Real-Time Observations of the Microstructural Evolution in Compressed Ice

By

Kurtis Galway

A thesis submitted to the

School of Graduate Studies

In partial fulfillment of the requirements for the degree of

Master of Engineering

Faculty of Engineering and Applied Science

Memorial University of Newfoundland

February 2024

St. John's, Newfoundland

Abstract

A total of fourteen (14) small-scale compression tests have been conducted using a specially designed apparatus in order to observe the processes which alter the microstructure of the ice due to an applied stress. All tests were conducted using a 5 MPa load applied to a 0.8mm thick, 60mm diameter ice sample. Tests were conducted at temperatures of -10°C to 0°C, -10°C to -2°C, -15°C to -20°C, and 0°C. These tests were then compared to a base case in which the ice sample temperature was allowed to change from -10°C to 0°C without any applied load. Various processes which impact the structure of the ice were observed in real-time using a borescope camera, and the videos were analyzed following the test. Cracking occurred in all tests and was dependent on the ice temperature. Ice at -10°C cracked in one short event indicating sudden brittle fracture, while ice closer to the melting point and ice at -15°C was time-dependent and cracked over the course of minutes. Crack healing is observed in two cases: as a result of prolonged application of stress and the resulting creep, and due to pressure melting at temperatures close to the melting point. Grain nucleation was the dominant dynamic recrystallization process at temperatures less than around -3°C and always occurred in response to the applied stress. At temperatures within -3°C of the melting point, grain boundary migration became the dominant recrystallization process. Pressure melting is observed to occur at temperatures within -0.1°C of the melting point. Generally, processes occurred at faster rates at warmer temperatures closer to the melting point. An in-depth analysis of the observed processes is presented in this thesis.

Acknowledgement

I would like to express my gratitude towards my supervisor, Dr. Rocky Taylor, for his guidance and support throughout the entirety of this research program. His guidance and advice regarding ice mechanics and experimentation were crucial to the success of this research program.

Funding for this work from Innovate NL, the Natural Sciences and Engineering Research Council (NSERC) of Canada, and Hibernia Management and Development Company Ltd. (HMDC) are gratefully acknowledged.

Graduate student funding from the Memorial University School of Graduate Studies is also gratefully acknowledged.

Table of Contents

List of Figures

List of Tables

List of Abbreviations and Symbols

P	Pressure
T_m	Melting Temperature
S	Entropy
V	Volume
E	Young's Modulus
v	Poisson's Ratio
F	Factor of Safety
A	Unsupported Area
M	Modulus of Rupture
hpz	High-pressure Zone
BPM	Bulk Pressure Melting
LPM	Localized Pressure Melting
LVDT	Linear Variable Differential Transformer
MUN	Memorial University of Newfoundland

Chapter 1: Introduction

1.1 Overview

Ice is a significant aspect of life in many cold climate areas – both on and offshore. As a result, much research has been conducted to gain a stronger understanding of ice and its mechanics. In this program, ice which has been subjected to high pressures during experimentation has been studied to reveal significant alteration to the grain structure – mainly due to the effects of dynamic recrystallization. Additionally, such ice is often devoid of air, appearing clear and without bubbles, which is believed to be the result of pressure melting that allows for easier transport of air during the liquid phase. There is much evidence that supports the theory that dynamic recrystallization and pressure melting are two dominant processes that effect the grain structure of ice which is subjected to high pressure – yet there has not been any observation of these processes in real time. This is due to restrictions surrounding current testing methods, as well as the high pressures which many experiments are conducted at, leading to difficulty observing these processes in real time. Using a new custom designed testing apparatus and by targeting modest pressures, experiments

have been conducted in which these processes were observed in real time. Given the complexities involved with theoretical analysis, this research aims to enhance the current understanding of the changes ice undergoes while under pressure. Furthermore, such observation of ice under pressure provides insight into processes such as how the grain structure melts or how the ice cracks and heals on a small-scale. This understanding is important as the real-time behaviour of ice on this scale and under these conditions is known primarily through force and stress analysis, not through the observation of real-time microstructural evolution. Thus, research into this area will support the evaluation of existing theories, while providing a basis for future research into this area. Additionally, results from this research can help improve models by linking changes in ice material behaviour to physical mechanisms.

1.2 Background

The processes of dynamic recrystallization and pressure melting are of particular interest when considering the goals of this research program. This section provides an overview of the current understanding of these two processes, as well as for high pressure zones. This is because these topics are crucial to the analysis of the experimental results – and were used to determine design constraints for the experimental apparatus.

1.2.1 High Pressure Zones

High-pressure zones refer to the localized, short-lived zones of high pressure that are located at the interface between ice and a structure. The load placed on the structure by the ice is mainly transmitted through these zones; thus, they are of critical importance to understand and account for in the design process. These zones are typically associated with a layer of damaged ice containing crushed ice and fine grains (Li, Barrette, & Jordaan, 2004). These zones are highly relevant and important in understanding both dynamic recrystallization and pressure melting

processes. As mentioned by Jordaan (2001), at the centre of these zones where the pressure is highest, both dynamic recrystallization and pressure melting at the grain boundaries are the primary failure mechanisms. Along the edges of these zones where the pressure is significantly lower, microcracking and dynamic recrystallization are the primary failure mechanisms. Figure 1 illustrates a typical high-pressure zone, including pressure distribution and primary failure mechanisms.

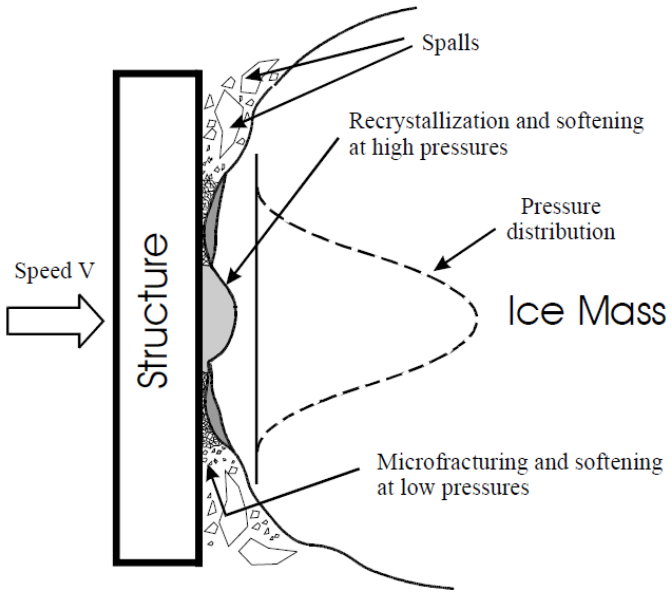

Figure 1 – Diagram demonstrating a typical high-pressure zone (Li, Barrette, & Jordaan, 2004).

1.2.2 Dynamic Recrystallization

Recrystallization refers to the restructuring and reorientation of the molecules from the original crystal lattice which has been placed under stress, and therefore disrupted, to a new lattice that is stress free. These disruptions are typically a result of slipping basal planes and the resulting

dislocations and are proportional to the applied stress. Recrystallization occurs once the energy stored due to the dislocations reaches a point known as the 'activation energy' upon which a new, stress-free grain will begin to grow (Gagnon R. , 2002). It should be noted that in a disrupted crystal, the molecules have, on average, a lower activation energy between the boundary zone compared to that of an undisrupted crystal and the boundary zone. This is because they have stored energy from the disruption. Thus, the boundary will move through the disrupted crystal as it has more thermally activated molecules available. More specifically, this means that new, stress-free grains that grow during the dynamic recrystallization process will have their boundaries grow into the disrupted grains. In ice, this process is both thermally and mechanically driven (Gagnon R. , 2002).

1.2.3 Pressure Melting

When a material's melt is denser than the solid, pressure melting can occur. Pressure melting refers to the decrease in melting point of a material subjected to a hydrostatic pressure and is governed by the Clausius-Clapeyron equation seen below in equation (1):

$$\frac{dp}{dT_m} = \frac{\Delta S}{\Delta V} \qquad (1)$$

In the above equation, T_m is melting temperature, p is pressure, ΔS is change in entropy, and ΔV is change in volume. For ice, 13.5 MPa of pressure will result in an approximate decrease of 1°C in melting point (Gagnon R. , 2002). This melting is expected to initiate on imperfections or at grain boundaries. Ice subjected to high pressures will be forced into a superheated state as its

melting point will be pushed to a temperature lower than its current temperature. The excess heat then conducts from this 'superheated' ice, as well as the pressure medium, into the areas in which melting has already started. This process can have significant softening effects on ice subjected to sufficiently high pressures and is a substantial component to understanding and modeling the failure of ice under compression and high amounts of pressure (Gagnon R. , 2002).

1.3 Objectives

The main objective of this research is to observe the development of the grain structure of a sample of ice when subjected to a constant pressure for an extended period of time with controlled temperature conditions. Particularly, processes such as localized pressure melting, bulk melting, cracking, crack healing and dynamic recrystallization are all processes which are of significance. The specific goal of this thesis is to investigate the following:

- The processes which influence the grain structure of the ice sample while under pressure.
- The identification of where and how the ice sample begins to bulk melt as it relates to the grain structure as a benchmark for comparison with pressure melting.
- The general pattern of evolution of the grain structure and the characteristics which denote these changes.
- The effect of temperature on the development of the ice sample under pressure.

1.4 Scope and Outline of Research

This thesis presents research focusing on the evolution of the grain boundaries of a sample of ice under a compressive load. In order to observe this evolution, a series of small-scale tests were completed in which a thin-section of ice was contained within a specially designed frame made of aluminum. The ice sample was then compressed between two polished, fused quarts glass discs and observed using a camera and polarized light. These experiments were performed in Memorial University of Newfoundland's Thermal Dynamics Laboratory using a deep freezer and a hydraulic handpump. The goal of this research is to observe and understand the processes which occur in the ice to develop the grain structure under compression at different temperatures.

This thesis is separated into six chapters. Chapter 1 provides an introduction and an outline of the research program. A literature review of general ice mechanics and processes, as well as past experimental programs which provided evidence of dynamic recrystallization and pressure melting, is provided in Chapter 2. Chapter 3 consists of a detailed explanation and overview of the experimental methodology, including an explanation of the new custom testing apparatus designed and used for these experiments. Chapter 4 describes the test matrix as well as the results of the experiments. Chapter 4 is separated into two parts: the first describing a base case, and the second describing four representative tests for the different types of tests conducted. In Chapter 5, the observed processes are analyzed, identifying various trends, and identifying the conditions under which these processes occur. An analysis focused on the effect of temperature as it relates to these processes is provided. Finally, Chapter 6 provides a summary of the main findings with recommendations for future work.

Chapter 2: Literature Review

2.1 Overview

The presence of ice presents a significant design challenge in many industries that operate in cold ocean environments. As such, there has been significant research conducted in order to understand various aspects of ice mechanics and properties that would aid in structural design and improve simulation models. In this chapter, these ice properties relevant to this research program are reviewed. Specifically, elastic behaviour of ice, viscoelastic behaviour of ice, and mechanics of compressive ice failure, such as dynamic recrystallization and pressure melting, are reviewed. Finally, an in-depth review of experimental programs focused on dynamic recrystallization and pressure melting is conducted to gain an understanding of common testing procedures and experimental apparatuses which are typically used.

2.2 Elastic and Viscoelastic Behaviour of Ice

2.2.1 Elasticity

Elasticity refers to a material's ability to return to its original shape and size once forces causing deformation are removed. According to Schapery (1997), in cases of fast loading, freshwater

granular ice is treated as an isotropic elastic material. Thus, the elasticity of ice is characterized by two constants – including the Young's modulus, E, and Poisson's ration, ν. The Young's modulus and Poisson's ration of sea ice has been studied by Mellor (1983). His findings demonstrate that, in a temperature range of -5°C to -10°C, the modulus ranges from 9 GPa to 9.5 GPa while the Poisson's ratio ranges from 0.3 to 0.33. Additionally, later research conducted by Sinha (1989) showed that, for temperatures ranging between -50°C to 0°C, the modulus only varied from 9 GPa to 10.16 GPa while the Poisson's ration ranged from 0.308 to 0.365. This suggests that temperature has a low impact on these values overall.

2.2.2 Viscoelasticity

Viscoelasticity of a material refers to it's ability to display both elastic properties and viscous properties when undergoing deformation. Viscoelastic materials display a time-dependent material response, generally depending on the strain applied and the rate of application. Ice is a viscoelastic material and will therefore demonstrate the following behaviour. Firstly, ice under constant stress will have increased strain overtime – commonly referred to as creep. Secondly, when strain is constant, the stress will decrease over time. Finally, after a load is applied, the ice will not fully rebound. These properties of viscoelastic materials are discussed by Lockett (1972).

2.3 Mechanics of Compressive Ice Failure

Compressive ice failure is a complex process dependent on a variety of processes. According to Jordaan et al. (2008), these mechanisms include microfracture, dynamic recrystallization, and pressure melting – all of which influence the development of high-pressure zones. Of particular interest is the role of both dynamic recrystallization and pressure melting.

2.3.1 Dynamic Recrystallization

Dynamic recrystallization can be described as a change in grain size, grain shape, and grain orientation without chemical change. This is driven by deformation and involves the nucleation of grains as well as the eventual migration of grain boundaries (Poirier & Guillope, 1979).

In ice, dynamic recrystallization results in an increase in creep and an increase in material softness. Duval et al. (1983) report that higher rates of strain results in more continuous dynamic recrystallization – with low rates of strain resulting in no recrystallization, intermediate levels resulting in periodic recrystallization, and high rates resulting in continuous recrystallization.

2.3.2 Pressure Melting

Pressure melting is another important mechanism, similar to dynamic recrystallization, for confined ice at high pressures. As discussed by Nordell (1990), the melting point of ice decreases as the pressure increases in accordance with the Clausius-Clapeyron Equation.

Using data from Nordell (1990), experimental data for the relationship between the melting pressure and temperature of ice is plotted by Taylor (2010) and can be seen in Figure 2.

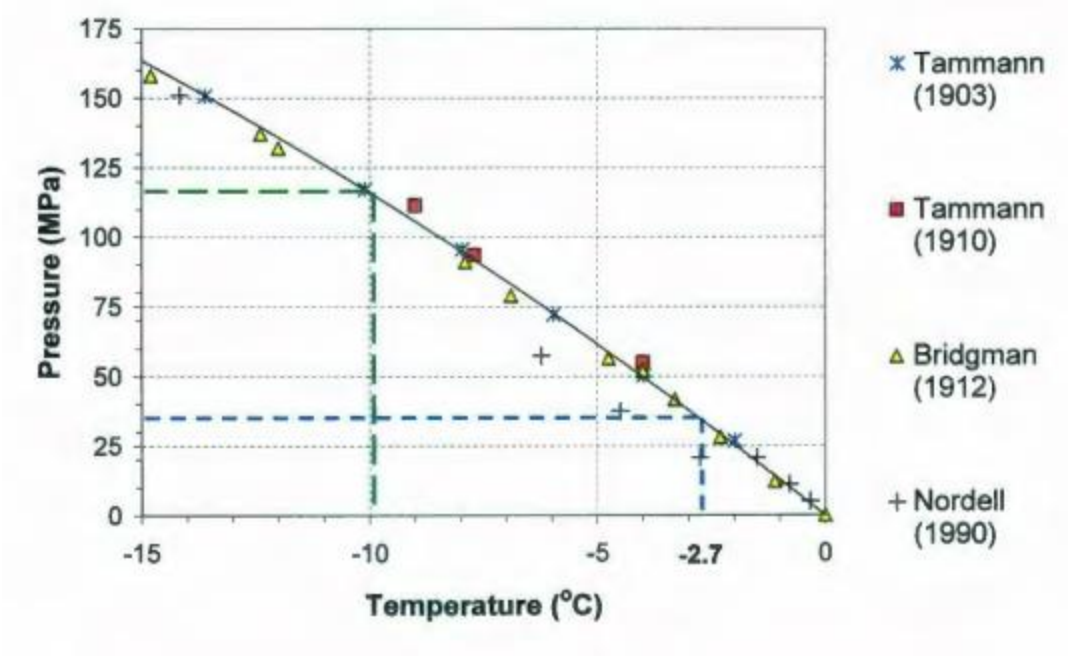

Figure 2 – Plot of pressure melting data for ice *(Taylor, 2010)*.

As seen in the above graph, at a pressure of 120 MPa, the melting point drops to -10°C, while at 35 MPa, the melting temperature drops to -2.7°C. Additionally, using this graph as a basis, it can be concluded that the melting point of ice changes even at relatively lower pressures of 5 MPa, where the melting point is around -0.5°C.

2.4 Dynamic Recrystallization Experiments/Research

2.4.1 Simple Shear Deformation

Some of the earliest experiments done investigating the mechanisms of deformation of ice under stress were experiments completed by Wilson et. al (1986). These experiments were intended to investigate the development of a preferred crystallographic orientation due to an applied shear stress of polycrystalline aggregates relevant to both geological and glacial environments. Ice was chosen for use in these experiments due to the similarity between shear-zones to those in larger crystalline rocks.

The apparatus used in this experiment allowed for the in-situ recording of an ice sample during progressive simple shear and can be seen in Figure 3 (Burg, Wilson, & Mitchell, 1986).

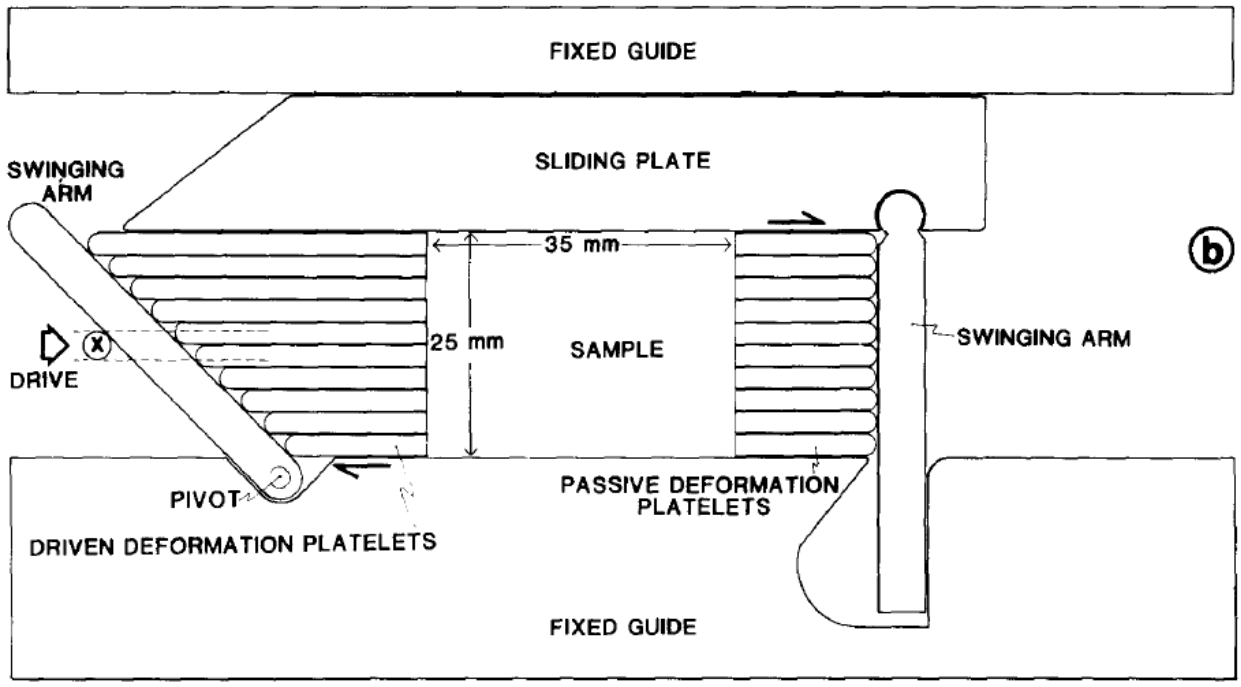

Figure 3 – Plan view at beginning of experiment of in-situ simple shear deformation apparatus (Burg, Wilson, & Mitchell, 1986).

The sample used in the experiments was a thin rectangular section of ice that was 25 x 35 mm and 0.85 mm thick. The ice was prepared in a laboratory by refreezing a mixture of sieved crushed ice and distilled water. It featured randomly oriented polygonal grains, which meant it did not demonstrate a preferred crystallographic orientation prior to experimental tests. The sample was confined between two fixed glass plates on its upper and lower surfaces. One long edge was confined by a fixed guide, while the other was confined by a sliding guide, which was also confined by another fixed guide. To apply the shear stress, the short edges were confined using "deformation platelets". A swinging arm controlled by a motor pushed against the platelets at one end at a swinging arc of 50°. The strain rate was set at approximately 3 mm per day and each experiment

lasted anywhere between 3 to 8 days. The platelets in contact with the primary swinging arm were of differing lengths and formed an angle to drive the deformation. The apparatus was confined in a sealed box and flooded with silicone oil for purposes of temperature stability during testing, which is seen in Figure 4. This box is then mounted on a Zeiss Invertoscope used to record microstructural data under crossed polarized light. This was done so via a time-lapse method – on 16 mm film every five minutes and 35 mm film every five hours (Burg, Wilson, & Mitchell, 1986).

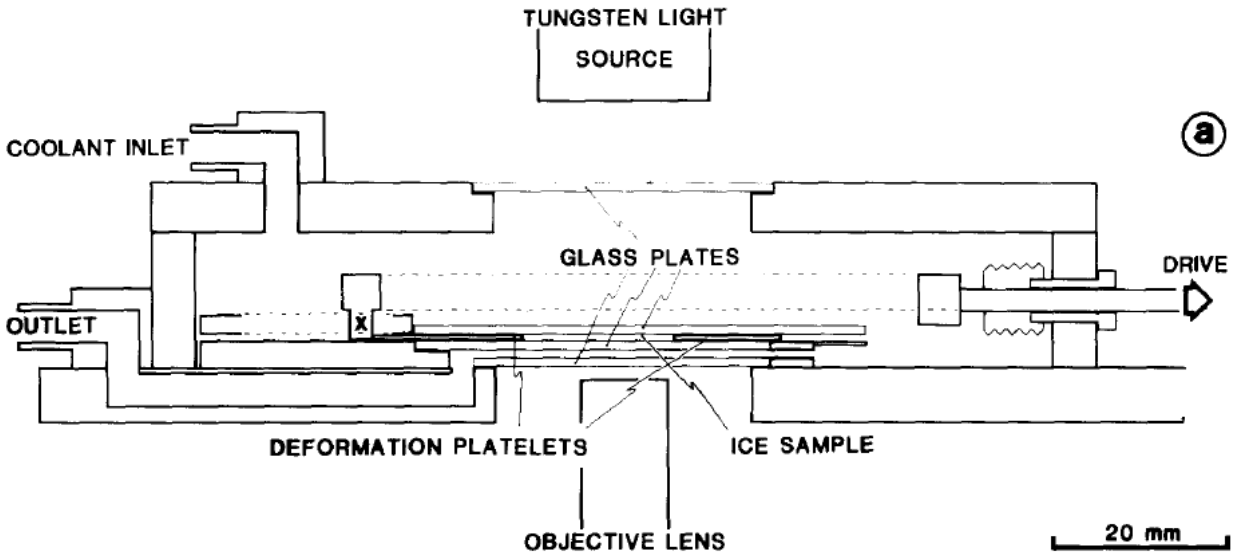

Figure 4 – Side view of in-situ simple shear deformation apparatus (Burg, Wilson, & Mitchell, 1986).

Note that for all but one of the experiments, the single crystal samples demonstrated plane-strain deformation as the grain orientation was aligned with slip on the basal plane. This meant that no "kinks" were formed during the experiments and the thickness of the ice sample did not significantly change. Slip bands, however, were apparent on grains early on in the experiment – forming parallel to (0001). Relevant to dynamic crystallization, it was found to be highly dependant on temperature – with experiments conducted at higher temperatures (-1 Celsius) showing earlier recrystallization. Generally, grain nucleation began at strains of around 2%. These

recrystallized grains generally had an equiaxed shape. In grains which were not suited to slip along the basal plane, kinks and deformation bands formed at higher shear strains (0.4). The recrystallization processes are dominated by migration of grain boundaries – both existing and new. There is notable break-up of old grains into sub-grains – particularly in grains unsuitable for glide along the basal plane. The new equiaxed grains mentioned above form at the grain boundaries. The recrystallization process continuously modifies grains and grain aggregates. Typically, there will be a reduction in grain size before the grain begins to grow via boundary migration. It is noted that it is difficult to identify a particular grain at differing strain rates due to the significant number of changes occurring in grain-size, shape, and number throughout the recrystallization process (Burg, Wilson, & Mitchell, 1986).

Based on this research, Wilson et. al come to two conclusions regarding dynamic recrystallization in ice undergoing simple shear. This is that dynamic recrystallization occurs at strains of 2-3% and can be considered a growth mechanism as well as a rotation mechanism. The second is that dynamic recrystallization is a strain softening process which partitions strain throughout a sample. It is argued that dynamic recrystallization contributes heavily to grain shape changes while preventing transition into a regime of fracture and preventing strain hardening from occurring. Thus, dynamic recrystallization is a key aspect of deformation of ice under stress (Burg, Wilson, & Mitchell, 1986).

As part of the experiments discussed above, Wilson (Wilson, 1985) also recorded a video of the dynamic crystallization process during the simple shear experiment. The purpose of the video was to allow for observation of flow mechanisms in polycrystalline aggregates. Specifically, dynamic recrystallization involving grain boundary migration is focused on during these experiments. The simple shear test took place over the span of days (3 – 8) and was observed and recorded using a

microscope while the specimen was under polarized light. In some instances, the video was recorded in real-time, while in others, a time-lapse method was used identical to the one described above. Refer to Figure 4 for a detailed illustration of the testing apparatus. Also considered in this video is the formation of slip bands and kinks. It is explained that the dominant glide plane is parallel to the basal plane, and that slip bands form on grains under stress. On grains which are in favorable position for glide, slip bands will more readily for as the glide occurs along the basal plane. Minor grain boundary adjustment accompanies the glide. In grains that are not favorably aligned, kink bands tend to form as the grain undergoes lattice bending in order to accommodate the strain. Such grains are unstable and may grow smaller as neighbouring grain boundary migration occurs. In some cases, grain nucleation and grain growth are observed to occur in the boundaries between two grains. This reduces the size of the original grains; although they do retain any deformations, such as slip bands or kinks. It is noted that these new grains are unstrained. It is later observed that grain nucleation may occur at kinks (Wilson, 1985).

Also included are experiments of pure shear, in which a load was placed on the vertical axis and the specimen was deformed by 30 % over a period of 5 days. A diagram of the apparatus used can be seen in Figure 5 (Wilson, 1985).

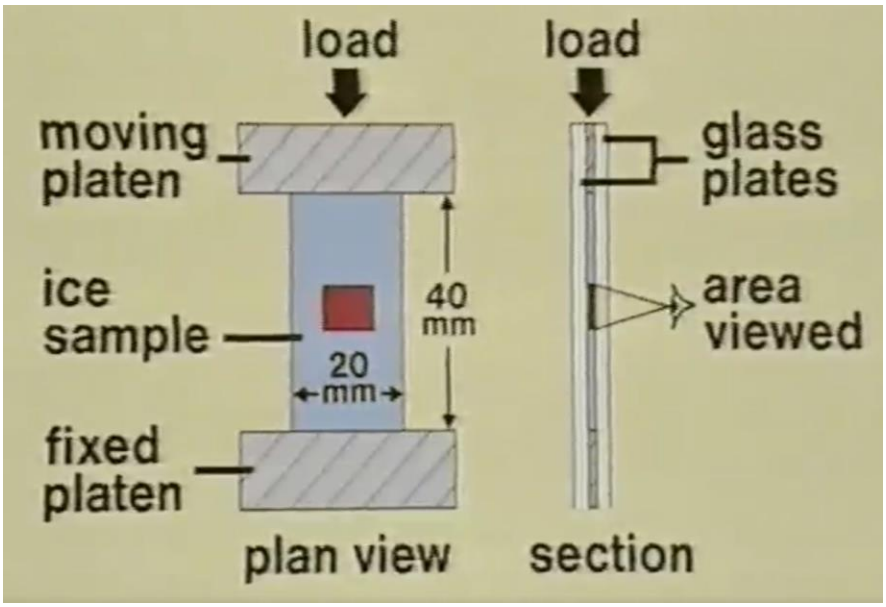

Figure 5 – Illustration of testing apparatus used in pure shear experiments (Wilson, 1985).

Deformation occurs as intracrystalline glide on the basal plane. Slip bands begin to form. Slip bands refer to plastic deformation within a grain that appear as a localized 'band'. An example of this can be seen in Figure 6 (Burg, Wilson, & Mitchell, 1986). To accommodate strain, kink bands may be formed – although not in every grain. Kink bands refer to rotational deformation within a grain and can be seen in Figure 7 (Burg, Wilson, & Mitchell, 1986). Dynamic recrystallization involving grain nucleation and grain growth occur in areas of grain boundaries and kinks. The original grain sizes are significantly reduced. The new grains undergo boundary migration and continue to grow until they themselves become deformed as deformation continues. The grains ultimately become aligned due to the competition between deformation and grain growth (Wilson, 1985).

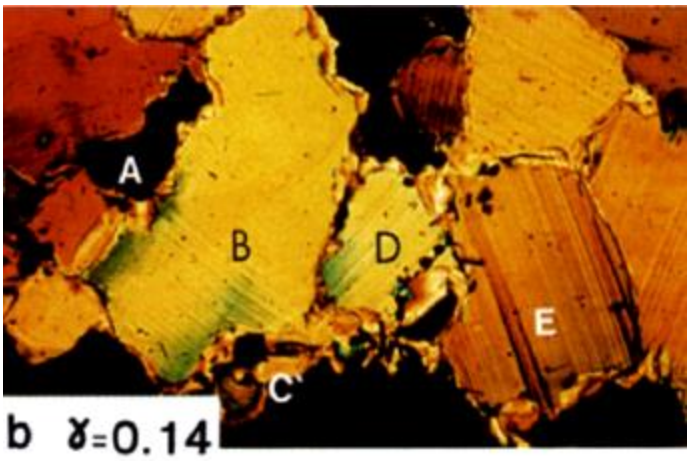

Figure 6 – Simple-shear deformation of ice. Slip bands are visible on grains B, D, and E (Burg, Wilson, & Mitchell, 1986).

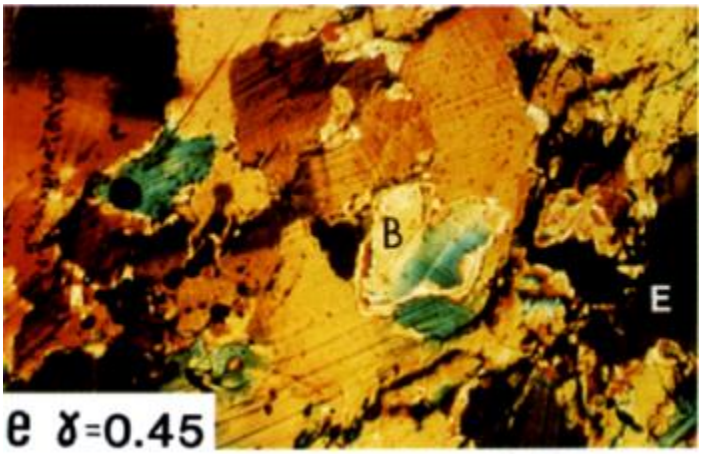

Figure 7 – Simple-shear deformation of ice. Kink bands are visible on grain B (Burg, Wilson, & Mitchell, 1986).

Finally, experiments were conducted at different temperatures. One at -10°C and the other at -1°C. It was noticed that dynamic recrystallization began earlier when the temperature is higher. Furthermore, grain boundary migration was seen to be much more rapid and extensive at higher temperatures (Wilson, 1985).

2.4.2 Triaxial Compression Tests

Jordaan et al. (1999) and Jordaan (2001) completed triaxial compression tests on a cylindrical ice specimen to determine the significant failure mechanisms at varying levels of pressure. In these tests, a cylindrical ice specimen was prepared by sieving crushed ice through a 2 mm and 3.35 mm

mesh, sealing this mixture in a mold, flooding with distilled and deionized water, and then allowing it to freeze. This block of ice was then machined into a cylinder of 70 mm diameter that is 155 mm long. This specimen is placed in a triaxial cell, which is pressurized using some fluid (commonly silicone oil). This hydrostatic pressure helps to prevent the specimen from failing and fracturing under pressure and mimics the pressure felt by ice in high pressure zones. Pressure is applied via a hydraulic press along a single axis. Strain, pressure, and temperature are measured throughout the experiment.

These tests revealed much regarding the significance of dynamic recrystallization as an ice failure mechanism. At lower shear stress, the significant/dominant deformation process is microcracking. At this point, dynamic recrystallization begins adjacent to the microcracks. As stress increases, these processes remain the same; however, dynamic recrystallization becomes increasingly important as it causes grain sizes to decrease and grain boundary volume to increase. Jordaan et al. (1999) suggest that this effect on grain boundaries is why dynamic recrystallization can be considered a 'damaging' process. As pressure increases further, while dynamic recrystallization remains a significant process, pressure melting that causes melt to form at the grain boundaries also becomes increasingly significant.

Another observation by Jordaan et al. (1999) was that dynamic recrystallization was seen as a continuous process. Particularly, it was observed that wherever the local stress was high, dynamic recrystallization would occur. Because the failure mechanisms at these high pressures cause constant stress redistribution, dynamic recrystallization would keep occurring in these areas of high local stress. Jordaan attempted to calibrate a FEA model in ABAQUS using a time-stepping approach. The observations concerning dynamic recrystallization were one of the failure mechanisms included in the model. The model produced plausible results – confirming that

microstructural changes are key to understanding the mechanical behaviour of ice under compression.

Triaxial test completed by Meglis et al. (1999) aimed to investigate creep behaviour under various triaxial stress conditions – including an analysis of the resulting microstructure. To prepare the ice sample, a near identical process to that of Jordaan et al. (1999), which is described above, was used to produce a cylindrical specimen of the same dimensions – 70 mm in diameter and 155 mm in length. One difference, however, is that a specimen was made using snow instead of crushed ice as the seeding material and another specimen was made using a large-grained block of ice (Meglis, Melanson, & Jordaan, 1999).

A Material Testing System was used to apply the axial load, which was controlled with the built-in MTS software. The ice samples were placed in latex jackets to isolate the specimen from the pressure medium (silicone oil). This was then placed in the triaxial cell, which was subsequently filled with the silicone oil. The confining pressure was increased at a rate of 0.5 MPa/s and, upon reaching the target pressure, was held for 1 minute prior to applying the axial creep load. This creep load was applied rapidly, reaching the target pressure in 0.1 s or less. The load was monitored throughout the experiment using two load cells positioned inside and outside the triaxial cell. The displacement of the MTS pistons was used to monitor the shortening of the sample since sample strain could not be directly monitored. Once the specimen reached its strain limit, the axial load was released, and the confining pressure was slowly decreased. It is noted that most samples were taken to approximately 44% of the true strain. Additionally, tests were halted at points to examine microstructural changes. The tests were conducted at temperatures of -10°C and the samples were held at this temperature for at least 12 hours prior to beginning the testing. It is noted that as confining pressure is increased, the center of the specimen tends to heat up at a rate of 0.02°C/MPa

while the silicone oil heats at a rate of 0.11°C/MPa. As such, at higher confining pressures, the specimens had a slightly lower initial temperature in order to compensate for these temperature changes. The test covered confining pressures between 5 and 60 MPa and with an axial pressure of 15 MPa. Samples were thin-sectioned using a microtome to a thickness of approximately 0.5 mm (Meglis, Melanson, & Jordaan, 1999).

During testing, some samples failed along a through-fault plane. Relevant to the microstructure, at maximum strain, the grain structure consisted mainly of fine grains surrounded by a few large grains. It is noted that the large grains are aligned with the load axis. At lower confining pressures, microcracking is present as a dominant deformation mechanism, although dynamic recrystallization is also present. As the confining pressure is increased greater than 15 MPa, microcracking becomes supressed and the formation of fine grains is primarily caused by dynamic recrystallization and pressure melting. It is concluded, however, that confining pressure is independent of grain size despite this change in dominant deformation mechanisms (Meglis, Melanson, & Jordaan, 1999).

2.4.3 Uniaxial Tests

Uniaxial tests refer to experiments in which stress is applied to a single axis. For example, Chauve, Montagnat, and Vacher (2015) utilized uniaxial tests to apply a stress of 0.5 MPa to a column of ice in order to investigate discontinuous dynamic recrystallization. Using Digital Image Correlation, in-situ images of this process were generated. It was found that grain nucleation and kink formation is correlated with high amplitude strain localization as a means to compensate for incompatibilities between grains. Additionally, it was found that nucleation, grain growth, tilt, and kink formation cause redistribution of stress, which decreases stress concentration (Chauve, Montagnat, & Vacher, 2015).

Fan et al. (2020) utilized uniaxial compression of a cylindrical ice specimen at 1.0 MPa to investigate grain boundary irregularity and quantify dynamic recrystallization. It was determined that the number of grains increased with strain at high stress but decreased with strain at low stress. Additionally, it was found that, as nucleated grains increase in size, their grain boundary irregularity also increases (Fan, et al., 2020).

2.4.4 Indentation Tests

Indentation tests completed by Li et al. (2004) were done so using varying indenter tip sizes in order to assess the behaviour of high-pressure zones at different sizes. Laboratory test results were compared to medium-scale field test results to determine the overall difference. Included in this analysis is a comparison between microstructures at the indentation area between the two data sets. As suggested by Jordaan (2001), microcracking and dynamic recrystallization were expected at the pressures and temperatures in which the tests were conducted. This was confirmed as seen in Figure 8. Here, in the indentation area there are both light and dark zones. The dark zones primarily consist of a layer of recrystalized ice – featuring a large number of fine grains. The light zones consist of dense microcracking – although at the resolution of Figure 8 this cannot be easily observed. It was noted that there is similar microstructural damage between the laboratory data and field data (Li, Barrette, & Jordaan, 2004).

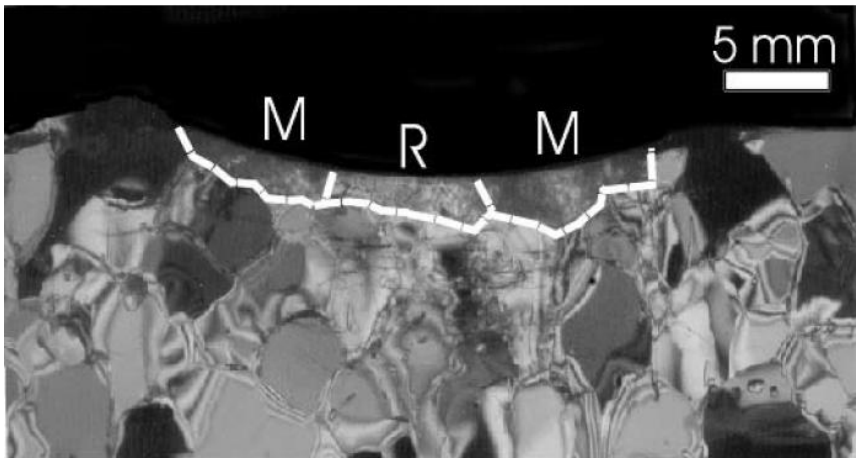

Figure 8 – Thin-section under polarized light following an indentation test. M – microcracking, R – recrystallization (Li, Barrette, & Jordaan, 2004).

The ice used for these indentation tests was prepared as follows: first, distilled, deionized water was frozen in a bucket and then crushed. It was then sieved to produce four different seed sizes depending on the mesh sizes (<2 mm, 2 – 3.35 mm, 3.35 – 4.75 mm, and > 4.75 mm), which were stored at -20°C in separate plastic bags. The seeds were then distributed to molds varying in size depending on indenter size. The bottom of these molds was surrounded by a thin, plastic membrane secured using a rubber band. Water of temperature 5 - 10°C flooded the molds and was stirred so that the seeds would form an ice cover of thickness between 10 – 30 mm. It was then placed on a Styrofoam sheet and left to freeze at -15°C. As the ice expanded, it pushed against the membrane and was raised. The plastic was then removed, and the ice was leveled to be flush with the steel mold. The specimen was then left in a cold room at -10°C where the tests would be conducted. Following the tests, the indented section was cut out using a chainsaw and then thin-sectioning was conducted such that the microstructure could be observed. The remaining cavity was filled with water and left to freeze for subsequent tests (Li, Barrette, & Jordaan, 2004).

The apparatus used was a Material Testing System (MTS) located in a cold room. The built-in MTS software was used to control the ram and a 10 KN load cell was used to measure the load cycling for the smaller indenters as the built-in load cell in the MTS (500 KN) was not sensitive enough. The built-in load cell was used for the indenters which produced greater loads. The indenter was made using steel. The setup can be seen in Figure 9 (Li, Barrette, & Jordaan, 2004).

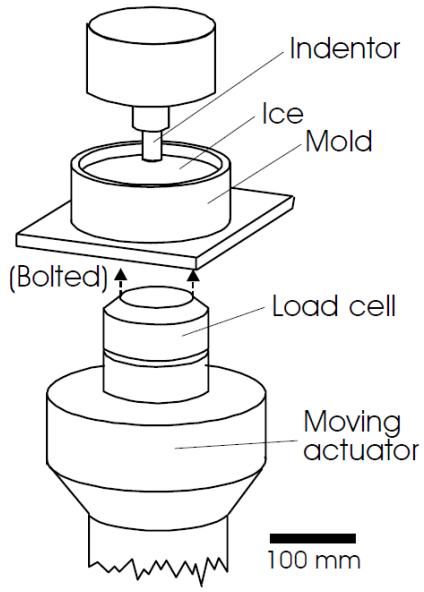

Figure 9 – Diagram of the testing apparatus used in indentation experiments (Li, Barrette, & Jordaan, 2004).

A similar uniaxial indentation experiment was run by Mackey et al. (2007) in an effort to study failure mechanisms in polycrystalline ice at varying loads. It is noted that an indentation test of this sort is essentially a model of a single high-pressure zone – meaning that results reflecting current understanding of high-pressure zones is expected. Particularly, at the center of the high-pressure zone where there is high confinement pressure, it is expected that a damage layer will form along the interface between the ice and indenter mainly consisting of recrystallized and

pressure melted ice. That is, a layer of recrystallized clear ice. This is surrounded by an area of extruded crushed ice and microcracking. Furthermore, depending on the location of the indentation relative to the edge of the ice block, other failure mechanisms can be observed – including spalling and large fracturing of the ice (Mackey, Wells, Jordaan, & Derradji-Aouat, 2007).

In this case, the polycrystalline ice had an average grain size of approximately 4 mm. During production, storage, and testing, the ice was kept at a temperature of -10°C. To start, a block of bubble-free ice, which was purchased to save time, was crushed and sieved using a 4.75 – 3.35 mm mesh. A fiberglass mold was filled with the crushed ice seed and then sealed with a rubber membrane over-top. Then, air was evacuated from the mold via application of a vacuum. Then, similar to most ice sample preparation, distilled and de-aerated water at 0°C was used to flood the mold, an insulated cover was placed on top of the mold, and it was left to freeze. The purpose of the insulated cover was to ensure that freezing would occur from the bottom up. As a result, any remaining air would be concentrated at the top of the block and could easily be trimmed off of the sample. The block was left to freeze for three days and then left upturned at 0°C until released from the mold. At this point, it was machined into a 20 x 20 x 10 cm block for testing (Mackey, Wells, Jordaan, & Derradji-Aouat, 2007).

The tests were completed using an MTS in a cold room at -10°C. The block was placed such that the indenter was above the desired impact location. It was then lowered manually such that the indenter was directly above the test location without being in contact with it. A thin metal strip was used as a spacer to maintain consistency between tests. The built-in MTS controller and equipment was used for these tests. A 25 kN MTS load cell at a sample frequency of 20 kHz was used and was chosen based on expected loads and frequencies. A 3dB cut-off frequency of 3kHz was used to filter the readings. Indenter speeds were between 0.2 mm/s and 10 mm/s and the

maximum displacement was 5 mm. To record the tests, three cameras were used. The first was a black and white camera capable of recording in 30 frames per second (fps). The second a color camera also capable of recording at 30 fps. Finally, a high-speed black and white camera capable of recording at 1000, 500, and 125 fps depending in the length of the test was used. Furthermore, the specimens were immediately photographed following the tests. To synchronize the load data and the videos, an electrical pulse which would both trigger the indenter and flash an LED visible by the camera was used (Mackey, Wells, Jordaan, & Derradji-Aouat, 2007).

Following the tests, a thin-sectioning technique called "Double Microtome" was used. Using a thin bead of water from a syringe, a section of ice between 1 – 2 cm thick was welded to a clean glass slide. A microtome blade was then used to shave off layers of ice until the desired thickness is reached. Then, the free side is welded onto a new glass slide and the first glass slide is removed using a small blade. Now, the newly freed surface is microtomed to approximately 0.5 mm in thickness. At this point, the crystal structure of the ice can be examined. It is noted that only 3 sides of the specimen were welded – leaving the indented side untouched to preserve it for observation. The thin-sections can then be photographed under polarized light to easily view the grain structure of the specimen. The specimens were also side lighted (45 degrees) under plain light and photographed to highlight microcracking specifically (Mackey, Wells, Jordaan, & Derradji-Aouat, 2007).

Results relevant to dynamic recrystallization are mainly associated with the observations of the damaged layer which is formed in the high-pressure zone as hypothesised. Again, it is noted that in the area of high-pressure, the microstructure consists of many small, fine grains – a product of dynamic recrystallization. Other results less relevant to dynamic recrystallization but still relevant to failure mechanisms was that large-scale fracture and spalling was abundant and occurred more

frequently when the indentation occurred closer to the edge of the sample. Additionally, slower load rates lead to a higher probability of fracture. Finally, it was determined that fracturing and spalling caused a noticeable drop in load felt by the specimen (Mackey, Wells, Jordaan, & Derradji-Aouat, 2007).

2.4.5 Medium Scale / Field Experimentation

Dynamic recrystallization has also been observed in tests conducted in the field. One such test is the field tests of ice indentation at a medium scale conducted by Frederking et al. (1990). These indentation tests were conducted on Hobson's Choice Ice Island, which was a 5 km wide by 8 km long 40 m thick ice island. This ice was primarily shelf ice but had an area of multiyear pack ice attached to it. At the time of testing, the temperature of the ice was roughly -14°C. A trench was dug out on the ice island to house the indentation apparatus. The apparatus was a hydraulic actuator with force capacity of up to 4.5 MN and a maximum velocity of 100 mm/s. A high speed data acquisition system was used to collect force data, displacement, and local ice pressure – with rates of up to 1000 readings per second. A schematic of the apparatus is seen below in Figure 10.

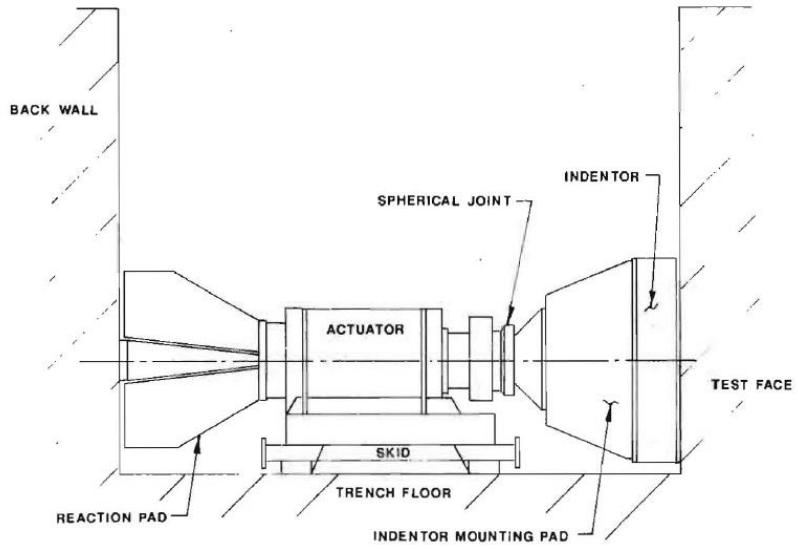

Figure 10 – Illustration of the apparatus used for indentation tests at Hobson's Choice Ice Island (Frederking, Jordaan, & McCallum, 1990).

The indentation experiments were recorded through a Lexan window using a video camera capable of 30 frames per second. To synchronise with the data, a red LED was set to blink on and off once the experiment was started. The LED was in view of the camera. To determine which is the first frame of the experiment, the frames showing the first blink of the LED were determined (Gagnon R. E., Analysis of visual data from medium scale indentation experiments at Hobson's Choice Ice Island, 1998). Results of this experiment are consistent with knowledge regarding high-pressure zones. That is, the centre of the impacted area withstood higher pressures than areas along the edges. This area was notably harder than other areas. It was later hypothesized by Gagnon (1998) that a thin layer of liquid formed along the interface, presumably due to pressure melting occurring at higher pressures. All of this reflects results from laboratory experiments involving ice indentation and the effects of the changing microstructure under these conditions on the mechanical properties of ice.

2.4.6 Other Experiments/Analysis

Another experiment relevant to dynamic recrystallization was completed by Duval and Castelnau (1995) in which recrystallization mechanisms in polar ice sheets was investigated. It is stated that in polar ice there are three recrystallization mechanisms at work. This includes grain growth, rotation recrystallization, and migration recrystallization – but it is suggested that each mechanism will only occur under specific circumstances, such as at a certain depth or temperature. Migration recrystallization refers to boundary migration and may occur in ice with strain less than 1% - and typically occurs near the bottom of ice sheets where there are higher temperatures. It is noted that dislocation glide on basal planes is the primary mechanism of deformation; however, as creep relaxes, these recrystallization mechanisms act to alter the grain texture (Duval & Castelnau, Dynamic Recrystallization of Ice in Polar Ice Sheets, 1995).

2.5 Pressure Melting Experiments/Research

2.5.1 Indentation Tests

The effects of pressure melting are often observed in experiments in which ice is placed under large amounts of pressure. Often referred to as "anomalies" in the deformation process, such effects were observed by Barnes and Tabor (1966) following indentation experiments aiming to measure the hardness of ice at different temperatures. These experiments were simple indentation experiments performed on ice of small grain size (approx. 2 mm) that were held at a constant temperature during each run. A steel indenter was used. At temperatures above the pressure melting point, there was a steep drop-off in hardness values, which can be seen in Figure 11. As seen, all curves to the left of the pressure melting curve have a significant drop-off. This is consistent for all strain rates shown. Furthermore, the grain size of the ice observed following the experiment was larger and there was significant bubble loss - creating a region of clear ice in the

area of indentation. This indicates that pressure melting is having a significant effect on the deformation of ice under certain conditions (Barnes & Tabor, 1966).

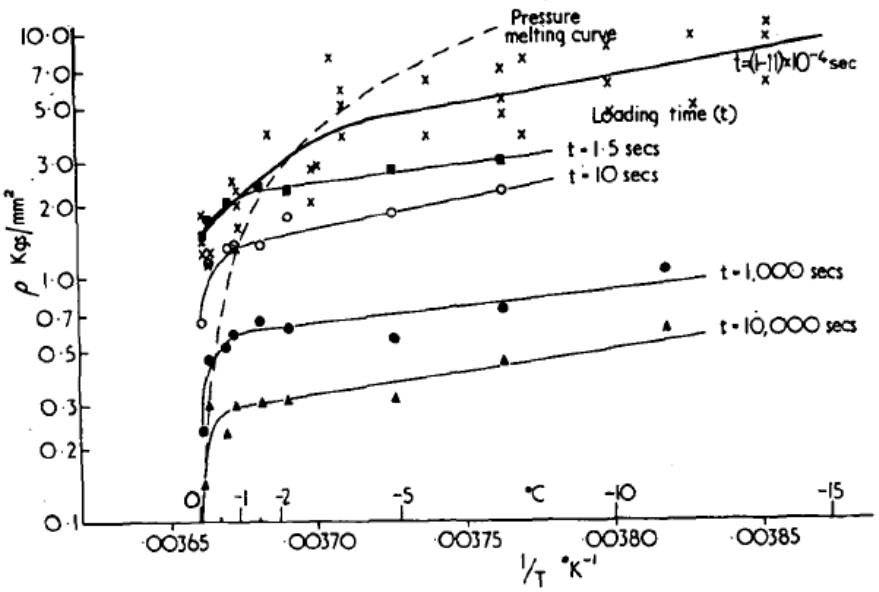

Figure 11 – Indentation hardness (log) vs. temperature (reciprocal) for various strain rates (Barnes & Tabor, 1966).

Barnes and Tabor suggest that at high pressures, the deformation of ice at 0°C is largely driven mechanisms taking place at grain boundaries – specifically, pressure melting processes. Essentially, a water-like layer would form at the ground boundaries, which would allow for growth, movement, and rotation of the grains without requiring a significantly large amount of heat. To confirm that this melting was intrinsic to the ice and not due to the indenter providing the ice with heat, additional indentation experiments were preformed using an ebonite tipped indenter. The thermal conductivity of steel is much higher – meaning that there is sufficient heat relayed into the ice from the indenter to cause relegation. In the case of ebonite, the thermal conductivity is much lower, meaning heat is mainly transferred through the ice. This means that relegation effects are negligible in experiments conducted using the ebonite. Thus, it was determined that processes above the pressure melting temperature must be leading to a decreased harness and an

increased flow of the ice (Barnes & Tabor, 1966). These experiments identified the presence of pressure melting in ice under compression while also identifying its significance in deformation and ability to soften the ice.

Further evidence of pressure melting occurring in a high-pressure zone is the clear ice, devoid of bubbles, seen in thin-sections of experiments completed by Mackey et al. (2007) discussed in section 2.4.3.

Gagnon and Tulk (2019) conducted crushing experiments in which pressure spikes induced by spallation caused rapid pressure melting. Using a high-speed camera, dendritic, fern-like features were observed during formation as the pressure was increased at a temperature of -5°C. The length of the feature was approximately 1.7 mm. These features were similar to melt figures and propagated laterally within a shallow depth of the ice. During spallation, spikes of up to 36 MPa were measured – and these melt features formed rapidly during the ascent of pressure. They then rapidly refreeze during the descent of the pressure. Additionally, it is noted that there are cases in which phase transition in ice is observed; however, the pressure required to theoretically induce this change was much higher than what was measured.

2.5.2 Triaxial Tests

Experiments involving triaxial compression to gain an understanding of ice disintegration under fast compression loading were completed by Jordaan et al. (Jordaan, Matskevitch, & Meglis, 1999). The intent of these experiments was to gain a stronger understanding of the mechanisms of failure at varying levels of pressure and to develop models to account for these varying mechanisms. High-pressure zones, which are somewhat randomized areas of high local pressure located on the interface between the ice and structure, are relevant to pressure melting because the high pressures in these zones may produce appropriate conditions for pressure melting to occur.

In fact, medium scale field experiments have shown pressures of up to 70 MPa across a 10 mm diameter pressure gauge (Jordaan, Matskevitch, & Meglis, 1999). This is important because it proves the existence of extraordinarily high pressures in the context of ice-structure interactions. It is also suggested that pressure melting occurs at the center of these high-pressure zones where the pressure is at its highest. Thus, understanding failure mechanisms, including pressure melting, in ice at these compressive loads is important.

In a triaxial test, the test specimen is confined in a triaxial cell which is pressurized with a fluid such that the specimen is confined by the hydrostatic pressure at all points. The benefit of this is that it will help prevent fracture/failure of the specimen when the high compressive load is applied. Thus, the specimen can be studied in a state of high pressure. Using a hydraulic press, pressure is applied along a single axis of the specimen and maintained for some period of time. This is a creep test. In this case, the ice specimen was prepared using crushed seed ice that was sieved between a 2 mm and 3.35 mm mesh. This mixture was placed in an acrylic mold, sealed, and then flooded with distilled, deionized, and de-aerated water. This mixture was allowed to freeze. Then, the resulting block of ice was machined into a cylinder that was 155 mm in length with a 70 mm diameter. Following the experiment, the cylinder is thin-sectioned and can be viewed under polarized light, as seen in Figure 12 (Jordaan, Matskevitch, & Meglis, 1999).

Figure 12 – Thin-sectioned view of ice under polarized light (Jordaan, Matskevitch, & Meglis, 1999).

Following the experiment, there were some results and conclusions relevant to pressure melting. Mainly, pressure melting is only a significant deformation mechanism at very high pressures, along with dynamic recrystallization. This means that these two processes are the primary mechanisms occurring at high pressure. Also noted is how the rate of deformation decreases as pressure increases until pressure reaches high enough to trigger pressure melting, at which point the rate of deformation increases. Also of interest is the observation that, at higher pressures, there is continuous softening and deformation of the ice, while this is not the case at lower pressures where the material approaches a steady-state. Finally, it is noted that the pressure melting process is continuous. This is because in areas of high local pressure, pressure melting may occur at the grain boundaries, relieve the stress locally, refreeze, which ultimately causes the pressure to rise again

in some local area and the process can continue. Thus, it is the rate of occurrence of these events which is most important when attempting to model these processes (Jordaan, Matskevitch, & Meglis, 1999). Jordaan also notes that, at the time, many models lacked the ability, or did not consider, pressure melting and its softening effect. This would result in higher results when modeling high loading rates compared to actual field results. It is noted that preliminary results of modeling the pressure-softening effect have produced better results (Jordaan, Matskevitch, & Meglis, 1999). Gagnon (2002) later analyzes this model and states that it is insufficient for use in instances of high strain rate, which are the most common type of ice-structure interaction. He states that there is insufficient time for heat conduction and recrystallization to occur. At lower strain-rates, however, Gagnon states that the model may be sufficient pending additional confirmation tests (2002).

Jordaan (2001) furthered the analysis of these experiments, ultimately coming to the conclusion that the ice "borrows" heat from the indenter in order to initiate melting at grain boundaries under high pressure. This is supported by work done by Gagnon and Sinha (1991), in which it is noted that the temperature of the indenter decreases as the load increases. Furthermore, Jordaan calculates that the melt concentrated at the grain boundaries would be approximately 0.5% of the total volume involved in the melting process at the interface (Jordaan I. J., 2001).

Barette and Jordaan (2003) also completed triaxial tests on ice in order to investigate the pressure-temperature relationship of ice under compression – including an analysis of failure mechanisms under conditions of high pressure. The ice was prepared in a similar manner as that of Jordaan (1999), although more detail is provided in this case. To start, the ice was grown in an insulated bucket filled with deionized and distilled water using a single crystal seed. This creates a block of ice without grain boundaries. This is then crushed and sieved through meshes of 2 and 3.5 mm.

These seeds were then placed in a cylindrical mold and filled with more distilled and deionized water under a vacuum. Once allowed to freeze, the specimen would be one of granular ice with a random crystallographic orientation. It is noted, however, that there were some cases in which air was entrapped within the specimen consisting of non-uniform bubbles throughout. From here, the cylindrical block of ice was cut into quarters and machined into a cylinder of 70 mm diameter and 155 mm length. This ice is stored at -25°C until needed for testing. Also used in this test was iceberg ice, which was purchased from a third-party company and stored at a temperature of -20°C (Barrette & Jordaan, 2003).

The testing apparatus used in this case is also similar to that used by Jordaan (1999); although, there is more detail provided in this case. The recorded parameters include platen displacement used to determine the strain, axial load, and the confining pressure and temperature. An MTS is used to apply the axial load via servo-controlled hydraulics. The MTS software was used to control the rams. A Structural Behavior Engineering Laboratories Model 10 Triaxial Cell using silicone oil was used to confine the specimen. The specimens were first wrapped in a latex membrane prior to being enclosed in the triaxial cell. It is noted that there was no window on the cell – meaning observation could not occur during the test. The confining pressure felt by the specimen ranged from 10 – 65 MPa while the temperature was held constant throughout the experiment and ranged anywhere from -26 to -5°C. The axial stress applied in all runs was 15 MPa (Barrette & Jordaan, 2003).

Results from this experiment relevant to pressure melting show that there is an extreme increase in activation energy at higher pressures, which suggests that the mechanisms operating at these higher pressures are very different to that at lower pressures. It is noted that when ice approaches its pressure melting point, the melt is expected to occur at the grain boundaries. Furthermore, it is

suggested that there is a possibility that this is concentrated between grains that are not oriented for easy crystal slip. Additionally, it is observed that there is an increased sensitivity to internal structure at high amounts of pressure, which may indicate that pressure melting introduces an element of randomness in that it randomly distributes liquid while softening the ice. Finally, it is suggested that because the ice undergoes a significant reduction in strength at high levels of pressure (~65 MPa at -20°C), that the collapse of high pressure zones is due to failure, presumably due to dynamic recrystallization and pressure melting, at the center where the pressure is highest (Barrette & Jordaan, 2003).

Meglis et al. also completed similar triaxial tests – coming to the conclusion that, at high confining pressures greater than 15 MPa and approaching 60 MPa, there is strong indirect evidence that pressure melting is a dominant deformation mechanism. Specifically, it is noted that samples tested at these high pressures were perfectly welded across the rupture plane when retrieved, which indicates that melting had occurred. Additionally, slight reduction in temperature of 1 or 2°C would result in no rupture occurring and lower creep rates. This suggests that when pressure melting did not occur the ice was able to withstand the stress. Finally, as noted in most tests, the ice was observed to be perfectly clear at higher confinement pressures, suggesting that pressure melting had occurred and removed all bubbles from the area (Meglis, Melanson, & Jordaan, 1999).

Chapter 3: Experimental Apparatus Design & Methodology

3.1 Overview

The goal of this study was to observe a thin-section of ice that was illuminated by a polarized light and under compression. The pressure melting process was initially the main process that was targeted for observation. As such, the experiments were designed with this goal in mind. All tests were completed using freshwater ice that was approximately 0.5 mm thick and 60 mm in diameter. A custom-built housing was designed to crush the ice sample in between two glass discs, while allowing for a camera to record the compressed ice with a polarized backlight to better view the developing grain structure, which is discussed in detail in section 3.2. A hydraulic hand pump was used to apply force on this housing, which applied pressure on the ice sample. A load cell was used to collect pressure data and temperature probes were used to collect temperature data of the housing and the freezer in which the experiments were conducted in. A self-reaction frame was used to contain the forces and prevent damage to the freezer. Because the original goal of these experiments was to observe the pressure melting process, the only independent variable is the target temperature. Other than the effects of this factor, the main results of these experiments were

the observation of the various processes which occur in ice under pressure. Due to the fact that this type of experiment has not been conducted before, this research aims to provide a basis for future research of this type.

All experimental tests, water preparation, and ice preparation was completed in Memorial University of Newfoundland's Thermal lab using a deep freezer.

3.2 Design of Experiment

3.2.1 Overview of Experimental Apparatus

The main goal of this experiment was to observe a sample of ice under compression with a focus on pressure melting. According to the Clausius-Clapeyron equation, it would take approximately 13 MPa exerted on the ice sample to lower the melting point by 1 degree Celsius. At this pressure, the ice sample should display pressure melting – thus, the apparatus was designed with a target pressure of 15MPa.

Initially, the idea was to create a frame out of metal to hold two pieces of glass that would crush the ice. The frame would house both a camera, as well as a light and the necessary polarizing films in order to view the grain structure in color. All of these components must be protected from the force exerted on the frame and glass. Thus, the design seen below in Figure 13 was created – and was used as a guideline throughout the remaining design process.

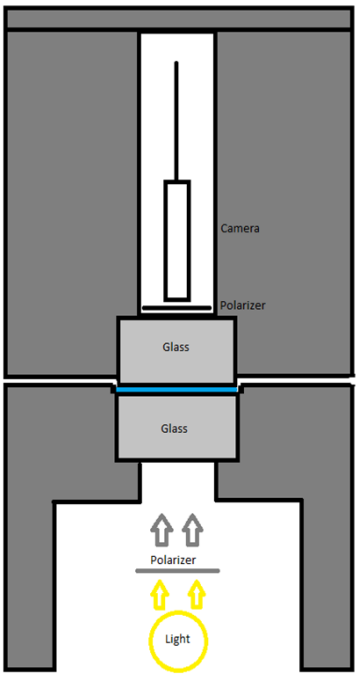

Figure 13 – Conceptual design of the pressure melting observation apparatus.

After consulting with Memorial University of Newfoundland's Technical Services engineers, it was determined that aluminum would be ideal for such a design due to its resistance to rust and it being of suitable strength when taking into account the target pressure and temperature. The design drawings can be seen in APPENDIX - B. Below in Figure 14 is the machined testing apparatus.

Figure 14 – Testing apparatus.

This apparatus can be separated into two parts. The top section housing the camera and the protruding glass disc which served as the indenter. The bottom section of the apparatus that housed a LED light strip and had a countersunk glass disc upon which the ice sample sits. Rectangular access holes in the bottom allowed easy access to the light during testing to allow adjustment as needed. In both top and bottom there was a polarizing film. Alignment pegs machined out of brass were used to align the top and bottom parts and to ensure that the glass discs did not come into contact with the metal frame during the connection process.

An example of the image this apparatus can produce is seen in Figure 15. As seen, the cross polarized light makes the ice crystals distinguishable among each other. Depending on their orientation in relation to the cross-polarizers, the individual ice crystals will appear in a different color, allowing for easier visualization (Shokr & Sinha, 2023).

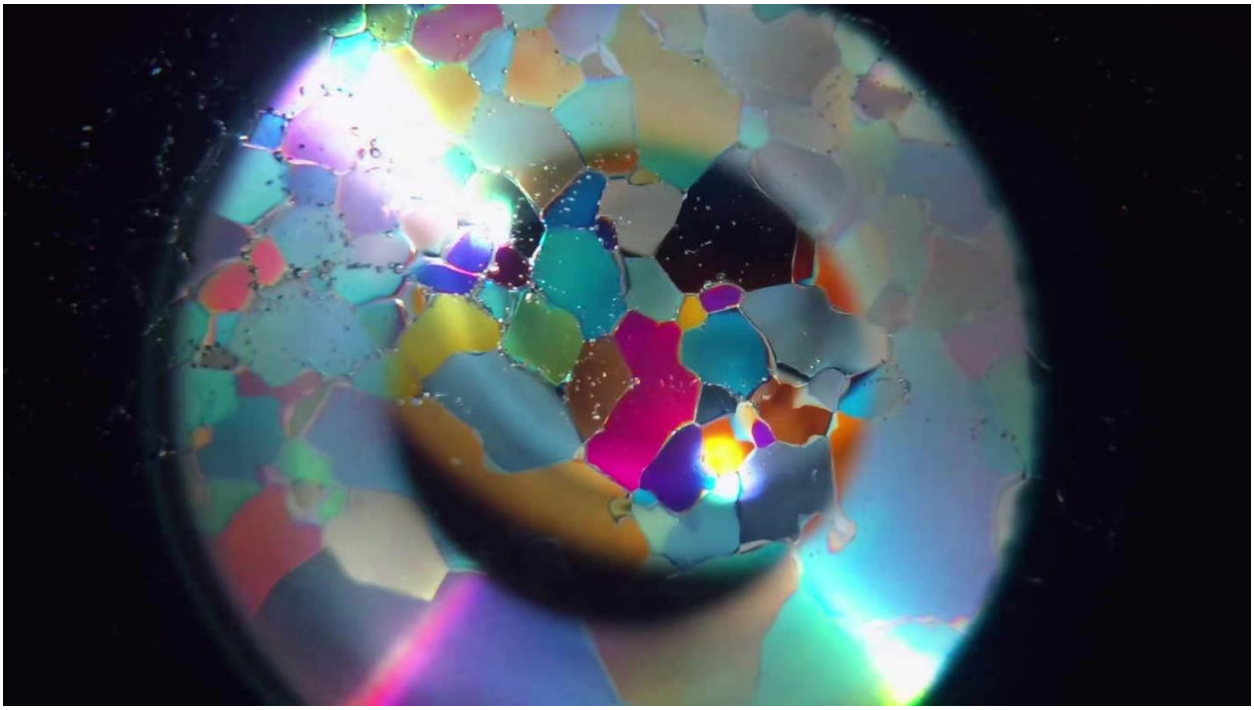

Figure 15 – An example of the image produced by the testing apparatus when viewing compressed ice.

For reference, Figure 16 shows the portion of ice which was observed by the camera, represented by the rectangle, and the portion which was illuminated compared to the overall size of the ice sample, represented by the inner circle.

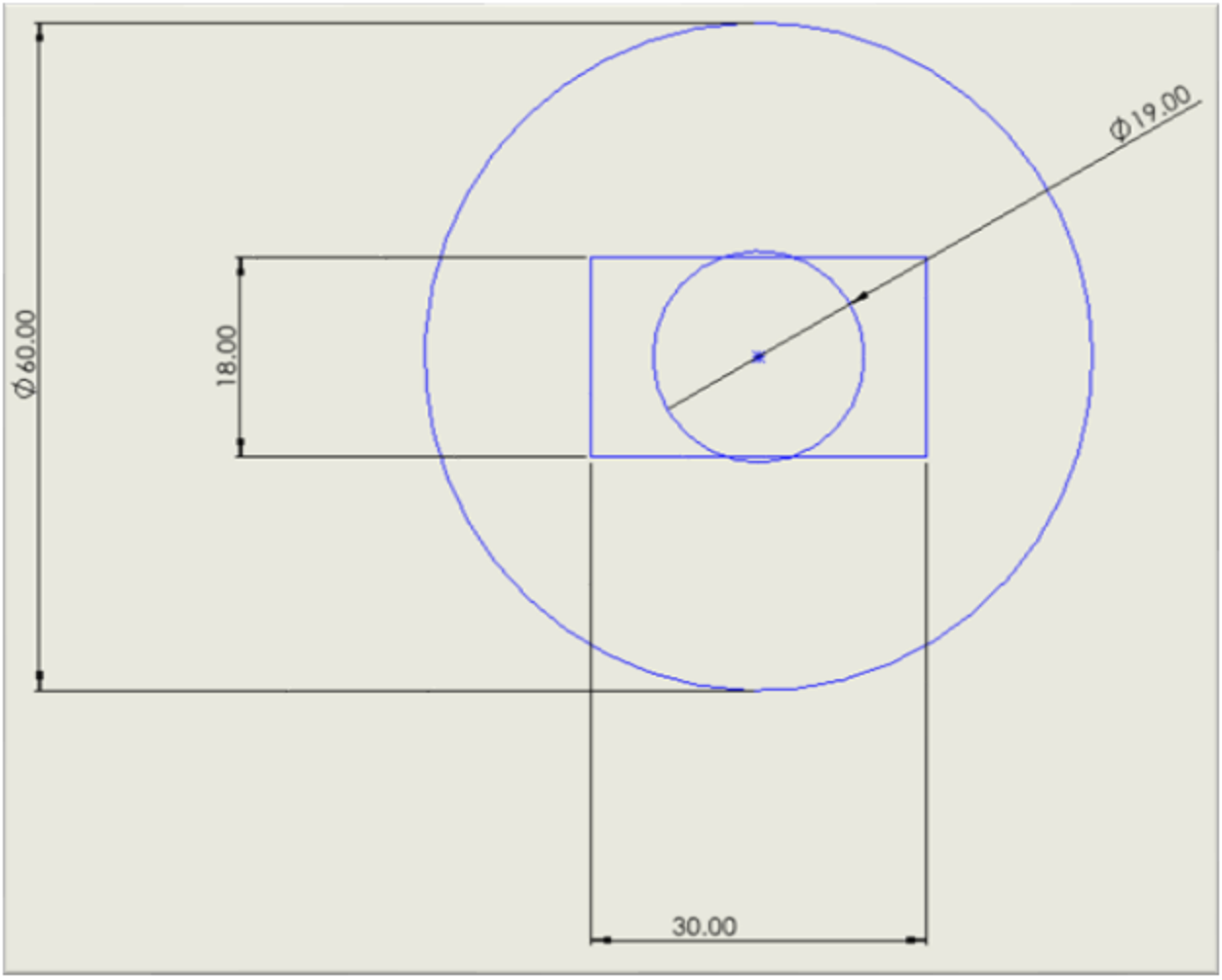

Figure 16 – Section of the ice sample observable by the camera, represented by the rectangle. The outer circle represents the entire ice sample, while the inner circle represents the portion of ice which is illuminated. Dimensions in millimeters.

3.2.2 Design of Glass Discs

As the ice needed to be observed in real time – it was required to compress the ice using two pieces of a suitable transparent material. Fused quartz silica was chosen due to its low coefficient of thermal expansion – meaning it is resistant to thermal shock. A diameter of 60 mm was chosen, with a 30mm viewing port in the center. To determine the thickness, it was determined that failure would first occur when the glass pushed up through the viewing port – creating a bend. Thus, equation (2) was used to calculate a thickness that would withstand the target pressure:

$$T = \sqrt{\frac{PxAxF}{3.12xM}} \quad (2)$$

This is the formula for calculating rupture pressure of a disc which was provided by the manufacturer of the glass disc, Technical Glass Products. In the above equation, T is thickness, P is pressure, A is unsupported area, F is factor of safety, and M is the modulus of rupture. Using a factor of safety of 7, a target pressure of 15 MPa, and a modulus of rupture of 48.2633 MPa, a thickness of approximately 22 mm was calculated. Values for Modulus of rupture were provided by the manufacturer (Technical Glass Products, 2022).

3.2.3 Top Half of Apparatus

The top half of the apparatus housed the camera, a polarizing film, and held the protruding glass disc that worked as an indenter. The top half of the apparatus can be seen in Figure 17. The four holes were for the alignment pegs attached of the bottom half of the apparatus.

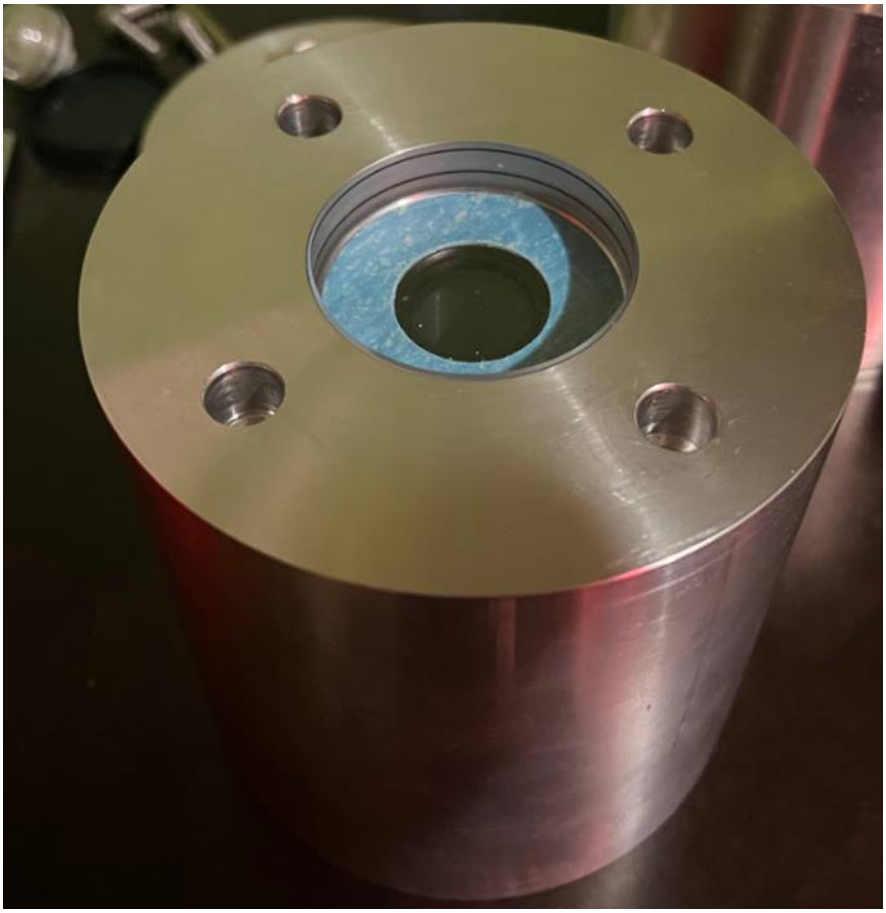

Figure 17 – Top half of the apparatus.

The glass disc fitted into the top half of the apparatus protruded approximately 0.5 mm. This allows, as the load is applied to the apparatus, only the glass disc contacts the ice sample ensuring that all of the force is transferred through the disc into the ice. The protruding glass disc is visible in Figure 18.

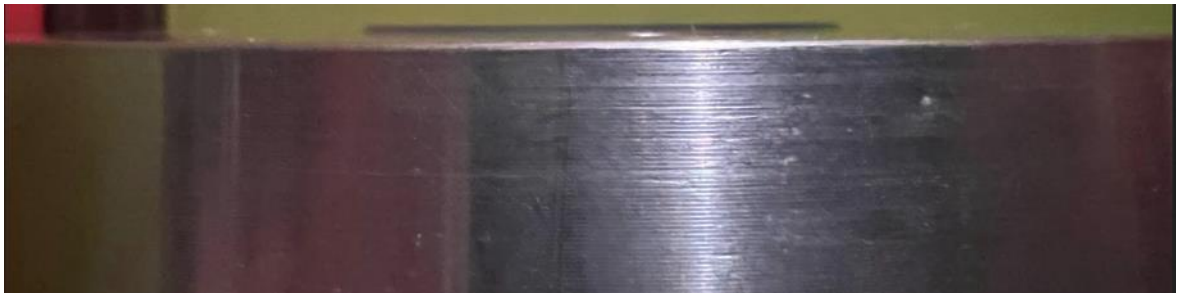

Figure 18 – Protruding glass disc in top half of apparatus.

A borescope camera was purchased to record the sample as it is compact. The maximum diameter of the selected camera was 30 mm – matching the port hole size chosen for the glass. For this purpose, a Teslong 3rd Generation USB Borescope was chosen. This camera had an outer diameter of 12.5 mm, is USB compatible, and can record video resolution up to 1080p. To secure the camera in the 30 mm cavity, two custom-made set screw collars were used. This ensured the camera was in the exact same position during every test. The camera with these collars attached can be seen in Figure 19. These collars were machined out of aluminum.

Figure 19 – Borescope camera with two set screw collars attached.

This camera was then placed into the top section of the apparatus as seen in Figure 20. A polarizing lens was placed on top of the glass disc between the glass and the camera. A small groove was machined into the top of the apparatus that allows for the camera cable to be run out of the apparatus to connect to a computer. A flat top was then placed over the top of the apparatus and secured using socket head cap screws.

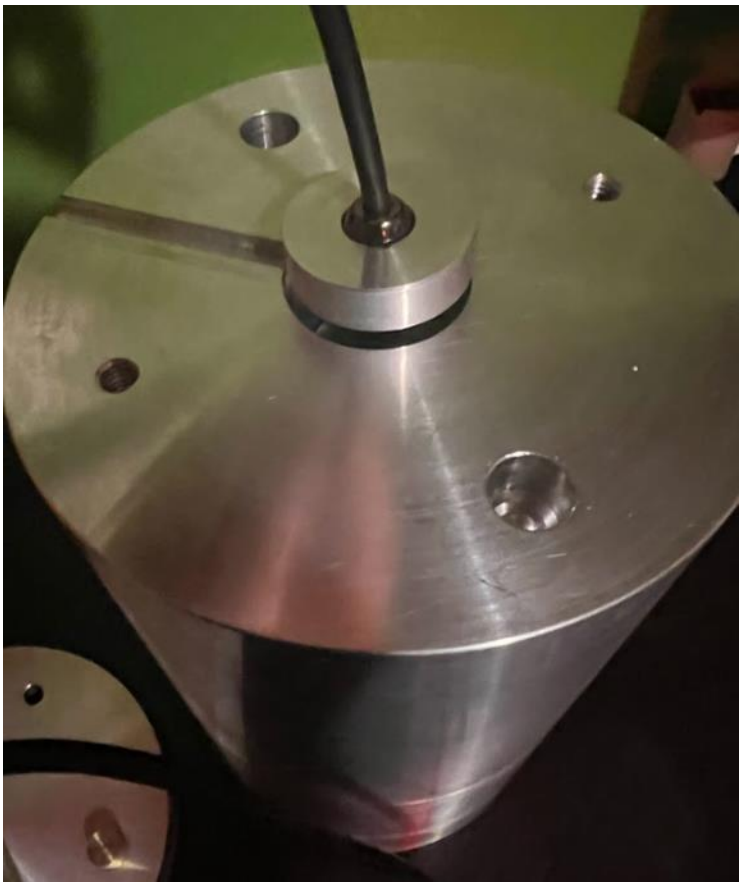

Figure 20 – Inserting the camera into the top half of the apparatus.

3.2.4 Bottom Half of Apparatus

The bottom half of the apparatus holds a countersunk glass disc which seats the ice sample and provided a space for a suitable backlight and a second polarizing film. It also holds the four alignment pins. The bottom half of the apparatus can be seen in Figure 21.

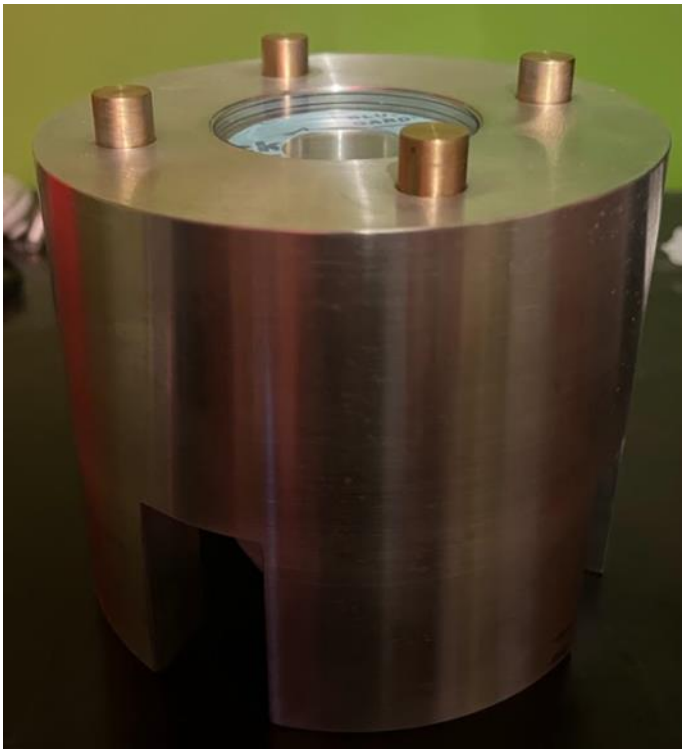

Figure 21 – Bottom half of apparatus.

The glass in the bottom half was countersunk such that there was a 0.8 mm gap between the top surface of the glass and the top surface of the bottom section of the apparatus. Thus, when the two parts were assembled, the top disc which protrudes 0.5 mm would never come into contact with the bottom disc while still compressing any ice which may be seated on top of the bottom disc. Additionally, there was a 1 mm ring along the edge surrounding the bottom disc. This was to ensure that the top disc never came into contact with the metal frame. When the apparatus was connected and pressure was applied, minimal evidence of initial ice extrusion was observed, and the ice sample appeared to be fully contained.

The interior of the bottom section was designed to allow adequate space for a light and the polarizing film, so light could be shined up through the view port and glass disc to illuminate the ice sample. This can be seen in Figure 22. The four rectangular gaps were intended to provide access to the light and polarizing film during testing to allow for adjustment if needed.

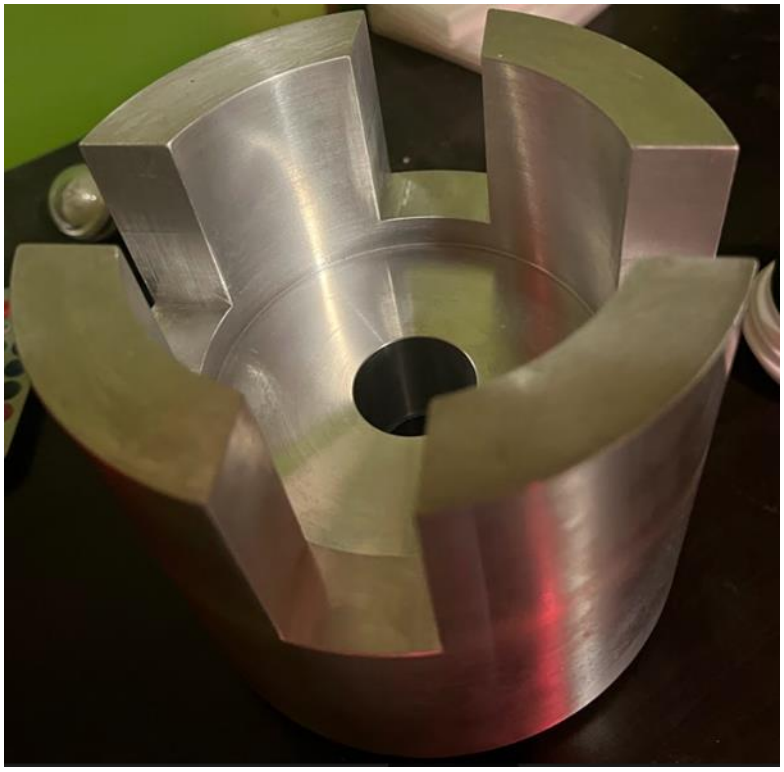

Figure 22 – Bottom half of apparatus flipped to show space for light.

3.2.5 Hydraulic Ram

To apply force to the apparatus and the ice, a hydraulic hand pump was used. The pump used was a Power Fist 4-ton hydraulic Porta-Power Hand Pump. This pump was chosen for its low-profile ram, which was an essential feature to allow all equipment to fit in the deep freezer. This pump was rated to 58.6 MPa (8,500 psi); however, attaching a hose and the ram cut this capacity almost in half, resulting in pressures of around 34.47 MPa (5,000 psi) during testing. This was still sufficient for this experiment as it would apply enough force on the apparatus to place the ice specimen under approximately 5MPa which, according to Clausius-Clapeyron, would cause the melting point to decrease to -0.5 degrees Celsius. This was sufficient to observe pressure melting during the experiments.

3.2.6 Data Acquisition

Both temperature data and pressure data were recorded as part of the experiments.

A load cell was positioned between the apparatus and the hydraulic ram.

The load cell was wired to the data acquisition system and recorded data every 20 seconds for the duration of the test. This is shown in Figure 23, which shows the positioning of the load cell. Figure 24, shows the data acquisition system which is set to run using the software Labview.

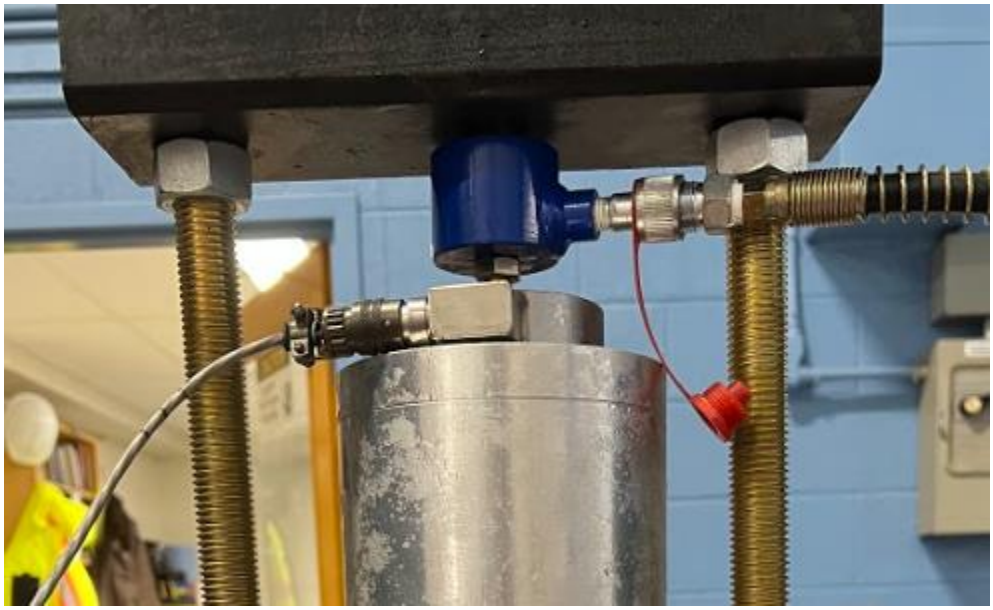

Figure 23 – Load cell positioning.

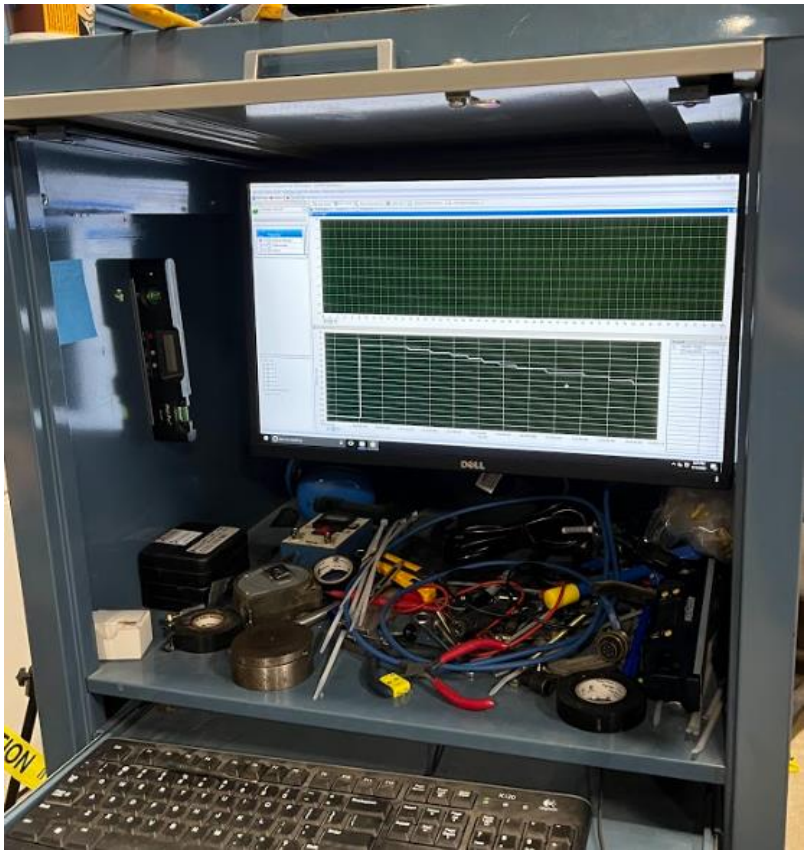

Figure 24 – Labview of Pressure data.

To record temperature data, small holes were drilled into both the top and bottom halves of the apparatus. These holes were drilled as close as possible to the glass indenter and as deep as possible without breaking into the interior surface. This allows temperature sensors to be placed as close as possible to the ice sample without damaging the integrity of the apparatus. Temperature probes were inserted into both holes, as well as in the freezer and outside in the lab. These probes were fed back to an OM-HL-EH-TC data logger, which logged the temperature data. This logger can be seen below in Figure 25.

Figure 25 – OM-HL-EH-TC temperature data logger.

3.2.7 Self-Reaction Frame

To provide a reaction structure to react force onto the apparatus and the ice without damaging the deep freezer, a self-reacting frame was designed. This frame consisted of two square steel beams connected using two 1-inch threaded rods. Using a target pressure of 15 MPa and a factor of safety of 2, simple beam calculation was conducted to determine the thickness of the hollow square steel beams. This resulted in ¼" thick, 4" x 4" low-carbon rectangular steel tube being selected. Rods were chosen simply based on tensile strength. By using threaded rods and hex nuts, the frame could be adjusted as needed. This frame with the apparatus mounted in it can be seen in Figure 26.

Figure 26 – Apparatus in self-reaction frame.

3.2.8 Freezer Temperature Controller

To control the temperature of the ice, an Inkbird temperature controller was used to maintain the deep freezer temperature at a chosen control point. This was accomplished by turning the freezer on or off depending on the temperature to help keep the temperature at a certain point. However, this controller had an offset of 0.3 degrees, meaning it only activated and deactivated when the temperature was +/- 0.3 degrees Celsius from the set point. For example, if the set point was 0 degrees Celsius, the freezer would turn off until it warmed up to 0.3 degrees, at which point it would turn back on until it hit -0.3 degrees. This meant that there was a slight fluctuation in freezer temperature which needed to be worked around. Ultimately, it was discovered that the apparatus would hit a temperature equilibrium, in which it would maintain a temperature despite the

fluctuating freezer temperature. This allowed that the temperature of the apparatus, and thus the ice, to be controlled. Figure 27 shows the temperature controller. The top number is the current temperature while the bottom is the set point.

Figure 27 – Inkbird temperature controller.

3.3 Water Preparation Procedure

Three processes were conducted in order to consistently prepare the water used for making the ice samples. These processes were water distillation, water deionization, and water deaeration.

Memorial University of Newfoundland's Thermal lab has a distillation system which was used to produce distilled water from tap water. This distilled water was then stored in a large glass container, seen below in Figure 28.

Figure 28 – Water distillation system.

This container was connected via a hose to the deionizer system. To begin the deionization process, once the 'operate' light turns on, the 'reset' switch must be turned on. The two valves in the connecting hose must then be opened, at which point the power button could be pressed. On the right side of the deionizer, the green valve is then opened, to allow the deionizer system to store the water after deionization. The deionization system described above is seen in Figure 29.

Figure 29 – Water deionization system.

Using the distilled and deionized water, the deaeration process was then started. Water was pulled into the deaerator, pictured below in Figure 30, using a vacuum.

Figure 30 – Water deaeration system.

For this part of the process, the isolation valve must be closed, and the gas ballast valve turned to the specified point to begin this process. Once this was done, the switching valve must be closed and then the pump can be powered on. The switching valve must then be opened, allowing the water to flow into the chamber. Once the water reaches the desired level marked on the chamber, the valves were closed, and the pump was turned off. The ballast valve was then closed to create a vacuum. The impeller was turned on, forcing the air out of the water and out of the system via the vacuum pump. Once there were no noticeable bubbles in the water, the system was shut down by closing the isolation valve and opening the gas ballast valve. The chamber was then brought to atmospheric pressure using the switching valve. This water was then drained from the deaerator and stored in a sealed container with as little air present as possible.

3.4 Ice Specimen Preparation

To prepare the ice specimen, the distilled, deionized, and deaerated water was placed in the testing area on the bottom half of the apparatus using a syringe. Pure water was used in order to ensure clear ice to improve visibility of the ice during testing. The entire area was filled – creating a dome of water due to the surface tension. This was then carefully placed in a freezer on a flat surface to ensure that the water is level and did not flow to one side prior to freezing. After 24 hours, the apparatus was removed. Generally, the ice at this stage was not flat, often being higher near the center of the sample. Using the flat side of a polished aluminum cylinder, the surface of the ice was melted in order to flatten it. The excess water was wiped off using a cloth, and the sample was placed back in the freezer for 15 minutes to refreeze any remaining water. At this point, the sample was ready for testing.

A microtome was considered to prepare the sample; however, this was not practical as the sample needed to be less than a millimeter thick. Thus, installing the sample after use of the microtome would be challenging. Additionally, the use of in-situ freezing allowed for a consistent thickness between samples in different tests which was important as high-precision was needed to ensure the ice was properly compressed.

3.5 Testing Procedure

Both halves of the testing apparatus, as well as the self-reacting frame, were stored in the freezer overnight such that they were all -15 degrees Celsius. The bottom half of the apparatus containing the ice sample was then taken out of the freezer. If the ice sample was not roughly flush with the surface of the apparatus, a polished aluminum cylinder was used to quickly melt the top surface of the ice and a cloth was used to remove any water. The apparatus was then placed back in the freezer to refreeze any remaining moisture.

Once the sample was flattened and chilled to the target temperature, both halves of the apparatus were removed from the freezer using gloves. The surface of the indenter was scrubbed with a cloth to remove any frozen condensation. This was important because condensation would block the camera's view of the ice if not removed. Next, the two parts were quickly connected. Delaying this would also result in condensation forming on the glass which would obscure the camera's view of the ice sample.

The deep freezer was opened to allow access to the self-reacting frame, which was already placed upright in the deep freezer. The LED light with the installed polarizer was placed, centered, on the plate where the apparatus was to be placed. The apparatus was then placed on top of the light with the light cable running out through one of the access holes in the bottom section of the apparatus. The load cell was then placed on top of the apparatus, and the hydraulic ram was positioned on top of the load cell. The top beam of the self-reacting frame was then adjusted once all components were mounted within it. Finally, the temperature probe was inserted into each of the mounting holes in the apparatus, one in the freezer, and one outside the freezer to capture the lab temperature. The freezer was then closed.

The light was then turned on and the video recording was started. The temperature logger and pressure data acquisition were then started. To synchronize the data, the light was turned on and off, which was visible on the video and recorded as a voltage spike by the data acquisition software recording the pressure. The set point of the freezer was changed as needed such that the ice would hit the final temperature as per the set point chosen for each experiment.

To start the loading process, the hydraulic pump was used to increase the pressure until the gauge reads 5,000 psi. At the start, the pressure bled off relatively quickly, so it was monitored and

reapplied using the jack for the first 15 to 30 minutes. After that, everything was left for approximately 24 hours.

After 24 hours, the pressure was then released and the light was then turned off. The video recording was stopped, and all data acquisition and logging was halted. The temperature logger connected to a computer to offload the data into an excel spreadsheet. The pressure data was offloaded from the data acquisition computer onto a USB drive and then onto a computer for analysis. The apparatus was removed from the deep freezer and disconnected. Both parts of the test apparatus were wiped clean, and any residual ice was removed. Then, the apparatus was placed back into the freezer in preparation for the next test, and distilled, deaerated water was placed into the bottom section of the apparatus to make another ice sample. The hydraulic ram and LED light were then removed from the deep freezer and stored while preparing for the next test.

This process was repeated until all test conditions included in the test matrix had been tested.

Chapter 4: Experimental Results

4.1 Overview

A total of fourteen (14) tests were completed as a part of this research program. There were five types of tests, each repeated between two and five times. The goal of these experiments was to observe various processes that work to develop the grain structure of the ice. The main factors altered in these tests are the initial temperature and final temperature – although there was some variation in test length, initial pressure, and final pressure. Tests 1 – 5 consisted of heating a specimen up to its melting point while it was under pressure. Tests 6 – 7 heated the specimen to -2°C under pressure. Tests 8 and 12 were a base case, heating the specimen to its melting point under no pressure. Tests 9 -11 were tests in which the temperature was maintained at melting point under pressure. Tests 13 – 14 were cold tests in which the temperature was lowered under pressure. The variation in testing length was due to lab availability, as not all tests could be started and stopped at the same time of day. This is ultimately inconsequential, as the processes to be observed would occur based on temperature and pressure conditions, and the variation in time was not

significant enough to affect these processes. The main concern was that each test had enough time for all processes to occur, and approximately 20 hours was determined to be more than sufficient. All testing conditions are recorded in the test matrix seen in Table 1.

Table 1 – Test Matrix

Test Number	Time (hours)	Initial Temperature (°C)	Final Temperature (°C)	Initial Pressure (MPa)	Final Pressure (MPa)
1	22.7	-6.1	0.4	6.2	5.2
2	26.1	-11	0	6.4	5.6
3	26.3	-9.3	-0.1	5.5	4.7
4	22.2	-11.8	0	4.6	2
5	19.2	-9.3	-0.1	6.9	5.4
6	26.2	-13.7	-2	6.3	5
7	23.9	-13.7	-2	6.5	5
8	25.7	-13.6	0	0	0
9	22	0	0	6.7	6.2
10	23.4	-0.8	0	6.7	6.2
11	25.5	0	0	7.6	6.5
12	23.9	-14.5	0.3	0	0
13	24.9	-10.4	-18.4	5.8	5
14	24	-10.4	-18.4	5.8	5

All test data was recorded using instrumentation. This included temperature probes for the temperature, and a load cell for the pressure. These tests were video recorded using a borescope camera, which allowed for study of the evolution of the ice specimen when exposed to the various conditions.

4.2 Base Case

The following details Test 8, which is the base case. Detailed screenshots of this test can be viewed in APPENDIX C. In this experiment, no pressure was applied, and the specimen was allowed to warm up from -13.6°C to 0°C while being recorded and backlit by a polarized light. This allows

for the observation of any processes that occur under no pressure while the ice specimen was warming.

While no pressure was applied using the hydraulic hand pump, the weight of the top half of the apparatus did apply a small amount of pressure to the ice specimen. This ranged from 0.09 MPa to 0.16 MPa, influenced by noise from the sensor, and can be seen below in Figure 31.

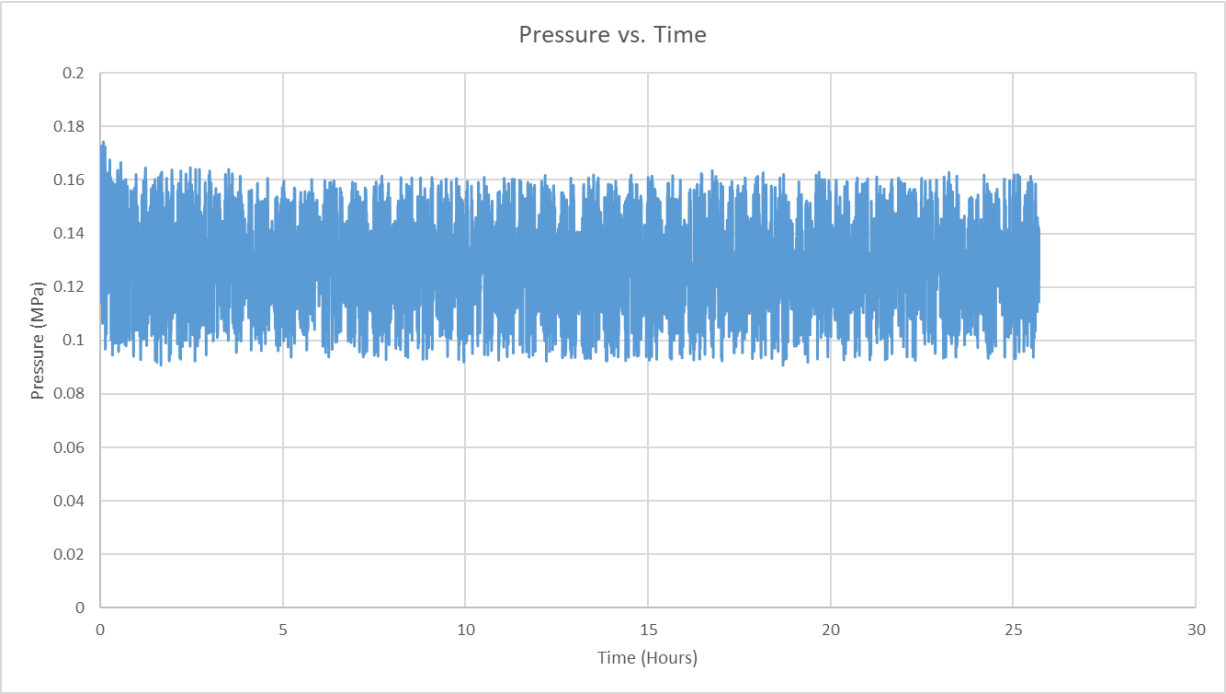

Figure 31 – Pressure curve for Test 8 – Base case.

The temperature curve for Test 8 can be seen in Figure 32. In this experiment, the temperature began at -13.6°C and rose to 0°C over 11 hours. At this point, the temperature sat at 0°C for another 14 hours until the experiment ended at 25 hours.

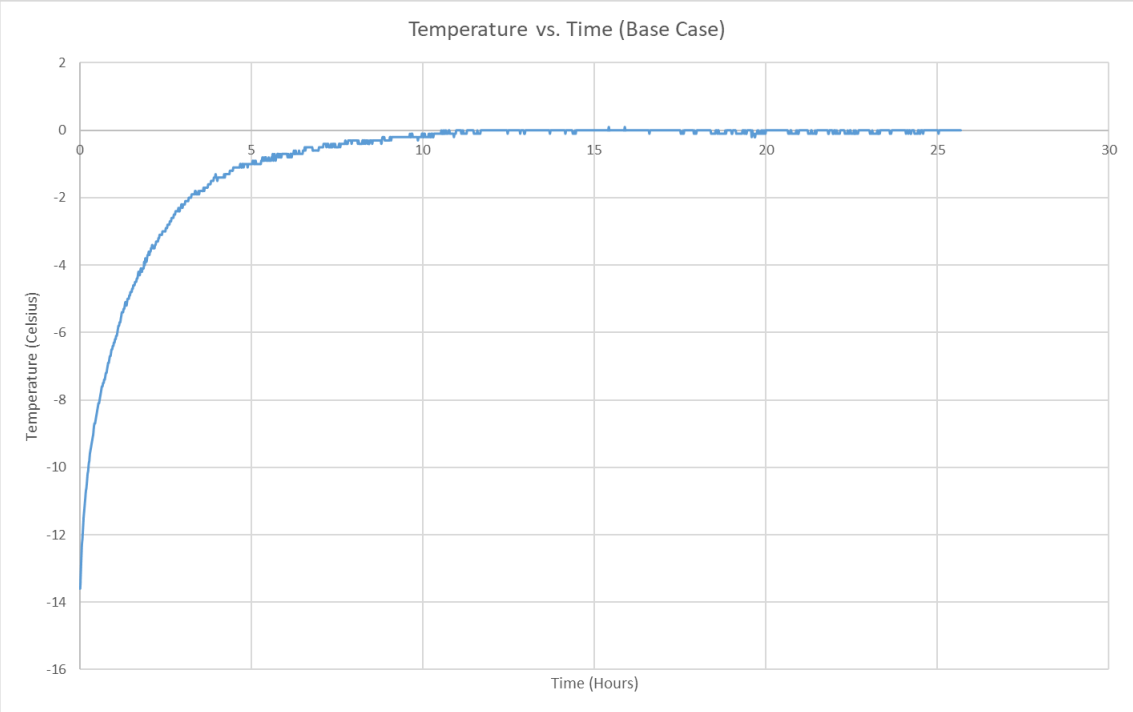

Figure 32 – Temperature curve for Test 8 – Base Case.

The initial state of the ice specimen, backlit by polarized light, can be seen in Figure 33 (a). The temperature was -13.6°C. Many bubbles were present throughout the ice specimen. There was damage done to the upper right corner of the ice specimen – caused by the connection of the top and bottom parts of the apparatus. This indicated that this part of the ice contained a bump and was therefore an area of pressure concentration. Some minor cracking was seen in this area.

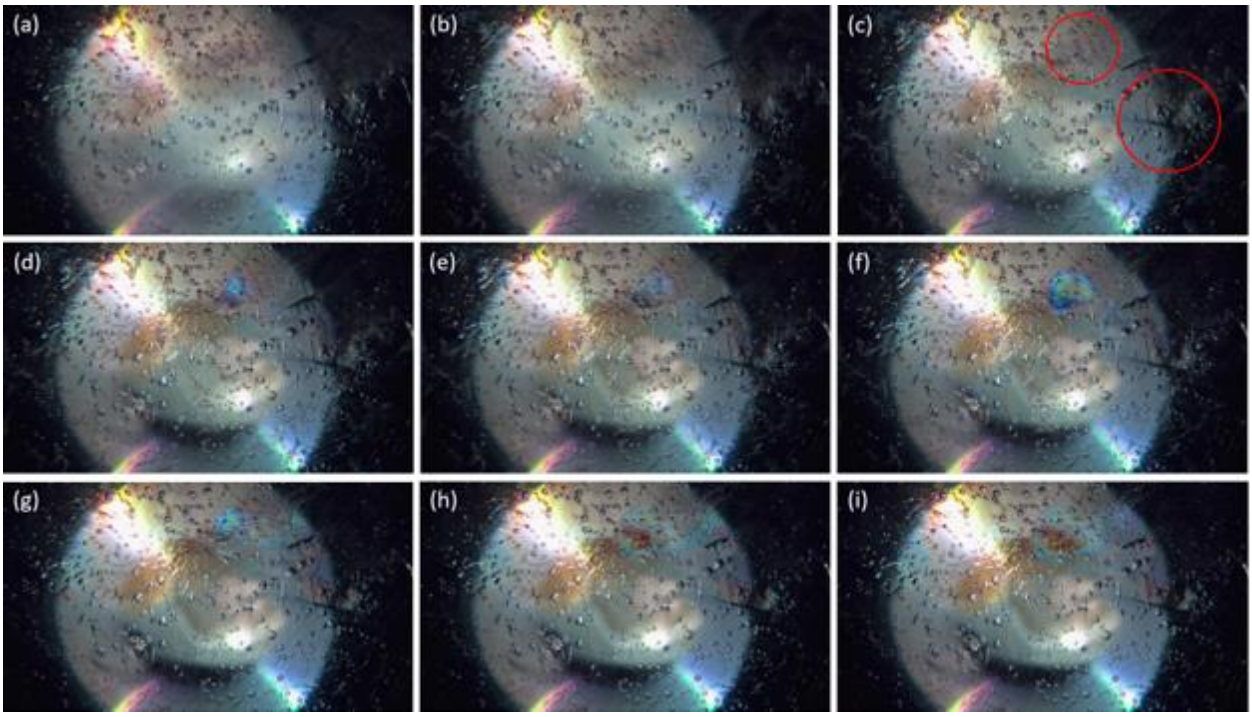

Figure 33 – Overview of Test 8 – Base Case: (a) initial state of sample, (b) 1.5 hours, (c) 4 hours w/ crack formation and discoloration, (d) 6 hours, (e) 8 hours, (f) 10 hours, (g) 15 hours, (h) 20 hours, (i) 25 hours and 42 minutes.

After 1 hour and 30 minutes, the ice temperature had risen to -4.8°C, see Figure 33 (b). At this time, frost began to form on the surface of the glass disc and was seen on the edges of the observable area. Additionally, the ice surrounding the damaged area was being slowly pushed away from the pressure concentration.

After 4 hours, the temperature of the ice specimen had risen to -1.4°C. The ice in the upper right corner continued to slowly drift away from the pressure concentration. This created a new crack in the ice which is circled on the right in Figure 33 (c). Furthermore, discoloration began to form, which is indicated by the left circle in Figure 33 (c).

After 6 hours, the temperature had risen to -0.7°C. The discoloration was now much more apparent, and more discoloration began to form around the tip of the upper fracture. The ice continued to be pushed downwards in the area of the pressure concentration, as shown in Figure 33 (d).

At the 8-hour mark of the experiment, the temperature reached -0.3°C. Discoloration began to flow in from the right side near the fractures in a leftward direction. The discoloration closer to the center of the sample continued to grow and change in color. A small portion of the ice below the pressure concentration continued to extrude downwards away from the pressure concentration. This is shown in Figure 33 (e).

At the 10-hour mark, the temperature rose to -0.1°C. The specimen at this time can be seen in Figure 33 (f). Of note, the discoloration near the upper center of the specimen grew and continued to change color from blue to a greenish/brown color. The extrusion away from the pressure concentration in the upper right slowed and stopped.

After 15 hours, the temperature was consistently at 0°C. The discoloration near the upper center of the specimen appeared to shrink in size. The discoloration on the right border of the specimen began to flow in towards the center – likely being melt from the bottom surface of the ice specimen. This can be seen in Figure 33 (g).

After 20 hours, the ice specimen remained at 0°C. The melt continued to push its way to the left, hitting the area of discoloration indicated in Figure 33 (c). At this point, the movement of the melt accelerated, creating a large, brown colored area. This suggests that the original area of discoloration was an air pocket – likely influenced by the small stress applied to the ice as a result of the weight of the apparatus. This is shown in Figure 33 (h).

Finally, after 25 hours and 42 minutes, with the specimen at 0°C, the test is concluded. The specimen at the end of the test can be seen in Figure 33 (i). The melt under the ice continued to push its way underneath the ice, creating discoloration in these areas. No crack healing was evident throughout this test. There was also no change in any of the bubbles from the start to the end of the test. No grains have formed.

Notable features observed in the Base Case are summarized below:

- Extrusion at a slow rate pushes the ice in a single direction for the first 10 hours of the test, this is a result of the weight of the apparatus on the ice sample.
- All cracking is caused by an uneven ice surface and the weight of the apparatus.
- The discoloration present throughout the test indicates the growing presence of fluid within the ice sample.
- The ice begins to melt from the edges of the sample inwards, followed by the top and bottom surfaces of the ice which are in contact with the glass.

4.3 Representative Tests

This section details four tests, each representing a type of test which was repeated two or three times each.

4.3.1 Heating to Melting Point at Constant Pressure

The following details Test 1. Detailed screenshots of this test are available in APPENDIX D. This test slowly heated the ice sample from -6.1°C to slightly above 0°C, where it was held at a constant temperature of 0°C and allowed to undergo bulk melting. This section reports on the processes and features observed during this test in a chronological order.

The pressure curve of this test can be seen below in Figure 34. The initial application of pressure reached 6.2MPa; however, this bled off over time. In this test, pressure was reapplied twice – once at three hours in and the second time at six hours in. After this, the pressure bled off until it reached a constant 5.2MPa. According to the Clausius-Clapeyron equation, this should result in a melting point of -0.4°C.

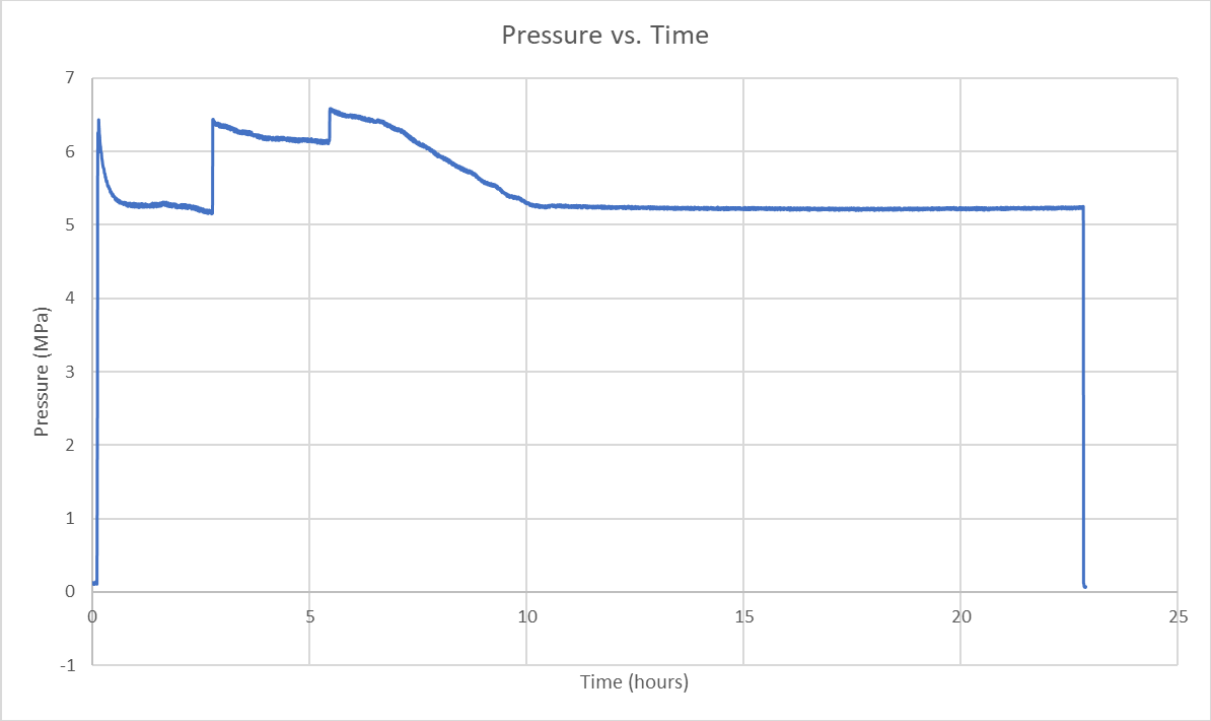

Figure 34 – Pressure (MPa) vs. Time (Hours) for Test 1

The temperature curve for Test 1 can be seen in Figure 35. The initial temperature was -6.1°C. This quickly rose until it hit 0°C six hours into the test. While the curve shows a further increase in temperature to 0.4°C, this was for the metal apparatus. The ice remained at 0°C until bulk melting occurred, and it turned into water.

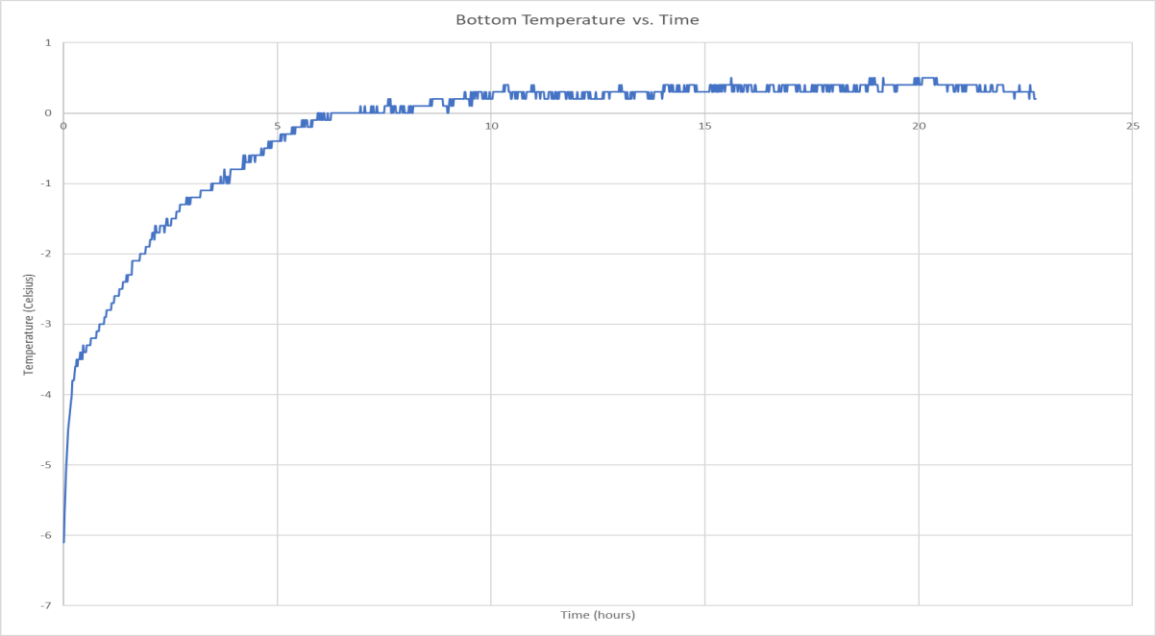

Figure 35 – Temperature (°C) vs. Time (Hours) for Test1

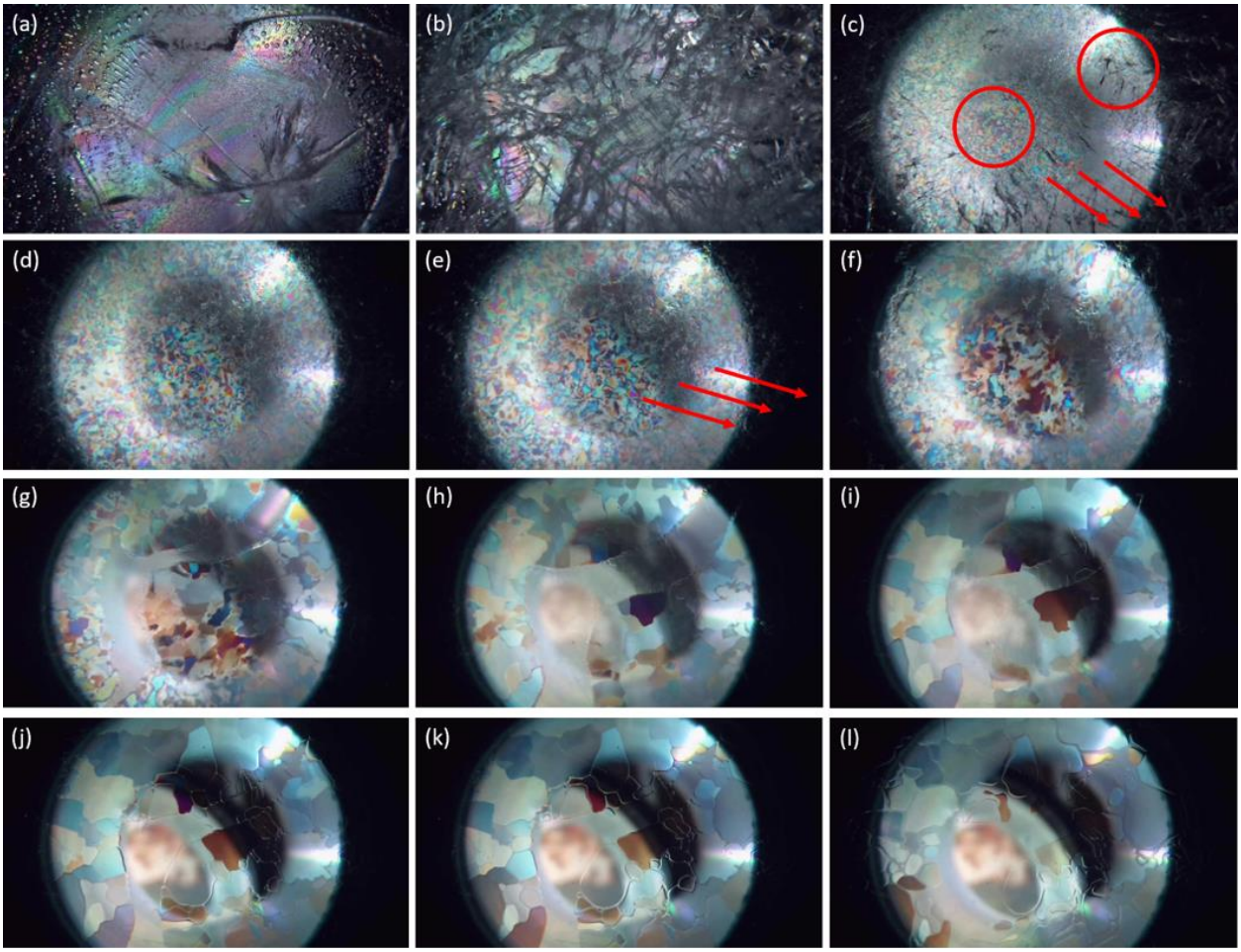

Figure 36 – Overview for Test 1: (a) initial ice sample, (b) initial fracture, (c) 1 hour w/ extrusion, grain nucleation, and crack healing, (d) 6 hours, (e) 7 hours w/ extrusion, (f) 8 hours, (g) 9 hours w/ melt, (h) 9 hours and 40 minutes, (i) 10 hours and 20 minutes w/ refreezing, (j) 11 hours and 48 minutes w/ grain boundary melting, (k) 16 hours and 28 minutes w/ bulk melting.

The initial ice sample, backlit by a polarized light, can be seen in Figure 36 (a). This sample was -6.1°C and had no pressure applied. As seen, there were a few cracks pre-existing in the ice specimen. This was caused by the connection of the top and bottom parts of the apparatus as the ice came into contact with the glass disc. Of note, the fracture in the bottom right corner was a result of an uneven ice surface and would briefly concentrate the applied pressure upon initial application. Various air bubbles were also present throughout the ice specimen.

Once the initial pressure is applied, fracture occurred. Figure 36 (b) shows the initial fracturing of the specimen.

In this test, the entire specimen is compressed and there was a myriad of micro-fractures. As noted, the bottom right featured a high concentration of fractures due to the bump that was present on the surface of the specimen at this location creating a pressure concentration. Some of the bubbles also disappeared as the air was able to escape through the fractures.

Over the next hour, the ice underwent an extrusion event due to the initial application of pressure and the significant fracturing that resulted. In this case, the ice slowly creeped down and to the right – visualized by the arrows in Figure 36 (c). Following application of pressure, grains started to form via dynamic recrystallization. The left circle in Figure 36 (c) shows what these developing grains looked like after 1 hour. Also evident was crack healing, seen in the right circle in Figure 36 (c). Many of the fractures have closed, which allowed for a clearer visualization of the ice. The temperature was -2.9°C.

The above processes continued until the six-hour mark, pictured in Figure 36 (d). At three hours and six hours, when the pressure was slightly increased, the rate of extrusion slightly accelerated in the same direction as previously indicated. The grain structure continuously changed, as dynamic recrystallization was constantly occurring and grains were growing, shrinking, and overlapping with one another. As seen, over time, the grains became slightly larger and were more distinguishable. At this point in the test, the apparatus temperature had hit 0°C with the ice shortly to follow.

Once the ice hit 0°C and the melting process began, there was a second extrusion event – this time driven by melting. This is illustrated in Figure 36 (e). This instance of extrusion was much faster compared to the previous event which was driven by fracture. Additionally, this event was in a slightly different direction compared to the fracture extrusion event – pulling more to the right and less downward in this case.

Once the ice began to melt, larger grains quickly began to form as seen in Figure 36 (f). However, these grains did not persist, and were quickly destroyed by the rapid dynamic recrystallization and the constantly growing newer grains. At this point, due to extrusion and bulk melting, the ice began to break apart. This was seen in the top left corner of the ice specimen.

Over the next hour, due to the extrusion and bulk melting processes, a large fracture formed in the sample as the two sides of the ice were pulled apart. This is clearly visible in Figure 36 (g). This fracture was filled with water. Also of note was the developing grain structure. At this point, the grain boundaries were easily distinguishable. There was a slight discoloration at some grain boundaries – suggesting overlapping grains in these areas. Each grain generally consisted of one color and the shape of the grains could be described as 'smoother' when compared to the smaller, irregularly shaped grains that formed at the beginning of the test. Additionally, many of these grains would persist throughout the remainder of the test – some growing in size and consuming their neighbouring grains. As the bulk melting process continued, the thickness of the ice sample decreased.

The fracture continued to widen over the next forty minutes and can be seen in Figure 36 (h). The grains became even more distinguishable – likely due to the thinning of the sample due to bulk melting.

Over the next forty minutes, the fracture began to close due to refreezing. The forming ice crystals can be seen in Figure 36 (i). The grains continued to grow, consuming their surrounding grains. This left fewer, larger grains when compared to earlier in the test. Again, slight discoloration was seen at some grain boundaries. At this point, there was no more extrusion.

After roughly ten and a half hours, the specimen demonstrated little change in its grain structure and was a mixture of ice and water. The grains which did remain; however, began to melt. Their grain boundaries appeared transparent and wet, which is seen in Figure 36 (j).

Over the next five hours, the specimen underwent bulk melting. This started from the edges of the grain boundaries. The grains themselves became individual pieces of ice floating in a pool of water. Some drifted to the left in the water. They continued thinning while melting from the edges inward towards their center, shrinking in size. Some grains shrank to the point where they completely melted, while others remained larger until they thinned and melted in that way. This process can be seen in Figure 36 (k). Following this, no ice remained and there were no instances of refreezing – so the test was concluded. The melting which is present in this test is distinct from thermal melting, in that the melt began at the grain boundaries rather than from the edges of the ice sample.

Notable features observed when heating the ice to melting point are summarized below:

- Fracture occurs in a single instance after pressure application on cold ice, and a dense network of micro-cracking is formed due to an uneven ice surface causing a pressure concentration.
- Crack healing occurs slowly over the course of 5 hours and is caused by extrusion.
- Extrusion starts in response to pressure application and slows over time. As additional pressure is applied, the extrusion accelerates. Bulk pressure melting causes additional acceleration of extrusion later in the experiment.
- Dynamic recrystallization occurs throughout the experiment until extrusion stops, which coincides with the beginning of bulk pressure melting.

- Grain boundary migration begins once the ice approaches melting point, and becomes increasingly dominant as extrusion, and therefore grain nucleation, slows and stops.
- Bulk pressure melting begins at the grain boundaries which appear transparent.

4.3.2 Heating to -2°C at Constant Pressure

The following details Test 7. Detailed screenshots of this test can be seen in APPENDIX E. Starting at a temperature of -13.7°C, the apparatus was slowly heated to -2°C and held at that temperature for the remainder of the experiment. This section details the observed processes during this test in chronological order.

The pressure curve for this test is seen below in Figure 37. As seen, the pressure was initially brought up to 6.5 MPa, where it bled off to 5 MPa over 3 hours. It continued to bleed off for another 14 hours down to 4.6 MPa, at which point the lab temperature began to influence the pump and the pressure rose to 4.75MPa where it remained for the rest of the experiment. There was no manual reapplication of pressure during this experiment.

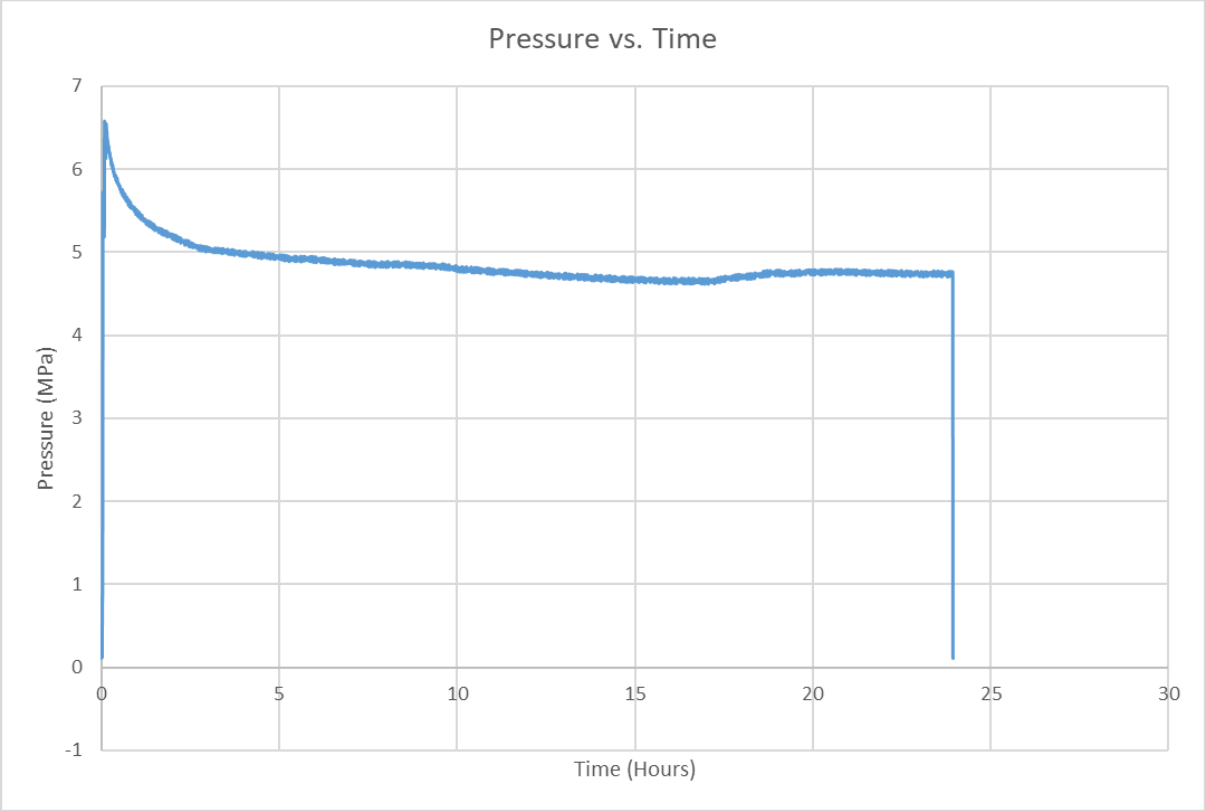

Figure 37 – Pressure curve for Test 7.

The temperature curve for Test 7 is seen in Figure 38. This curve was based off data collected by the temperature probe located in the bottom section of the apparatus – as close to the ice as possible. As seen, the initial temperature was -13.7°C. This quickly rose until the temperature reaches -2°C at the 9-hour mark. At this point, the temperature remained roughly consistent, cycling between -1.9°C and -2°C for the remainder of the experiment.

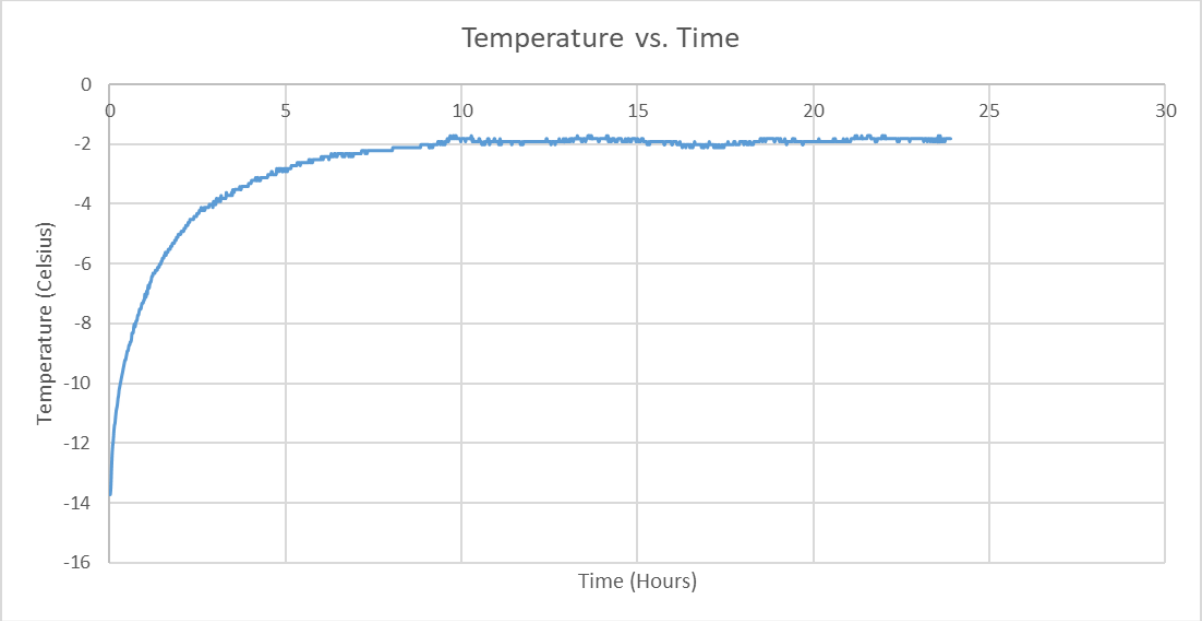

Figure 38 – Temperature curve for Test 7.

The initial ice sample, backlit by a polarized light and prior to the application of pressure, can be seen below in Figure 39 (a). The color seen at the center of the ice specimen was an ice crystal which had formed within the sample during the freezing process. There was a crack present at the top left of the sample. Bubbles were seen along the surface of the ice specimen – a result of the surface flattening process.

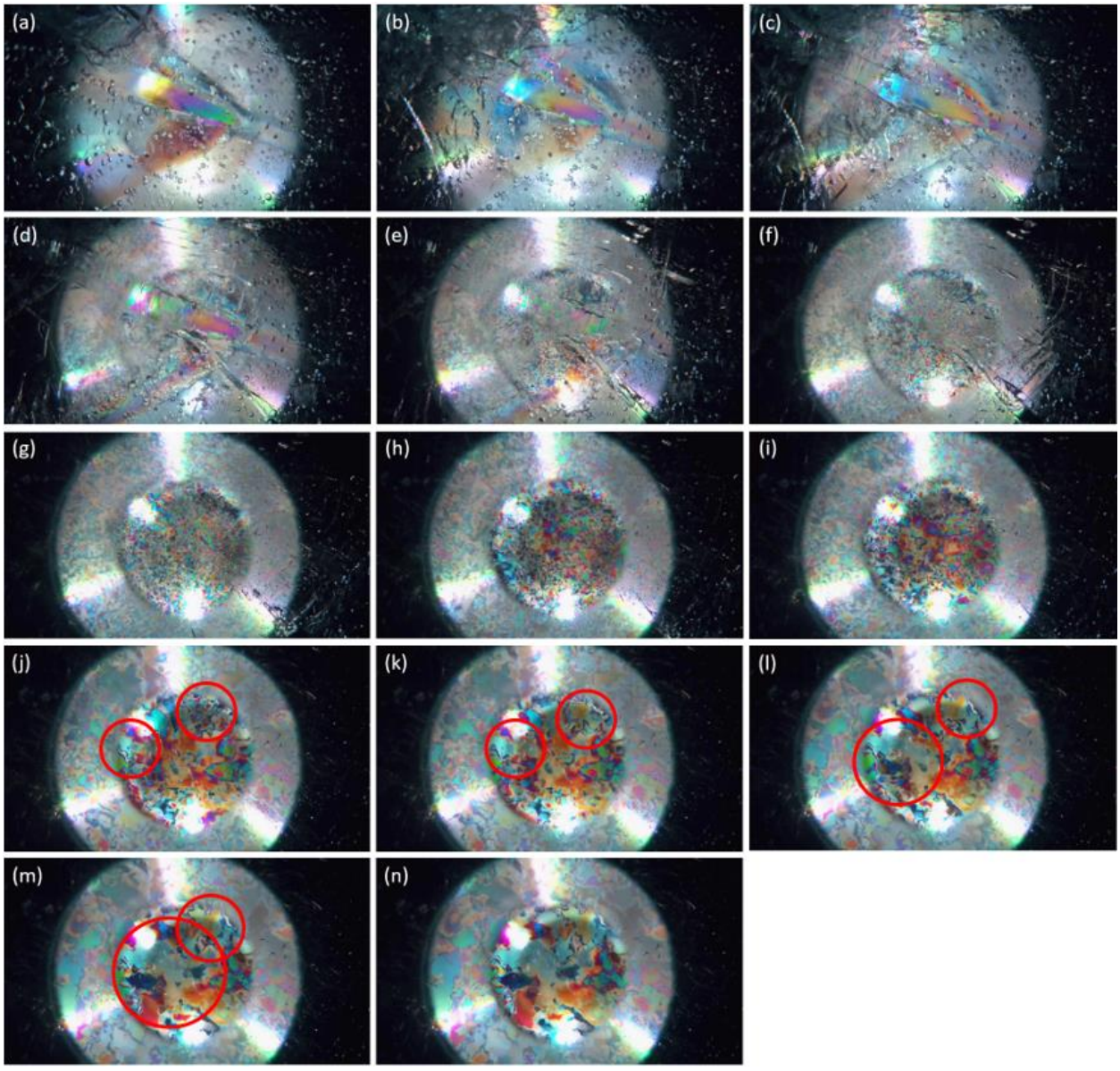

Figure 39 – Overview of Test 7: (a) initial sample, (b)initial fracture, (c) 5 minutes, (d) 20 minutes, (e) 1 hour, (f)2 hours, (g) 4 hours, (h) 6 hours, (i) 8 hours, (j) 15 hours, (k) 17 hours, (l)20 hours, (m) 22 hours, (n) 24 hours.

The initial pressure of 6.5 MPa was applied. This was concentrated in the area of the fracture seen in the initial specimen. This indicated that this area was an elevated bump on the surface of the specimen. The specimen after application of pressure can be seen in Figure 39 (b). Beyond the fractures concentrated around the top left of the specimen, extrusion began – which extruded the specimen to the right.

A visible pressure front was slowly pushed down and to the right, appearing to deform the parts of the ice specimen that were behind it. Figure 39 (c) shows the specimen after 5 minutes of pressure application – at which point the pressure front was visible. On the left behind the front, the ice was significantly fractured. The bubbles in these areas escaped through the many cracks and are no longer visible. There were indications of grains formed due to the stress in these areas. On the right of the specimen which has not been impacted by the pressure front, the ice appeared to be mostly the same as it was initially besides a few, distinct cracks. Bubbles were still clearly visible and there was no indication of developing grains.

After 20 minutes, the pressure front had continued to move along the ice specimen, which can be seen in Figure 39 (d). The cracks behind the wave were beginning to heal, and the initial development of grains due to stress was clearer. Again, as the ice behind the front fractured, the air bubbles were released from the specimen. The ice specimen continued to extrude to the right, and a split formed at the bottom right area, creating two sections of ice which continued extruding at different rates.

After 1 hour, the front has almost crossed the entirety of the observable ice specimen, which can be seen in Figure 39 (e). The area behind the front had tiny, irregular grains formed. The large ice crystal in the center of the specimen had been compressed and was also transforming into these grains. There were no observable bubbles in this area of the ice. The initial fractures in the top left of the ice sample continued to heal as extrusion occurred over time. The crack in the bottom right had become more evident. As noted, the ice to the left of the crack appeared to extrude faster compared to the ice on the right of the crack.

Figure 39 (f) shows the ice specimen 1 hour later, at a temperature of -7°C. The wave of pressure continued to move along the sample, crushing the ice and causing cracking. In these areas, the air

bubbles were released. The bubbles remained on the right side of the specimen. The ice crystal originally located in the center of the specimen was no longer distinguishable. Instead, small grains had formed due to the stress in this area. There was also further evidence of crack healing in the areas behind the pressure front – particularly the cracks in the top left corner, which had nearly 2 hours to heal. The crack in the bottom right continued to widen, as the two sections of ice extruded at different rates.

After 4 hours of pressure application, the wave of pressure had crossed the entirety of the observable ice specimen. Thus, the entirety of the observable specimen was now under stress. The small grains continued to develop, growing slightly larger in size. There was rapid, constant recrystallization occurring – causing grains to grow and overtake existing grains in such a way that any single distinguishable grain did not exist for a large amount of time. The crack in the bottom right corner had begun to close – being forced back together by the extrusion. At this point, there were very few observable bubbles – existing mainly in the lower right corner. This is observable in Figure 39 (g). The temperature at this time was -3.3°C.

After 6 hours of pressure application, the temperature reached -2.5°C, and the grains continued to grow in size and appeared to be larger. The blotchy appearance of these grains indicated significant grain overlapping. Additionally, overlapping grains caused discoloration seen at the boundaries of some grains. The crack in the bottom right had completely closed and was now beginning to heal. The ice specimen continued to extrude towards the right. This can be seen in Figure 39 (h).

After another 2 hours, the grains were now becoming distinguishable – as the rapid recrystallization began to slow down. The temperature at this point was -2.2°C. This can all be seen in Figure 39 (i). While the grains continued to grow in size, there were fewer instances of new

grain growth. This still occurred, however, and new grains tended to overtake and consume any pre-existing grains. These grains remained 'blotchy' and multicolored in appearance.

Recrystallization and grain growth continued over the next 7 hours – resulting in the specimen seen in Figure 39 (j). The temperature from this point onwards fluctuated between -1.9°C to -2°C. At this point, a final instance of significant recrystallization occurred – and there were several new grains which grew and began to dominate the final grain structure. Two of these are indicated by circles in Figure 39 (j) and are tracked for the remainder of the experiment. The left circle demonstrates a light blue grain, which had already had a small amount of growth. The right circle indicates a dark green/blue grain which had just started growing.

After another 2 hours, these grains continued to grow and develop. This can be seen in Figure 39 (k). Here, the left grain was roughly the same size as before, although it had begun growing towards the right into the larger orange grain. The right grain was now much more distinguishable and had consumed many of the smaller grains in this area. The specimen continued to extrude to the right.

After another 3 hours, the left grain exploded in growth and completely consumed the central orange grain. The right grain also continued to grow, developing more distinguishable grain boundaries. The off-color at the grain boundaries was an indication of two overlapping grain boundaries. The discoloration within the grains suggested smaller grains overlapping within the larger grain. This can be seen in Figure 39 (l).

After another 2 hours, the left grain continued to grow, becoming the largest visible grain in the sample. Some grain boundaries were very distinct – as seen with those on the left side of the sample. However, others do not have a distinguishable boundary – instead transitioning into

another grain such as the large orange grain bordering the left grain to its right. The right grain continued to grow, overtaking grains in its surroundings. This can be seen in Figure 39 (m).

The final grain structure can be seen in Figure 39 (n). In this case, because the temperature remained at -2°C, bulk melting did not occur. The existing grains continued to grow larger, with many grains overlapping and creating many instances of multi-colored grains. Extrusion continued in the same direction until the end of the test. All initial cracks have healed significantly, and there were no more instances of air bubbles. At this point, dynamic recrystallization had slowed down. New grains rarely formed – while existing grains continued to grow and consume some of their smaller neighbouring grains. After 24 hours, the test was concluded.

Notable features observed when heating the ice to -2°C are summarized below:

- Fracture occurs in one instance after pressure application. The area impacted by the pressure is visible and slowly moves across the ice over the first few hours of the test.
- In areas impacted by the pressure, dynamic recrystallization and crack healing are present. Areas unaffected by the pressure do not show any microstructural development.
- Extrusion occurs throughout the test but slows considerably near the end.
- Grain nucleation coincides with extrusion and shear, slowing near the end of the test.
- Grain boundary migration begins once the temperature increases to higher than -3°C and becomes increasingly apparent as grain nucleation slows.

4.3.3 Applying Constant Pressure at Melting Point

The following details Test 9. This ice specimen was warmed up over the course of 24 hours without any pressure applied. Starting at a temperature of 0°C, pressure was applied up to 6.8 MPa initially. The temperature was kept constant throughout the experiment. This section reports on the

processes which occurred during this experiment in a chronological order. Refer to APPENDIX F for larger scale screenshots of Test 9.

Below in Figure 40 is the temperature curve for Test 9. Beginning at a temperature of 0°C, the temperature was held roughly constant throughout the experiment. Near the beginning of the experiment, the range was between 0.1°C and -0.1°C, with the most common temperature being 0°C. After 8 hours, the temperature began to occasionally drop as low as -0.2°C, with the most common temperature remaining at 0°C. After 15 hours, the temperature began to drop as low as -0.3°C with the most common temperature being -0.1°C.

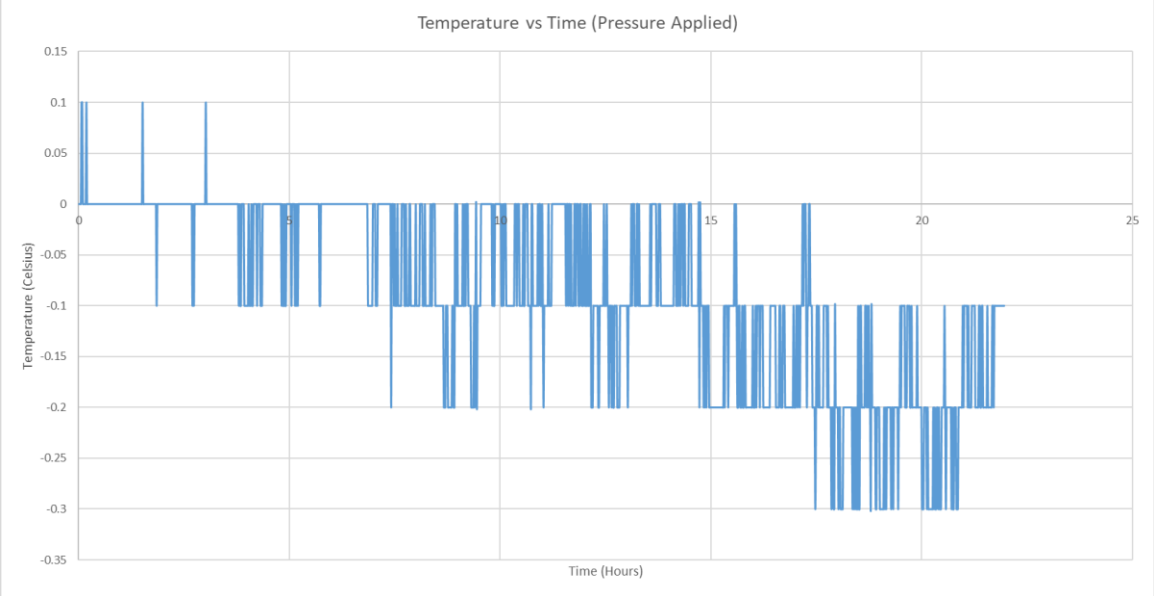

Figure 40 – Temperature curve for Test 9.

The pressure curve for Test 9 can be seen below in Figure 41. At the beginning of the experiment, the pressure was applied up to 6.8MPa. This bled off quickly, stabilizing at around 6.3MPa and never dropping below 6.2MPa. There was no additional pressure application at any point during this test.

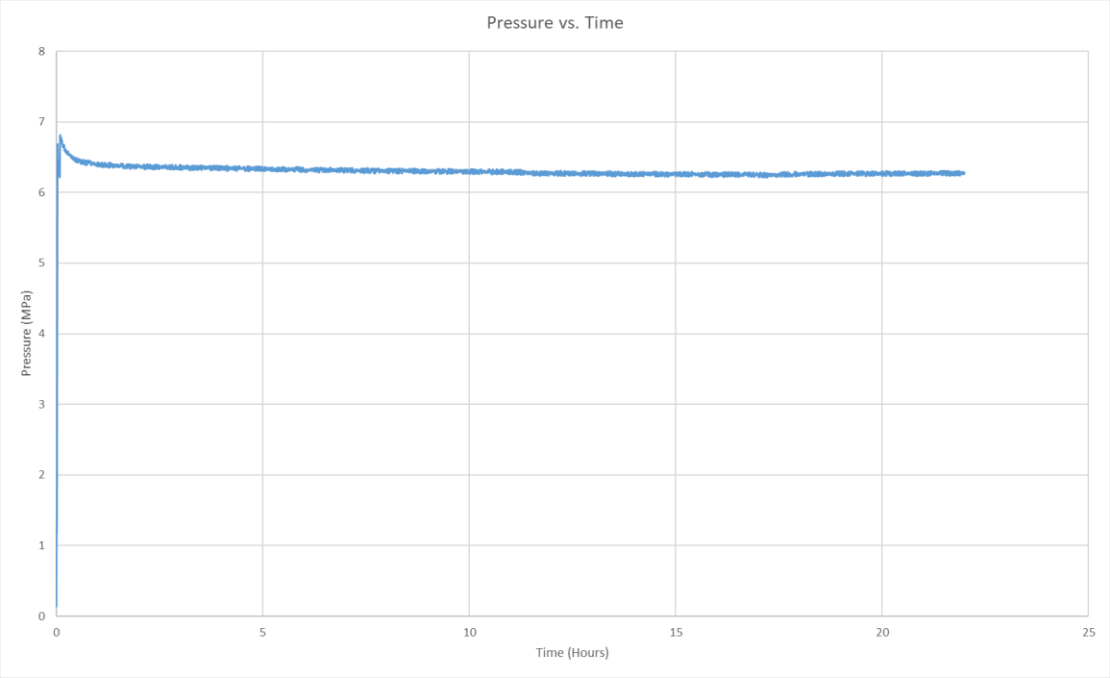

Figure 41 – Pressure curve for Test 9.

The initial state of the ice specimen can be seen in Figure 42 (a). There are many bubbles present along the surface of this specimen. There was a minor crack at the right of the specimen, which resulted from the connection of the top and bottom of the apparatus. The black band near the bottom of the specimen was due to the backlight being off-centre. Of importance, the colored area in the top right was a slight bump containing air and water.

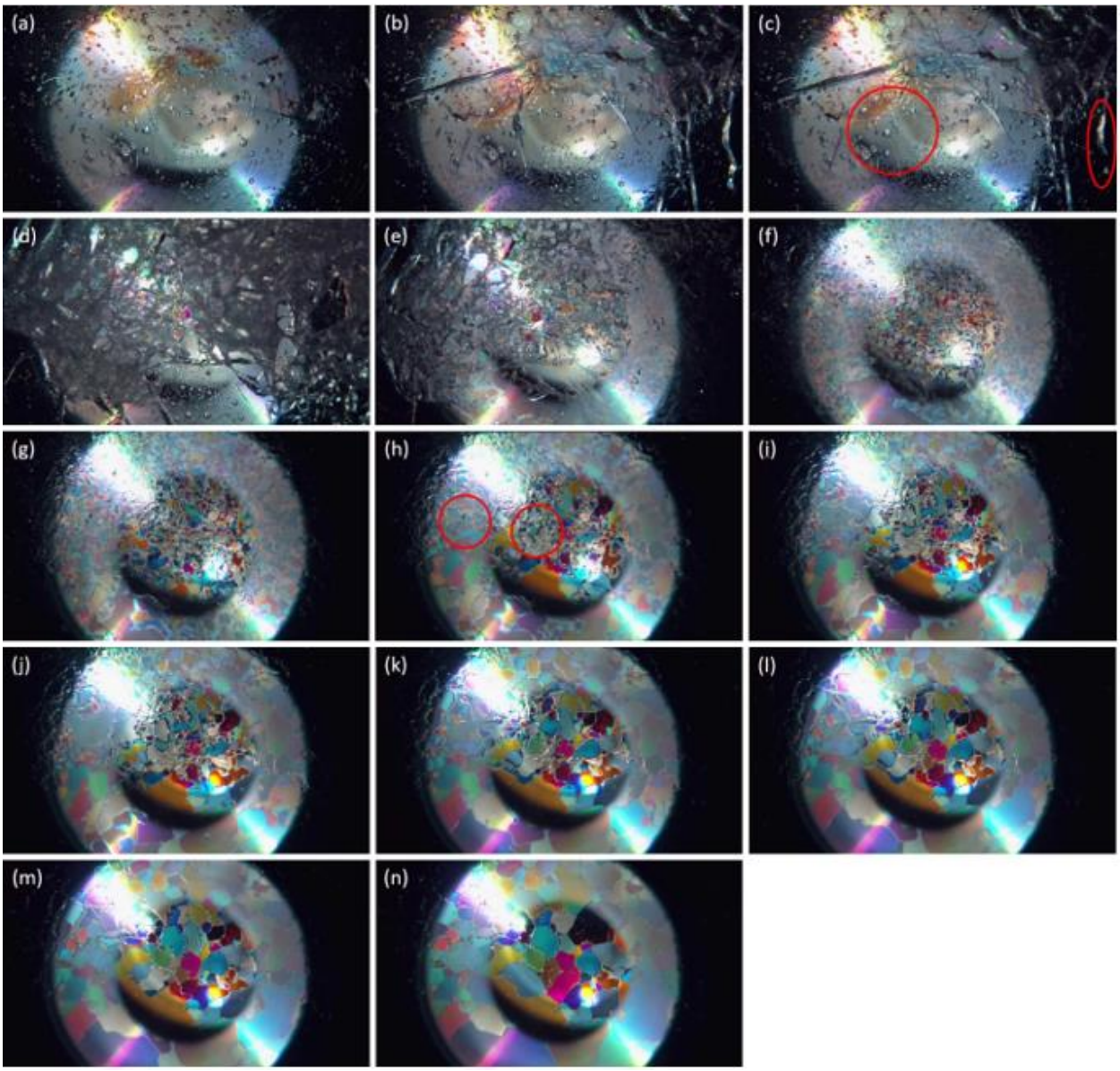

Figure 42 – Overview of Test 9: (a) initial state, (b) initial fracture, (c) rapid crack healing, (d) dense cloud of micro-cracks, (e) extrusion event, (f) 10 minutes, (g) 30 minutes, (h) 1 hour w/ localized pressure melting, (i) 1.5 hours, (j) 2 hours, (k) 5 hours w/ refreezing, (l) 7 hours, (m) 9 hours, (n) 22 hours.

After the application of pressure, the specimen fractured as seen in Figure 42 (b). The fracture was centered around the identified bump, with many cracks in the top right of the specimen and fewer, larger cracks on the left side of the specimen. Liquid water was seen flowing out from this bump, giving the ice near the bottom a watery appearance, and making some of the deeper bubbles more visible. Bubbles surrounding the bump were no longer present.

Over the next 14 seconds, some of the cracks rapidly healed. This is indicated in Figure 42 (c). These cracks closed relatively fast and appeared to do so in a 'fluid-like' manner.

After another minute, the ice sample violently fractured again under the pressure. This caused countless cracks which cover the majority of the ice sample. Many of the existing bubbles can no longer be seen – although some remained near the bottom area of the sample. The color near the center of the sample indicates dynamic recrystallization and the initial formation of grains. All of this is visible in Figure 42 (d).

Over the next minute, rapid extrusion occurred – causing crack healing and the removal of more bubbles. The sample is now much more visible – particularly on the right side. The initial formation of grains was then more easily observed. Also of note are the thin fractures which appeared in the bottom area of the ice sample. These cracks slowly appeared over a minute. Water and air were seen travelling along many of the fractures. All of this can be seen in Figure 42 (e).

At the 10-minute mark of Test 9, there was significant development of the ice specimen's grain structure. Many small sized grains were seen throughout the specimen. Extrusion continued to occur, pulling the ice downwards and to the left. As a result, much of the air was pulled towards the left. As the air was travelling along the cracks, it moved with those cracks due to the ongoing extrusion event. Once those cracks healed, however, the air could no longer travel – and was confined in place within the ice. Thus, bubbles formed on the left side of the specimen. This is seen in Figure 42 (f). Figure 42 (g) shows the sample 30 minutes into the experiment. Here, the rapid dynamic recrystallization and subsequent grain growth was clearly visible. The bottom of the sample appeared to have a greater concentration of large grains when compared to the rest of the sample which has smaller grains. Extrusion continued pulling the ice sample down and to the left.

30 minutes later, at approximately 1 hour into the experiment, there was indication of localized pressure melting. This occurred near the center of the sample as well as surrounding the bubble present on the left side of the sample. These areas are circled in Figure 42 (h).

After an additional 30 minutes, the areas of melt became more visible, as seen in Figure 42 (i). Additionally, many of the grains continued to grow in size and there was less new grain growth. The bubble circled in Figure 42 (h) had become smaller, as the air appeared to dissolve into the water. Again, the grains on the bottom and towards the right side were larger than those on the upper left. It should also be noted that these grains were mostly one solid color – with only some discoloration on grain boundaries. This indicates minimal grain overlap beyond the grain boundaries.

After another 30 minutes, the existing grains continued to grow, and the area of melt no longer expanded. The bubble was now completely dissolved into the water. The extrusion event had stopped. The temperature of the apparatus at this point in time was 0°C. A snapshot of the ice specimen at the 2-hour mark is seen in Figure 42 (j).

Over the next three hours, there was relatively minimal change. The existing grains continued to slowly grow, and there were few instances of new grain growth. Over this time, the areas of melt began to shrink in size as refreezing occurred. The grains surrounding the melt appeared to expand into the melt, and in some cases, there were new ice crystals which formed within the melt. Figure 42 (k) shows a snapshot of the ice specimen at this time.

Over the next 2 hours, the existing grains continued to grow with no new grain growth. The areas of melt continued to shrink, as the surrounding grains grew in size and refreezing continues. At

this point, the previously indicated bubble returned – as the air could no longer exist in the frozen water. This is indicated in Figure 42 (l).

At the 9-hour mark of the experiment, refreezing was completed. In the areas in which there was melt present, there were now bubbles which were previously dissolved in the water and have been ejected once the water refroze. Other than this, the existing grains continued to grow and change in shape. All of this can be seen in Figure 42 (m).

For the remainder of Test 9, there was continued grain growth and grain boundary migration. These changes occurred continuously, and slowly, throughout the remaining 13 hours of the experiment. The final ice specimen can be seen in Figure 42 (n). As can be seen, there were a few different grains which grew and consumed a neighbouring grain. For example, the dark blue grain in the top right, the dark pink grain directly in the center, and the light blue grain on the left above the large orange grain. Compared to Figure 42 (m), all of these grains have consumed a neighbouring grain and grew larger. This ultimately leaves fewer, larger grains.

Notable features observed when applying pressure on an ice sample near 0°C are summarized below:

- Fracture occurs immediately after pressure application, with a second fracture event forming a dense network of micro-cracks approximately 1 minute after application.
- Crack healing occurs immediately following pressure application due to pressure melting, and then occurs again minutes later due to extrusion and melting.
- Localized pressure melting occurs in areas of high pressure creating small pockets of melt which refreeze over hours.

- Dynamic recrystallization occurs soon after fracture and continues as long as extrusion, and therefore shear, is present.
- Grain boundary migration follows dynamic recrystallization and continues for the remainder of the experiment.
- Bubbles are observed to dissolve into pressurized melt, and reform once the melt refreezes.

4.3.4 Cold Test at Constant Pressure

The following details Test 13. Detailed screenshots for this test can be seen in APPENDIX G. This test applied pressure up to 5.7MPa to an ice specimen, which was then cooled from -10.4°C to -18.6°C. The purpose of this test was to observe the processes which occurred in compressed ice at cold temperatures where melting should not be possible.

The temperature curve for this test can be seen in Figure 43. Beginning at a temperature of -10.4°C, the ice was cooled over the next 8 hours to -18.5°C. It was then held at this temperature for the remainder of the experiment. The increase in temperature around the 24-hour mark was a result of the freezer being opened to check on the apparatus.

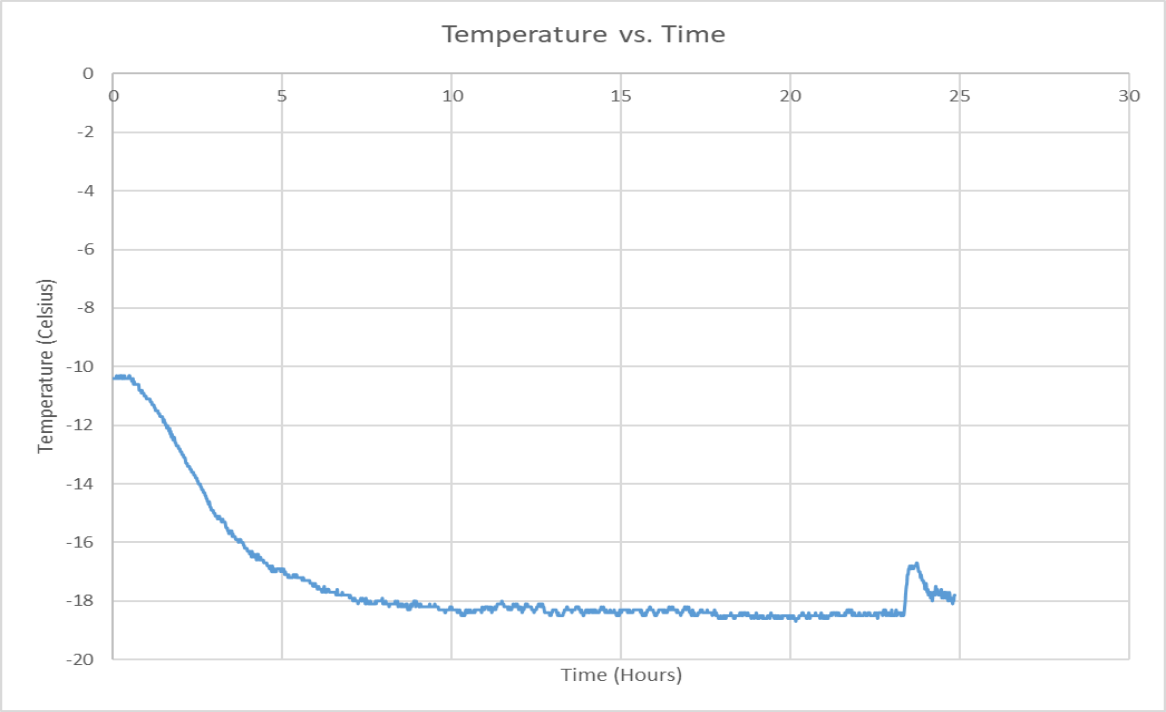

Figure 43 – Temperature curve for Test 13.

The pressure curve for Test 13 can be seen in Figure 44. Initially, the pressure was increased to 5.77MPa. It quickly bled off to 4.9MPa over the next 40 minutes, at which point additional pressure was applied to 5.5MPa. The pressure continued to bleed off until it stabilized at around 5.2MPa for the remainder of the experiment.

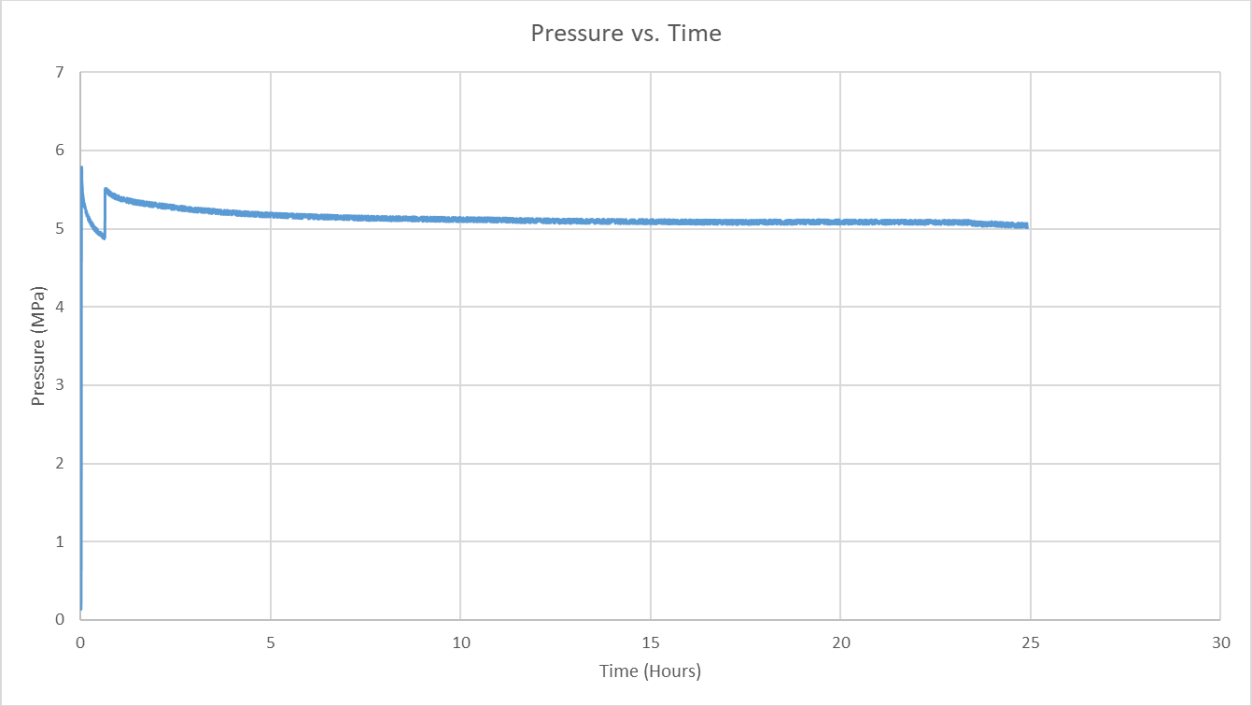

Figure 44 – Pressure curve for Test 13.

The initial state of the ice specimen can be seen below in Figure 45 (a). There is a crack on the right which was a result of connecting the top and bottom parts of the apparatus. Many air bubbles can be seen on the right side of the specimen. The temperature at this point was -10.4°C and the pressure was 0 MPa.

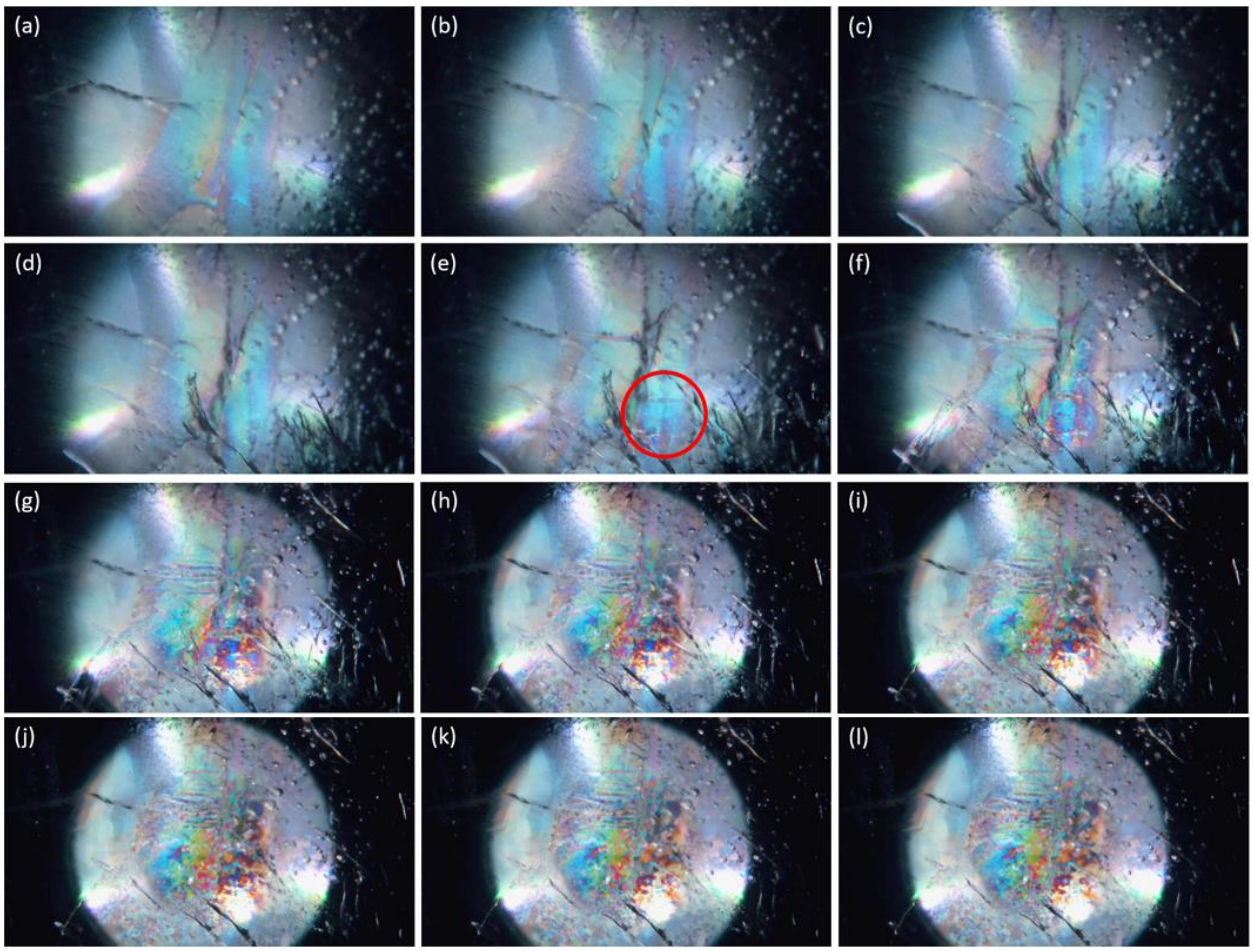

Figure 45 – Overview of Test 13: (a) initial sample, (b) initial fracture, (c) delayed fracture, (d) delayed fracture, (e) delayed fracture w/ stress indication, (f) 15 minutes, fracturing concluded, (g) 1 hour, (h) 2.5 hour, extrusion concluded, (i) 5 hours, (j) 10 hours, (k) 20 hours, (l) 24 hours.

Once the initial pressure of 5.77 MPa was applied, the ice slowly began to fracture. The first crack appeared at 1 minute and 22 seconds into the test and can be seen in Figure 45 (b). This crack appeared at the bottom of the sample near the center. The temperature at this point was still -10.4°C.

After another 23 seconds, additional fracturing occurred. This can be seen clearly in Figure 45 (c). At this point, extrusion began – pushing the ice to the left and in a slight upward direction.

Another instance of fracturing occurred 2 minutes and 5 seconds into the test – this time in the bottom right area. These cracks appeared finer and more concentrated than the previous cracks.

This is seen in Figure 45 (d). Extrusion continued in the same direction as previously indicated. The temperature remained at -10.4°C while the pressure dropped slightly to 5.36 MPa.

Around 3 and half minutes into the test, more fracturing occurred. These cracks were located at the center of the ice specimen. Additionally, deformation of the grain structure was now evident, as the highlighted area became blotchy in appearance and started to show more orange instead of blue. This is circled in Figure 45 (e). The temperature remained at -10.4°C while the pressure continued to drop – now at 5.27 MPa.

15 minutes into Test 13, the fracturing had completed. Additional cracks were visible in the top right area as well as in the bottom left area of the ice specimen. This can be seen in Figure 45 (f). Furthermore, additional deformation of the grain structure, and the initial formation of grains, was seen in the same area as indicated in Figure 45 (e). At this point, the orange color had become more apparent. Extrusion continued as the ice was pushed up and to the left. The temperature was still -10.4°C and the pressure was 5.1 MPa.

After 1 hour of pressure application, additional development of the grain structure was seen. A screenshot of the ice specimen at this time can be seen in Figure 45 (g). As seen, there was now more orange on the right area of the specimen – indicating stress in this area and grain growth. To the left of this, a greenish hue was seen – also suggesting grain growth in this area. By the cracking in the bottom left, very small grains, less than 1mm in size, had appeared. Extrusion continued and the ice was pushed up and to the left. The temperature was -11.1°C and the pressure was 5.38 MPa.

After 2 hours and 30 minutes, extrusion had concluded. As seen in Figure 45 (h), there was additional indication of a developing grain structure. The orange and blue on the right had become more distinct – and irregularly shaped grain-like structures were observed. There was almost no

new grain growth, and existing grains only grew slightly, remaining very small. The temperature was -13.9°C and the pressure was 5.27 MPa.

5 hours into Test 13, there was little change. The image of the sample, which can be seen in Figure 45 (i), appeared sharper because the condensation on the glass disc which was slightly obscuring the view of the camera had disappeared. Some crack healing was seen on the thin cracks at the bottom left and bottom right areas of the specimen. There was a very small amount of grain growth present in the orange/blue area on the right side of the specimen. The top left of the specimen remained unaffected by the pressure and appeared to not be affected by any stress. Instead, the stress seemed to be concentrated towards the bottom right of the specimen where most of the cracking was located – and somewhat in the center of the specimen where discoloration was present. The temperature had now dropped to -16.9°C and the pressure was 5.17 MPa.

At the 10-hour mark, there were few changes. A screenshot of the specimen at this time can be viewed in Figure 45 (j). Slight grain growth had occurred in the blue/orange region on the right side of the specimen. There were also many small, less than 1mm in size, grains on the outskirts of the specimen. The temperature was -18.2°C and the pressure was 5.12 MPa.

Over the next 10 hours, there continued to be minimal change in the structure of the ice specimen, which can be seen in Figure 45 (k). Grain growth continued in the area on the right, which now featured more orange than blue. The greenish area to the left remained virtually unchanged. There were many small grains on the edges of the specimen, although somewhat difficult to view as they were not under direct polarized light. The temperature was -18.6°C and pressure was 5.09 MPa.

At the end of the test, there was almost no ongoing changes to the grain structure. Irregularly shaped grains were present at the center of the specimen. Small grains, less than 1mm in size,

surrounded the bottom edges of the specimen, with a few small grains located on the right-side edge and in the center of the specimen. The temperature at this point was -17.4°C and the pressure was 5.08 MPa. The final image of the ice specimen can be seen in Figure 45 (l).

Notable features observed in cold ice under pressure are summarized below:

- There is relatively less fracturing after pressure application, with time-dependant fractures occurring over the first 15 minutes.
- There is very slow extrusion occurring for the first 2.5 hours.
- Minimal dynamic recrystallization occurs due to the lack of shear, although some small grains are present along with discoloration indicating stress within the ice sample.
- The tips of the cracks close over hours, but ultimately, crack healing is not apparent throughout the test.
- No grain boundary migration is present during the test.

4.4 Summary

Five representative tests were selected and described in this chapter. One test was a base case, while the other four tests had varying temperatures and pressures intended to induce evolution of the ice specimen grain structure over time. The base case showed that the grain structure did not develop when there was no applied pressure on the ice specimen. When under pressure and at all temperatures, a wide variety of processes are observed – including fracturing, crack healing, time dependent cracking, dynamic recrystallization, bulk melting, pressure melting, and extrusion. Some of these processes occurred no matter the temperature conditions, such as dynamic recrystallization. However, the specific behaviour of these processes appears to depend

significantly on the temperature and the presence of extrusion, which indicated shear. The videos taken of these tests allowed for in-depth analysis of these processes, the conditions under which they occurred, and the order in which they occurred in.

Chapter 5: Analysis

5.1 Overview

In this chapter, the results and data which were collected from the series of compression tests are discussed. Primarily, this section provides an overview of the processes which occurred in the ice sample under applied stress. This included dynamic recrystallization, grain boundary phenomena, cracking and fracturing processes, extrusion events, melting, and bubble behaviour. In general, comparisons between tests provided insight on the effect of temperature on an individual process. Thus, in cases where temperature had an effect, it was discussed along with the discussion of that feature. The main objective of this research was to not only determine the processes that occur in compressed ice, but to also gain a stronger understanding of how and why these processes occurred – all of which is discussed in this chapter.

5.2 Dynamic Recrystallization

Dynamic recrystallization refers to the nucleation and subsequent growth via grain boundary migration of new grains within the ice that is subjected to constant pressure. In order to compensate for the effect of the applied strain, the ice sample underwent new grain growth to better distribute and transmit the force/stress.

5.2.1 Grain Nucleation

Grain nucleation refers to the process in which new grains form within the ice sample. These grains, while initially being small (less than 1mm) in size, were able to grow.

Once the ice was placed under stress, fracturing and rapid extrusion occurred for the first ~10 minutes. After this point, the extrusion slowed down and cracking no longer occurred. Extrusion of the sample indicated that there was strain throughout the depth of the ice. Areas of high strain developed patches of orange and dark blue, which can be seen in Figure 46.

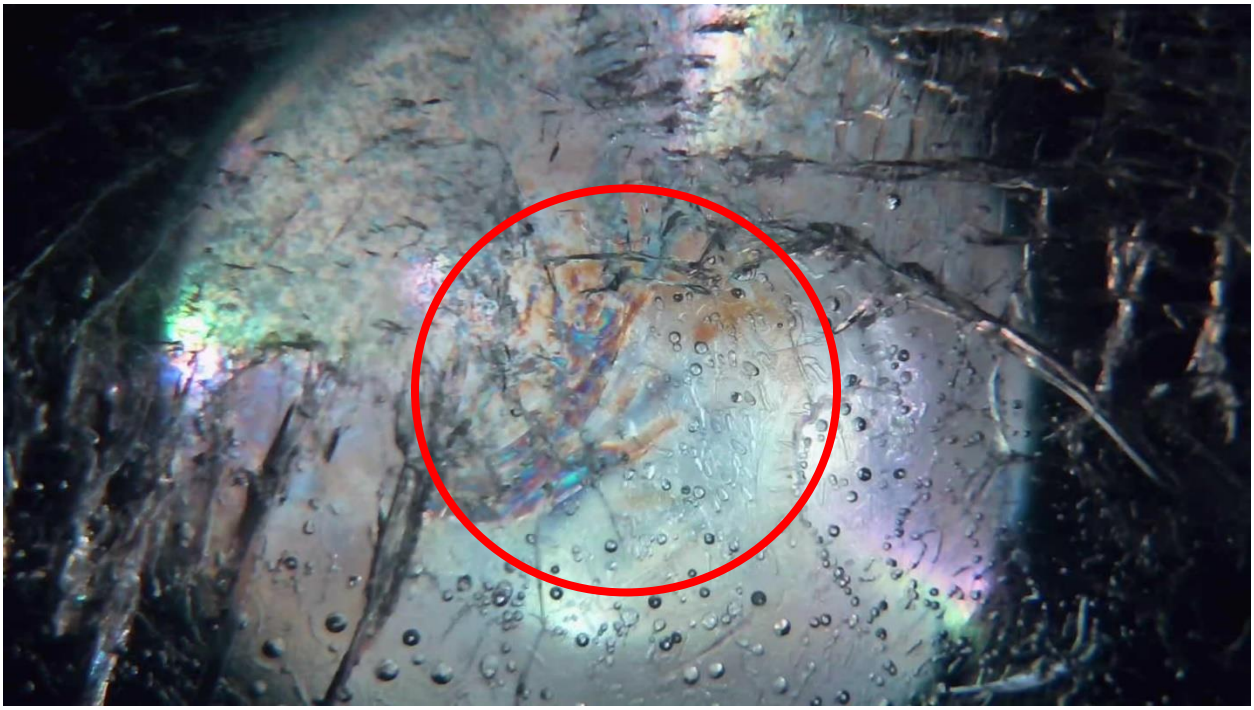

Figure 46 – Circled indication of stress in ice sample for Test 3. 18 minutes, -6.8°C.

In theses areas, rapid dynamic recrystallization in the form of grain nucleation occurred. These initial grains were very small and did not have much time to grow before they were consumed by a new grain. This was a constant process which occurred rapidly at the beginning of the experiment, typically for the first 8 hours. This process slowed over time until the process occurred rarely, if at all, near the end of the experiment. In all tests, grain nucleation always occurred in reaction to the stress applied on the ice sample. This occurred no matter the ice temperature – although it did so at different rates depending on the temperature – with colder temperatures featuring slower grain nucleation, and the rate of nucleation increasing as the ice approached melting point temperatures. This may be linked directly to the rate of extrusion, or shear, which is impacted by the ice temperature. At colder temperatures, the ice was harder and may be resistant to extrusion. At warmer temperatures, the ice became softer, meaning extrusion would accelerate. This suggested that, as the temperature increased, the magnitude of shear also increased. Thus, the main driver of grain nucleation was shear. This was further supported using Test 9, where the extrusion and shear stopped partway through the test and grain nucleation stopped at the same time. Additionally, there was minimal extrusion and shear present in Test 13, the cold test, which resulted in relatively less grain nucleation. Over time, as the ice increased in temperature and approached -3°C, grains began to grow via grain boundary migration. Figure 47 demonstrates this by showing the developing grain structures at 1 hour (a), 2 hours (b), 3 hours (c), and 4 hours (d).

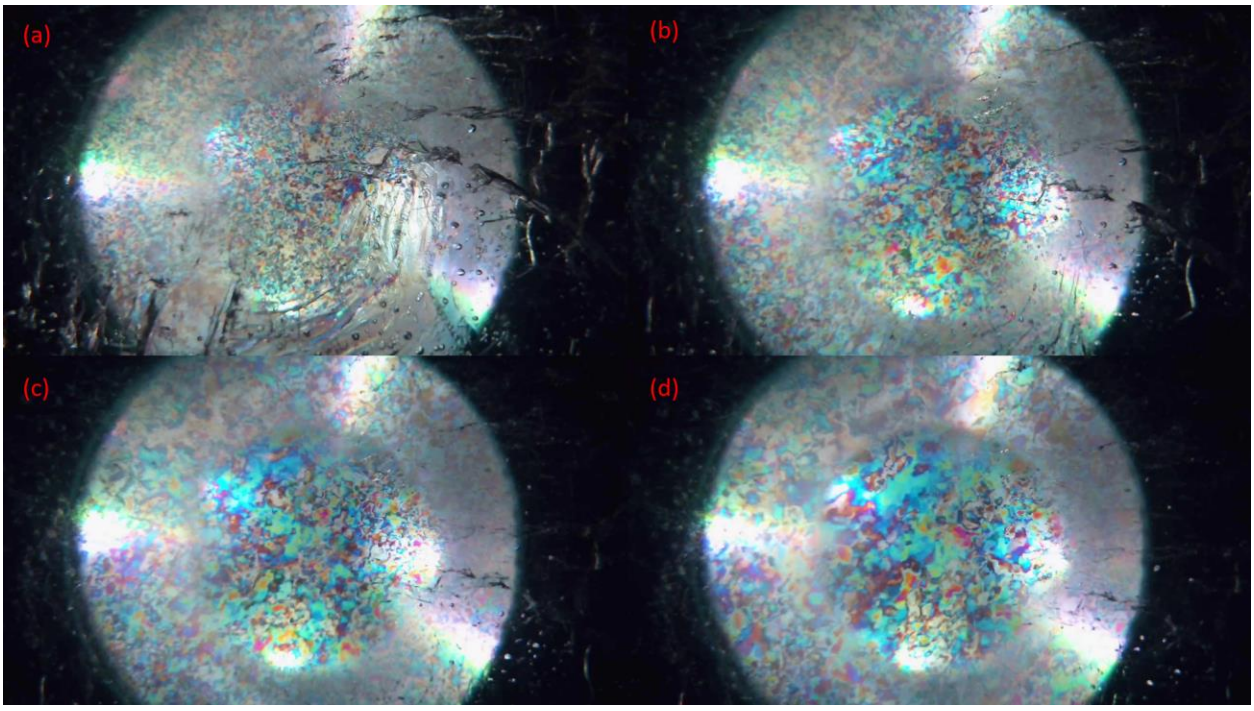

Figure 47 – Test 3 grain nucleation over time. (a) 1 hour at -5°C, (b) 2 hours at -3°C, (c) 3 hours at -2.1°C, (d) 4 hours at -1.5°C.

Ultimately, grain nucleation became less frequent as the test went on – suggesting that the ice specimen reached an equilibrium point where the existing grain structure allowed for efficient transfer of stress throughout the sample. Again, this coincided with the presence of extrusion and shear. In some tests, there was one last significant instance of grain nucleation, in which grains formed and dominated the final grain structure via grain boundary migration. As an example, Test 3 demonstrated a grain appearing at around 10 hours which grew for the remainder of the test. This can be seen in Figure 48.

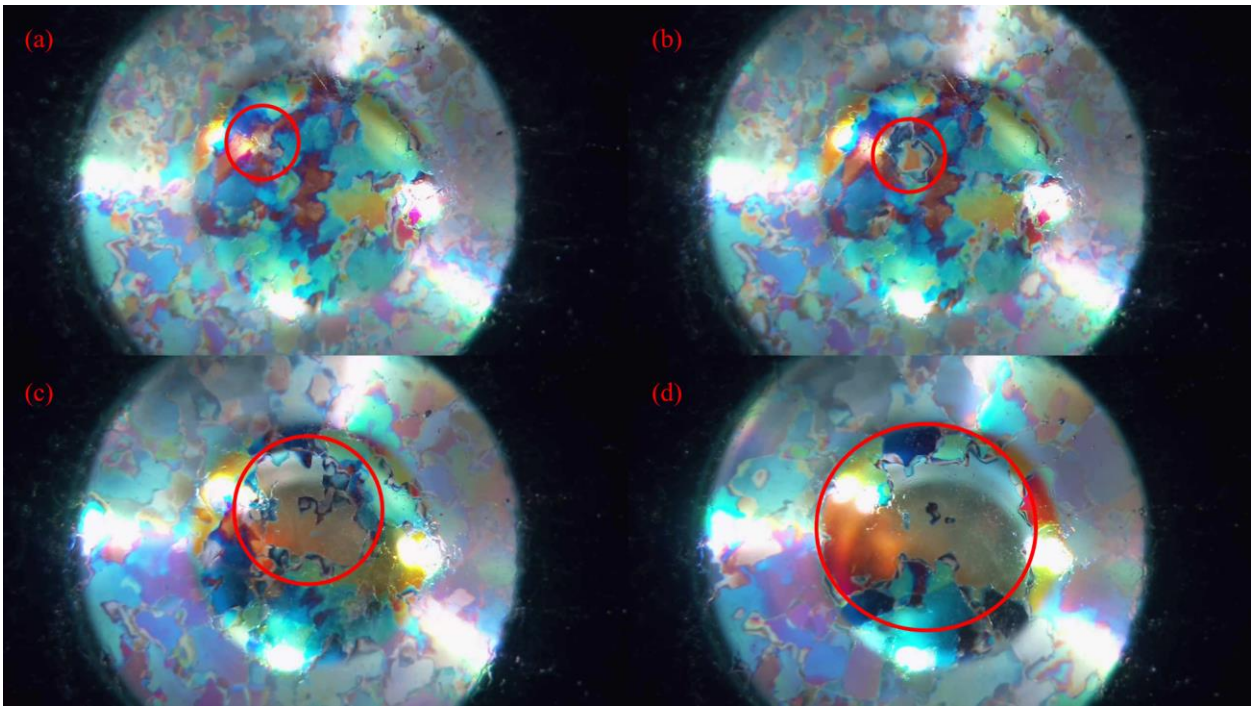

Figure 48 – Circled grain nucleation and subsequent growth via grain boundary migration. (a) 9 hours 42 min, (b) 10 hours 42 min, (c) 15hours 42 min, (d) 26 hours 15 min.

5.2.2 Grain Boundary Migration

Grain boundary migration refers to the material of one grain being absorbed by a neighbouring grain – thereby changing the position of the grain boundary. This process resulted in grains both increasing and decreasing in size, although typically resulted in fewer, larger grains by the end of the experiment.

As the temperature approached melting point, grain boundary migration became the dominating form of dynamic recrystallization. At an ice temperature warmer than -3°C, grain boundary migration began to occur. This is evident in both cold tests (sub -10°C), in which grain boundary migration was negligible and grains remained relatively small, and in tests in which the temperature was increased from a temperature below -3°C to a warmer temperature above -3°C. As the ice began to warm and approached the melting point, nucleation slowed significantly as the ice became softer and the extrusion process concluded. Here, grain boundary migration began to

dominate the recrystallization process, which allowed certain grains to consume their neighbouring grains and grow in size. The following Figure 49 demonstrates this process clearly. Over the course of two hours, both grain (a) and grain (b) grew by consuming some of the material in their surrounding grains. In this case, both grains mainly grew in an upward direction. This process continued throughout the remainder of this experiment, ultimately resulting in a grain structure consisting of relatively fewer, larger grains.

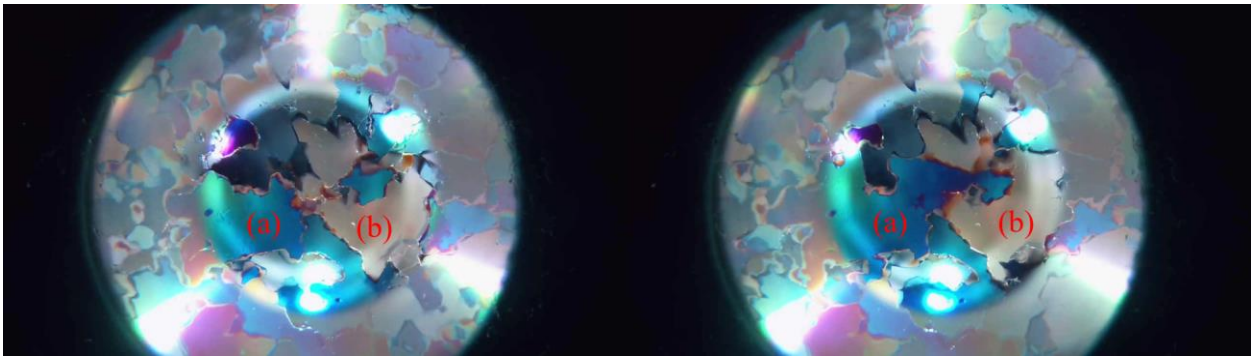

Figure 49 – Grain boundary migration at 12.5 hours to 14.5hours – Test 10.

5.2.3 Effect of Temperature

At colder temperatures, there was significantly slower grain nucleation and grain growth. Tests 13 and 14 demonstrated this as, after 24 hours under 5 MPa, new grains had formed; however, there had been almost no grain growth. Additionally, grain boundary migration did not seem to occur significantly at this temperature, which was likely the reason for the small grains. The grains formed during the cold test, as seen in Figure 50, were less than 1mm in size. This indicated that colder ice, being less ductile and harder, was able to resist physical change due to the applied stress. Thus, dynamic recrystallization processes required more energy to occur at this temperature.

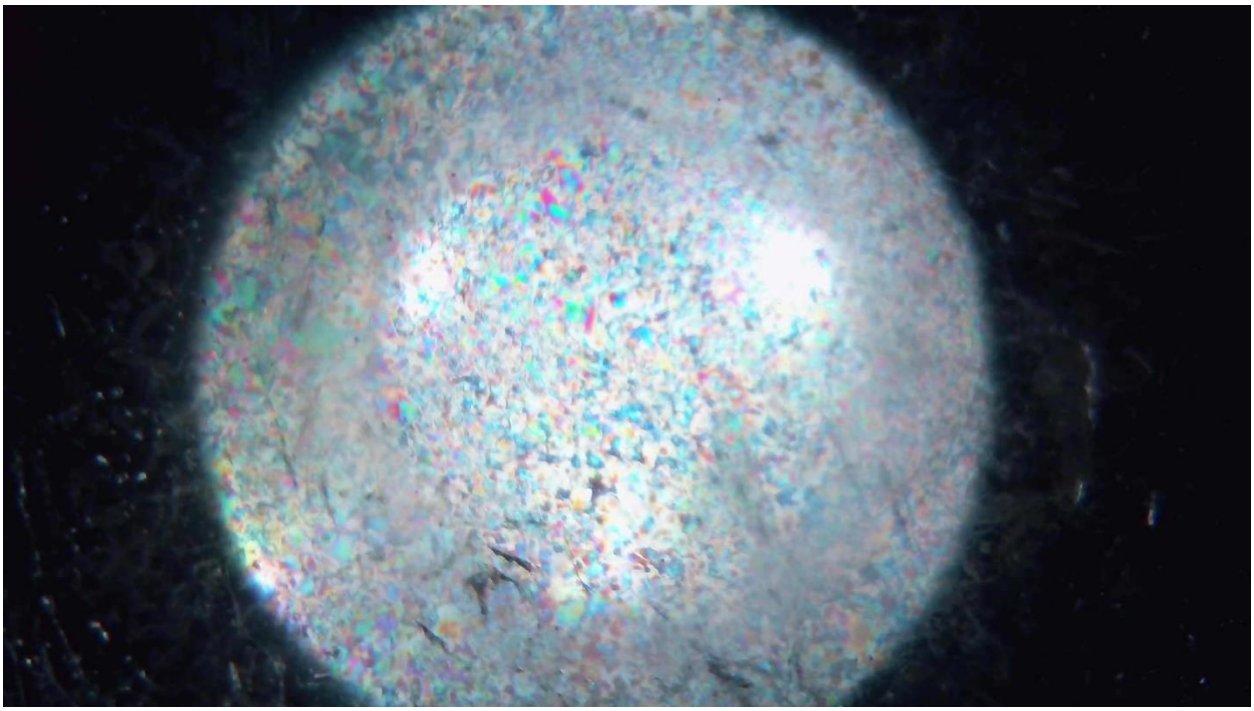

Figure 50 – Final state of Test 14 after 24 hours under 5MPa at -18°C. Grains are less than 1mm in size.

5.2.4 Summary

When subjected to an applied stress, the ice sample underwent dynamic recrystallization. This was in the form of grain nucleation and grain boundary migration. Initially, grain nucleation was the dominant process – as grains were rapidly forming on top of one another – slowly getting larger over time. This occurred to allow the ice to easily transfer and divert the applied stress throughout the sample. This process took a different amount of time depending on the temperature. At colder temperatures, the dynamic recrystallization and subsequent grain growth was relatively slow. As the temperature approached melting point, these processes accelerated. Once close to melting point, the ice underwent an additional wave of recrystallization until it settled on a particular grain structure. This process was also linked to extrusion, which indicated shear. The rate of extrusion, and therefore the magnitude of shear, drove the grain nucleation process. It was likely that the ice being closer to the melting point allowed for easier rearrangement of the sample under pressure. This meant that grain nucleation and growth occurred more quickly and in a way which best

allowed for the ice to respond to the applied stress. Thus, it was typical to observe the ice undergo a final instance of nucleation once it reaches 0°C. This would typically coincide with the conclusion of the extrusion process and the relief of shear stress on the sample. Finally, it was clear that, as the temperature of the ice approached the melting point, grain nucleation slowed, and grain boundary migration becomes the dominant process. Typically, grain boundary migration was seen at temperatures above -3°C, while it was rare to see this process at colder temperatures.

5.3 Grain Boundaries

There were a few other characteristics involving grain boundaries, outside of grain boundary migration, which were significant or frequently occurred. This included discoloration along grain boundaries as well as melting at grain boundaries during bulk melting.

A common characteristic of the grains formed during these tests was a slight discoloration along the grain boundaries. It was likely that this is caused by two grains overlapping along their grain boundaries. This can be seen in Figure 51.

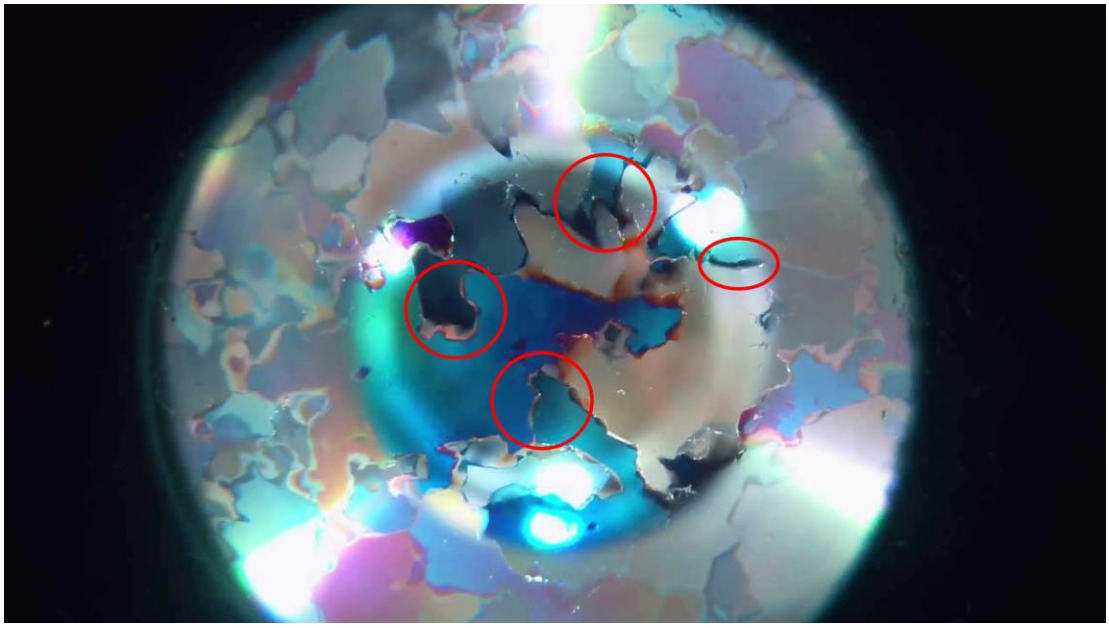

Figure 51 – Circled discoloration at grain boundaries – Test 10, 14 hours 30 minutes.

When bulk melting occurred, an initial characteristic that developed was the 'wetted' grain boundaries. Essentially, the grain boundaries required less activation energy in order to melt, resulting in them appearing translucent and melting first prior to the bulk melting of the entire ice sample. This can be seen in Figure 52.

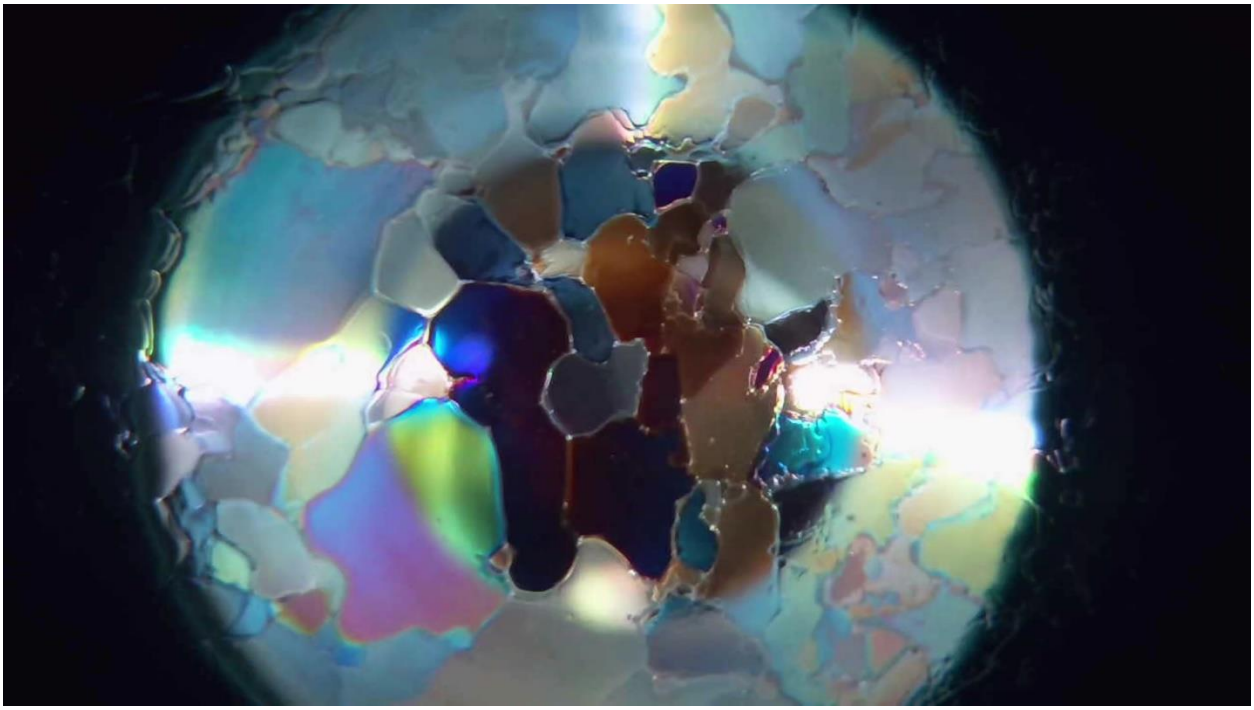

Figure 52 – Melting occurring first at the grain boundaries. Test 2 at 17 hours, temperature at 0°C.

5.4 Cracks/Fractures

5.4.1 Fracture Process

The fracturing of the ice sample was heavily influenced by two factors – the temperature of the ice, and whether or not there was a pressure concentration, or high-pressure zone, caused by an uneven surface. These two factors consistently influenced the fracturing in all tests.

Generally, the initial temperatures of most tests during pressure application were between -10°C to -15°C. In these cases, the ice fractured in a more abrupt manner, with the cracks often being

deep and long, as seen in Figure 53. In most tests, the majority of the fracturing occurred within the first 30 seconds after application of pressure on the ice sample.

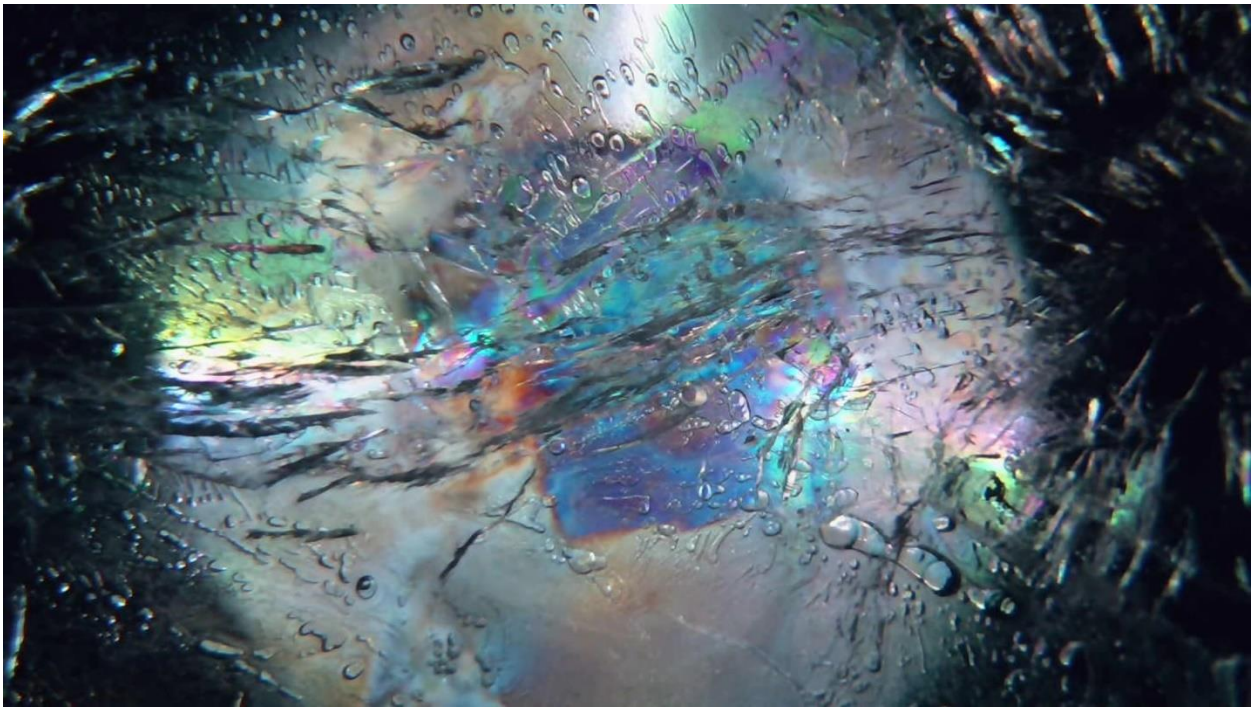

Figure 53 – Typical long, deep cracks formed during 'cold' tests – Test 2, 15 seconds after pressure application.

In some cases, the ice sample included an uneven surface, or a bump, which caused a pressure concentration. An example of this can be seen in Figure 54, where the 'bump' has caused a circular fracture around its perimeter when attaching the top and bottom parts of the apparatus. This caused a pressure concentration in this area, which resulted in a large, catastrophic fracture event in which the sample was quickly shattered into a dense network of micro cracks, seen in Figure 55.

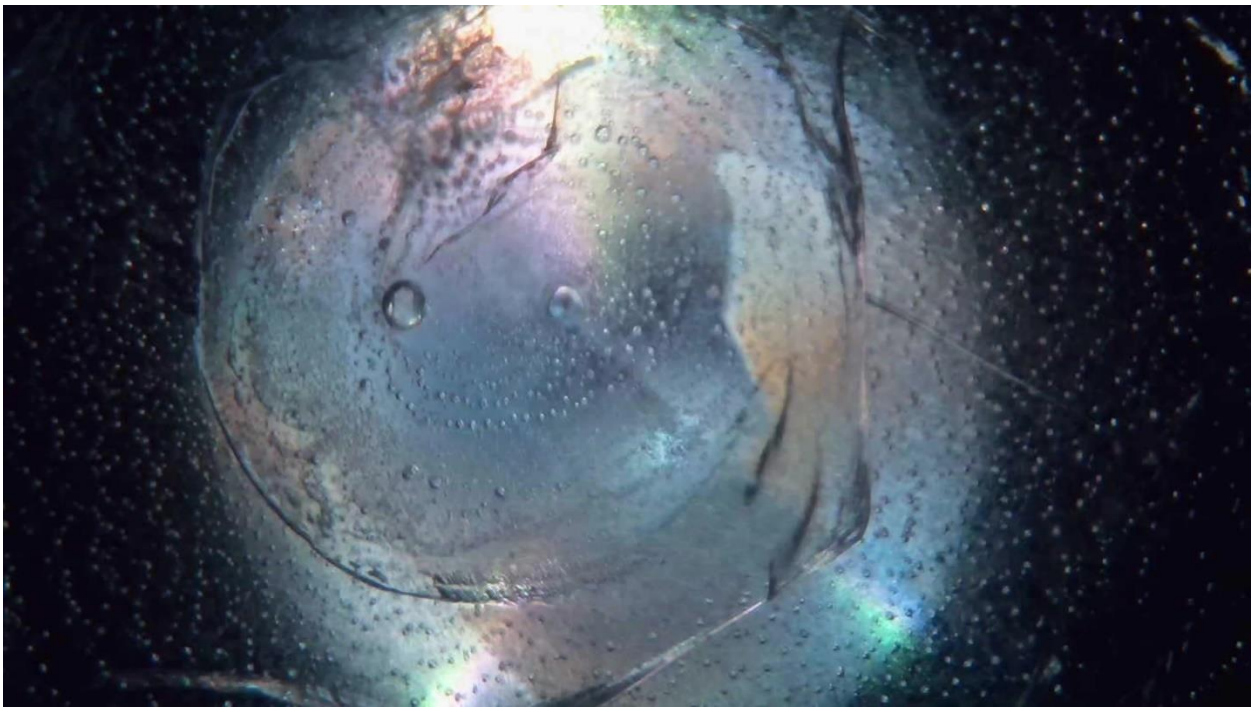

Figure 54 – Visible 'bump' located in the center of the ice sample – Test 5, start of experiment.

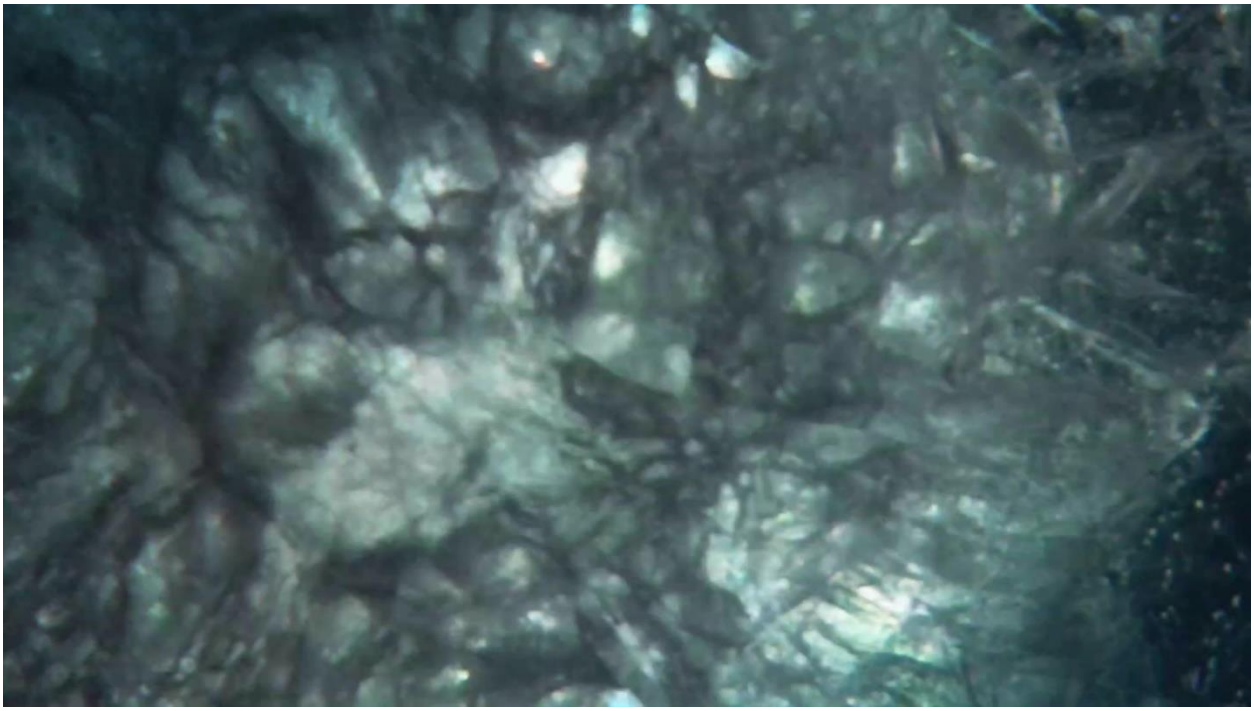

Figure 55 – Large micro-fracture event resulting from uneven ice surface – Test 5, 10 seconds after pressure application.

5.4.2 Time Dependent Cracking

In cases where pressure is applied on 'warm' ice around 0°C, the fracturing of the ice tended to be over a period of minutes instead of seconds – referred to as time dependent cracking. The ice sample at this temperature contained some amount of melt and behaved in a more fluid-like manner. Thus, it was likely easier for the ice to distribute the stress and delay the fracturing process. For example, in Test 11, the sample exhibited ductile crack growth continuously for approximately 2 minutes after the application of pressure. Typically, these cracks are thinner in appearance, as can be seen in Figure 56. Additionally, these cracks quickly filled with melt that refreeze, causing some cracks to appear and then immediately disappear. It should be noted that in Test 9, there was an eventual 'catastrophic' fracturing event, causing the ice to appear shattered as seen in Figure 57. This was caused by an uneven ice surface. In this case, the shattering of the ice was delayed, happening a full minute after pressure application. This suggested two things. First, that a warmer ice specimen behaves in a ductile and fluid-like manner, and that the ice specimen was easily able to adjust and accommodate the stress introduced into the sample, thereby delaying and extending the fracture process. Second, it further indicated that an uneven surface area would create a large pressure concentration and cause a 'catastrophic' failure independent of the temperature of the ice sample. Thus, it is clear that the time delay associated with cracking can be attributed to internal microstructural defects as, after application of pressure, the migration and pile up of dislocations in the crystalline lattice creates stress concentrations that suddenly cause fracture once it reaches a critical level. Depending on the temperature of the ice, this process happens at different rates – leading to the observed differences in the timing of fracture events between tests.

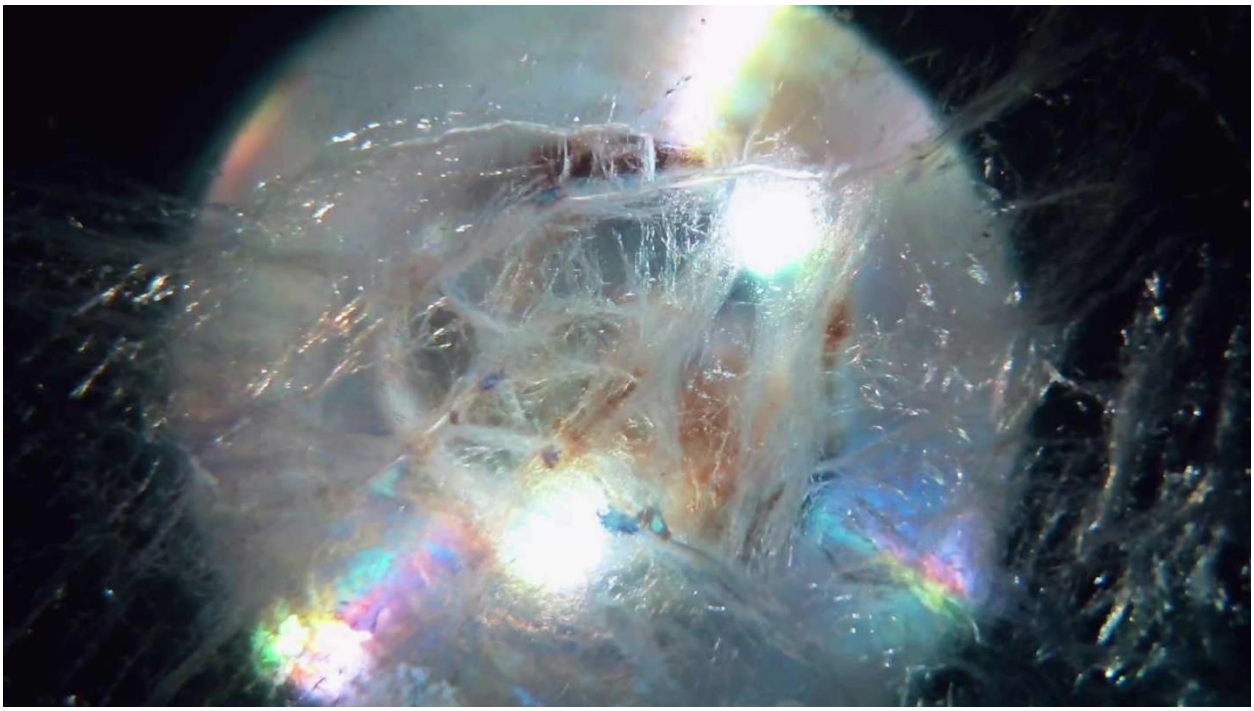

Figure 56 – Many thin cracks observable in a 'warm' test – Test 11, 50 seconds after pressure application.

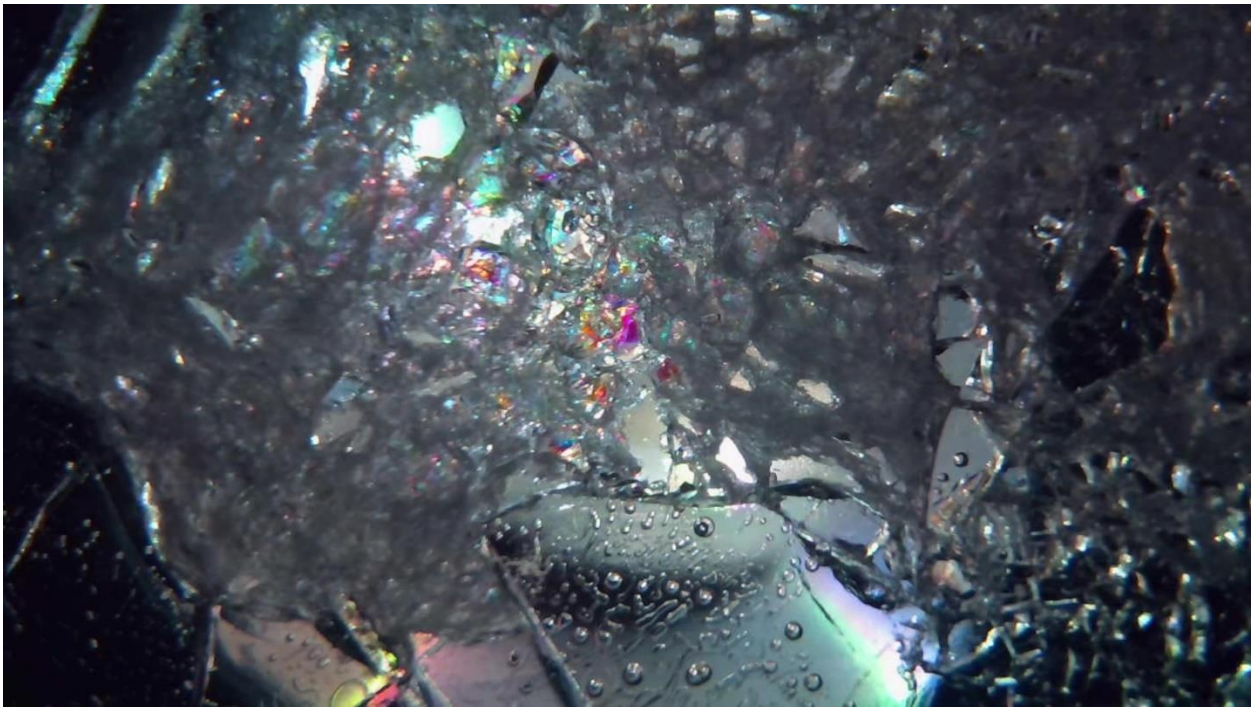

Figure 57 – Ice sample shattered a full minute after application of pressure during a warm test – Test 9.

In Test 13, a cold test, time dependent cracking is also evident. In this case, cracking occurred over a period of 15 minutes after pressure application. Compared to the warmer tests, there was less

cracking overall. This suggested that colder ice is more resilient to cracking compared to the warmer ice – and prolonged stress caused cracking over time rather than in one instance.

5.4.3 Crack Healing

Crack healing refers to the process which causes a crack to shrink or disappear over time. This process was evident in all tests conducted. Figure 58 demonstrates crack healing during Test 1 by observing a crack 2 minutes after pressure application, again after 15 minutes, and then finally at 2 hours and 30 minutes into the test. The temperature at this point during the test went from -5.7°C in (a), to -3.8°C in (b), and to -1.6°C in (c). The pressure was consistently above 5 MPa. Many of the smaller, shallower cracks close within minutes, while the longer, deeper cracks took hours to close completely. During this time, there was an ongoing extrusion event caused by the initial fracture and application of pressure.

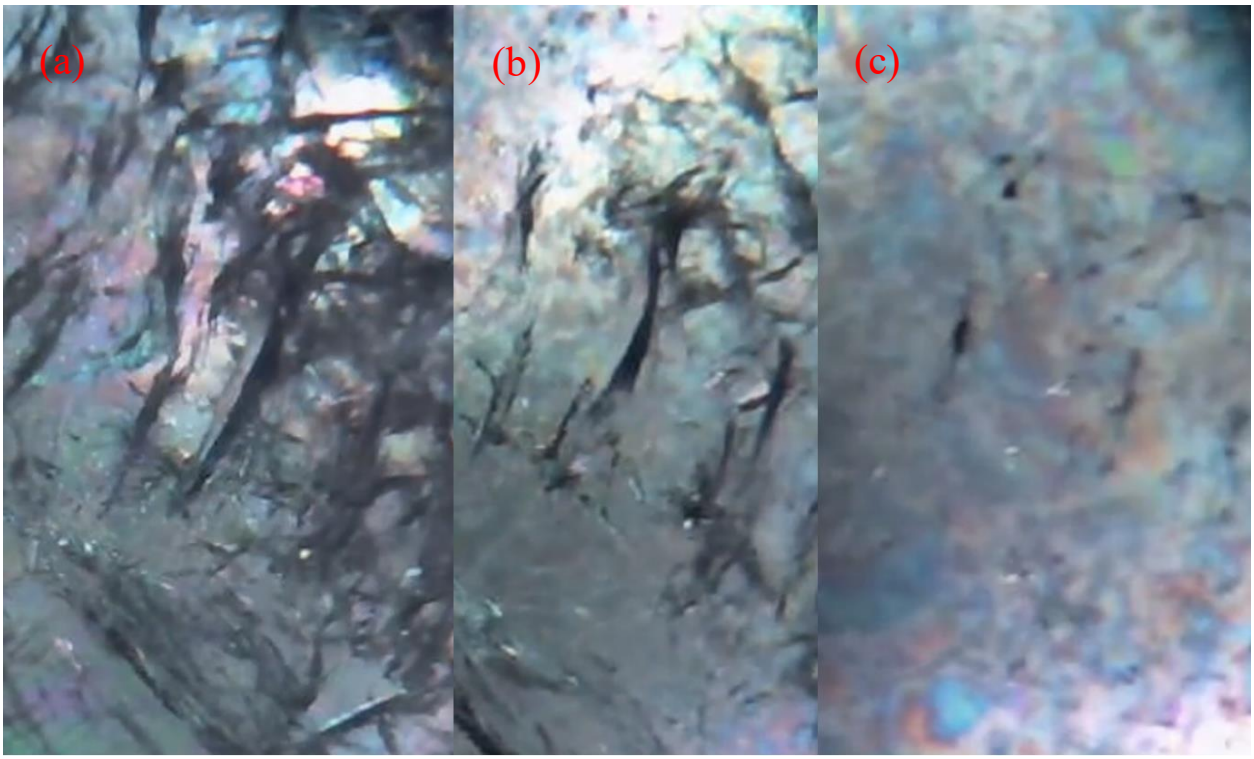

Figure 58 – Crack healing in Test 1. (a) 2min, (b) 15min, and (c) 2.5hours.

Crack healing was also observed in cases in which the ice is at melting point when initial pressure is applied. In these cases, some cracks became filled with melt which rapidly refreezes in under 30 seconds. While this was most common in the thinner cracks which tended to form under these temperature conditions, there were instances of larger cracks exhibiting the same behaviour, such as the crack examined below in Figure 59. Here, within 15 seconds, this crack filled with melt, refreezes, and closed completely. Such behaviour was not present in tests at lower temperatures in which melt was not present. Cracks of this size would typically take hours to close. This suggested that temperatures near the melting point would cause the crack healing process to accelerate. Additionally, while there was some extrusion present in this test, the ice hardly extruded at all over 15 seconds, suggesting that, for this crack specifically, extrusion was not a factor in its healing. The many other cracks that heal over a larger period of time, however, were likely influenced by the extrusion event.

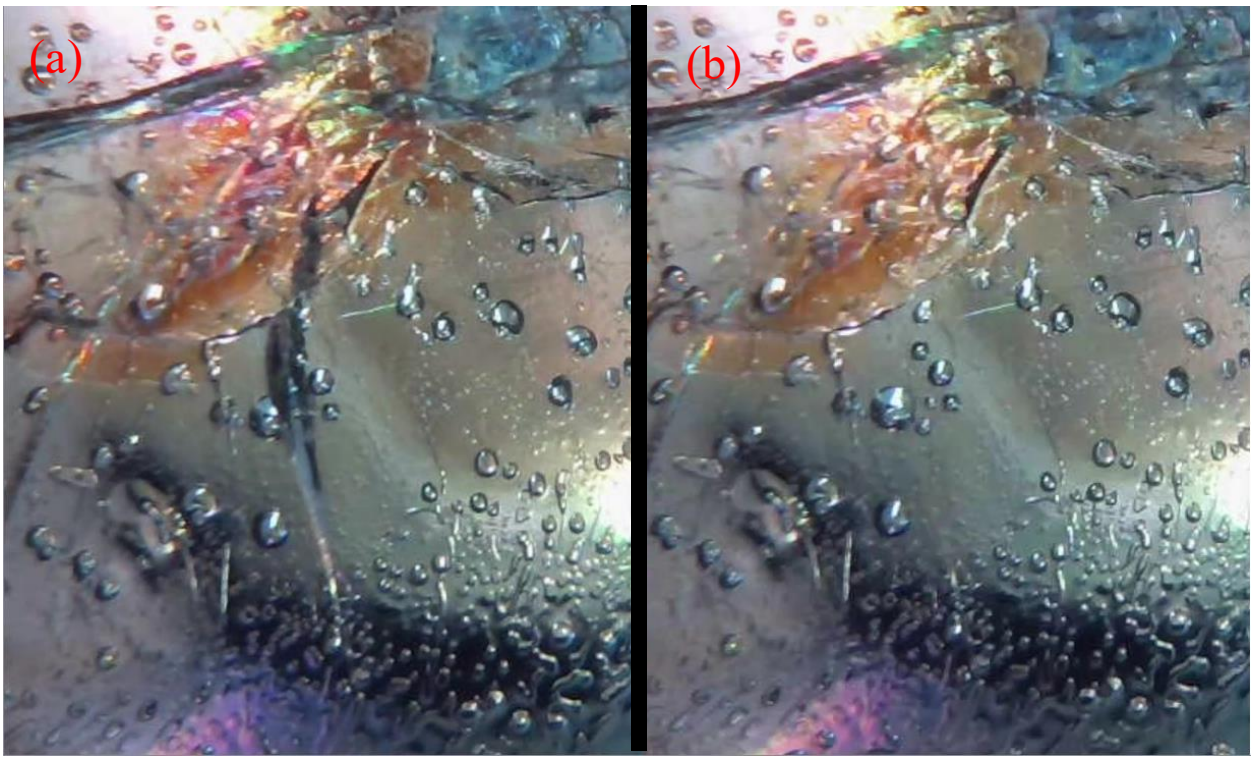

Figure 59 – Rapid crack healing in Test 9. (a) 1min 15s, (b) 1min 30s.

Experiments conducted at much lower temperatures under -15°C demonstrated slower crack healing. In Test 14, there were many small cracks which obstructed the view of the ice that healed and are no longer present at the end of the test. However, some of the larger cracks, while they shrunk in size, remained almost 24 hours later. In Test 13, some thin cracks healed completely, but the larger cracks only shrunk by a few fractions of a millimeter, and only at the thinner tips of the crack, over 24 hours. This case, however, featured less extrusion. This further suggests that both the temperature of the ice and the presence of an extrusion event greatly influences the speed at which cracks heal.

To further demonstrate the impact of temperature and localized pressure melting (LPM) on crack healing, Test 4 was observed. Pressure was initially applied when the ice was cold, around -11°C. Over the next 12 hours and 45 minutes, the crack slowly healed under 2 MPa of pressure and

constant extrusion. At this point, the ice was now at 0°C, and LPM occurred as illustrated in Figure 60. (a) demonstrates the initial crack. Figure 60 (b) shows crack healing after an hour and a half, unaffected by temperature. The crack at this point had shortened slightly, as the pressure and extrusion had closed the crack at the tips. Figure 60 (c) shows the crack midway through LPM. The edges of the crack appear wetted, and the crack was noticeably closing widthwise throughout the entire length of the crack – something which was not happening prior to LPM. Finally, Figure 60 (d) demonstrates the closed crack, filled in with melt which has quickly refrozen. All that remains was two air bubbles, a result of the air trapped within the crack.

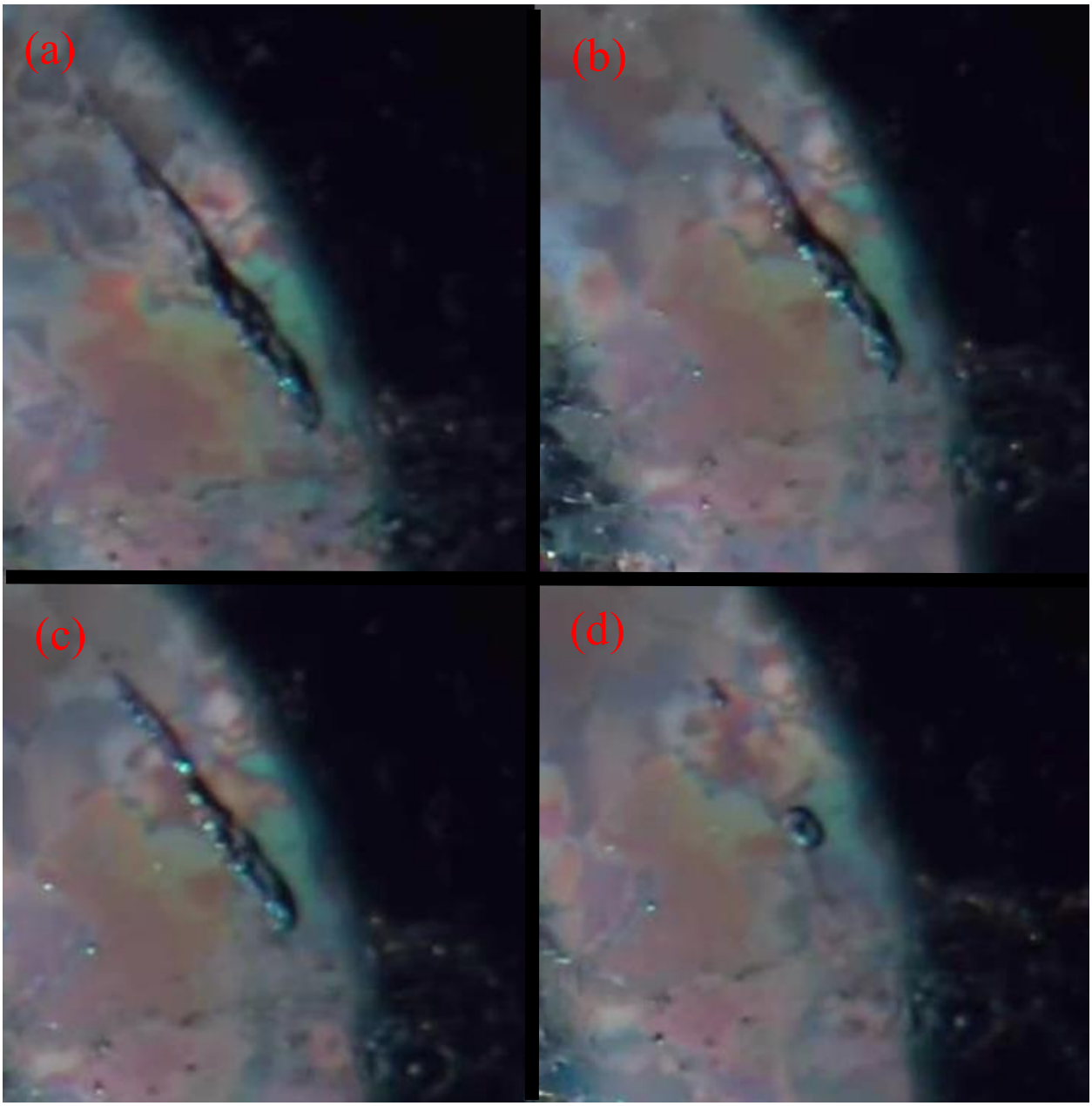

Figure 60 – (a) crack at 11hours, (b) 12 hours 45 minutes, (c) 13 hours, (d) 13hours 30 minutes – Test 4.

In the Base Case, there was no evidence of crack healing – despite there being a minor extrusion event in the area of the cracks and the ice being at 0°C with melt present in the sample. What this suggested is that high pressure was the key requirement to initiating this process in the ice sample. While temperatures at melting point accelerated this process, these temperatures alone did not

appear to cause crack healing. The high pressures were critical due to it forcing the fractured ice to fuse back together, as it provided the energy required to repair and create new bonds. Additionally, pressure melting could, under the right temperature and pressure conditions, contribute to crack healing. Cracks indicated areas of high stress within the ice sample; thus, these areas may be subjected to high pressures. This lowered the melting point of the ice and caused localized pressure melting. The melt then flowed into the crack and quickly refreezes, thereby healing the crack.

Based on these testing observations, it can be concluded that high pressure was the primary driving force behind crack healing; without high pressure, crack healing cannot occur. Lower temperatures coincide with faster crack healing, with temperatures close to 0°C allowing for localized pressure melting that could rapidly heal cracks. Extrusion events also helped accelerate the rate of crack healing, as this helped push the ice together and close some of the cracks.

5.5 Extrusion Events

Extrusion refers to the shear movement of the ice sample in a particular direction, often radially outwards from a high-pressure zone, due to the external pressure applied to the ice sample resulting in internal deformation processes. Extrusion events were present in all experiments, driven by one of two processes. One such process which drove extrusion was the initial fracture events after pressure application. The other process which was observed to trigger extrusion was localized melting.

5.5.1 Pressure/Fracture Events

The main driver of extrusion was the initial application of pressure and the subsequent fracture event which occurred in every test. The extrusion occurred for two reasons. First, the crushed ice when compressed was forced to become denser due to the application of pressure. This caused

movement within the ice sample. Second, the ice was not perfectly contained, with a small, less than 1 mm gap along the edge of the indenter that it could extrude out of. While most of the ice remained contained within the testing area, a small amount was occasionally forced away from the indenter.

To illustrate how uneven pressure application could cause extrusion, Test 3 is considered below. In this test, the pressure was concentrated in the top left of the sample. This section of the ice was compressed first, triggering an extrusion event away from this area. This resulted in excess ice being forced out and away from the center of contact. This gave the appearance of a wave, or pressure front, originating from the point of pressure concentration. This can be seen in Figure 61.

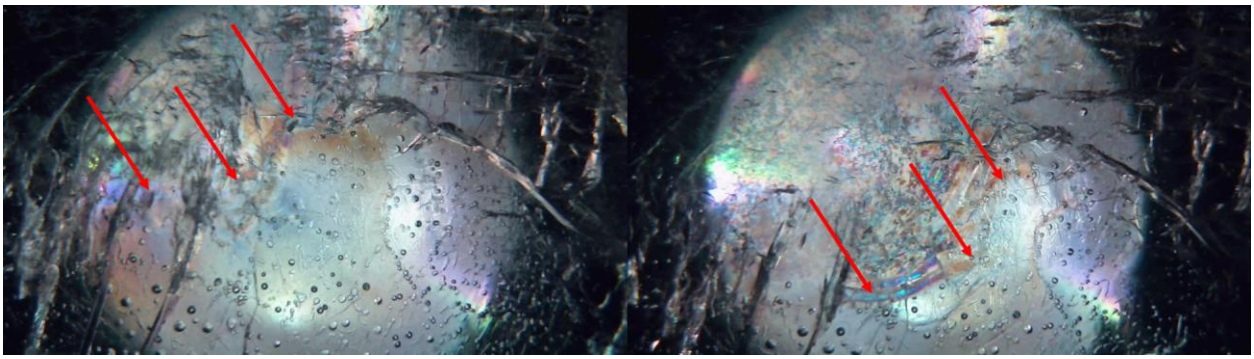

Figure 61 – Linear extrusion due to uneven pressure application – Test 3.

During the extrusion process, the ice was sometimes pushed away radially from a pressure concentration point. In many cases, it appeared as though the ice was moving in a single direction, which was generally because the area of pressure concentration was located outside the observable area. Other factors, such as a gap or uneven application of pressure, may have created some roughness in the ice and caused it to extrude in one direction more than other directions. An example of radial extrusion was seen in Test 5 and is illustrated in Figure 62. It should be noted, however, that the radial extrusion only occurred for approximately 1 hour and 30 minutes. Additionally, this extrusion coincided with another extrusion event which pushed the ice in a

singular direction, which is denoted by the dashed arrow in the figure below. This second linear extrusion event continued for the entirety of the experiment, lasting for 17 hours and 40 minutes in total.

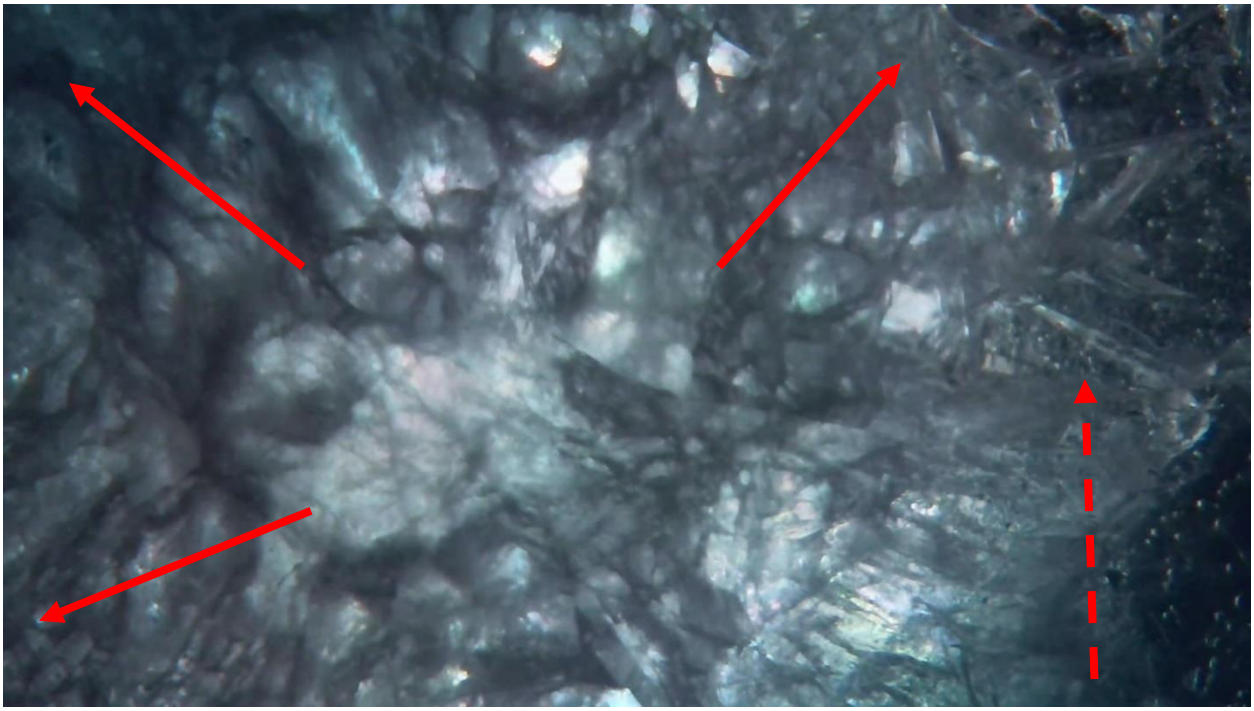

Figure 62 – Radial extrusion due to a pressure concentration/fracture event – Test 5 at 35 seconds, 5.4MPa. Solid arrows represent radial extrusion due to pressure concentration. Dashed arrows represent linear extrusion.

Immediately after pressure application, linear extrusion was observed and typically occurred at its fastest rate. This generally continued throughout the entire experiment, slowing down over time. In some cases, the extrusion stopped completely, indicating that the ice was either no longer under pressure or that the ice had reached a point of equilibrium, in which all mobile dislocations in the ice moved to stable parts, and it was able to support the force without any substantial physical changes. This process was observed in Test 11. In this test, the initial fracturing occurred in the top left of the specimen where the pressure was concentrated. The bottom right area of the specimen began to also deform laterally, ultimately causing fractures. After only 20 minutes, the extrusion stopped completely. However, changes to the grain structure continued for the remainder of the

24-hour experiment. This suggested that the ice was still under pressure, and that the extrusion had stopped because the ice was both contained and able to accommodate the applied pressure without further internal dislocation glide.

In Test 7, two adjacent areas of ice were extruded in different directions, causing a large crack in between them. This is shown in Figure 63. The bottom area extruded first, moving down and to the right in a linear manner. The rate of extrusion for the bottom region was much faster than the rate of extrusion in the upper area. Different to the bottom area, the upper area extruded in a clockwise direction, rotating slightly over time. The direction indicated by the dashed line in Figure 63 represents the initial direction this section of ice extruded towards. As mentioned, this section of ice rotated – slowly changing direction until it aligned with the direction of the bottom area approximately 7 hours into the test.

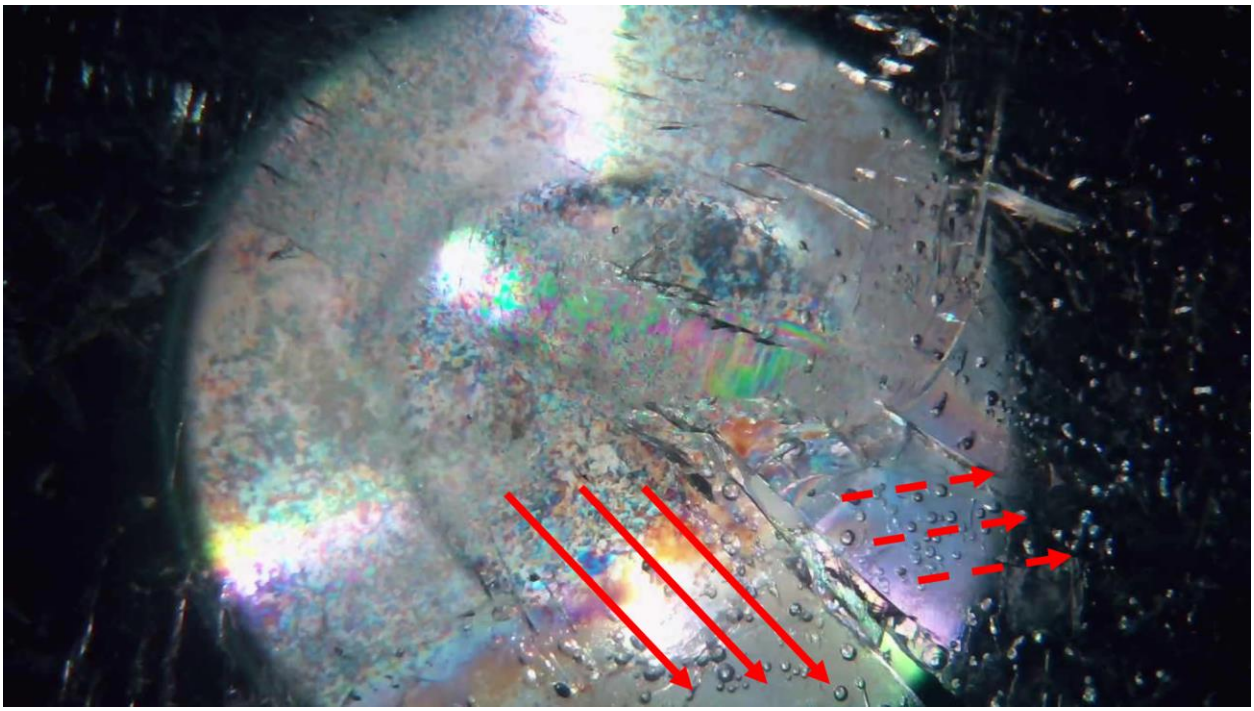

Figure 63 – Extrusion in multiple directions. The solid arrow represents the extrusion of the bottom area in a linear direction. The dashed arrow represents the extrusion of the upper area in a clockwise rotation. Test 7 at 1 hour.

5.5.2 Melting/Recrystallization Events

In some cases, bulk melting caused additional movement and extrusion events late into the test. Test 1 provided an example of this. The initial extrusion event was caused by the application of pressure and subsequent fracture event, which was represented in Figure 64 (a). Over time, the rate of extrusion caused by this event slowed down. At the 7-hour mark, the ice temperature reached 0°C and bulk melting began. This caused a second extrusion event as water was ejected from the ice specimen. The rate of extrusion increased, and the ice was pushed in a slightly different direction than that of the extrusion caused by fracture. This is illustrated in Figure 64 (b). Once the ice began to melt, it became more susceptible to the pressure as the ice became softer at higher temperatures and less energy was required to separate the ice crystals. This caused the ice to easily separate, as is reflected in the split which forms during this test.

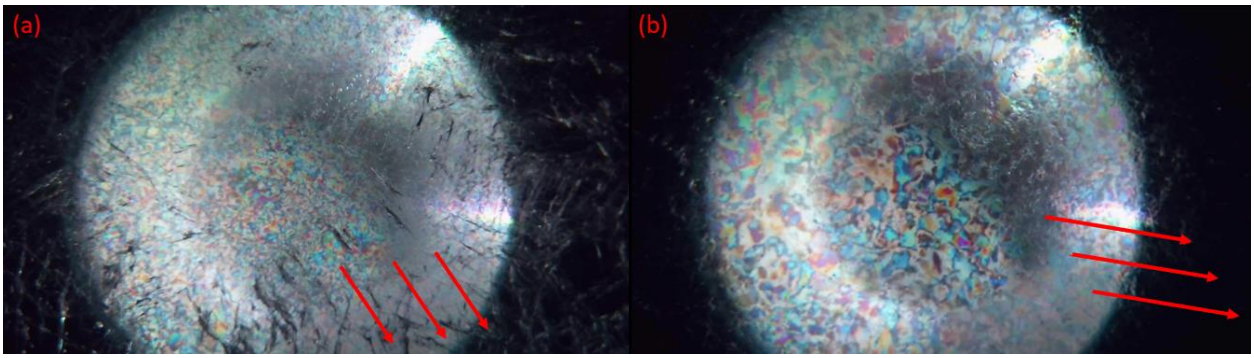

Figure 64 – Shift in extrusion direction caused by melting. (a) fracture event at 1 hour, (b) melting event at 7 hours – Test 1.

5.6 Melting

Melting is a process which, while frequent, was not present in every experiment. Melting was only observable in experiments that approached or reached 0°C. During the experiments, melting occurred under two circumstances – bulk pressure melting (BPM) and localized pressure melting (LPM).

It should be noted that without applied pressure, the ice sample simply exhibited thermal melting, wherein it melted from the outside edges inwards. This was because the outside edges are closest to the apparatus and therefore heated up first. Because there were no grains formed as a result of pressure application, the bulk melting process was different when compared to the experimental results. Additionally, LPM cannot occur without any pressure applied to the sample. Thus, all LPM discussed in this section did not occur without pressure applied to the sample.

5.6.1 Bulk Melting Under Pressure

Bulk pressure melting refers to the entirety of the ice sample reaching its typical melting point of 0°C and changing phases from solid to liquid by absorbing heat energy. This process was only observed in two instances in which the apparatus temperature reached a temperature higher than 0°C. In these instances, the entirety of the ice sample began to melt, starting at the grain boundaries.

The first visual indication of bulk pressure melting was a 'wet' appearance of the grain boundaries. This can be seen in Figure 65. The grain boundaries appeared to be transparent, making the grains look as though there is a small gap between them. The grains themselves continued to slowly grow and change shape, maintaining their wet boundaries.

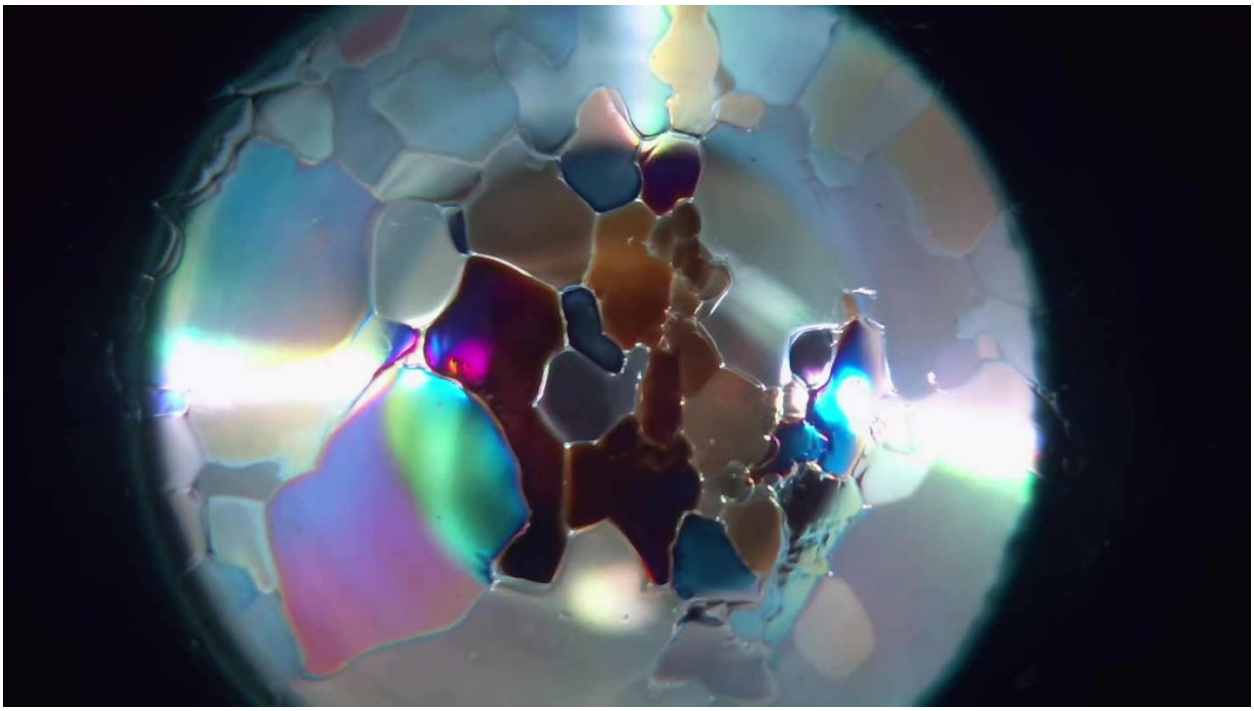

Figure 65 – 'Wet' grain boundaries appearing due to bulk melting – Test 2 at 24 hours.

Once the sample absorbed enough energy, melting began at the grain boundaries. Test 1, for example, showed the entirety of this melting process and is shown in Figure 66. Figure 66 (a) shows the initial grain structure for reference. In Figure 66 (b), the grain boundaries appear wetted and transparent. In Figure 66 (c), the grains begin to melt inward and begin to shrink in size. As seen in Figure 66 (d), the grains quickly begin to melt inwards from their top and bottom surfaces, reducing thickness. Due to the specimen being very thin relative to the width, the grains primarily melted in the vertical direction, with grains which were less than 1 mm in size melting from their sides inward. Ultimately, the grains appeared to fade away as they lost their color and the phase changed into water. Bulk pressure melting was observed in cases of high uniformly distributed pressures, such as cases with negligible shear.

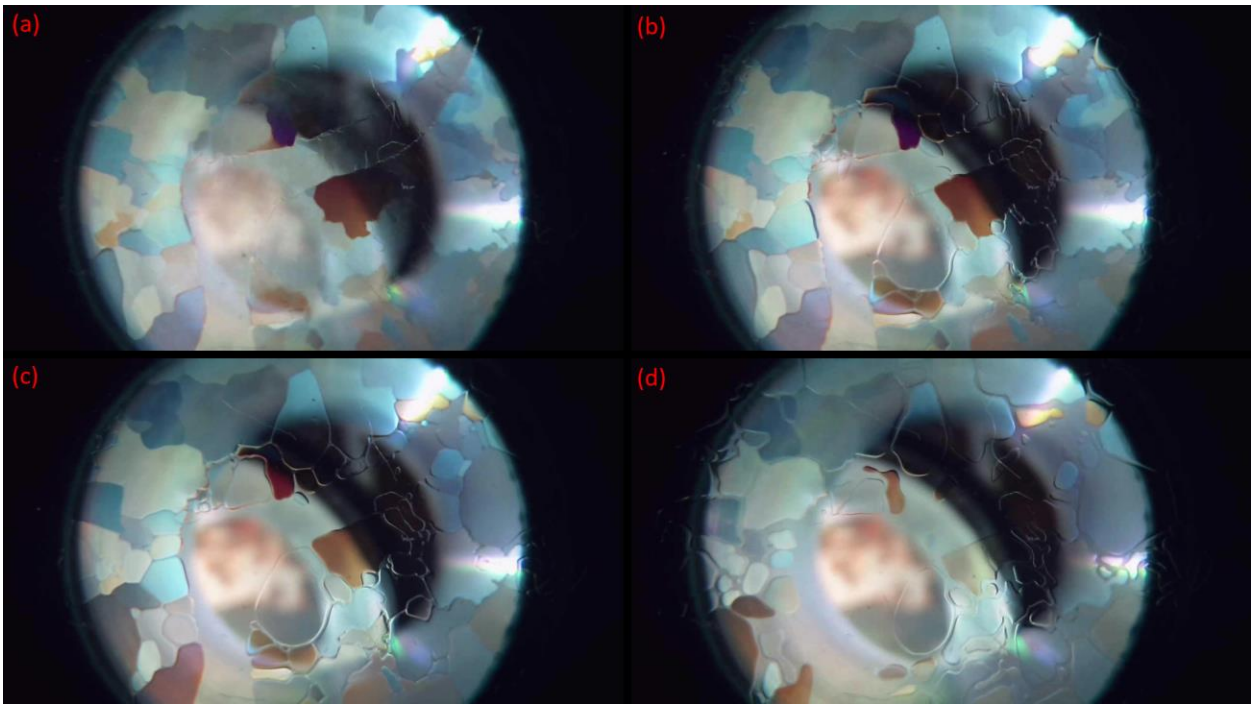

Figure 66 – (a) initial grain structure at 10 hours 20 minutes, (b) wet grain boundaries at 11 hours 48 minutes, (c) melting inwards at 14 hours 50 minutes, (d) melting top to bottom at 16 hours 28 minutes – Test 1.

Bulk pressure melting occurred when the entirety of the ice sample reached its melting point and began the phase change process. Melting began at the grain boundaries and was characterized by thinning along the boundaries creating a wet and transparent appearance. The grains then began to melt inwards, shrinking in size, causing them to break apart from each other. Smaller grains would continue to shrink until they completely transitioned into water. Larger grains would shrink until they melted completely from top to bottom. As the grains melted, they lost color under polarized light. As the grains detach from the larger sample, they began to move within the water, influenced by the high pressure.

5.6.2 Localized Pressure Melting

Localized pressure melting (LPM) refers to smaller scale, localized instances of melting which occurs due to the effect of localized pressure gradients on the melting point of ice. In high pressure zones, or areas of high pressure within the ice sample, the melting point dropped by up to -0.4°C

based on the Clausius-Clapeyron equation at a pressure of 5 MPa. Throughout the experiments, there were multiple incidents of observable local pressure melting. In most cases, this occurred in experiments in which pressure is applied at a 'warmer' temperature of 0°C. However, there were also instances in which pressure is applied at a cold temperature and LPM occurs once the ice sample had warmed up to near 0°C.

During all experiments in which pressure was applied at near 0°C, LPM was observed. After applying pressure, melting was induced locally as the ice already had enough heat energy that only small amounts of mechanical energy were needed to trigger phase change in the various localized areas of high pressure. This resulted in individual pockets of melt within the ice sample. Much of the ice remained as is, presumably due to these areas being under less local pressure. An example of LPM can be seen in Figure 67. In this case, after pressure is applied, pockets of melt formed around 30 minutes in. These continued to expand for approximately 2 hours.

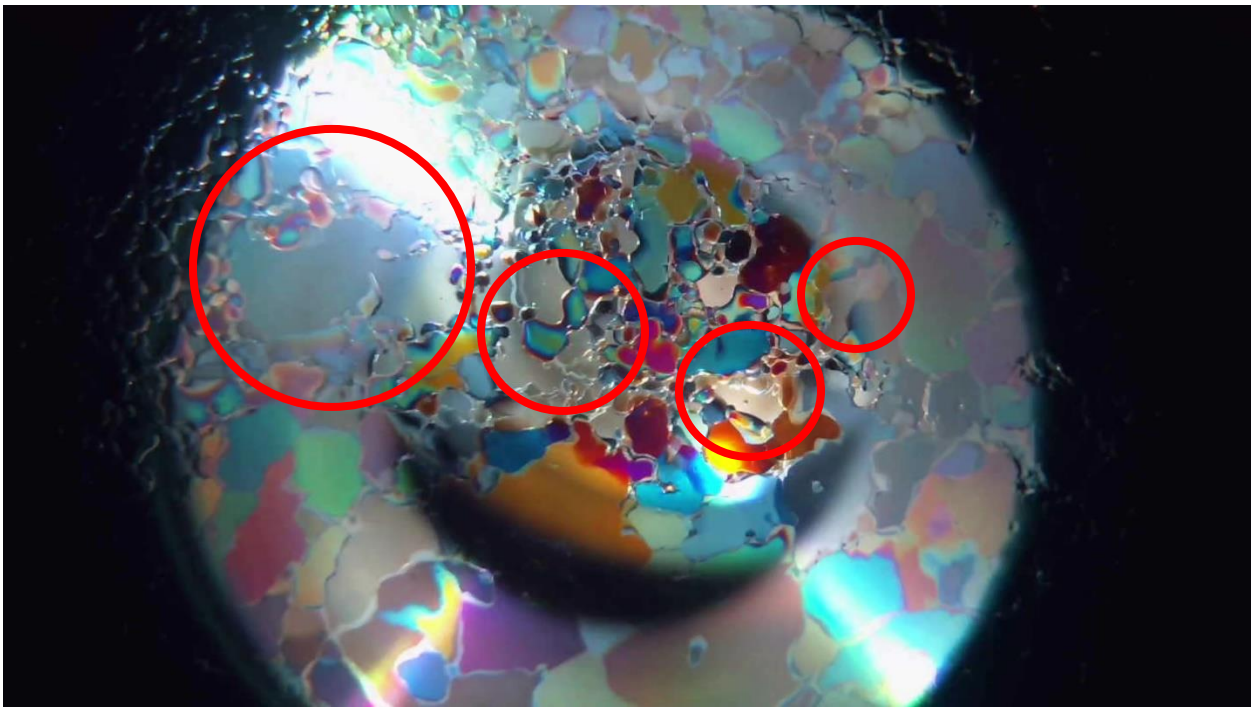

Figure 67 – Circled instances of localized pressure melting – Test 9 at 2 hours.

Following the instances of LPM, there was typically refreezing. That is, the growth of new ice crystals within the melt as well as the growth of surrounding grains into the melt. An example of this is circled in Figure 68. In this case, once the pool of water stopped expanding at the 2 hour and 30 minute-mark, the pool of melt slowly began to shrink as the surrounding grains started to refreeze and expand into the melt. At the same time, some of the small pieces of ice floating within the melt acted as nucleation sites for new ice crystals. These processes continued until all of the melt had turned back into solid ice around the 10-hour mark. The temperature of this experiment was at near 0°C and pressure at 6.2 MPa. These values remained consistent throughout the experiment, suggesting that the melting and refreezing were due to internal processes occurring in the ice sample rather than any external factors. It was likely that, by melting, the ice relieved itself of stress and pressure by diverting or redistributing it to other parts of the ice. Once the localized pressure dropped, the melting point and freezing point rose, and the water was able to freeze back into ice.

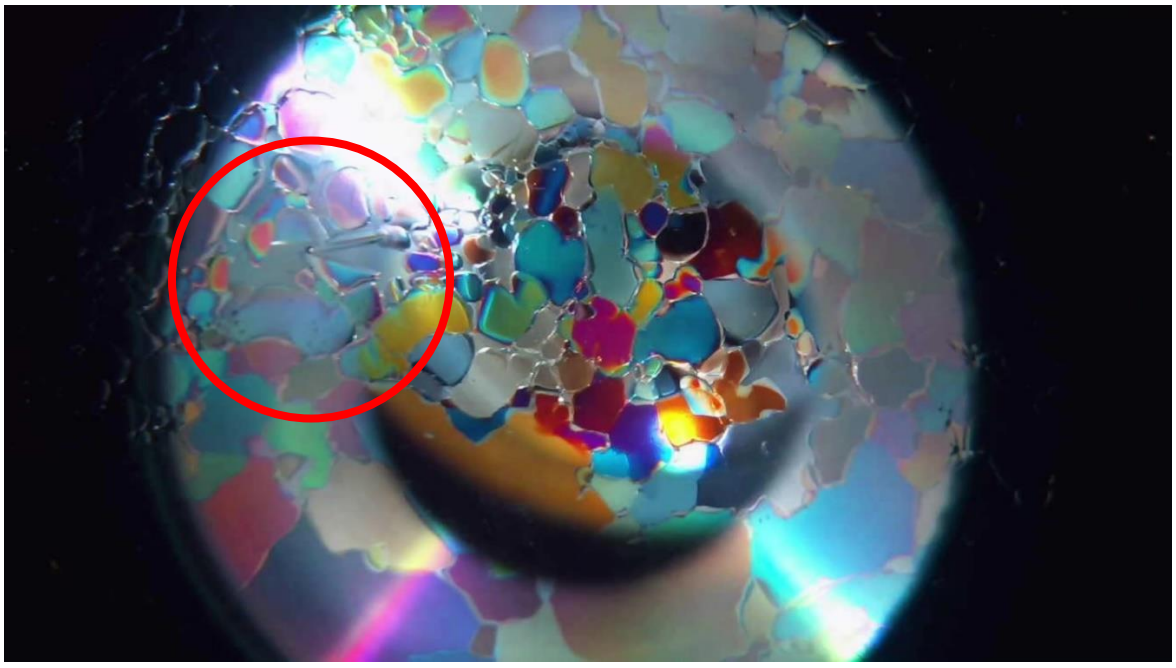

Figure 68 – Circled instance of refreezing and grain growth following LPM – Test 9 at 5 hours.

LPM was also seen in some cases in which pressure was applied at a cold temperature. In these instances, the temperature was slowly increased towards 0°C, crossing the lowered melting point created by localized areas of high pressure. This, again, resulted in small pockets of melt within the ice. This is seen in Figure 69. In this case, the pockets were much smaller than those in the warmer cases. Additionally, there was no observation of new ice crystals forming. Instead, the surrounding grains tended to expand into the pocket of melt.

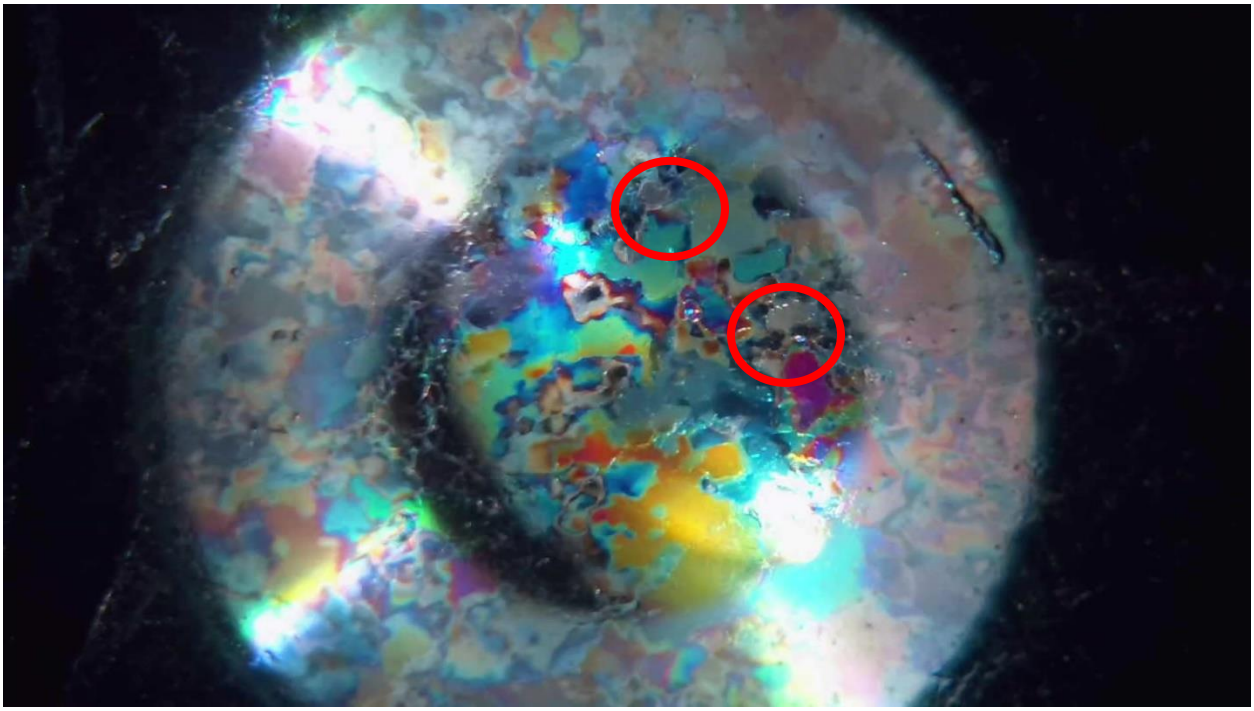

Figure 69 – Localized pressure melting. Temperature 0°C, Pressure 2MPa – Test 4 at 13 hours.

These instance of LPM were much less predictable compared to the previous examples. In these warming tests, by the time the temperature crossed the lowered melting point, the ice had already been under pressure for hours – meaning it had sufficient time to extrude, thin, crack, and develop a modified grain structure. This resulted in instances of relatively lower localized pressure as the sample was better able to distribute the applied stress – meaning that LPM would be less likely to occur. It was only in the test at 2 MPa where LPM was seen after heating. It is speculated that the lower pressure in this test had slowed the deformation of the ice – resulting in more localized areas

of higher pressure despite the lower applied stress. This may explain why LPM was seen in this instance; however, additional testing would be required in order to validate this speculation.

5.6.3 Overview of Observed Melting Processes

Overall, there were three different types of melting processes observed, all of which are illustrated in Figure 70. One type of melting which was observed is bulk pressure melting, which is illustrated in Figure 70 (b). This occurred when pressurized ice reached melting point and was unique in that melting began first along the grain boundaries. A second type of melting was bulk thermal melting, seen in Figure 70 (c), which refers to the specimen reaching its melting point and melting from the outside edges inward due to heat transfer from the apparatus. The final type of melting observed was localized pressure melting. This occurred when areas of high pressure formed within the sample, which caused the local melting point to drop in the preheated ice and melting to occur in small pockets. This is illustrated in Figure 70 (d).

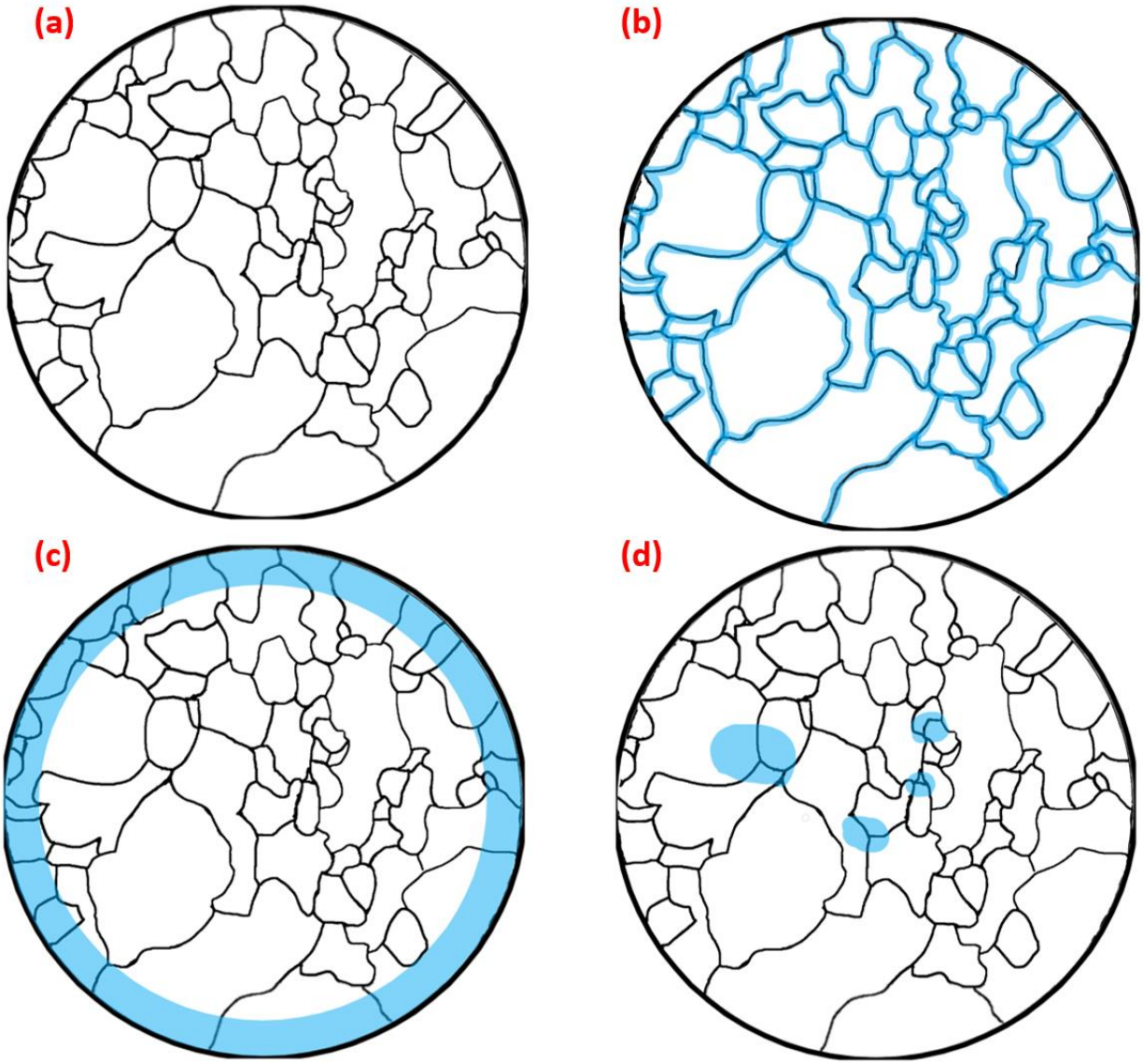

Figure 70 – Observed types of melting, where the blue highlights represent the melting. (a) is cold ice with no melting. (b) is Bulk Pressure Melting, in which pressurized ice reaches melting point and begins to melt along its grain boundaries. (c) is Bulk Thermal Melting, in which non-pressurized ice reaches its melting point and begins to melt at its sides due to heat transfer from the apparatus. (d) is Localized Pressure Melting, in which localized areas of high pressure causes small pockets of melt to form within the ice sample.

5.7 Bubbles

Bubbles are commonly seen throughout all experiments. Although the water was deaerated prior to freezing into the test samples, this did not eliminate all of the air in the sample. Furthermore, the process of smoothening the surface of the sample by melting it reintroduced air into the surface

of the sample. As a result, bubbles were commonly observed during testing. Figure 71 shows how bubbles were present along the surface of the ice sample.

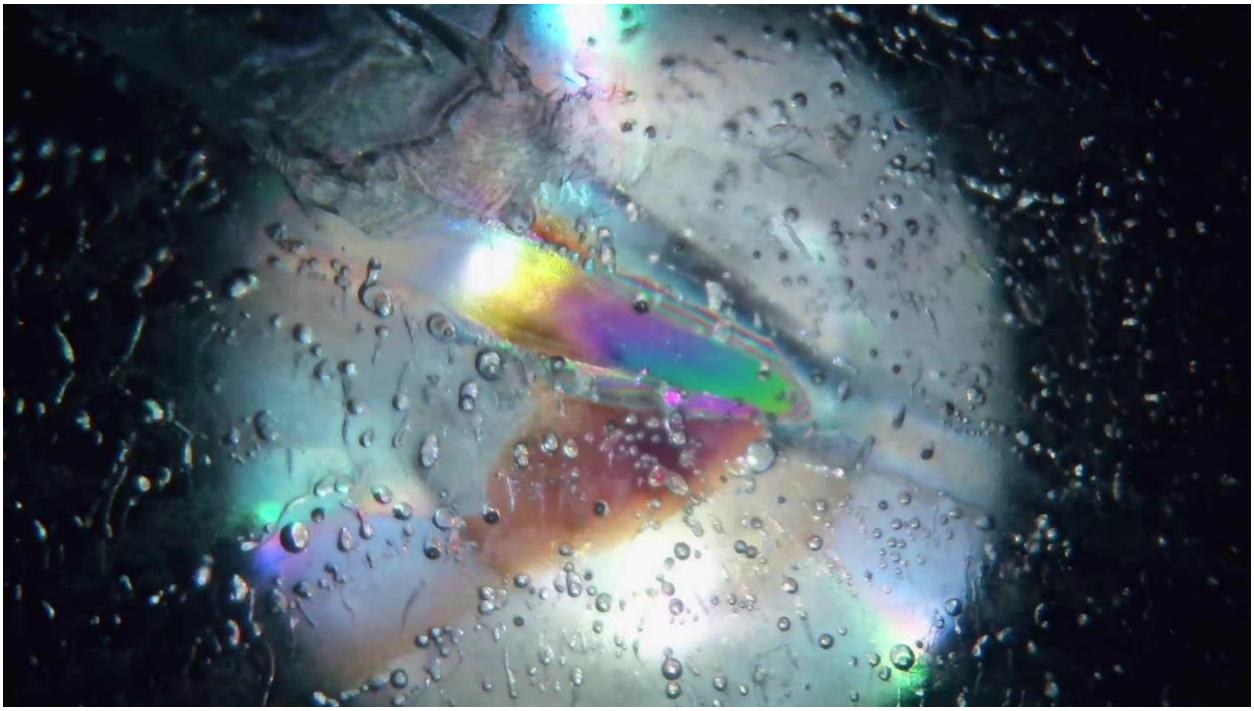

Figure 71 – Bubbles present at the surface of an ice sample prior to testing – Test 7.

During the fracture process, most bubbles were released into the newly formed cracks. This can be seen in Figure 72 when compared with the previous Figure 71. Here, the area in the top left, which had been compressed and fractured, was now devoid of bubbles. The area on the bottom right, which had not yet been affected by the pressure front still contained bubbles.

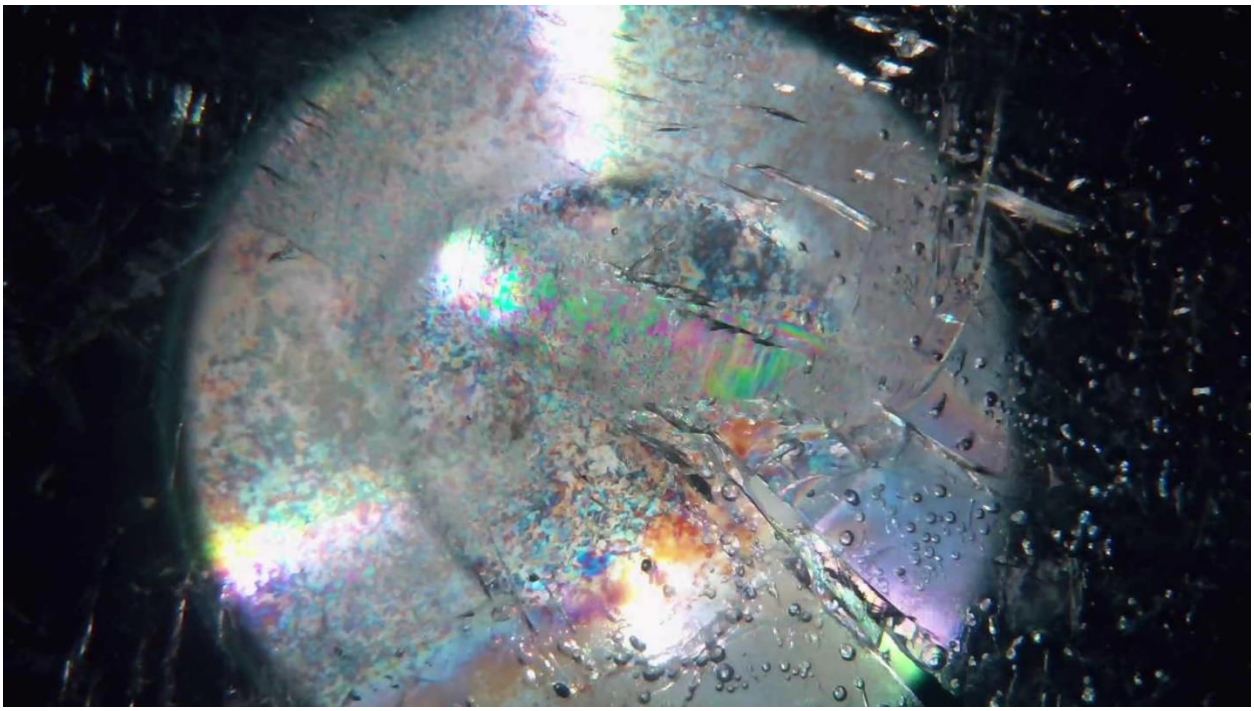

Figure 72 – Bubbles removed from ice in compressed/fractured area, while remaining in unaffected area – Test 7 at 1 hour.

Some interesting behaviour of bubbles was observed in instances of LPM. In these cases, as the ice melts, the bubbles trapped within the ice, seen in Figure 73 (a), were released into the pool of melt. Then, over time, the bubble began to shrink, seen in Figure 73 (b). Eventually, the bubble completely dissolved within the pool of melt, which can be seen in Figure 73 (c). Finally, as the ice refroze, the air was ejected from the melt solution, causing a bubble to re-form. This can be seen in Figure 73 (d).

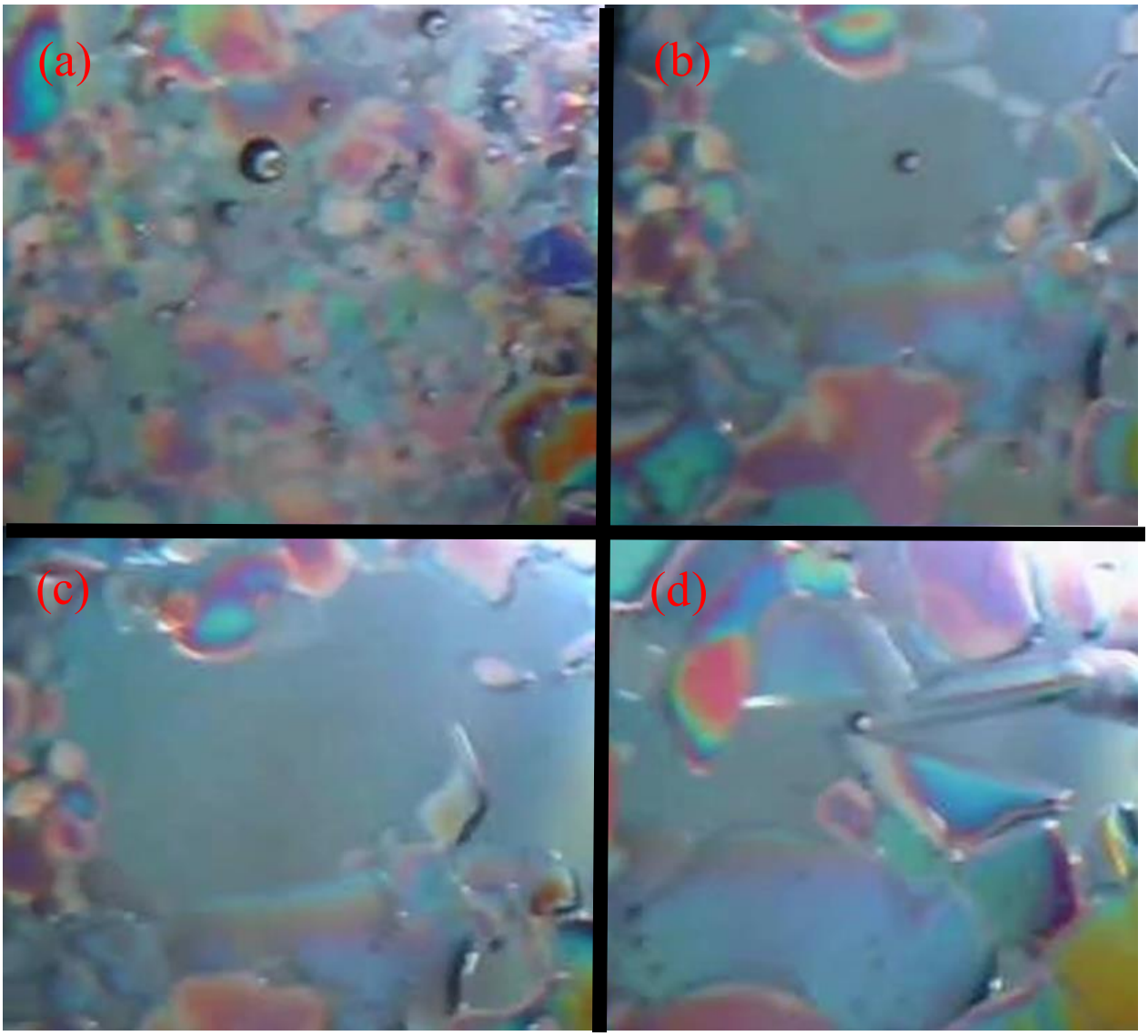

Figure 73 – (a) initial bubble prior to melt at 30 minutes, (b) bubble shrinking in pool of melt at 1 hour 30 minutes, (c) bubble completely dissolved in melt at 2 hours, (d) bubble re-forms as melt refreezes at 7 hours – Test 9.

5.8 Summary

Fourteen (14) tests in total were completed in order to observe the various processes which occur in ice under pressure in real-time. In ice which was at a temperature higher than -3°C, the general order in which the observed processes occur was as follows. First, within seconds of pressure application, cracking occurred throughout the specimen – followed by extrusion. Two types of

extrusion were identified: a radial type, pushing ice outwards away from a pressure concentration – and a linear type, pushing the entire sample in one direction which lasted for the majority of the experiment. Due to the applied pressure as well as the ongoing extrusion, the cracks healed over time. Within a minutes of pressure application, stress was visualized within the ice sample via the presence of color patches that formed in areas of high stress. Within 30 minutes, small grains began to nucleate in these areas of high stress. Generally, the areas of high stress changed throughout the experiment due to extrusion, grain nucleation, and melting. For approximately 8 hours, grain nucleation continued rapidly, with newly forming grains appearing larger over time. These new grains grew on top of one another – allowing little time for any individual grain to grow before it was overtaken by a newly formed grain. This process was driven by the presence of shear stress throughout the sample. Once the temperature of the ice became warmer than -3°C, grain boundary migration became the dominating process driving microstructural evolution while grain nucleation began to slow down and eventually stop. This ultimately resulted in a final grain structure consisting of relatively larger, randomly oriented, and irregularly shaped grains.

In some cases, localized pressure melting was directly observed, creating localized individual pools of melt in areas of high stress. These pools of melt, no longer under high stress, were either consumed by subsequent growth of neighbouring grains or refreezing to from a new fine-grained ice crystal. This happened only at temperatures close to the melting point and was mainly observed in cases in which pressure was applied to ice already near 0°C. This was because the sudden depression of the melting point following the application of pressure means that the warmer ice then had enough energy to undergo phase change without requiring additional heat from outside the apparatus. Also observed was the bulk pressure melting process in cases in which enough heat energy was allowed into the apparatus. In this case, the applied pressure was more uniform as

temperature was increased to 0°C, and melting begins along the grain boundaries and continues as each grain shrinks inward until melting completely.

The effect of temperature was also apparent throughout the experiments. At lower temperatures, many processes were slowed, such as grain nucleation and crack healing. Other processes, such as grain boundary migration, did not significantly occur. This was attributed to a higher activation energy required for many of these processes at colder temperatures, or due to the harder, less ductile properties of colder ice. This caused a greater resistance to extrusion, thereby causing a lower magnitude of shear stress, which was a primary driver of processes such as grain nucleation.

Finally, the behaviour of bubbles and air within the ice sample was discussed – showing how the air collected within cracks, escaped through deep cracks, or dissolved in melt.

Chapter 6: Discussion and Conclusion

6.1 Summary and Conclusion

Small scale ice compression tests were conducted using a custom designed apparatus to observe the different transformative processes that occur in highly compressed ice. The main objectives of this research were to identify, observe, and understand the processes which work to develop the ice and its grain structure under a compressive load. This includes processes such as dynamic recrystallization, pressure melting, and related processes.

To produce the ice sample, distilled, deionized, and deaerated water was placed directly into the apparatus and placed into a freezer for 24 hours. This ice was then flattened by melting the top surface using polished aluminum. The apparatus was placed in a deep freezer and pressure was applied using a hydraulic pump. A load cell and temperature probes recorded the force and temperature respectively. Tests were roughly 24 hours in length, with a constant nominal pressure of 5 MPa, and specified temperature profiles. A borescope camera was used to record the ice

throughout the test. This allowed for observation of the various processes that occurred in the ice microstructure throughout the experiment.

Throughout this research program fourteen (14) tests were completed. Due to delays resulting from cold room issues, the length of each test, the prep time required to create a single sample, as well as limitations and laboratory availability, it was not possible to do additional tests. The implications of this research, all of which is summarized below, can be used to improve analytical models. This is because many models are phenomenological that model properties as a function of temperature, pressure, or rate, without direct consideration of the evolution of the microstructure. This new information opens new avenues for linking changes in ice material behaviour to the underpinning physical mechanisms.

6.1.1 Observation of Dynamic Recrystallization

Dynamic recrystallization, primarily observed as a result of grain nucleation and grain boundary migration, was directly observed under various conditions. At colder temperatures below -3°C, and mainly for the first half of test, grain nucleation is the dominant recrystallization process. During grain nucleation, new grains continuously form on top of one another – meaning that no single grain exists for long enough to undergo sustained grain growth. Grain nucleation occurs in direct response to applied stress on the ice. Over time, nucleation naturally slowed until it became a rare occurrence around 8-12 hours into the experiment. Temperature also influenced this process, resulting in slower recrystallization rates at colder temperatures. Once the ice reached a temperature of approximately -3°C, grain boundary migration became the dominant recrystallization process, resulting in fewer, larger grains. As the temperature approached the melting point, this process of grain growth accelerated.

6.1.2 Observation of Grain Boundary Development

There are three phenomena directly observed in the grain boundaries. Firstly, grain boundaries became more pronounced and apparent following grain boundary migration, which works to create larger, more distinct grains. The grains and their boundaries formed by this process were irregularly shaped. Second, when bulk melting occurred for apparatus temperatures above 0°C and pressures greater than atmospheric, all grain boundaries begin to melt first, appearing transparent and wet. Finally, discoloration was often seen along grain boundaries, suggesting some angularity (non-orthogonal) of the grain boundaries, and resulting in two overlapping grains in these areas.

6.1.3 Observation of Cracking, Time Dependent Cracking, and Crack Healing

Cracking, time dependent cracking, and crack healing were all directly observed. Cracking occurred in every test within the first several seconds of the pressure being applied. At cold temperatures, the cracks appeared to be long and deep into the specimen. At warmer temperatures, closer to melting point, the cracks were thin and shorter in length. If the ice surface was not flat, a natural high-pressure zone was created, causing the ice to fracture catastrophically, which resulted in a dense network of micro cracks.

In cases where pressure was applied to ice that had been warmed to very close to 0°C, the cracks were slower to form and occurred over time frames of a few minutes, which is referred to as time dependent cracking. This was the case for warm crack formation on flat specimens, as well as cracking in warm ice caused by a high-pressure zone. This time dependent cracking was likely the result of the ice being warmer and more ductile as it approaches the melting point. This allowed the ice to better redistribute the applied stress and delayed the fracturing process. Time dependent cracking was also observed for cold ice tests at around -15°C, but in this case, cracking occurred

over 15 minutes, likely due to the colder ice being less prone to dislocation motion, resulting in long times for sufficient dislocation pile up to trigger cracking.

Crack healing was also observed in all testing cases. This was driven by compressive forces on the ice and was observed to correspond with extrusion events as well as melting. Crack healing was observed to occur slowly over hours for colder temperature ice and the rate of healing speeds up as the temperature increases. In cases where pressure was applied at melting point, cracks healed within seconds of forming. In some cases, pressure melting causes the crack to fill with melt and quickly refreeze, thereby healing it.

6.1.4 Observation of Extrusion Events

Extrusion events were observed during all tests. After the application of pressure, two types of extrusion were seen. The first is referred to as 'linear' extrusion, in which the ice specimen was slowly pushed in one direction for the entirety of the test. This is believed top be driven by some initial unevenness in the specimen. The seconds is 'radial' extrusion, in which the ice was locally pushed radially, outward from a point of pressure concentration. Radial extrusion was observed to typically only last for a period of time (1-2 hours) before stopping completely.

In some cases, when bulk melting began, the linear extrusion of the ice sample accelerated and slightly changed direction. Extrusion appeared to occur faster at warmer temperatures, with almost no extrusion occurring during the cold tests. This is possibly due to some accumulation of pressure melt at the interface between the glass and the specimen, which resulted in a lubricated layer that promoted extrusion. The extrusion observed is associated more with continuous creep deformation rather than the flow of crushed ice.

6.1.5 Observation of Bulk and Pressure Melting

Both bulk thermal melting and pressure melting were observed during testing. Bulk thermal melting occurred when the apparatus temperature exceeded 0°C and the entirety of the sample reached its natural unconfined melting point. Bulk pressure melting begins at the grain boundaries and continues until the ice fully changed phase into liquid water, which is distinctly different than both localized pressure melting and bulk thermal melting.

Localized pressure melting occurred on a much more localized, smaller scale in areas of locally high pressure. In these areas, the melting point was lowered such that these areas have enough energy to melt, which ultimately resulted in pockets of melt forming within the sample. These pockets of melt either formed new metastable ice crystals, which grew until the melt disappears, or disappeared when the surrounding grains grew into the melt. This resulted in a process of LPM-induced recrystallization of the ice. This behaviour was only seen when the ice was very close to 0°C and was more apparent in cases where pressure was applied on warm ice versus when pressure was applied on cold ice and the temperature was then raised to the melting point. This is different than bulk melting in that only small portions of the ice melt, that it originates from points of high pressure, and that other characteristics that denote bulk melting, such as transparent grain boundaries, are not present. Moreover, bulk melting exists directionally and is indicative of heat transfer, which is notably absent during localized pressure melting.

6.1.6 Observation of Entrained Bubble Behaviour

The behaviour of entrained bubbles was observed during testing. Generally, air bubbles frozen into the ice sample were released once these areas are placed under pressure due to cracking. In some cases, air was observed to dissolve into the pressurized melt, but that dissolved air was eventually

released when that melt refreezes during cycles of pressure melting and refreezing, which caused bubbles to reform within the ice.

6.2 Recommendation for Future Work

Real-time observation of compressed ice is now possible using the specially designed apparatus presented in this thesis. Modifications of this apparatus could allow for a plethora of new types of observations and additional methods of data collection.

Tests which maintain constant temperature can be conducted in order to better compare these processes at different temperatures. For example, tests could be completed at -20°C, -10°C, -5°C, -2.5°C, and 0°C. This would prove useful in providing additional insights into processes, such as grain boundary migration, at different temperatures. It would also provide an opportunity to estimate the speed at which processes such as extrusion, grain nucleation, and crack healing occur as a function of temperature and pressure.

The current apparatus is designed to withstand 15 MPa, however, the hydraulic hand pump used was only able to consistently output 5 MPa for a full test. By improving the capacity of the hydraulic system, higher pressures could be applied to ice samples in fracture tests. This would be useful in more broadly studying the conditions under which localized pressure melting occurs. It may also allow for easier observation of localized pressure melting by expanding the range of temperature under which this process can occur. A higher-pressure capacity and better pressure control would also allow for tests in which pressure is increased at specific intervals or at key moments in the melting process in order to observe the effect that this has on the ice sample during dynamic loading.

A linear variable differential transformer (LVDT) should also be installed on the bottom portion of the apparatus to measure the gap length, and therefore the evolving thickness of the ice sample, while it is being compressed. This would provide better extrusion data, as the amount of material within the testing area could be estimated if the change in gap height is known. An inline load cell that directly measures the indentation force acting on the glass could also offer better measurement accuracy.

Using a similar design to apply pressure to an ice sample while observing it under polarized light, it could also be possible to modify the top and bottom portion of the apparatus as well as the pressure applicator to allow for the application of shearing loads to the ice sample. This would allow for direct, real-time observation of ice under continued pressure and shear. Thus, processes such as dynamic recrystallization can be observed in ice under shear and compared with the results from this study.

Additional analysis can be conducted on the video and data gathered throughout this research program. Utilizing Python code, dimensionless parameters could be generated to generalize results and create a dataset which future work could be added to. For example, the rate of recrystallization or a comparison of crack length between samples at different conditions could be analyzed using these methods.

Through continued experiments as discussed above, a deeper understanding of how ice behaves under compression can be gained, which will ultimately improve the ability to model ice loads, and account for the contributions of important processes such as dynamic recrystallization and local pressure melting to ice behaviour.

Bibliography

Barnes, P., & Tabor, D. (1966). Plastic Flow and Pressur eMelting in the Deformation of Ice I. *Nature, 210*(5039), 878-882.

Barrette, P. D., & Jordaan, I. J. (2003). Pressure-temprature effects on the compressive behaviour of laboratory-grown and iceberg ice. *Cold Regions Science and Technology, 36*, 25-36.

Burg, J. P., Wilson, C. J., & Mitchell, J. C. (1986). Dynamic recrystallization and fabric development during the simple shear. *Journal of Structural Geology*, 857-870.

Chauve, T., Montagnat, M., & Vacher, P. (2015). Strain field evolution during dynamic recrystallization nucleation; A case study on ice. *Acta Materialia*, 116-124.

Duval, P., & Castelnau, O. (1995). Dynamic Recrystallization of Ice in Polar Ice Sheets. *Journal De Physique, 5*, 197-205.

Duval, P., Ashby, M. F., & Anderman, I. (1983). Rate-controlling processes in the creep of polycrystalline ice. *Journal of Physical Chemistry*, 4066-4074.

Fan, S., Prior, D. J., Cross, A. J., Goldsby, L. D., Hager, F. T., Negrini, M., & Qi, C. (2020). Using grain boundary irregularity to quantify dynamic recrystallization in ice. *Acta Materialia*, 1-22.

Frederking, R., Jordaan, I. J., & McCallum, J. S. (1990). Field Tests of Ice Indentation at Medium Scale Hobson's Choice Ice Island. *Proceedings of the 10th International Symposium on Ice.* Espoo.

Gagnon, R. (2002). Can Dynamic Recrystallization and Bulk Pressure Melting Explain Characteristics of Ice Crushing? *Ice in the Environment: Proceedings of the 16th IAHR International Symposium on Ice.* Dunedin.

Gagnon, R. E. (1998). Analysis of visual data from medium scale indentation experiments at Hobson's Choice Ice Island. *Cold REgions Science and Technology, 28*, 45-58.

Gagnon, R. E., & Sinha, N. K. (1991). Energy dissipation through melting in large scale. *Proc. of the 10th International Confernece on Offshore MEchanics and Arctic Engineering.* Stavanger.

Gagnon, R. E., & Tulk, C. A. (2019). Evidence for Tyndall melt-figure production during spallation-induced. *Cold Regions Science and Technology*.

Jordaan, I. J. (2001). Mechanics of ice-structure interaction. *Engineering Fracture MEchanics, 68*, 1923-1960.

Jordaan, I. J., Matskevitch, D. G., & Meglis, I. L. (1999). Disintegration of ice under fast compressive loading. *International Journal of Fracture, 97*, 279-300.

Jordaan, I. J., Wells, J., Xiao, J., & Derradji-Aouat, A. (2008). Ice crushing and cyclic loading in compression. *19th IAHR Symposium on Ice,.* Vancouver, British Columbia, Canada.

Li, C., Barrette, P., & Jordaan, I. (2004). High Pressure Zones at Different Scales During Ice-Structure Indentation. *23rd International Conference on Offshore Mechanics and Arctic Engineering.* Vancouver.

Lockett, F. J. (1972). *Nonlinear Viscoelastic Solids.* London and New York: Academic Press.

Mackey, T., Wells, J., Jordaan, I., & Derradji-Aouat, A. (2007). Experiments on the Fracture of Polycrystalline Ice.

Meglis, I. L., Melanson, P. M., & Jordaan, I. J. (1999). Microstructural change in ice: II. Creep behavior under triaxial stress conditions. *Journal of Glaciology, 45*(151).

Mellor, M. (1983). Mechical behaviour of sea ice. *U.S. Army Cold Region Research and Engineering Lab, Honover, CRREL Report 83-1.*

Nordell, B. (1990). Measurement of a P-T coexistence curve for ice-water mixture. *Cold Regions Science and Technology,*, 83-88.

Poirier, J. P., & Guillope, M. (1979). Dynamic recrystallization during creep of single-crystalline halite: An experimental study. *Journal of Geophysical Research*, 5557-5567.

Schapery, R. A. (1997). Nonlinear viscoelastic and viscoplastic constitutive equations based on thermodynamics. *Mechanics of Time-Dependent Materials*, 209-240.

Schulson, E. M., & Duval, P. (2009). *Creep and Fracture of Ice.* Cambridge: Cambridge University Press.

Shokr, M., & Sinha, N. K. (2023). Laboratory Techniques for Revealing the Structure of Polycrystalline Ice. In M. Shokr, & N. K. Sinha, *Sea Ice: Physics and Remote Sensing* (pp. 231-255). John Wiley & Sons, Inc.

Sinha, N. K. (1989). Elasticity of natural types of polycrystalline ice. *Cold Regions Science and Technology 17*, 127-135.

Taylor, R. (2010). *Analysis of Scale Effect in Compressive Ice Failure and Implications for Design.* St. John's, NL, Canada: Memorial University of Newfoundland.

Technical Glass Products. (2022). *Presssure Calculations*. Retrieved from Techncial Glass Products: https://technicalglass.com/pressure-calculations/

Wilson, C. J. (Director). (1985). *Dynamic Processes in shear of ice as a rock analogue* [Motion Picture]. Australia.

APPENDIX A - Test Results: Applied Pressure and Temperature during Testing

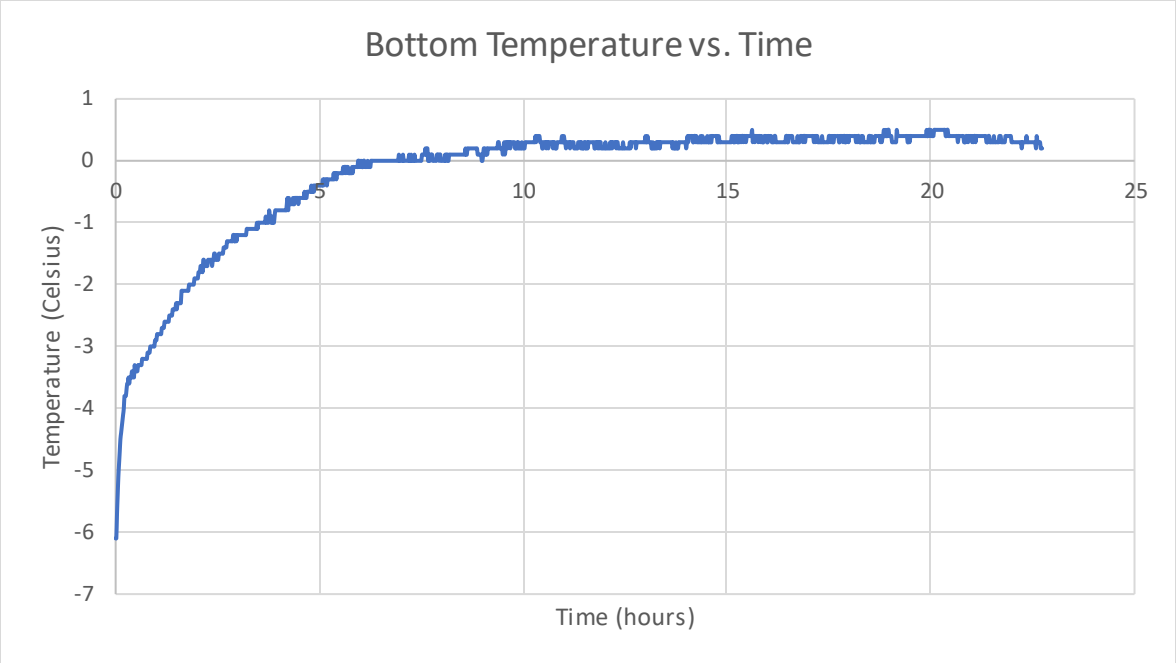

Figure A1 - Test 1: Temperature plot

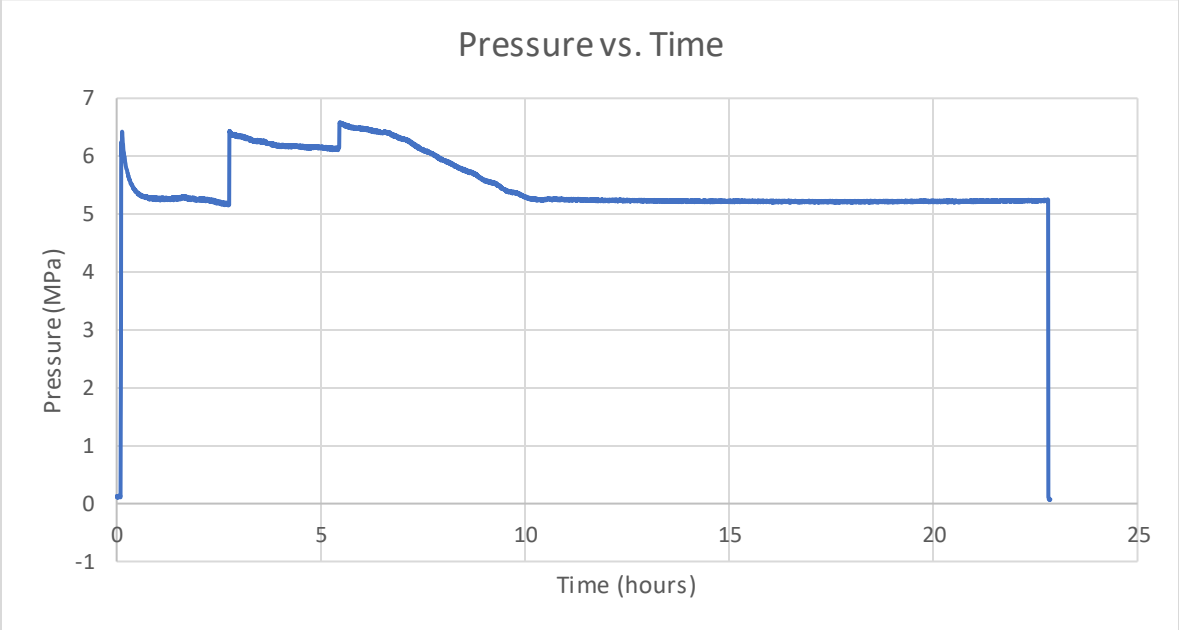

Figure A2 - Test 1: Pressure plot

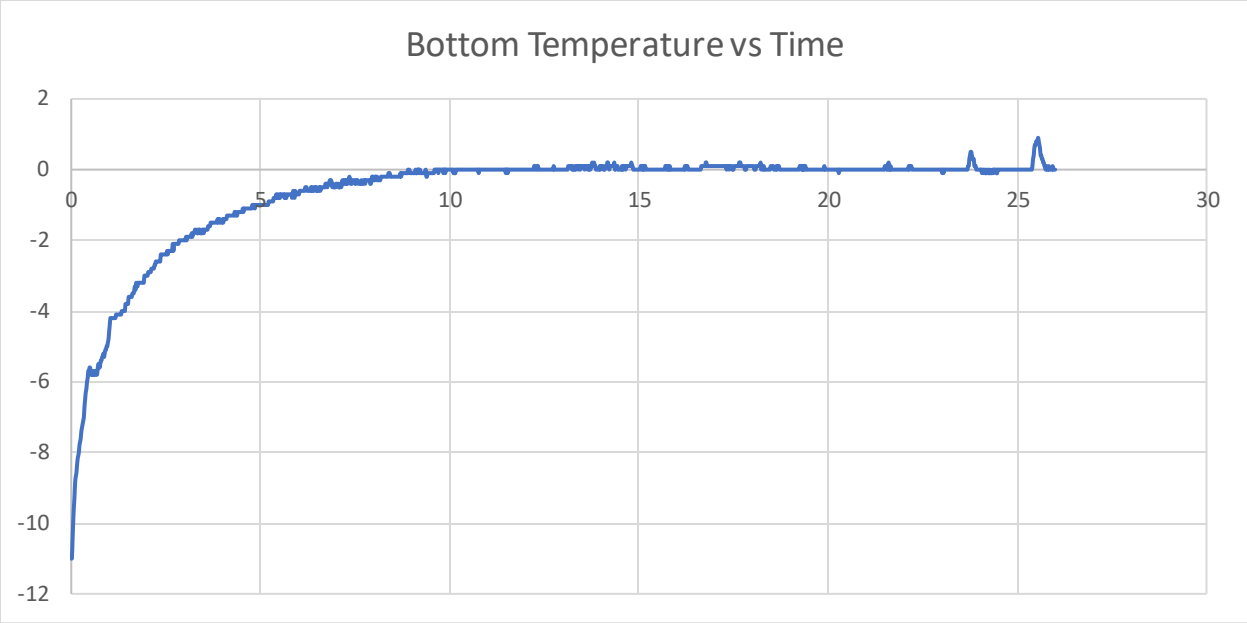

Figure A3 - Test 2: Temperature plot

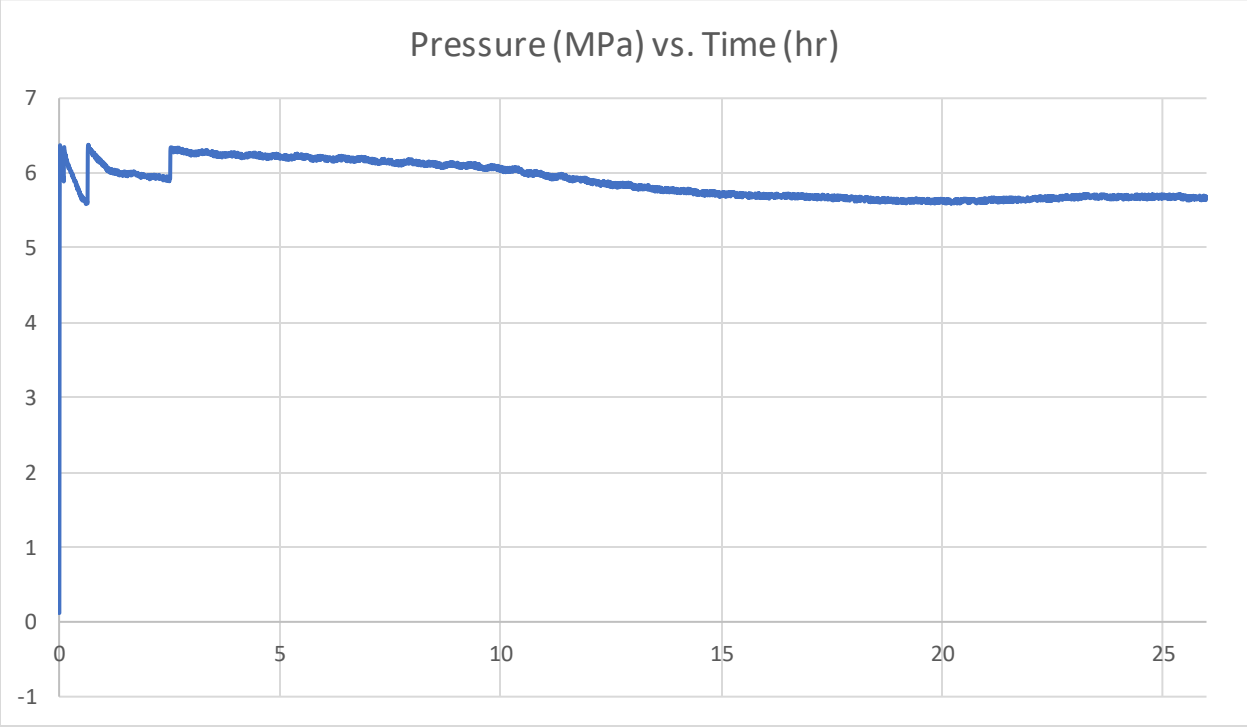

Figure A4 - Test 2: Pressure plot

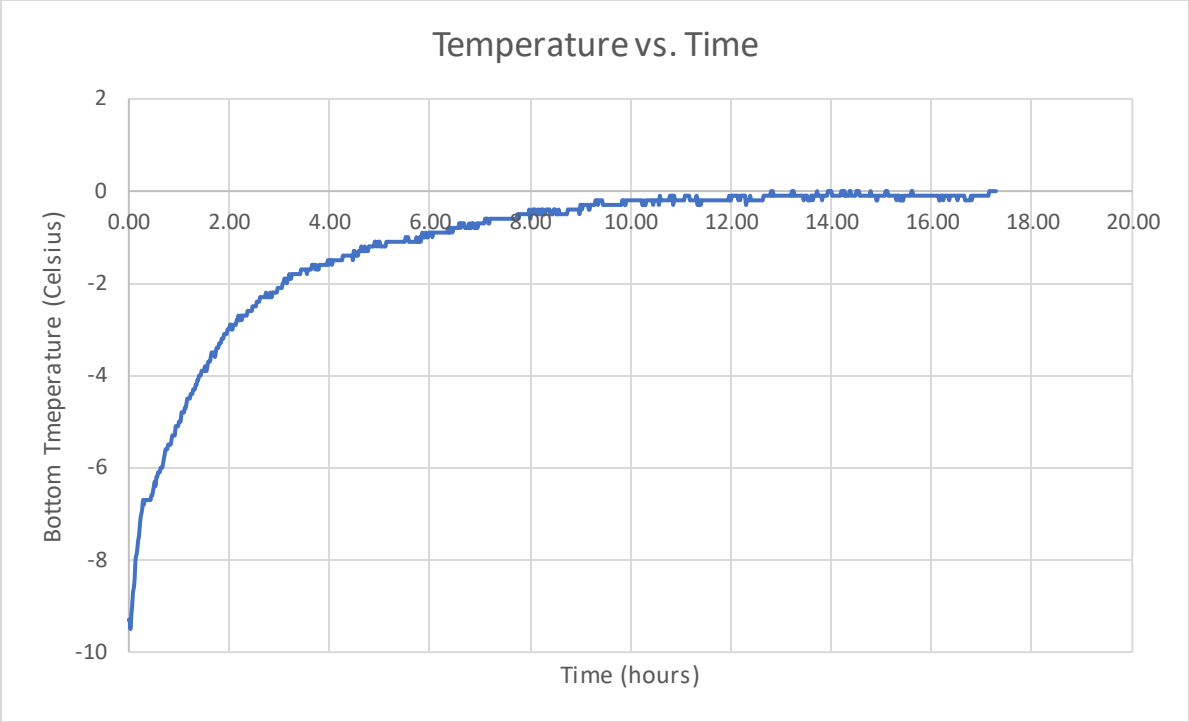

Figure A5 - Test 3: Temperature plot

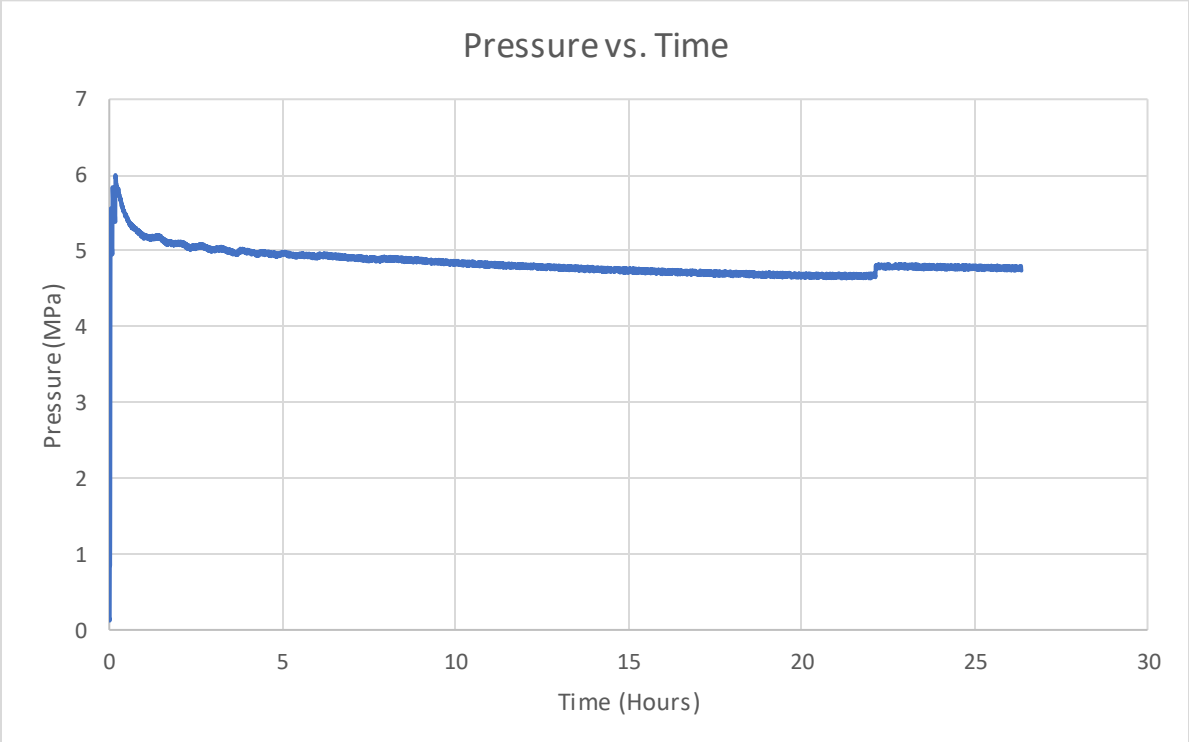

Figure A6 - Test 3: Pressure plot

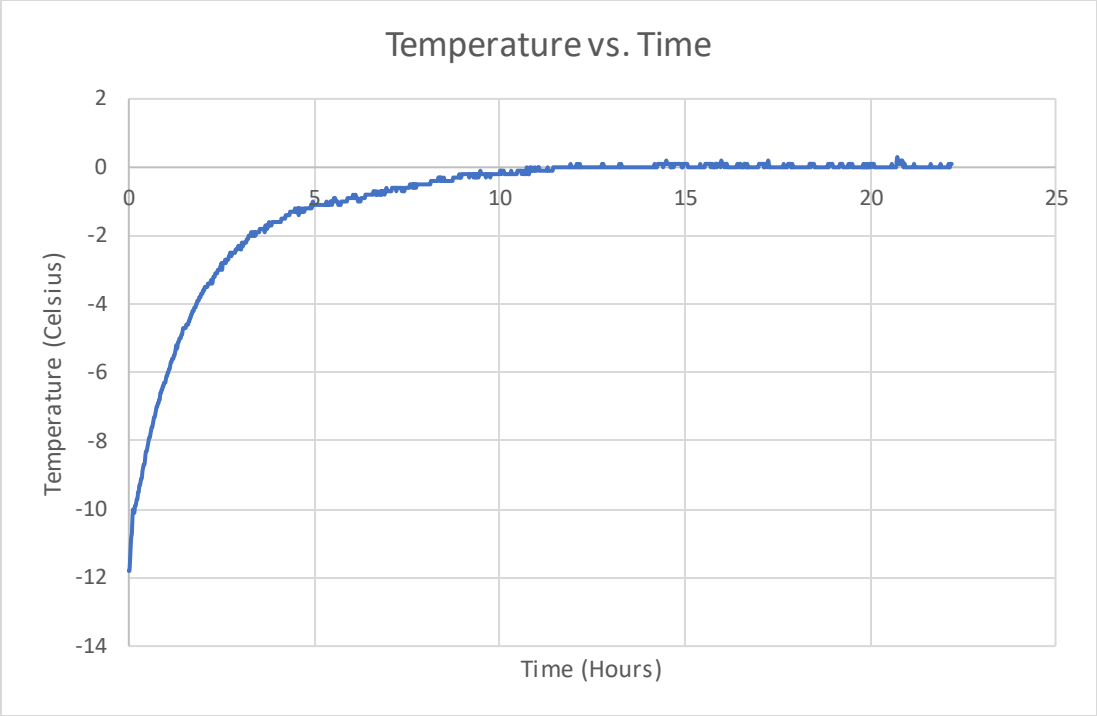

Figure A7 - Test 4: Temperature plot

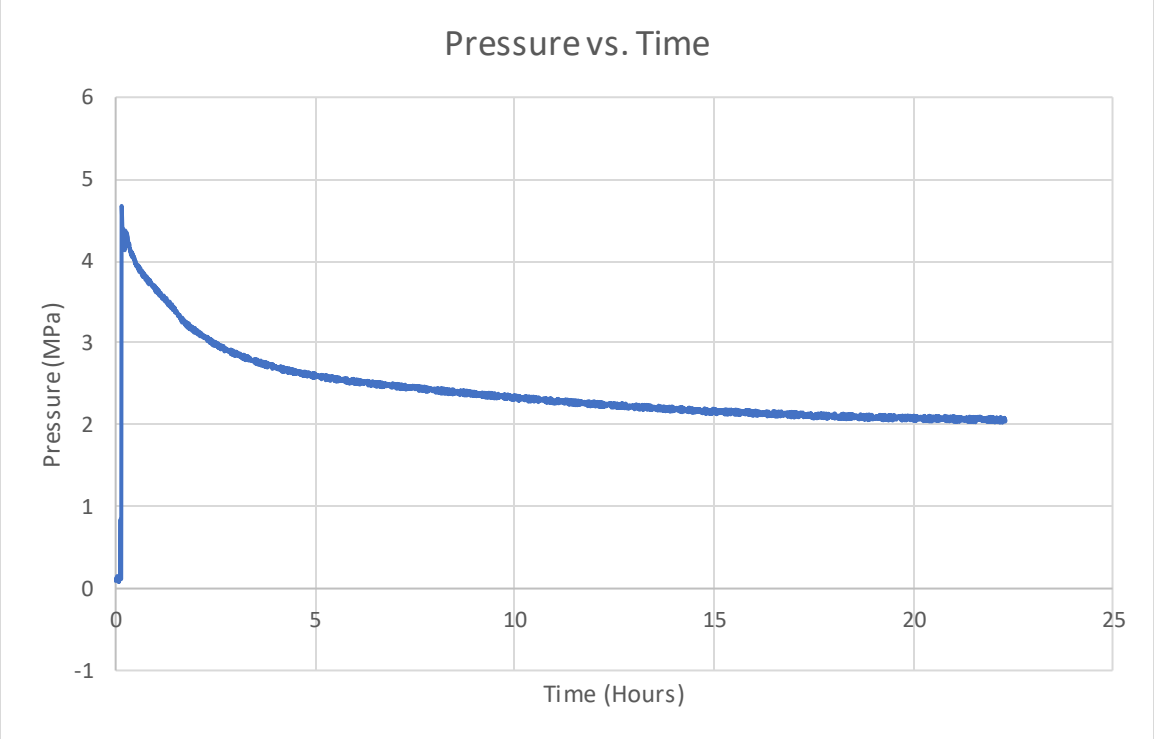

Figure A8 - Test 4: Pressure plot

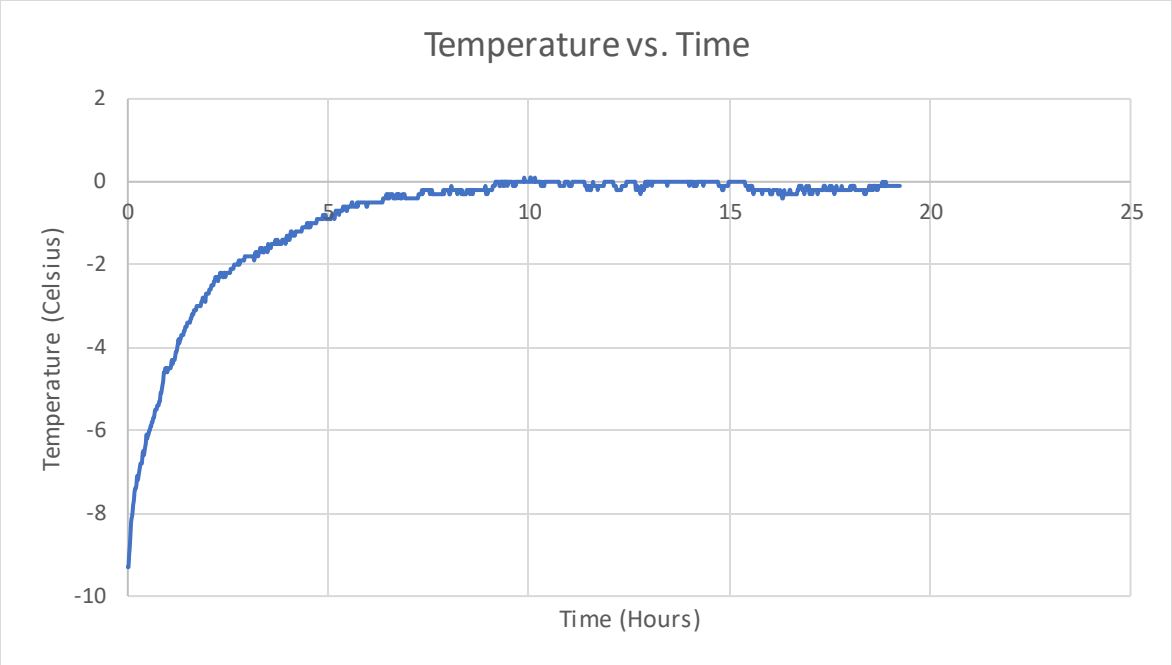

Figure A9 - Test 5: Temperature plot

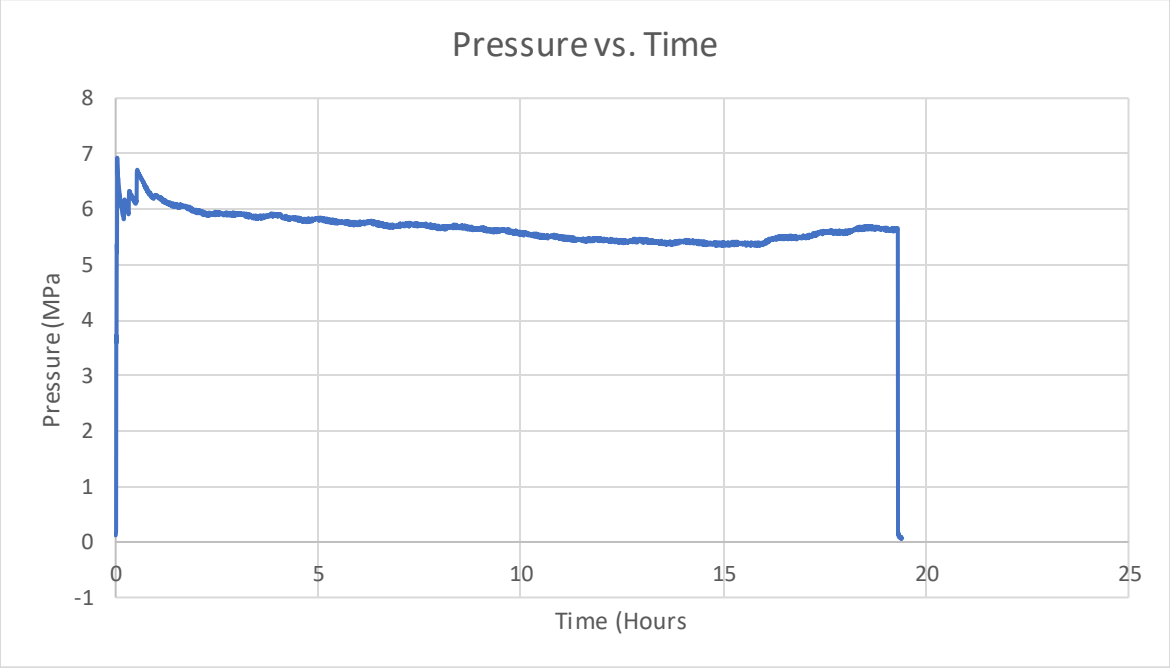

Figure A10 - Test 5: Pressure plot

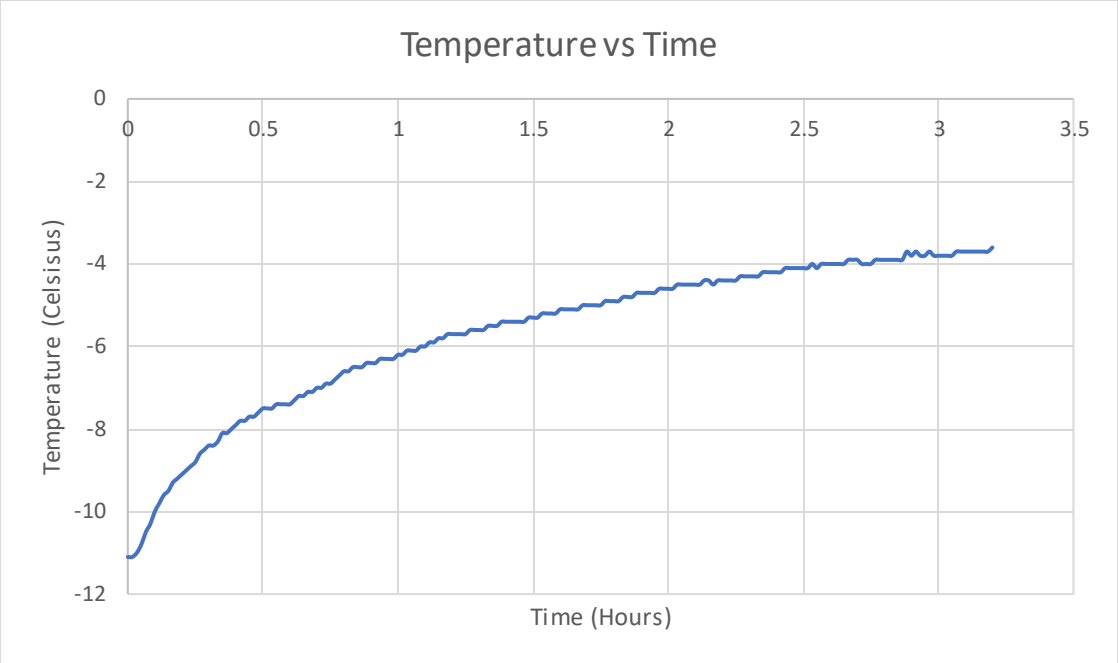

Figure A11 - Test 6: Temperature plot

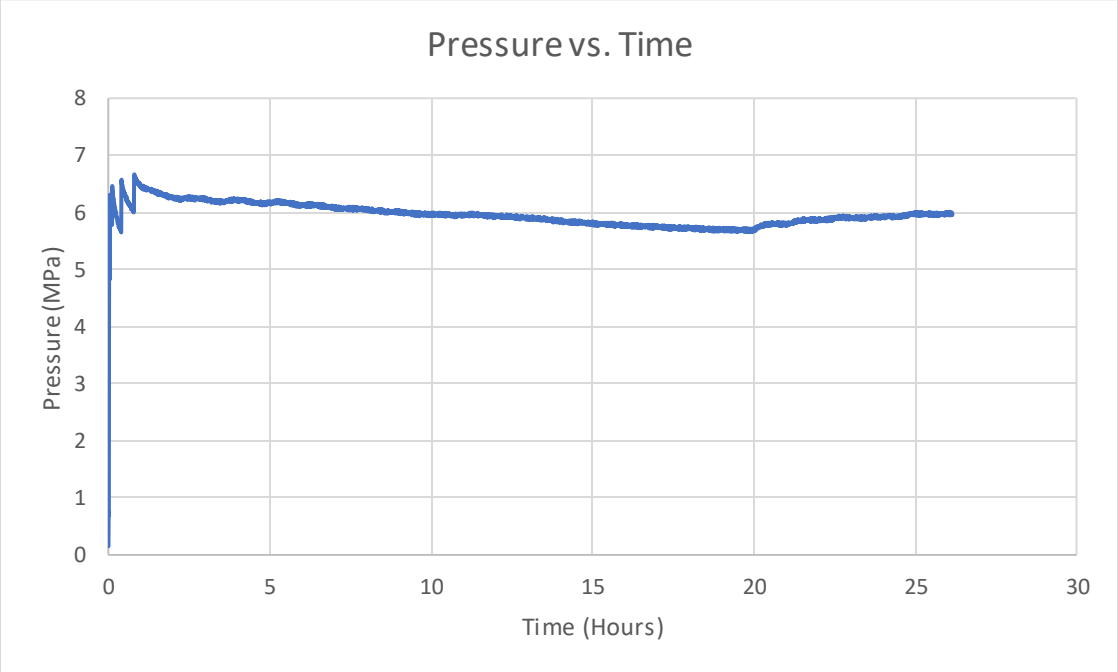

Figure A12 - Test 6: Pressure plot

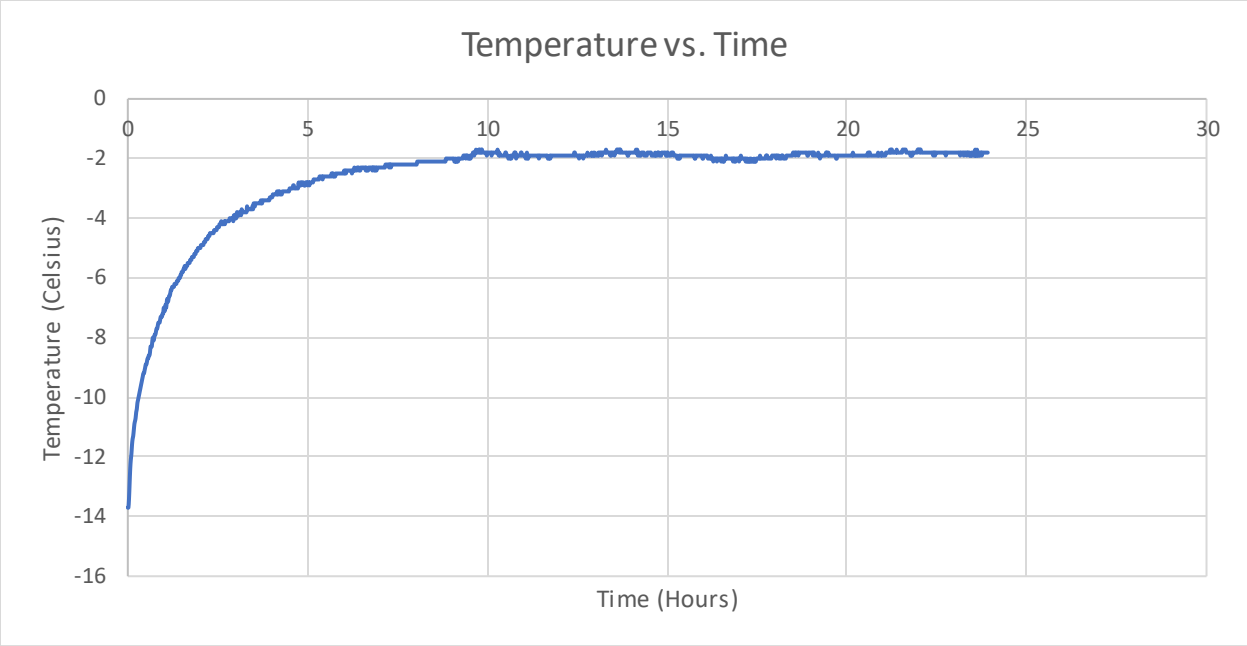

Figure A13 - Test 7: Temperature plot

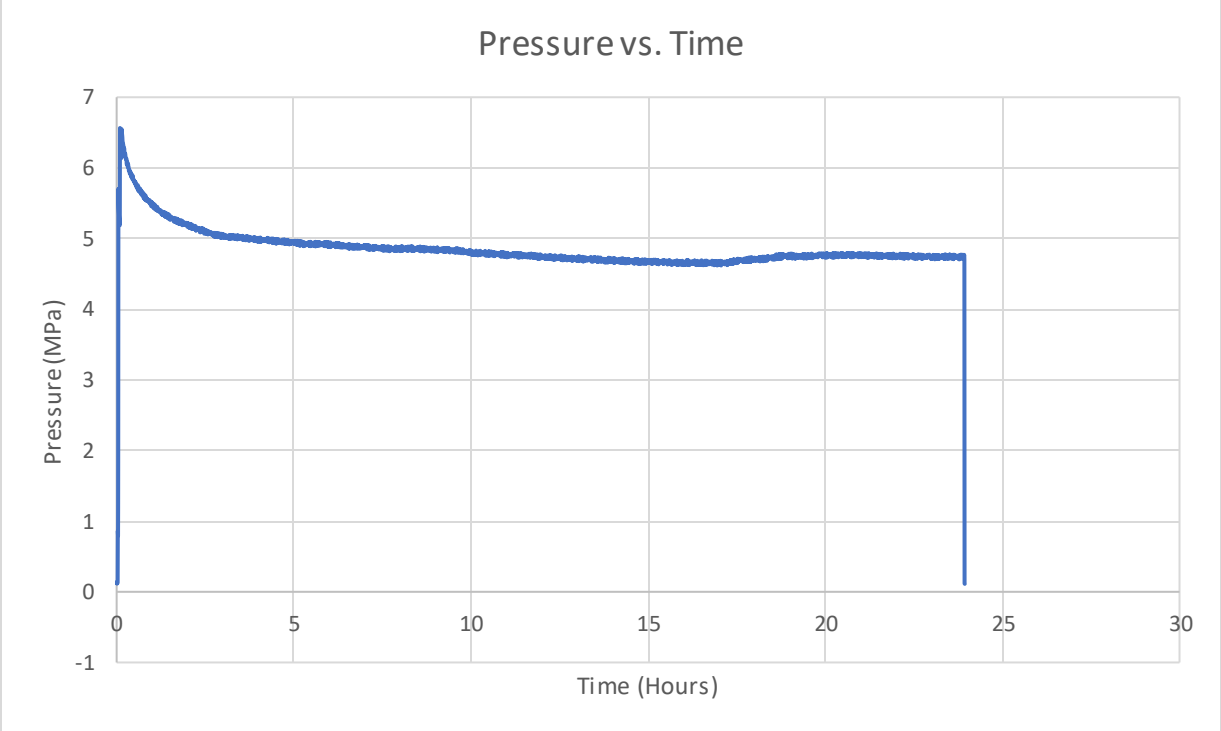

Figure A14 - Test 7: Pressure plot

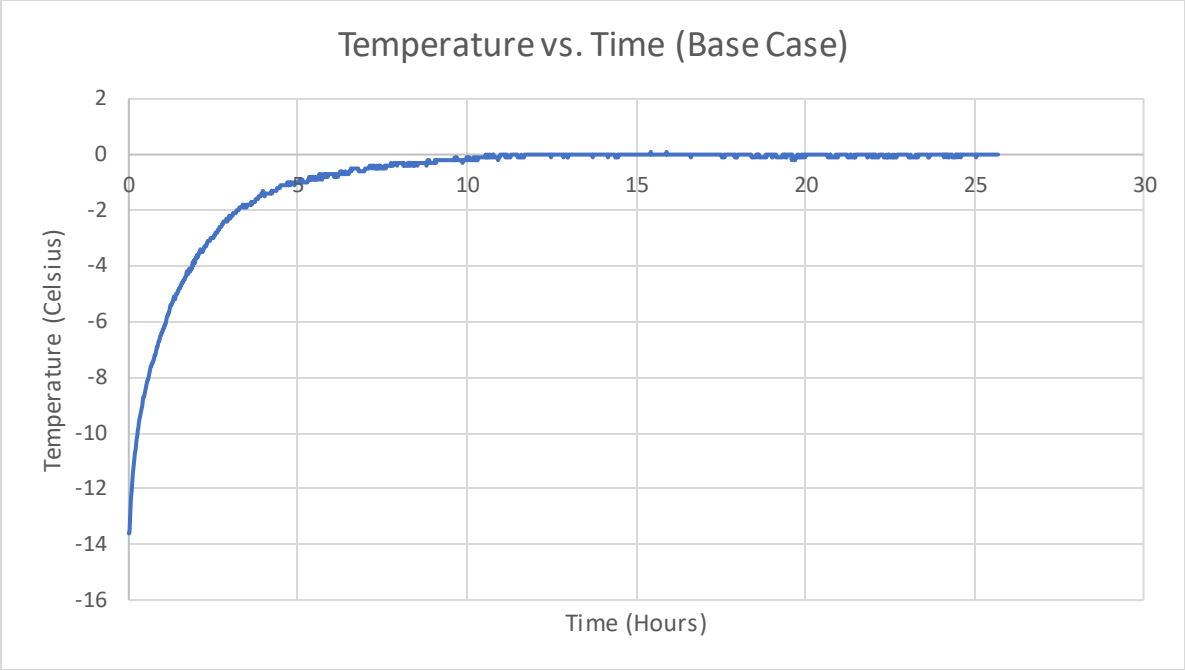

Figure A15 - Test 8: Temperature plot

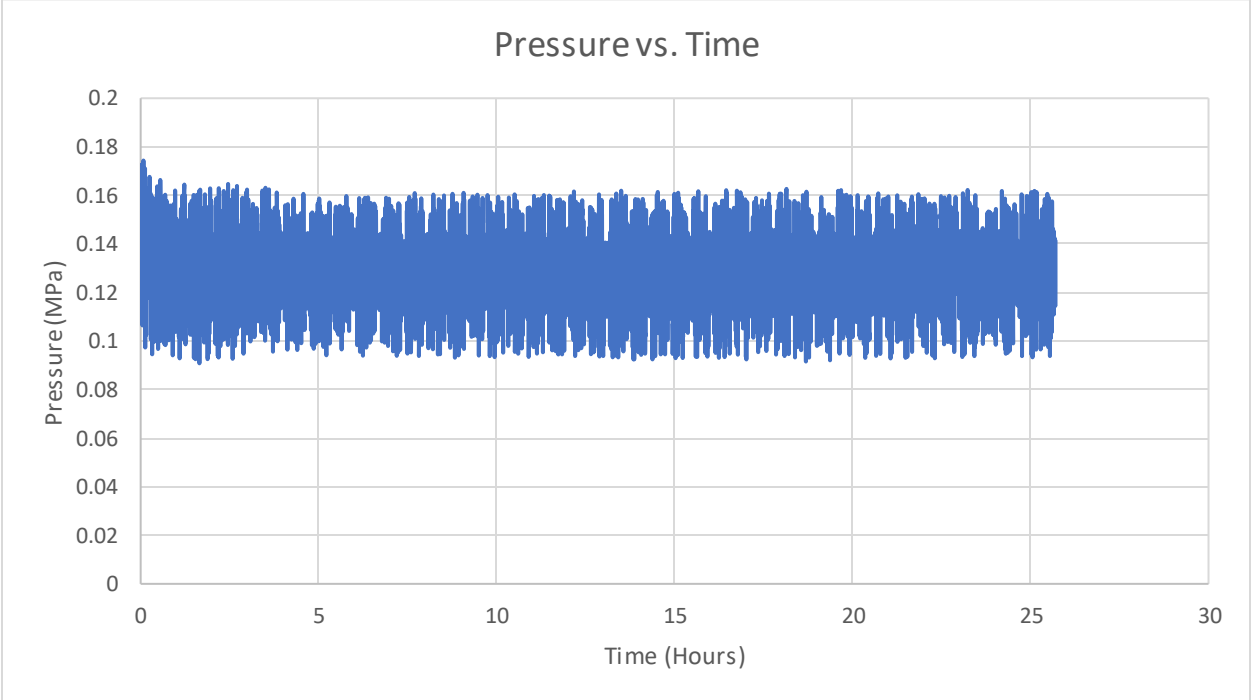

Figure A16 - Test 8: Pressure plot

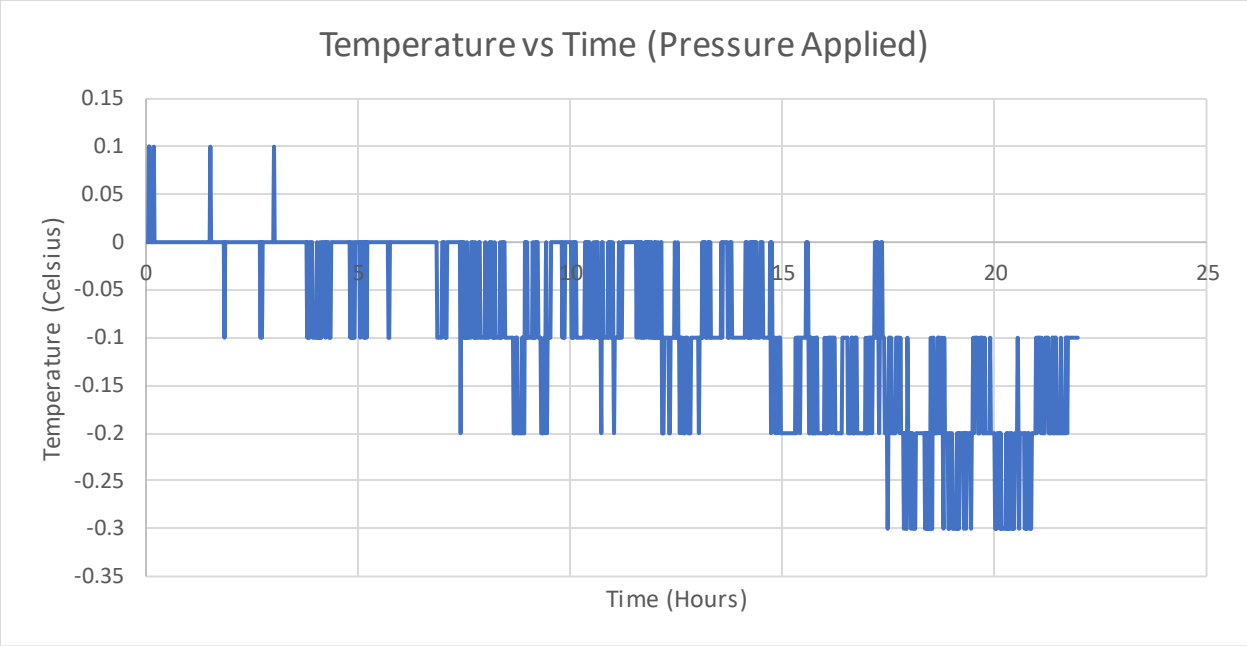

Figure A17 - Test 9: Temperature plot

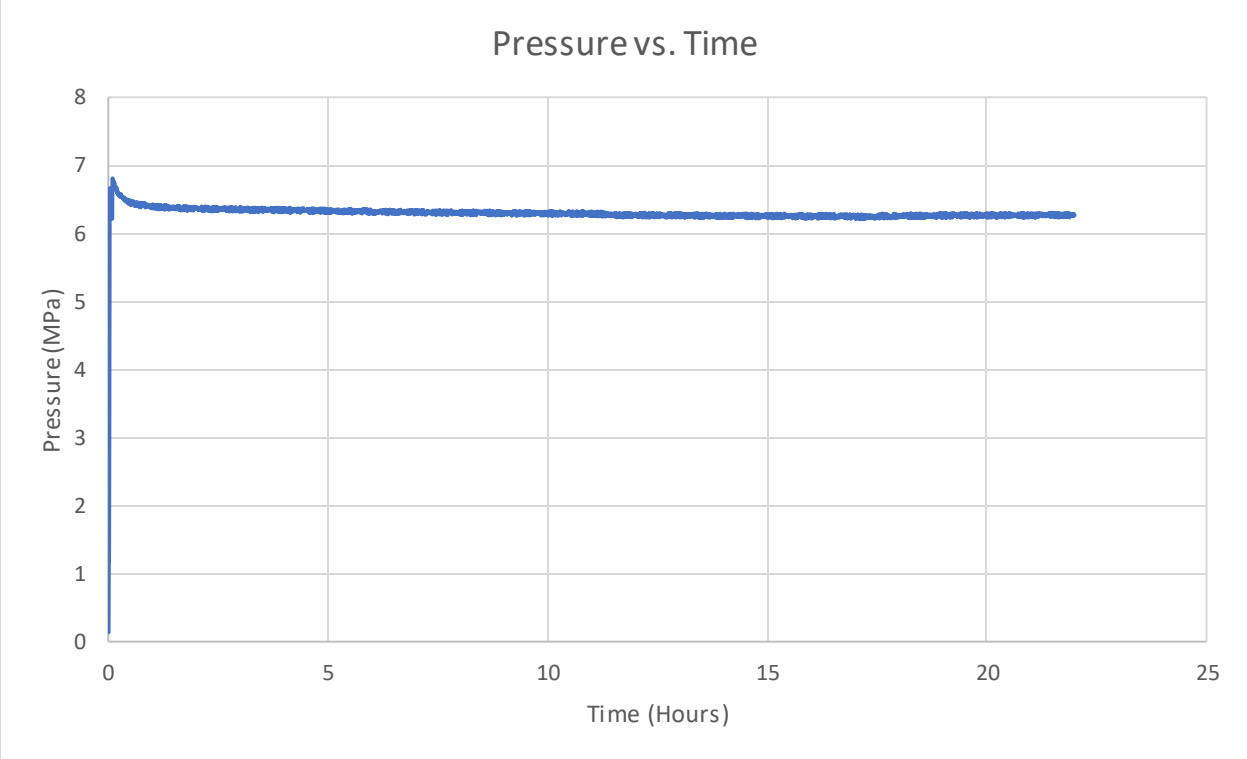

Figure A18 - Test 9: Pressure plot

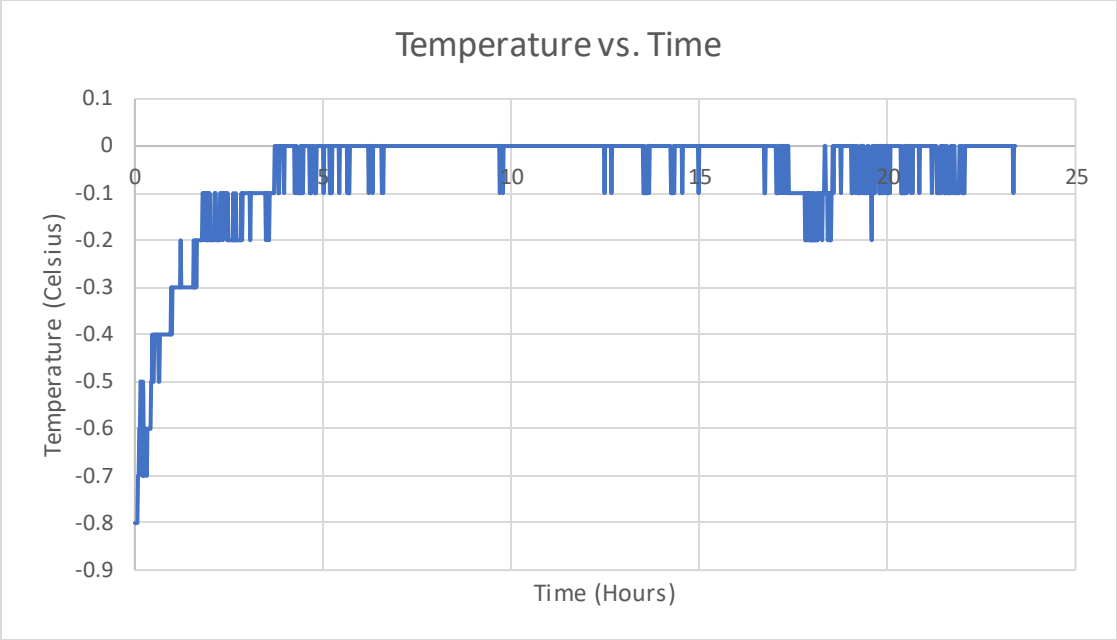

Figure A19 - Test 10: Temperature plot

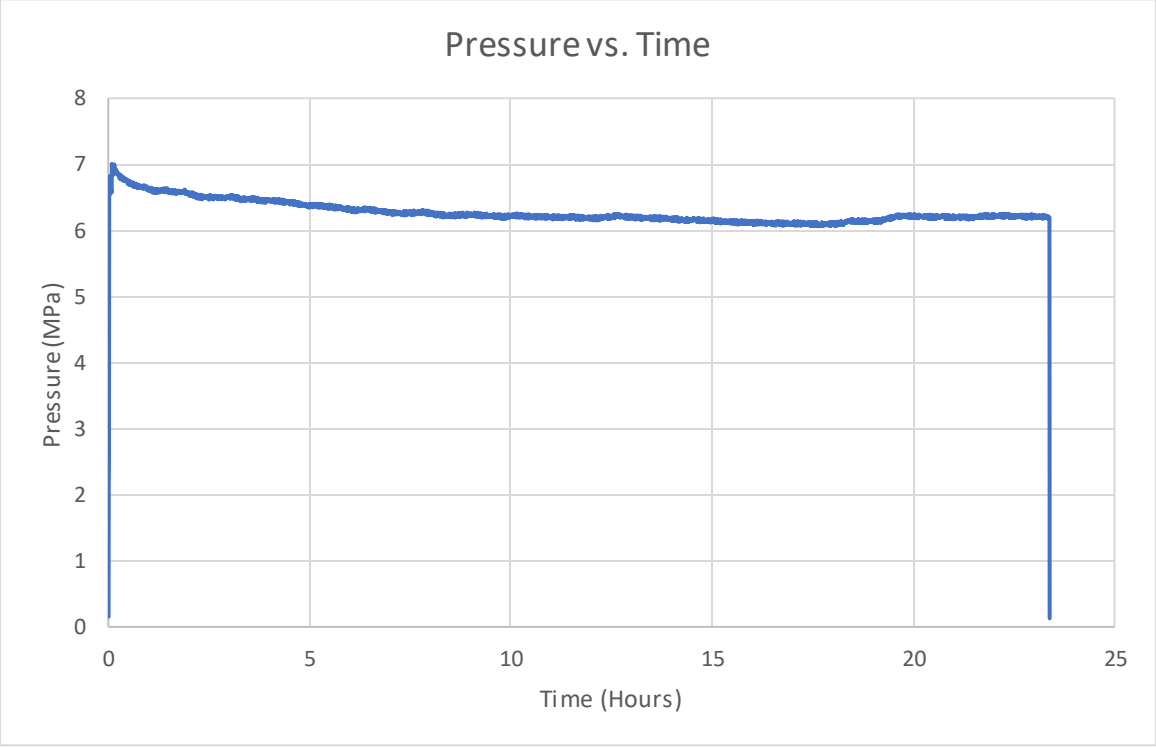

Figure A20 - Test 10: Pressure plot

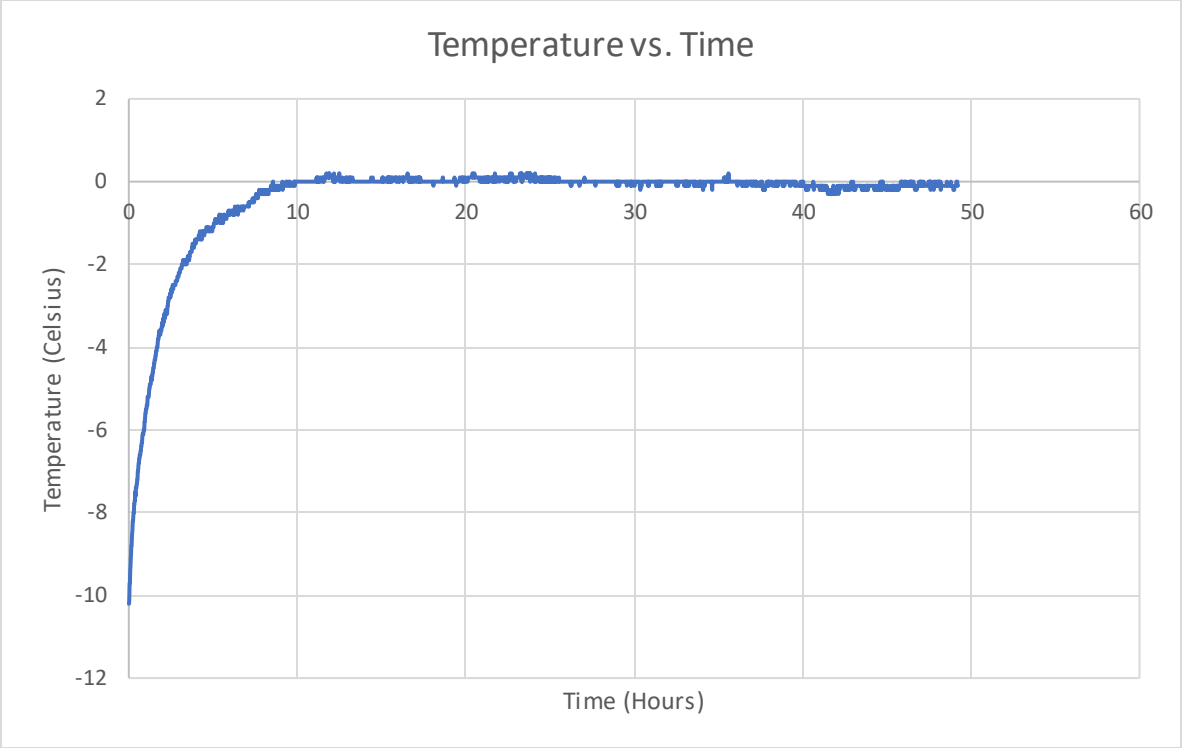

Figure A21 - Test 11: Temperature plot

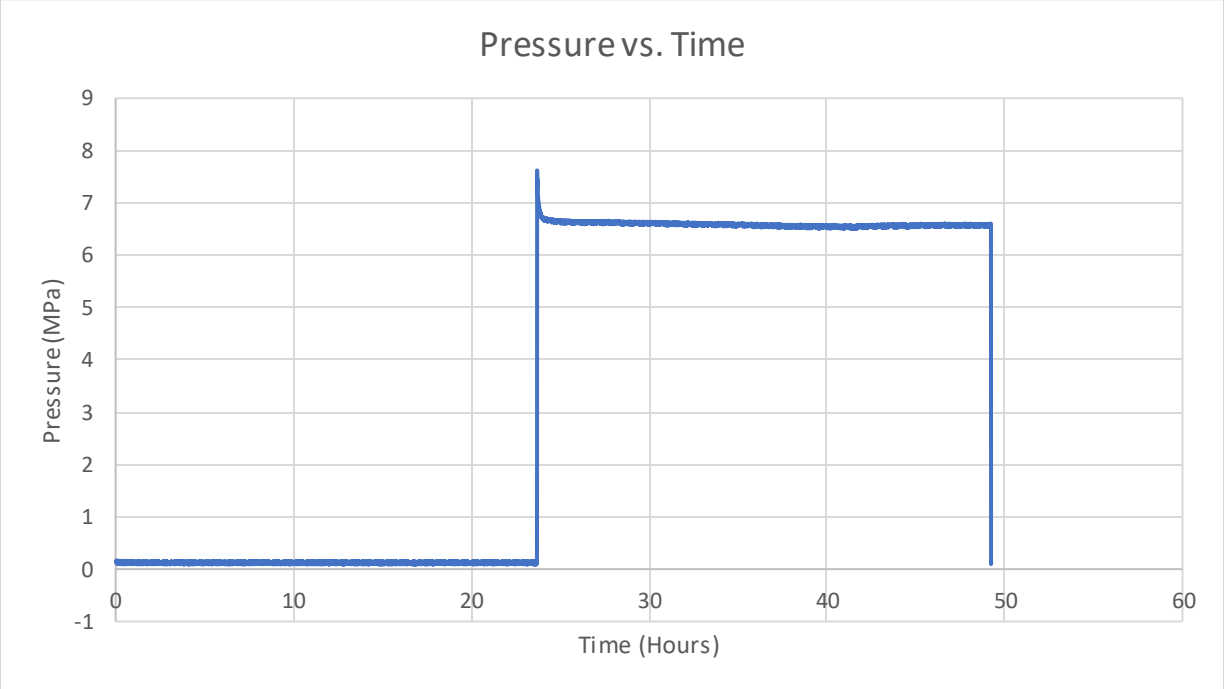

Figure A22 - Test 11: Pressure plot

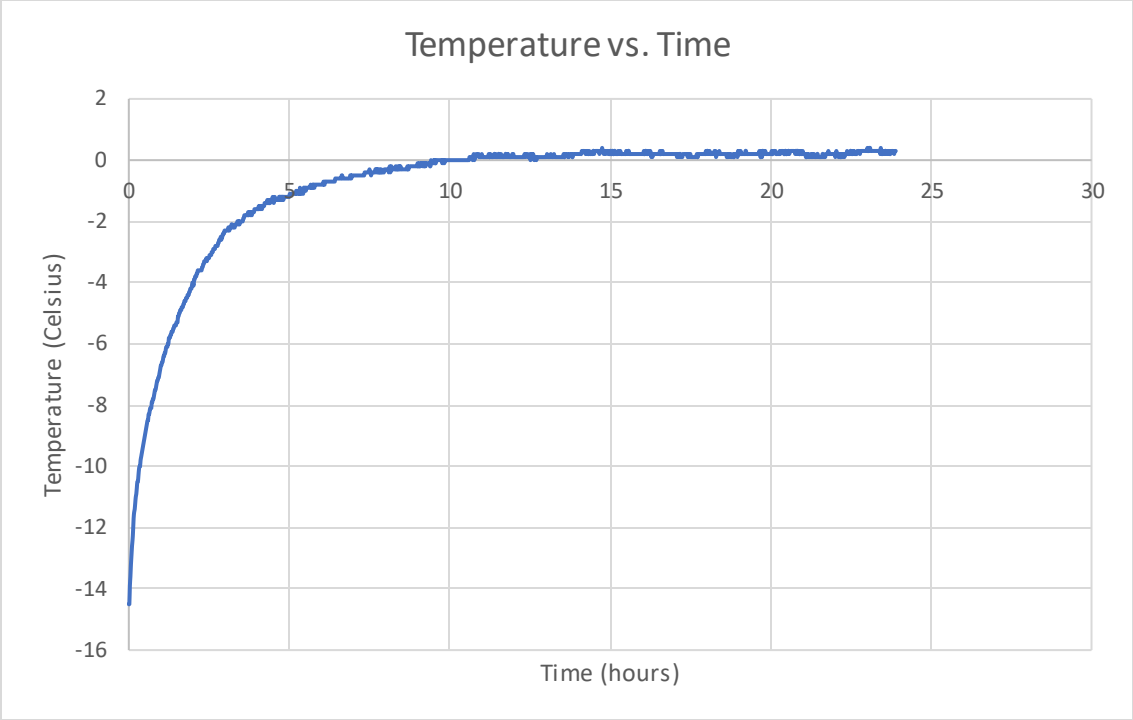

Figure A23 - Test 12: Temperature plot

No pressure plot because no pressure was applied in this test.

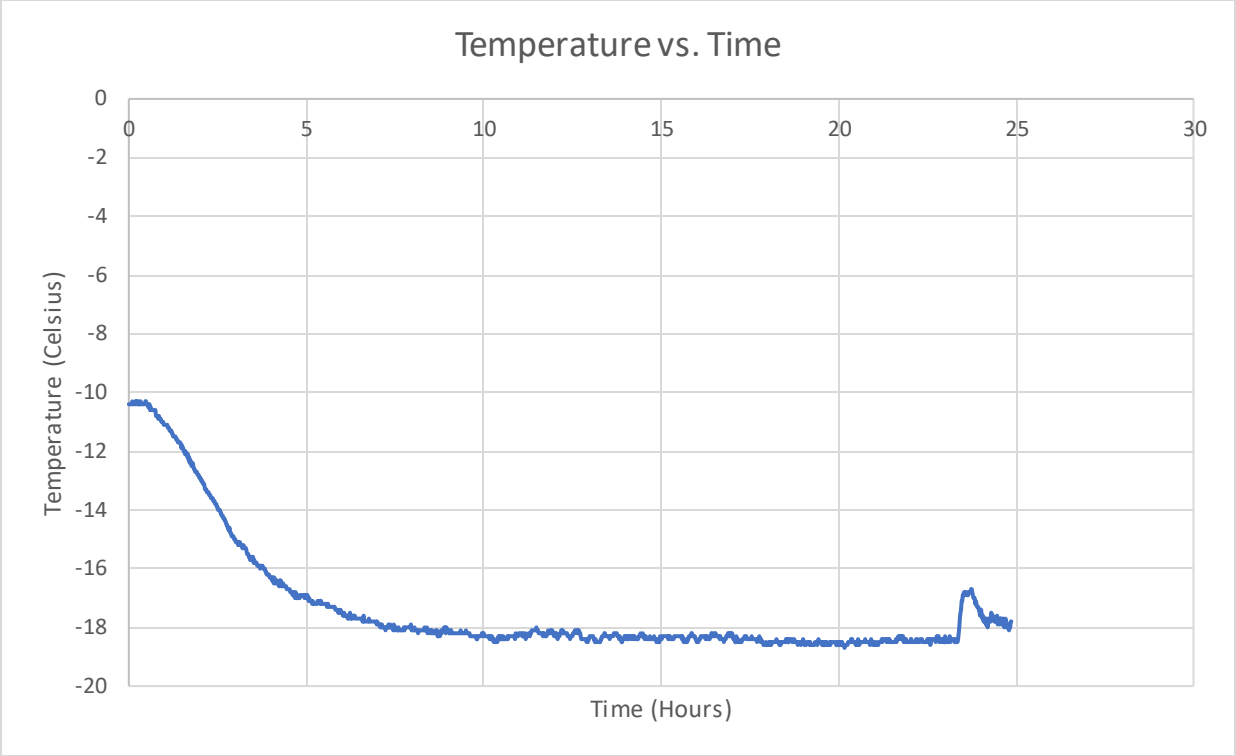

Figure A24 - Test 13: Temperature plot

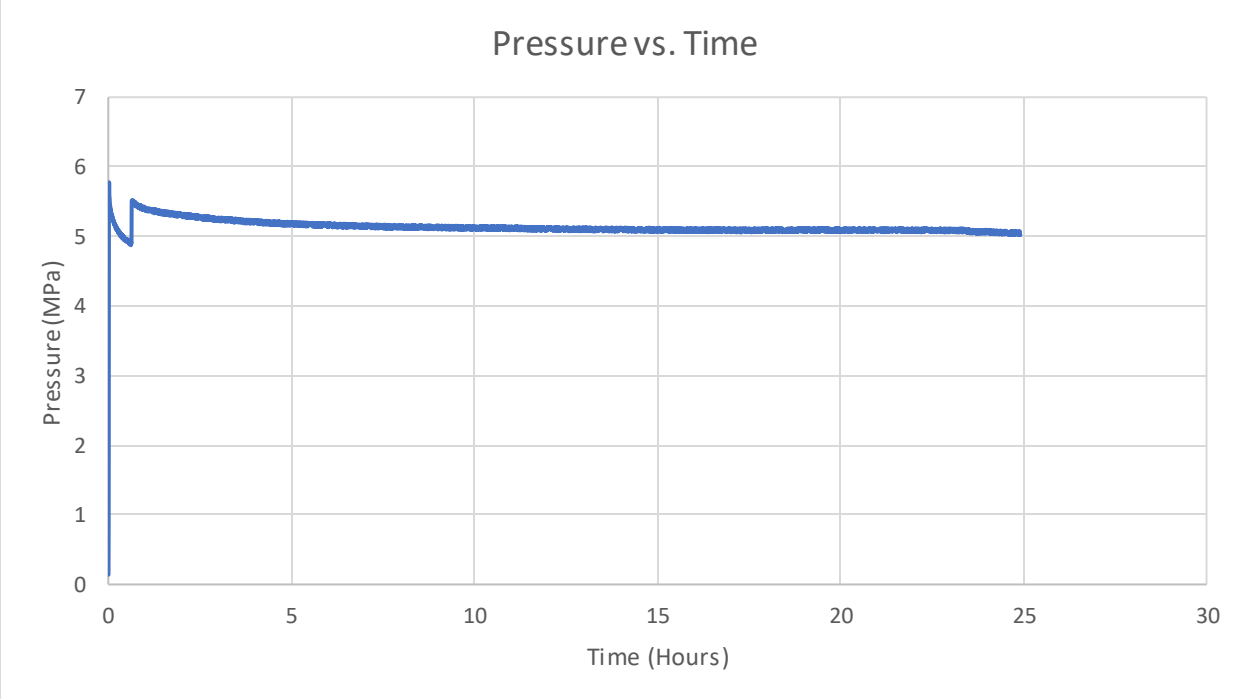

Figure A25 - Test 13: Pressure plot

Test 14 data corrupted – expected profile is similar to test 13.

APPENDIX B - Drawings of Apparatus

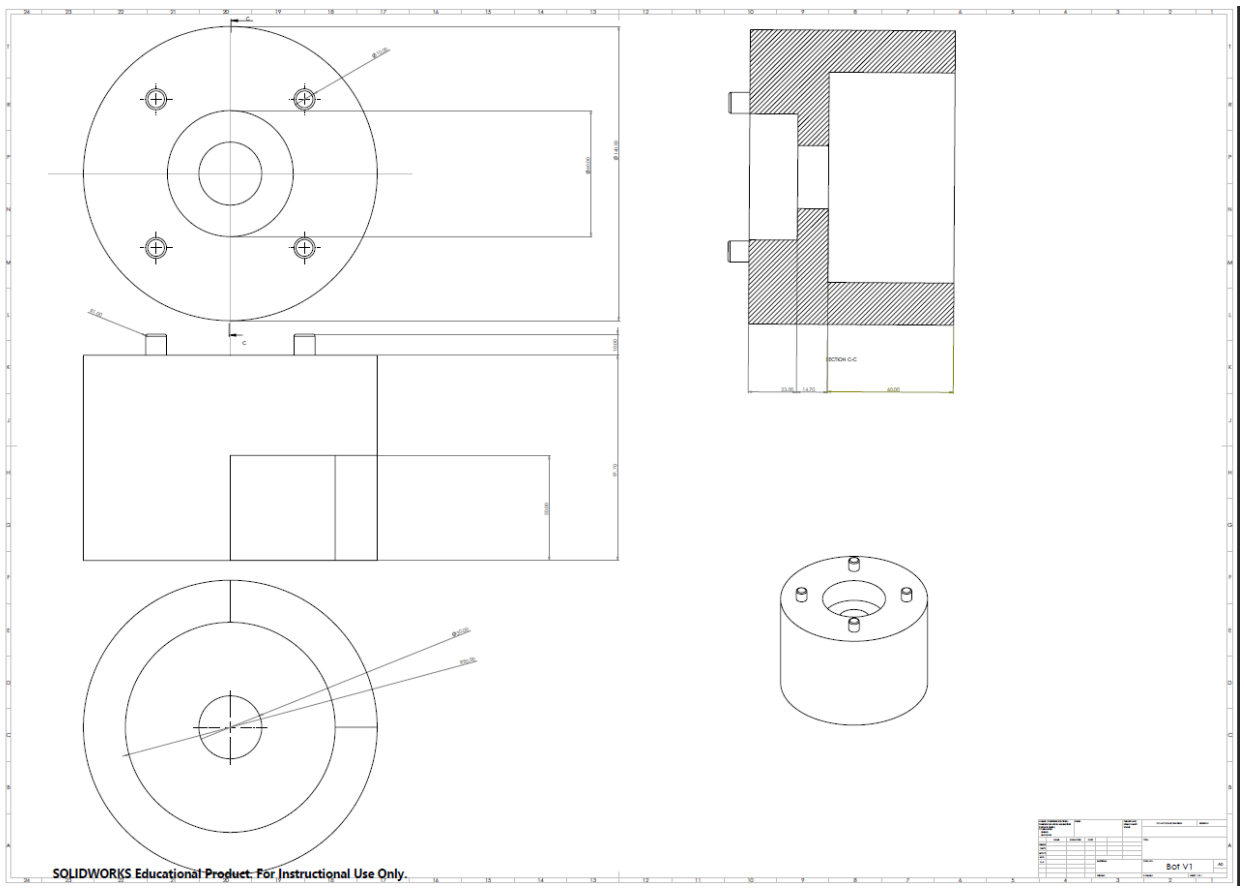

Figure B1 - Bottom part of apparatus

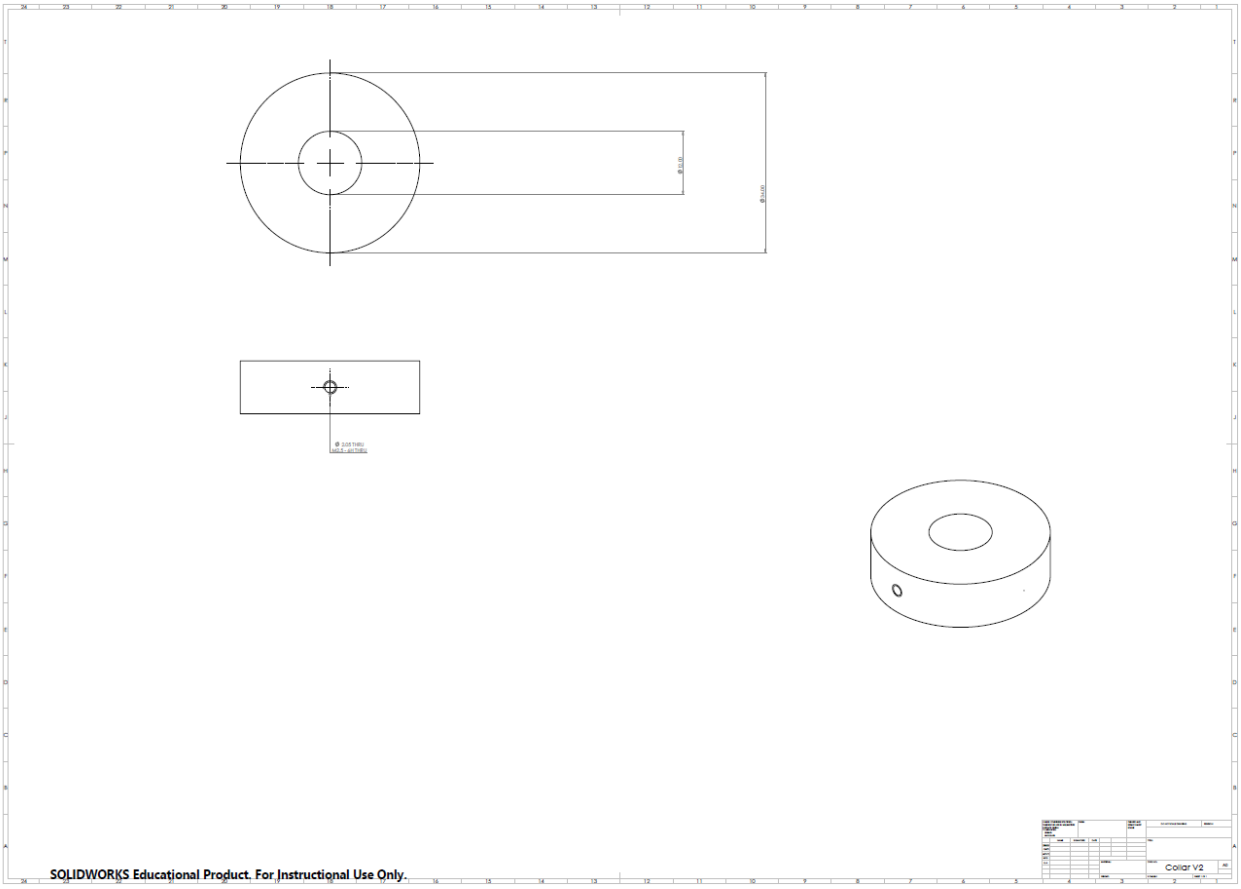

Figure B2 - Camera set screw collar.

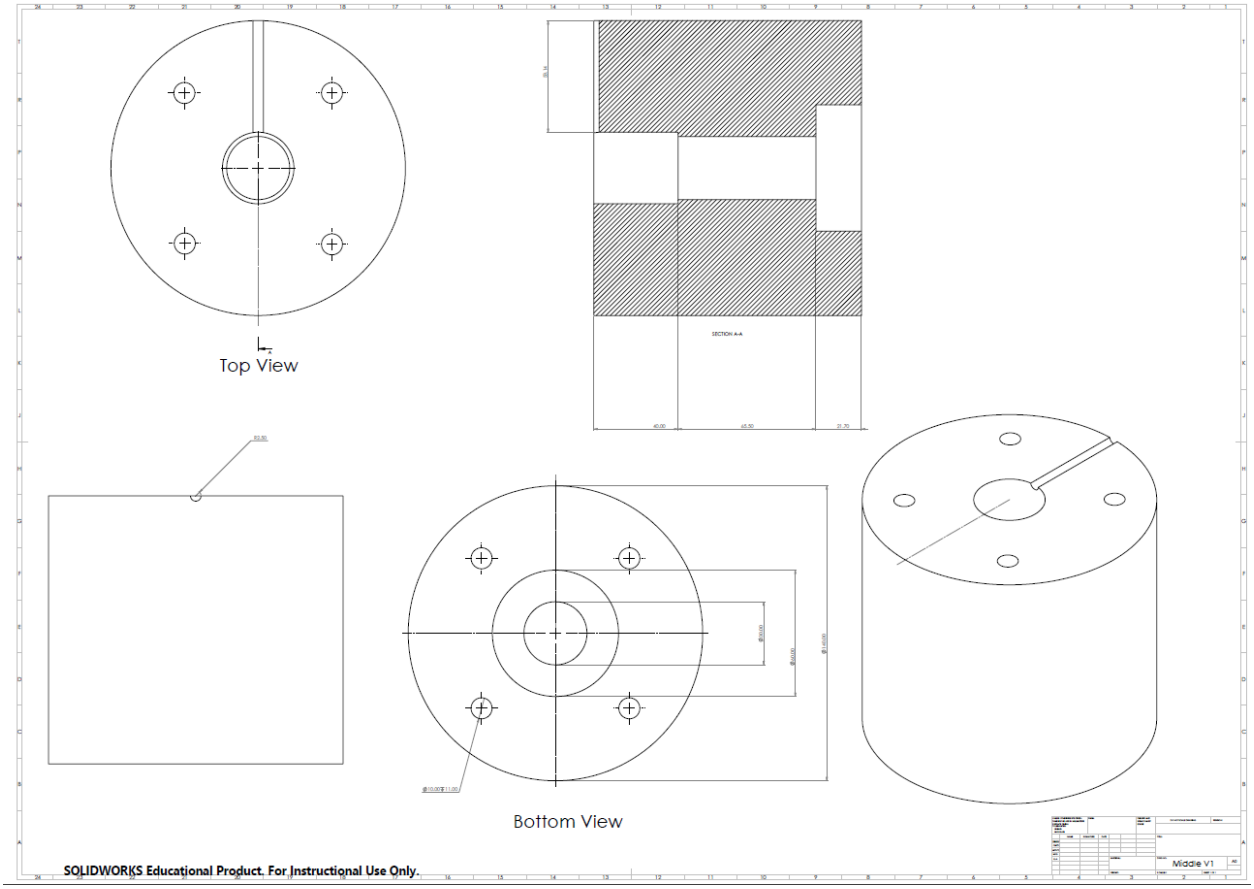

Figure B3 - Apparatus camera housing

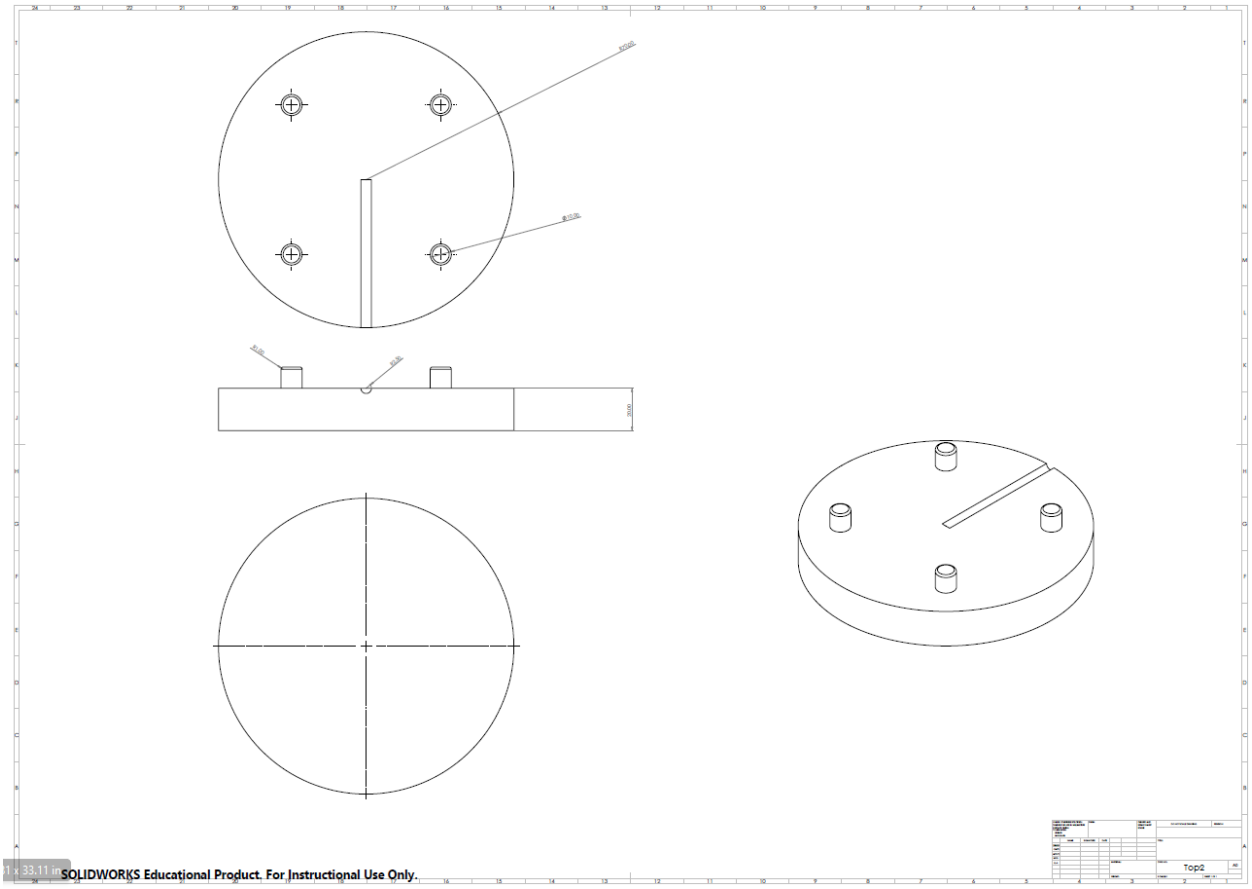

Figure B4 - Top of apparatus

APPENDIX C – Base Case Screenshots

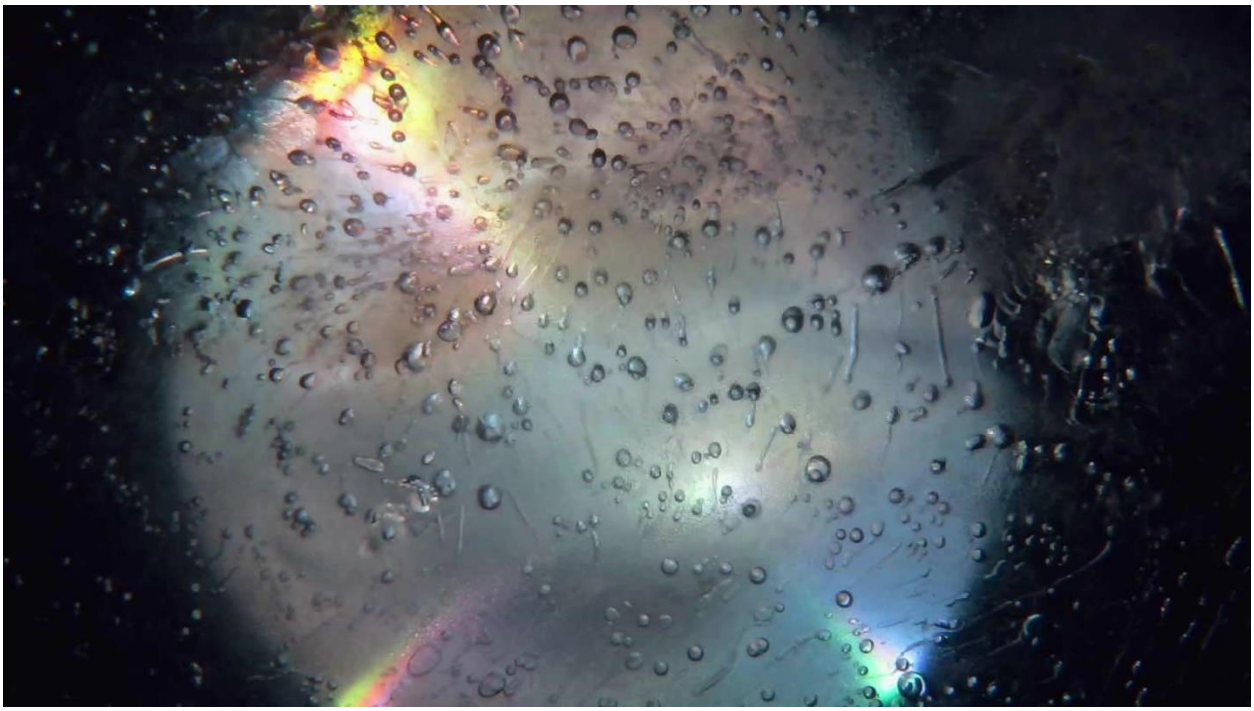

Figure C1 – 0 hours, 0 minutes, 0 seconds

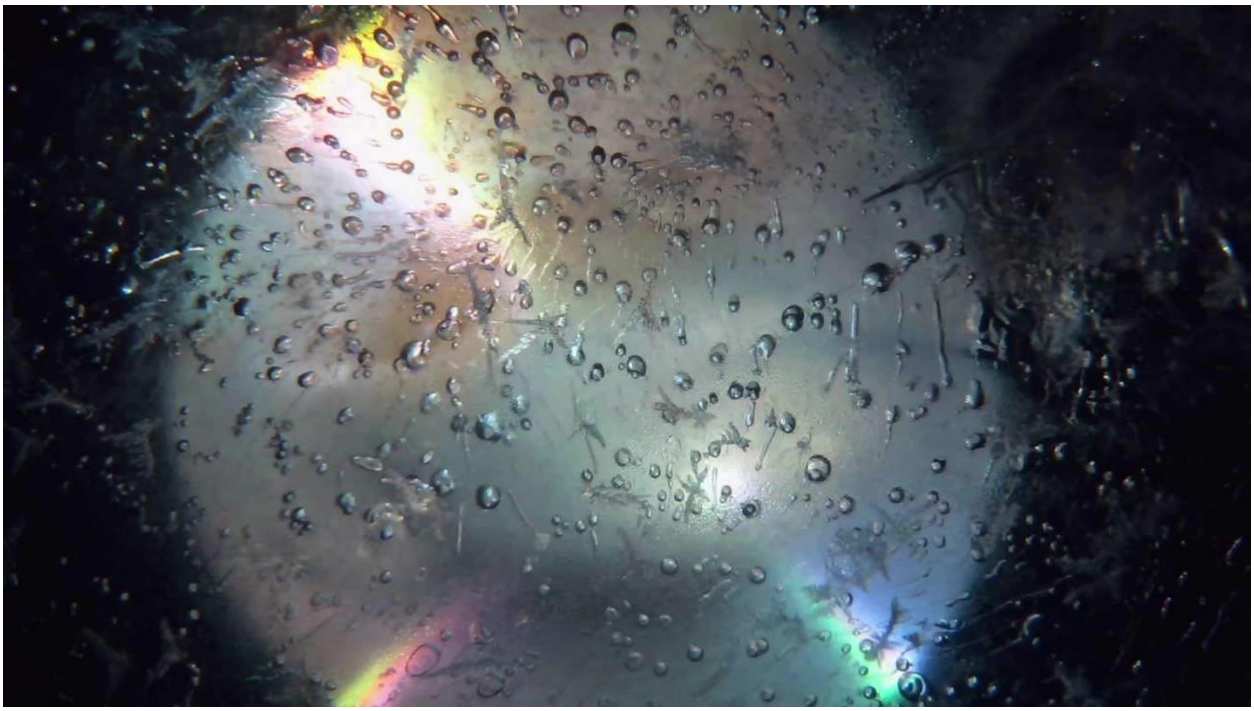

Figure C2 – 1 hour, 30 minutes, 0 seconds

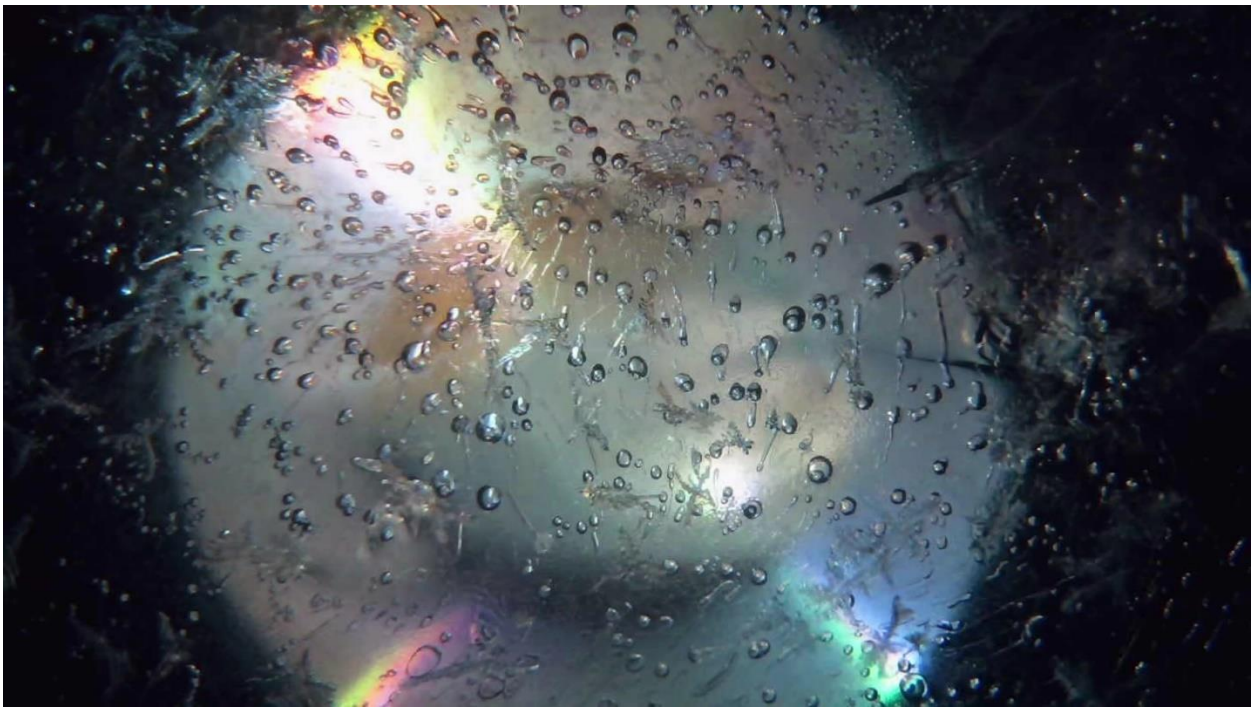

Figure C3 – 4 hours, 0 minutes, 0 seconds

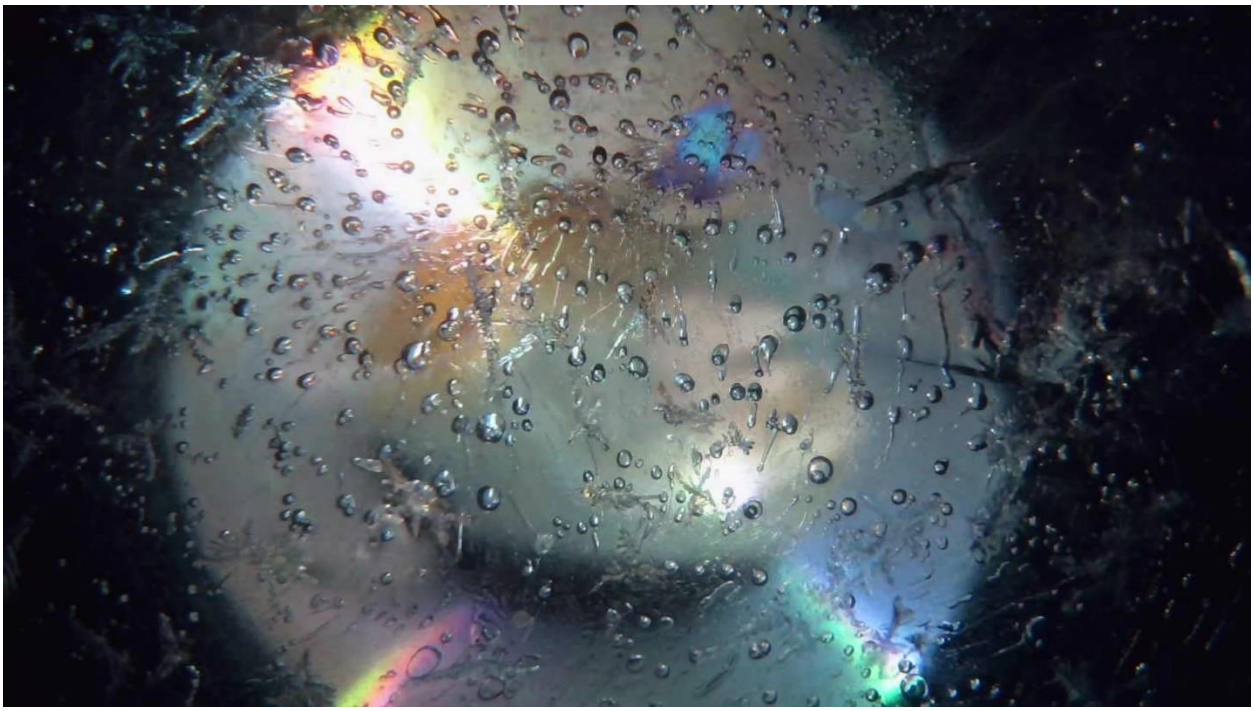

Figure C4 – 6 hours, 0 minutes, 0 seconds

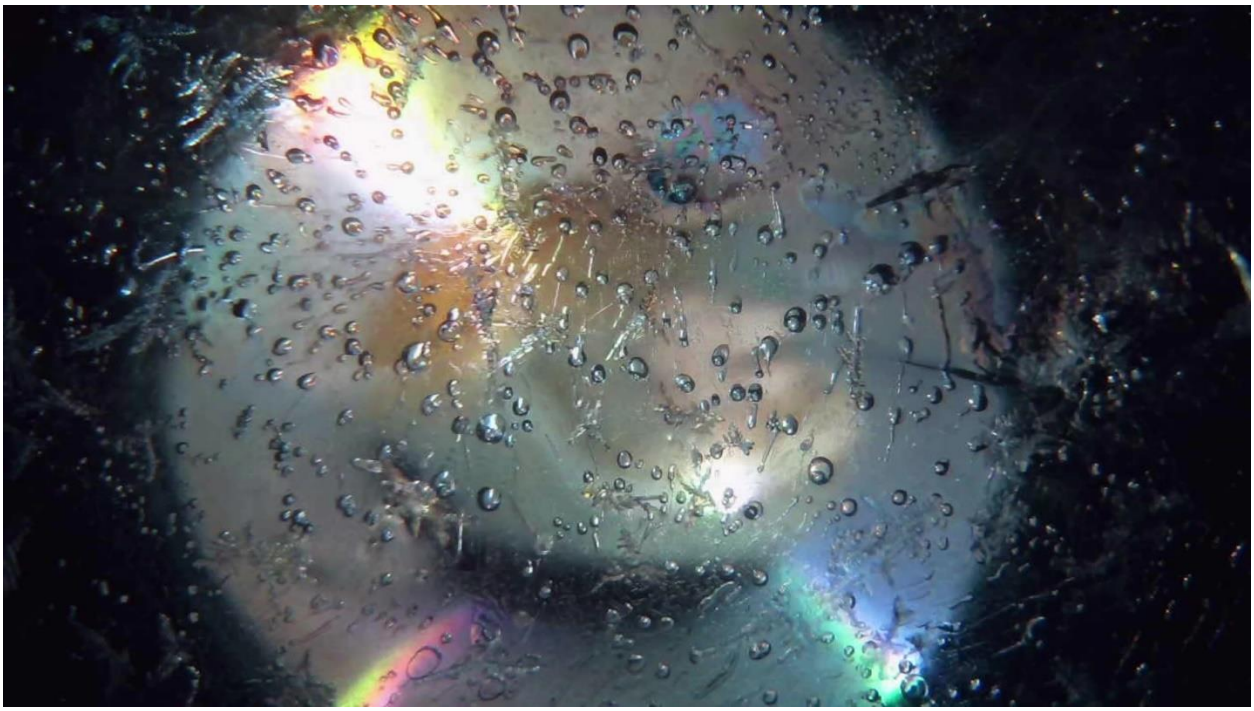

Figure C5 – 8 hours, 0 minutes, 0 seconds

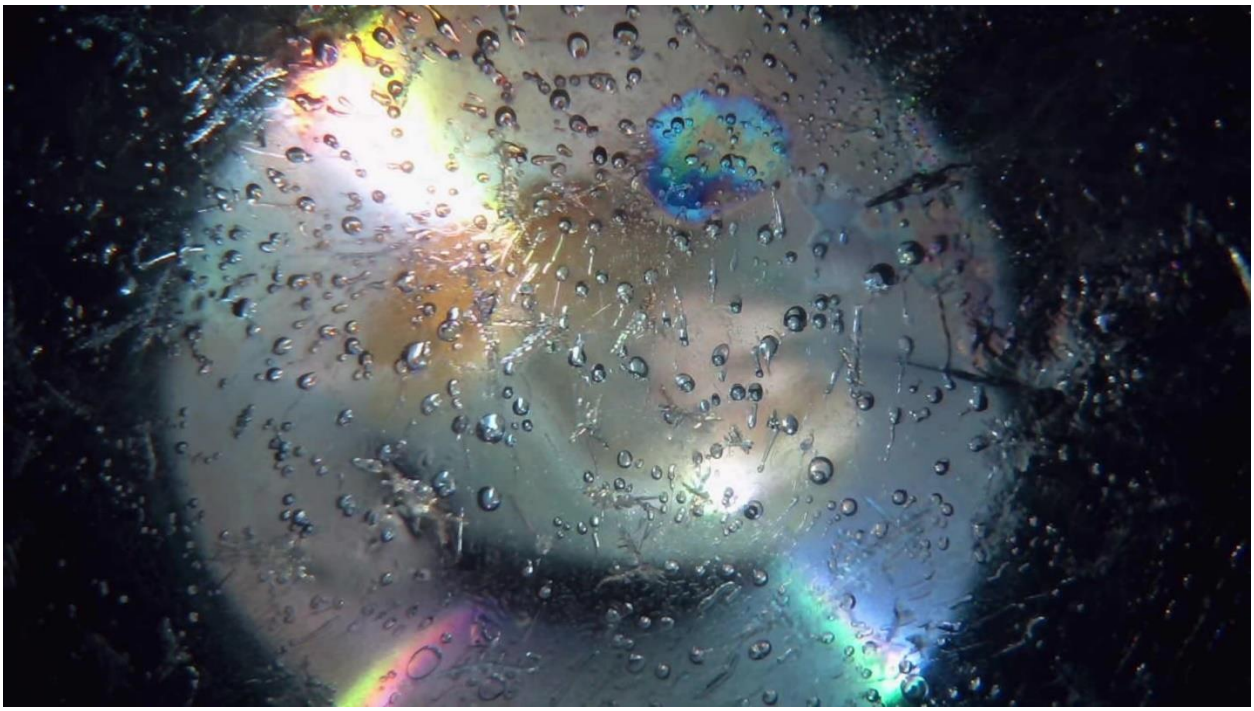

Figure C6 – 10 hours, 0 minutes, 1 second

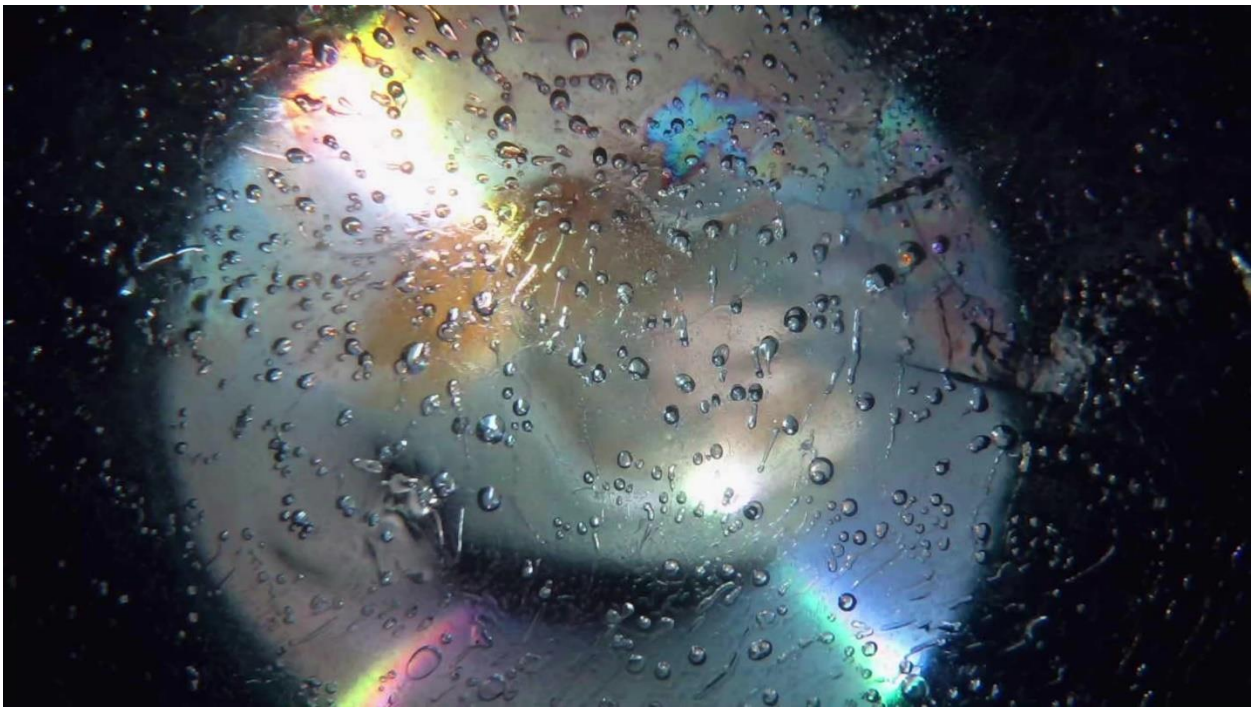

Figure C7 – 15 hours, 0 minutes, 0 seconds

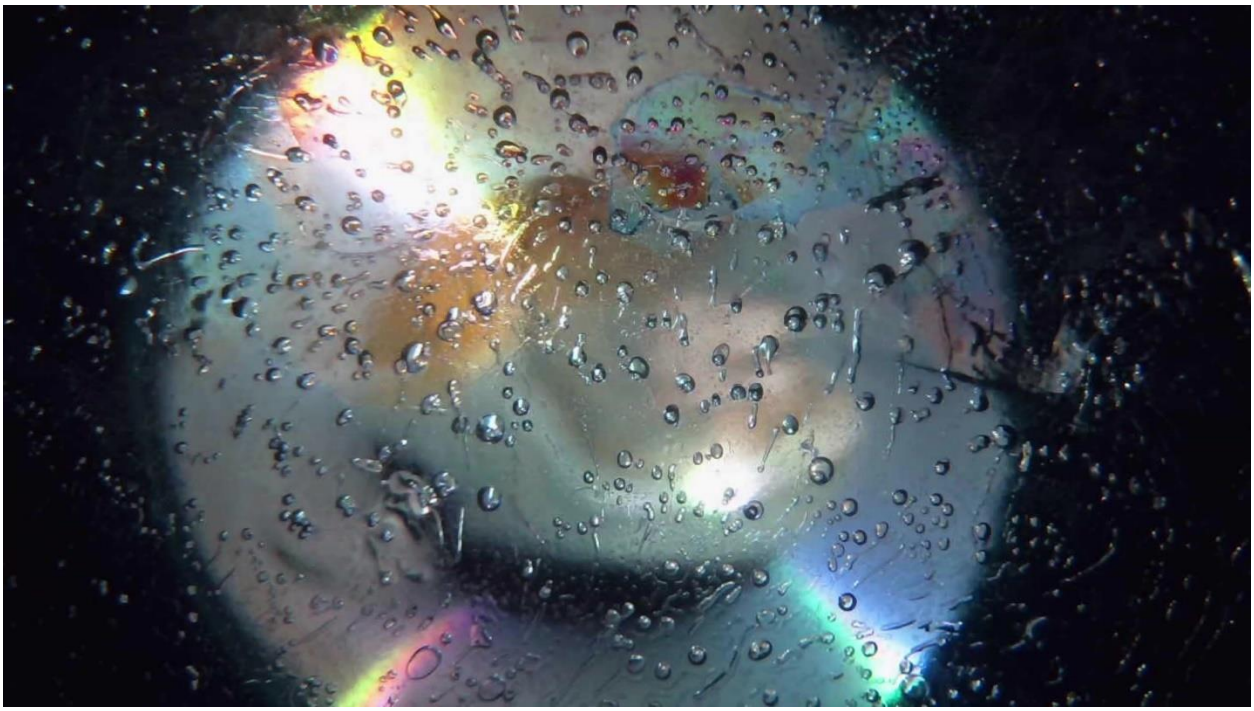

Figure C8 – 20 hours, 0 minutes, 0 seconds

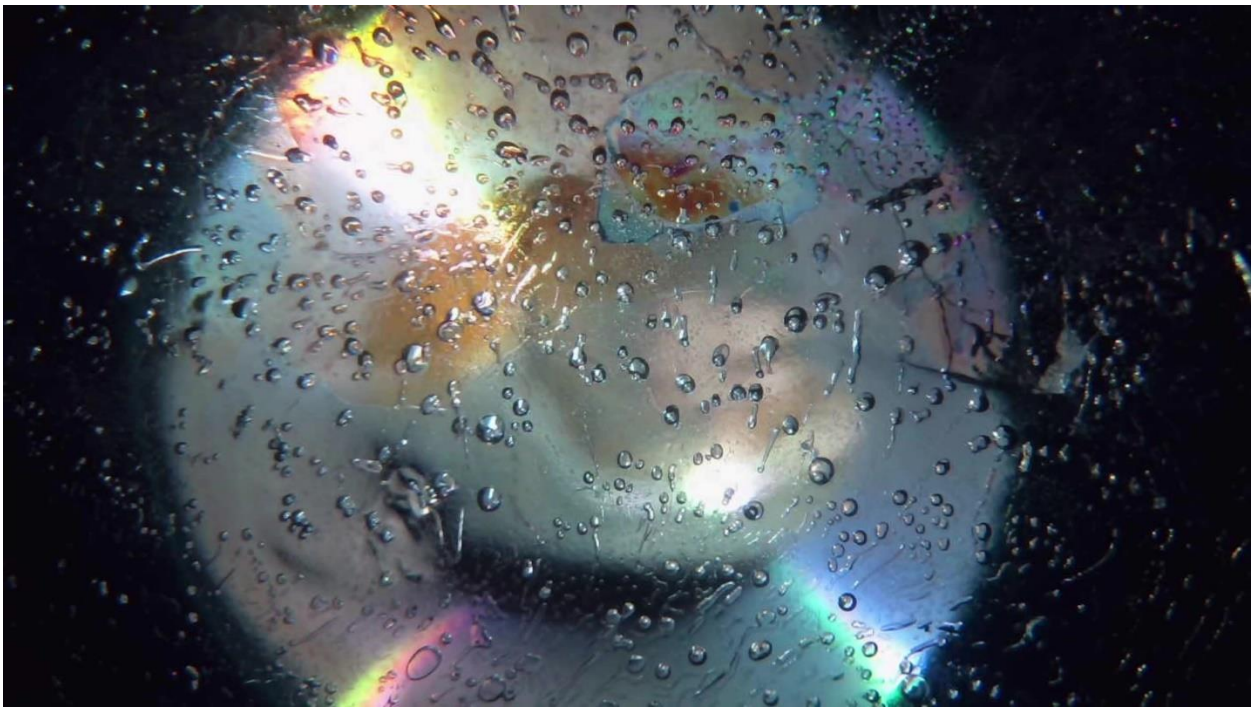

Figure C9 – 25 hours, 42 minutes, 24 seconds

APPENDIX D – Heating to Melting Point at Constant Pressure Screenshots

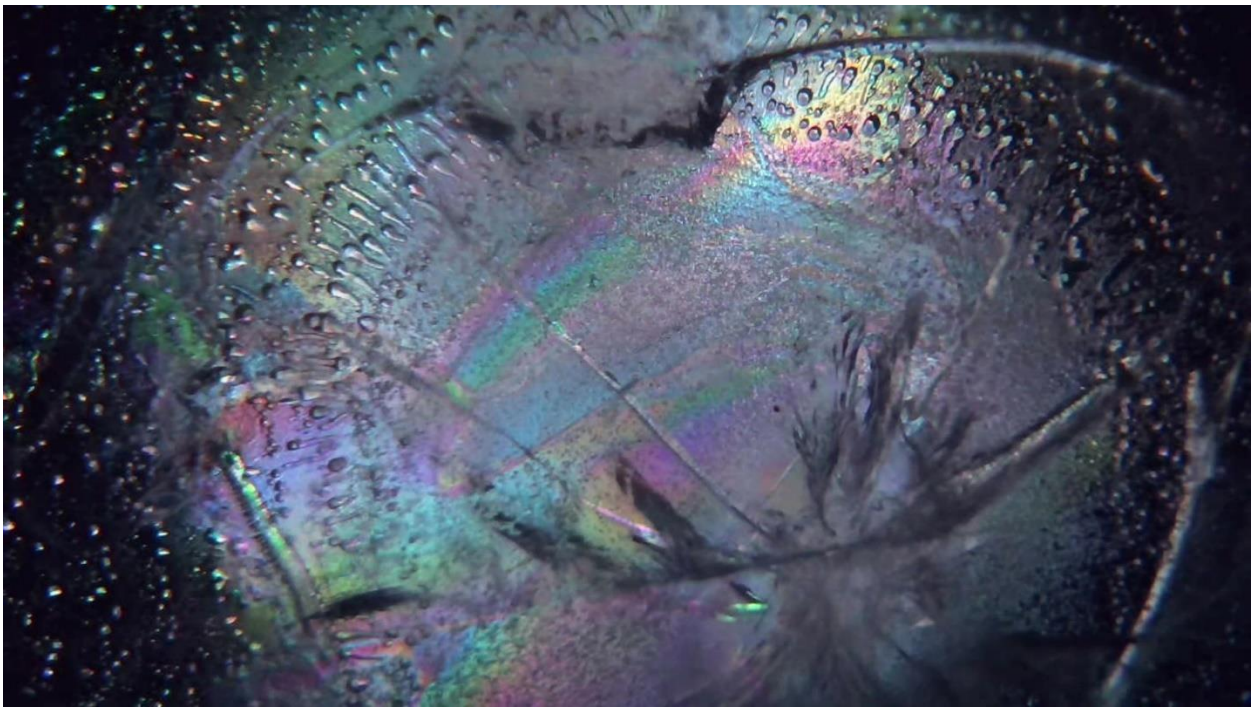

Figure D1 – 0 hours, 0 minutes, 0 seconds

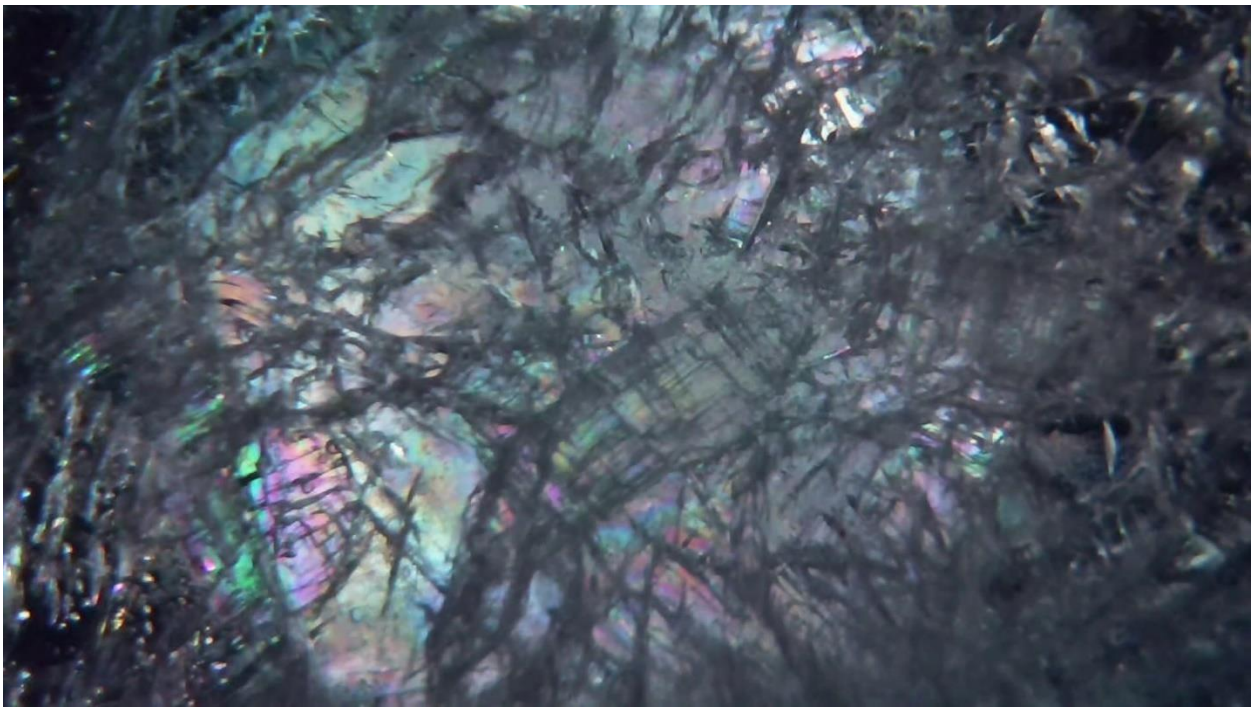

Figure D2 – 0 hours, 2 minutes, 17 seconds

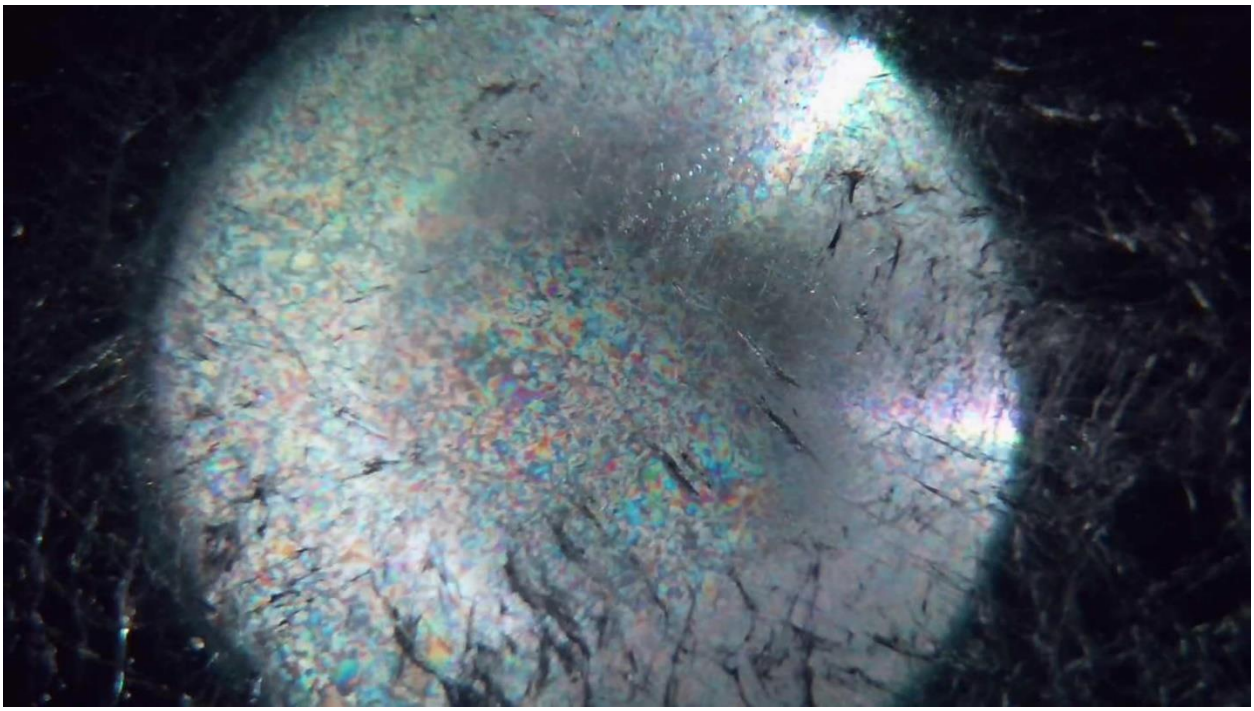

Figure D3 – 1 hour, 0 minutes, 0 seconds

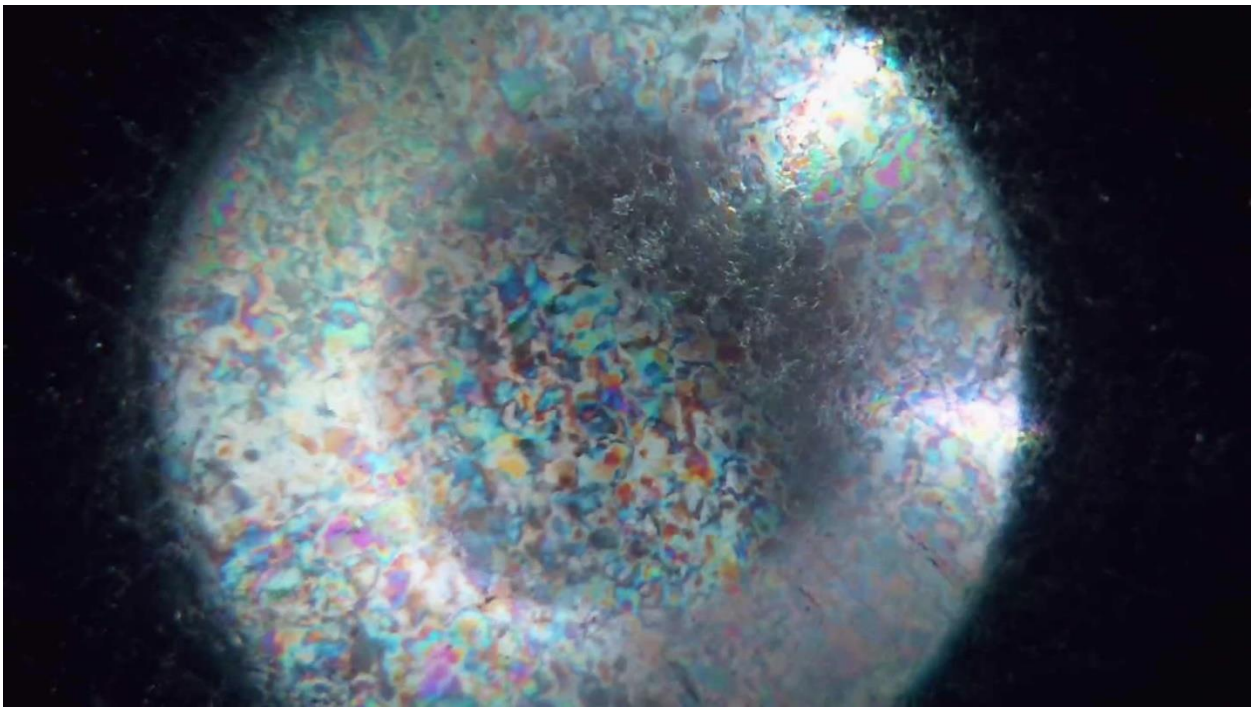

Figure D4 – 6 hours, 3 minutes, 45 seconds

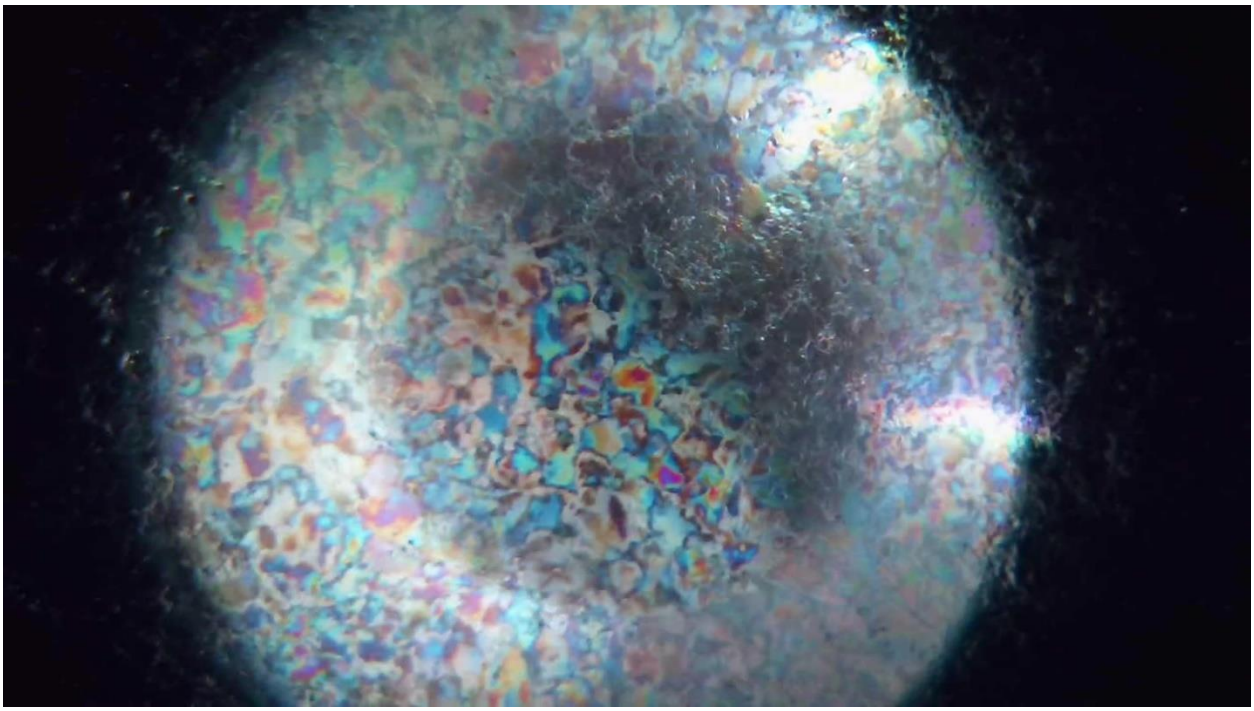

Figure D5 – 7 hours, 0 minutes, 0 seconds

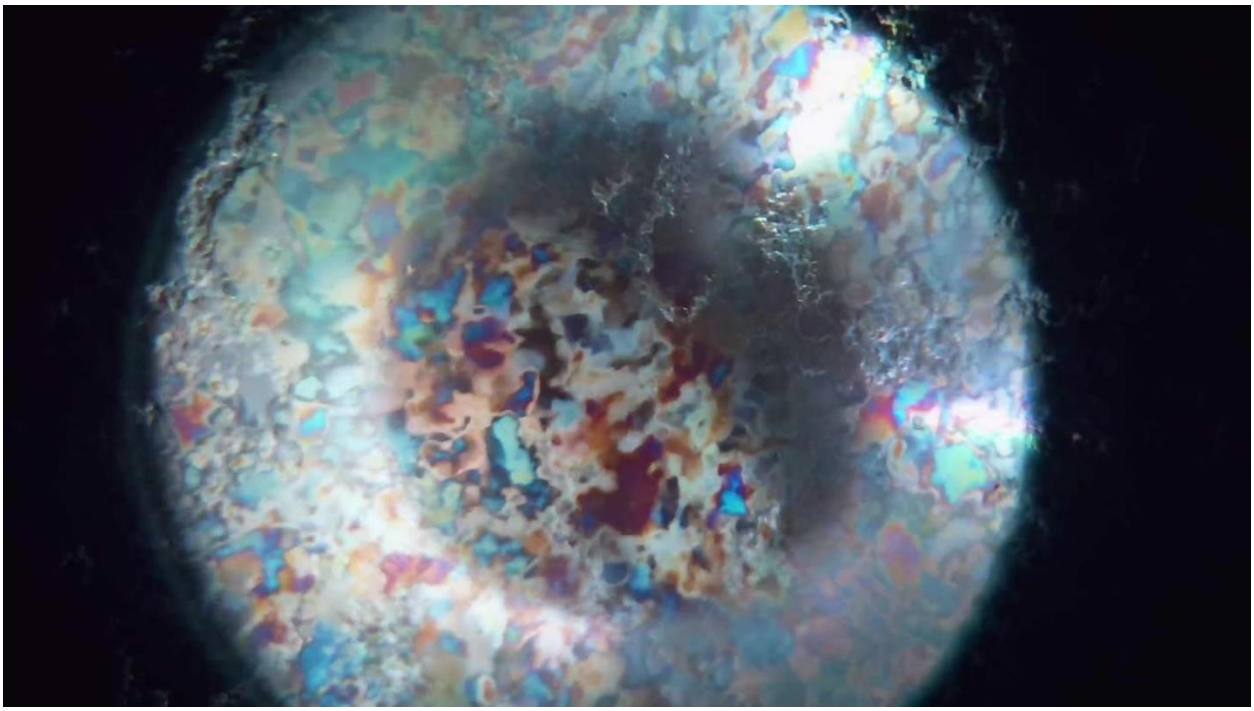

Figure D6 – 8 hours, 0 minutes, 0 seconds

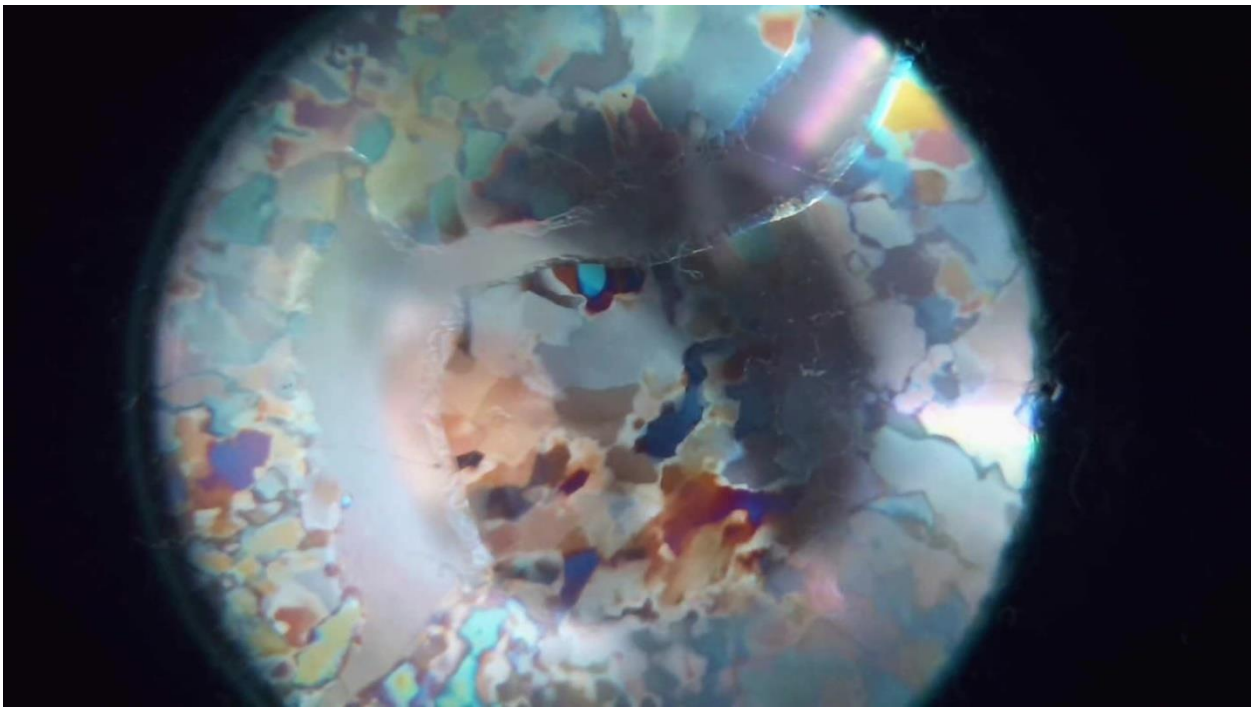

Figure D7 – 9 hours, 0 minutes, 0 seconds

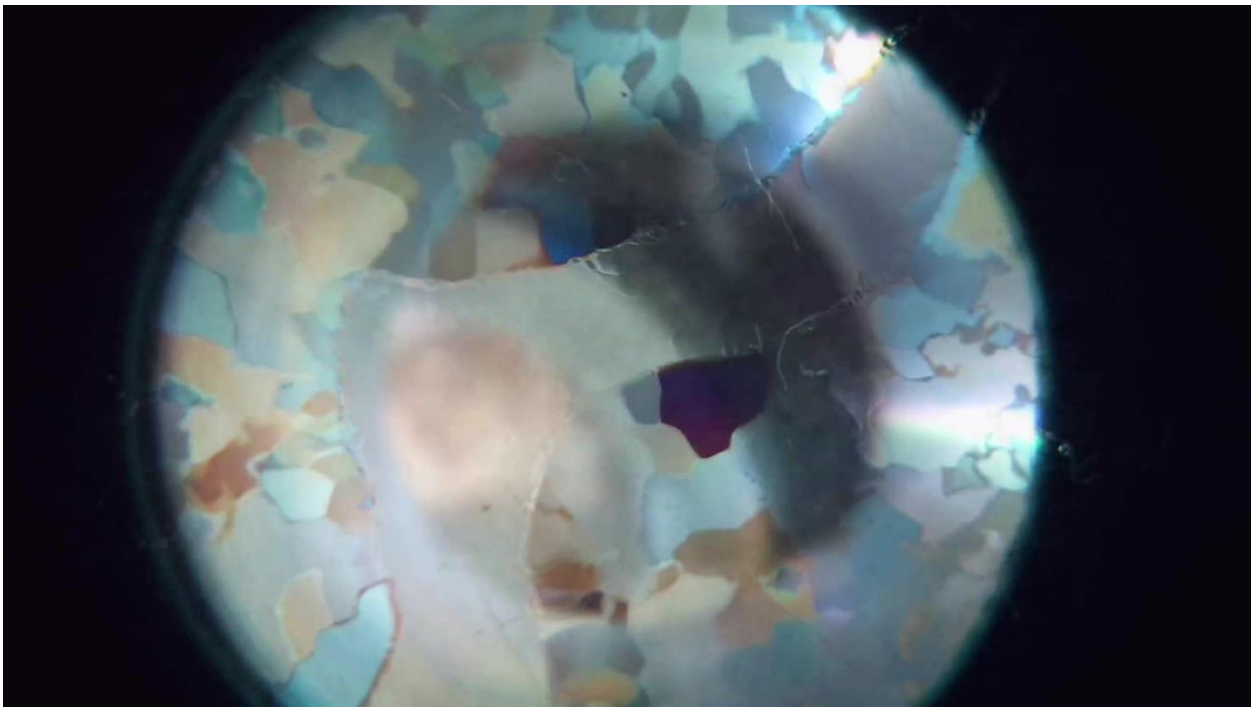

Figure D8 – 9 hours, 40 minutes, 18 seconds

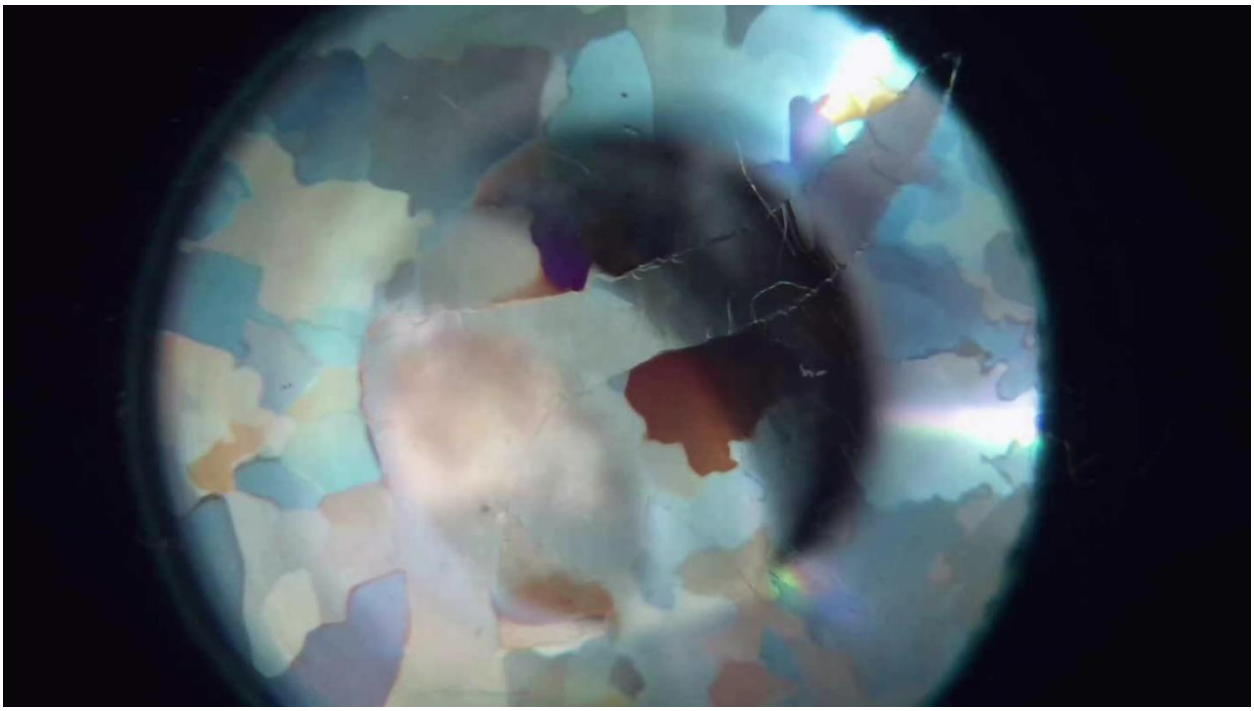

Figure D9 – 10 hours, 20 minutes, 27 seconds

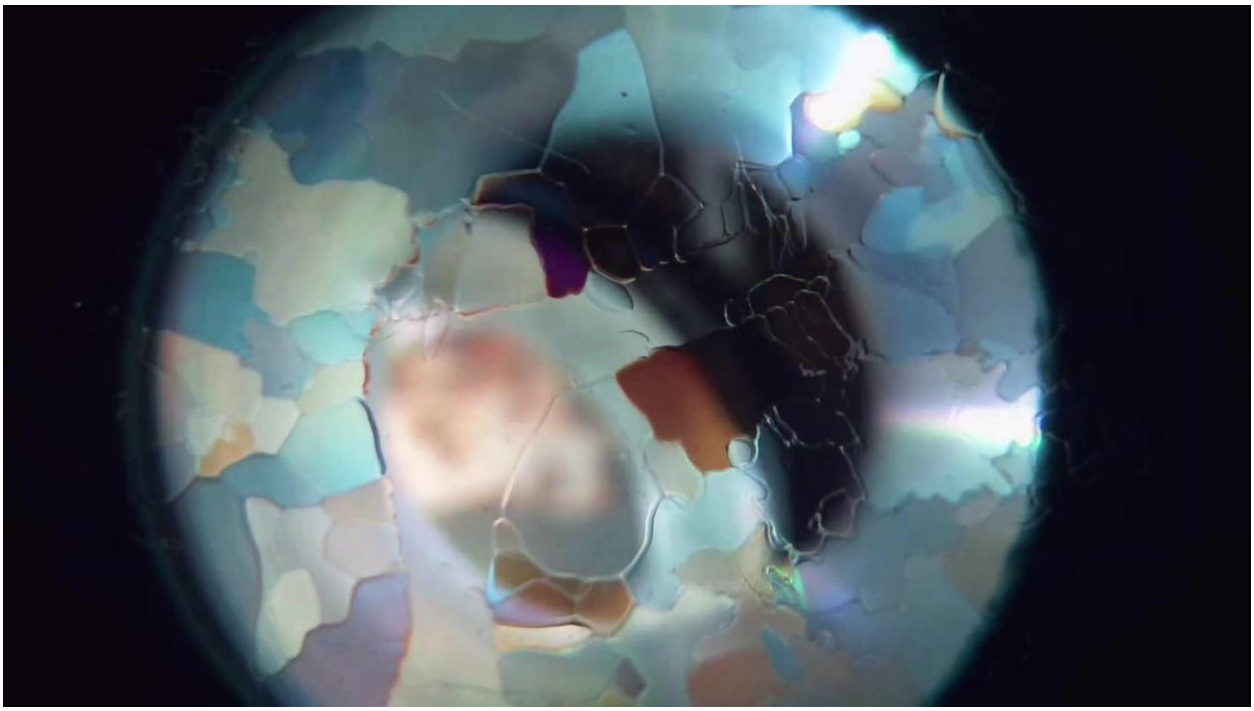

Figure D10 – 11 hours, 48 minutes, 36 seconds

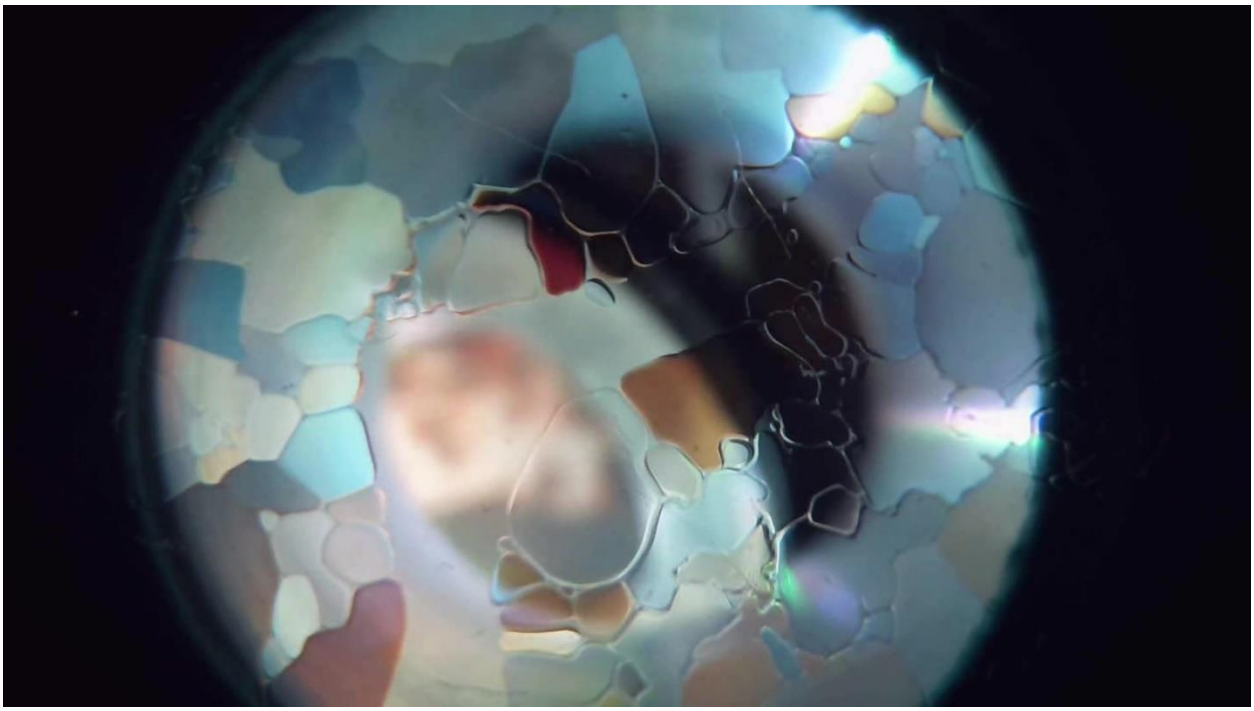

Figure D11 – 14 hours, 50 minutes, 28 seconds

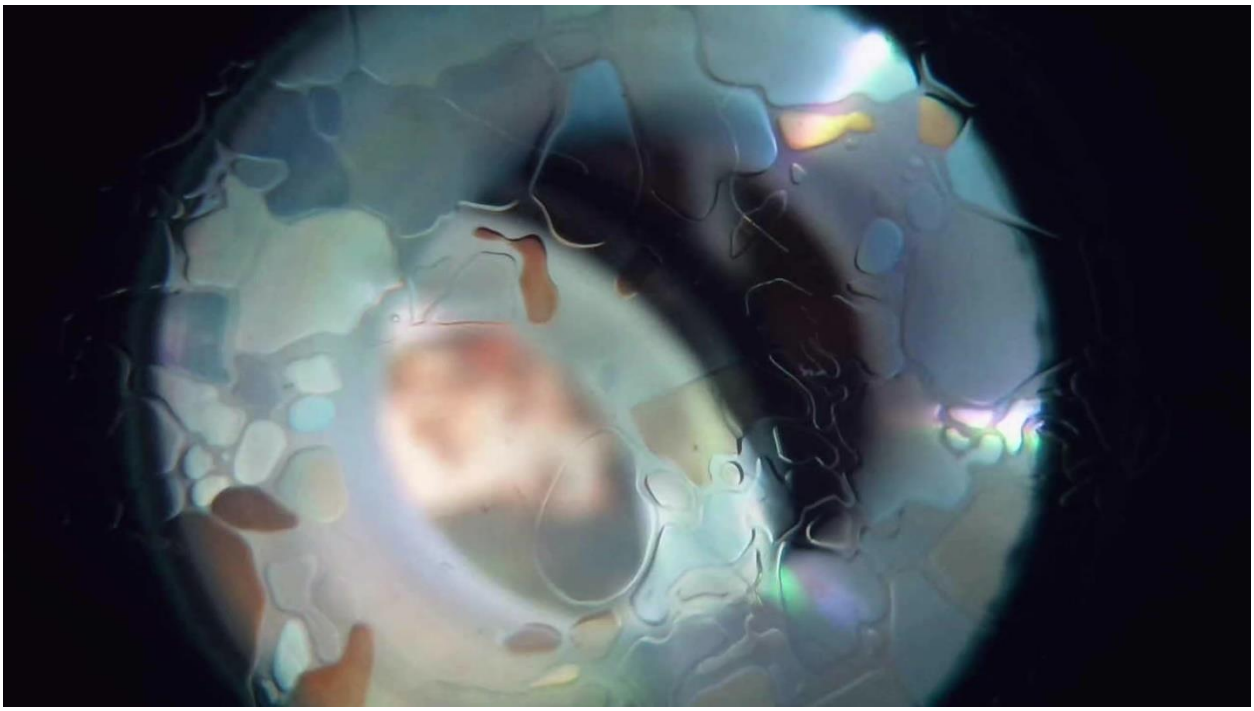

Figure D12 – 16 hours, 28 minutes, 42 seconds

APPENDIX E – Heating to -2°C at Constant Pressure Screenshots

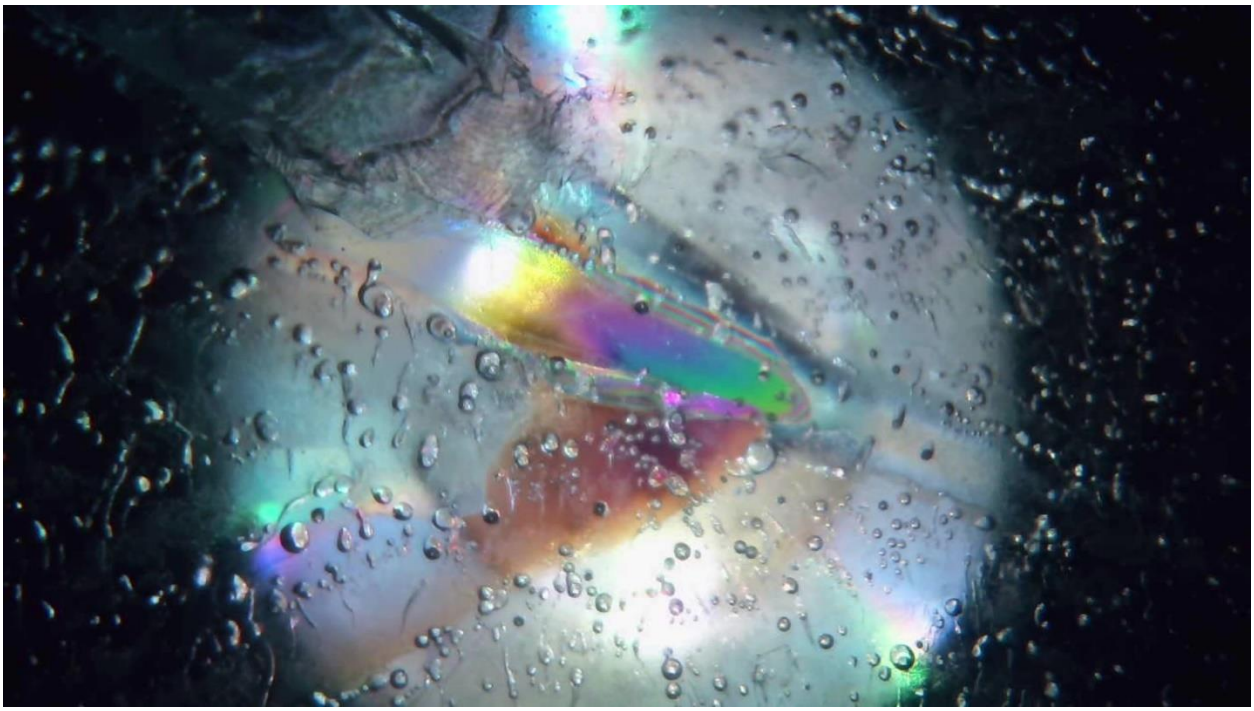

Figure E1 – 0 hours, 0 minutes, 0 seconds

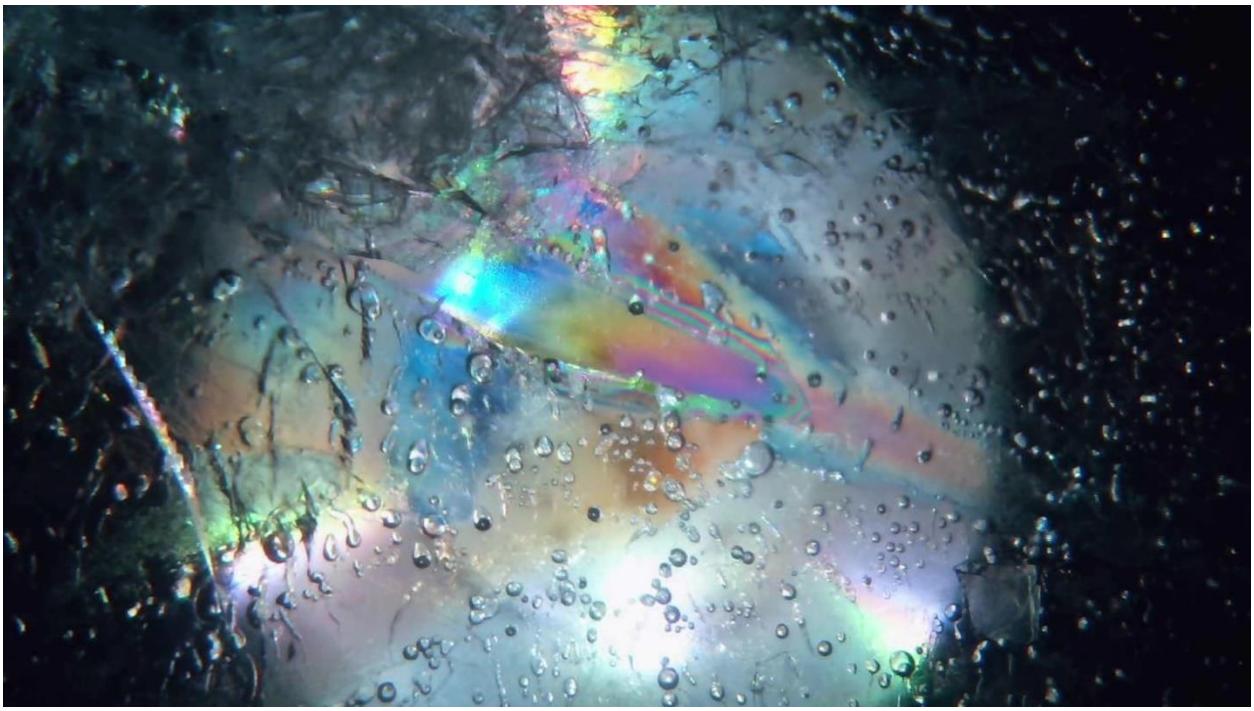

Figure E2 – 0 hours, 3 minutes, 13 seconds

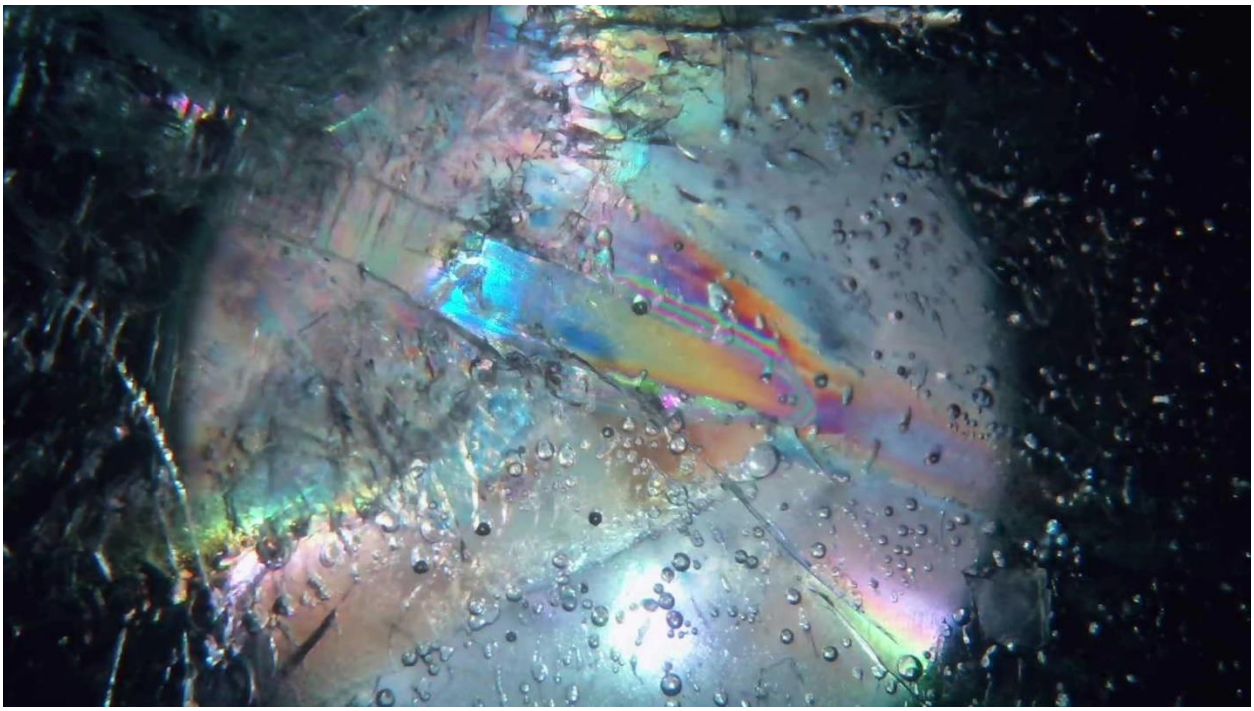

Figure E3 – 0 hours, 5 minutes, 0 seconds

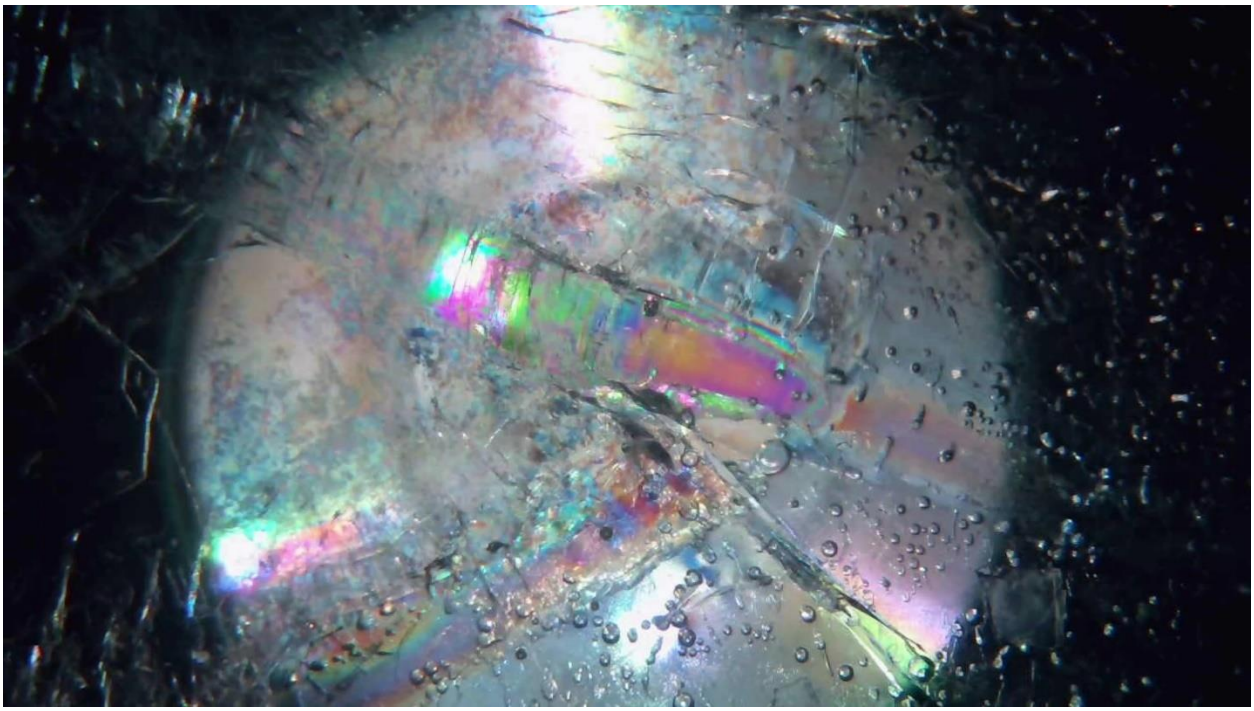

Figure E4 – 0 hours, 20 minutes, 0 seconds

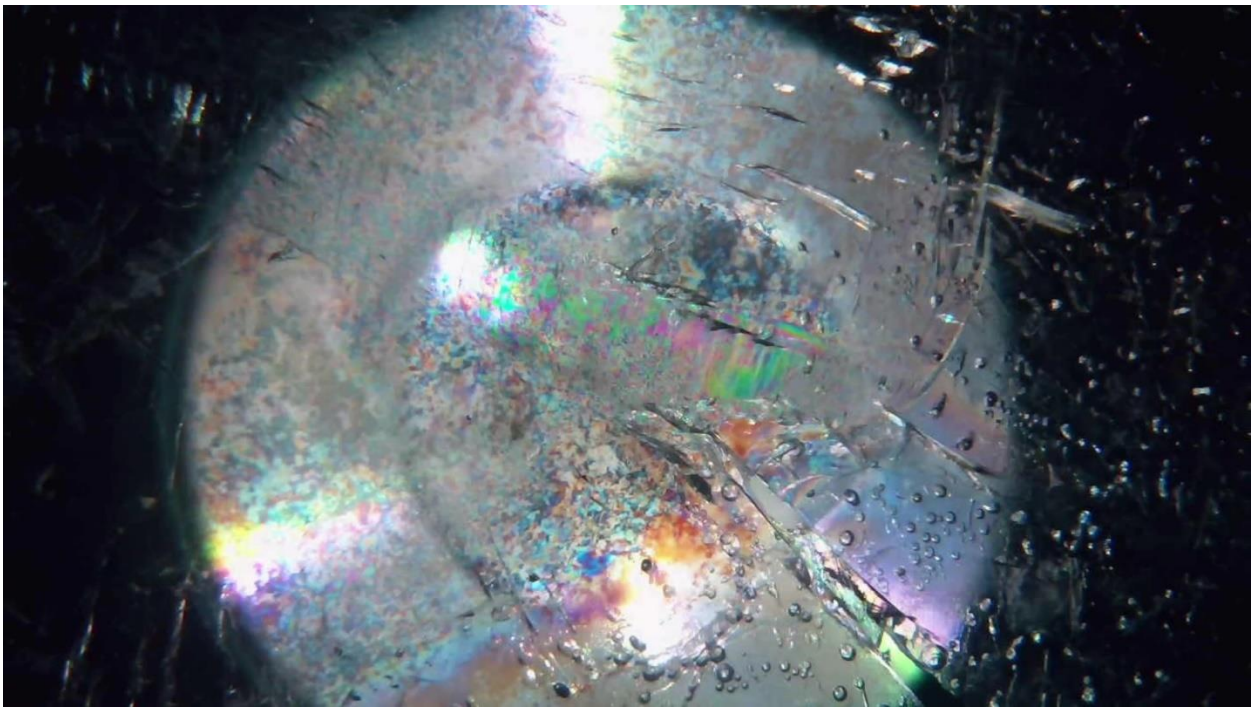

Figure E5 – 1 hour, 0 minutes, 0 seconds

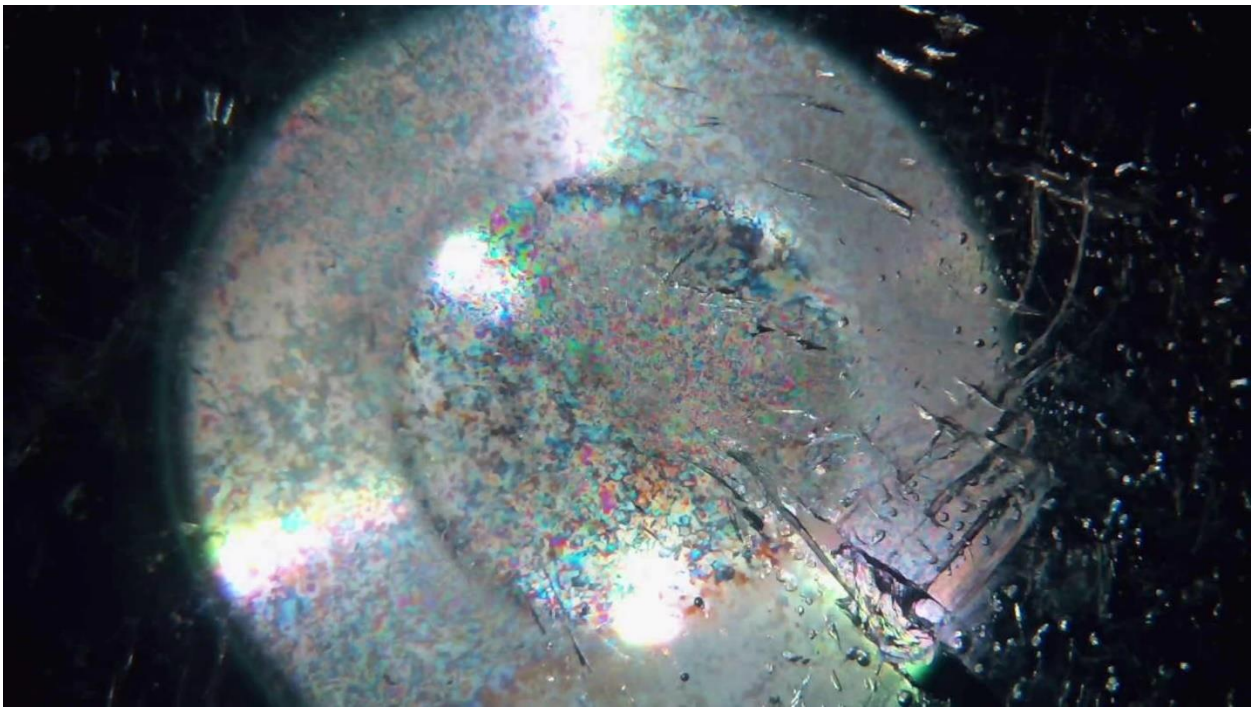

Figure E6 – 2 hours, 0 minutes, 0 seconds

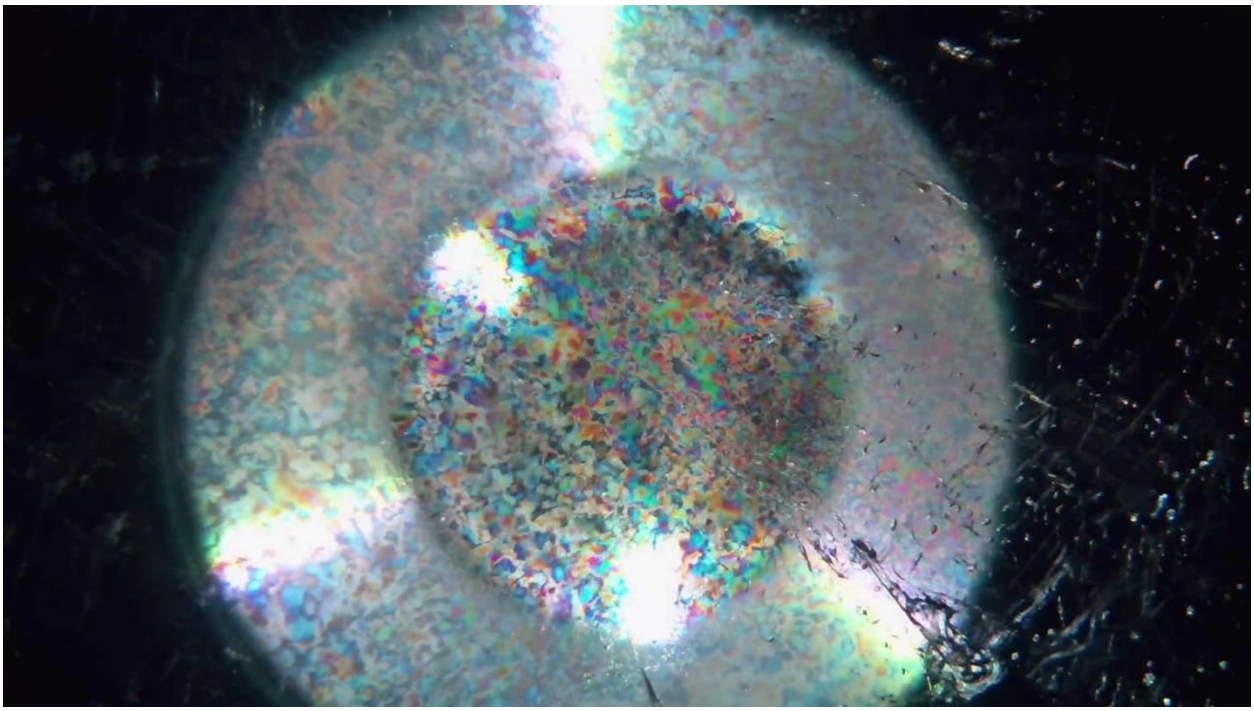

Figure E7 – 4 hours, 0 minutes, 0 seconds

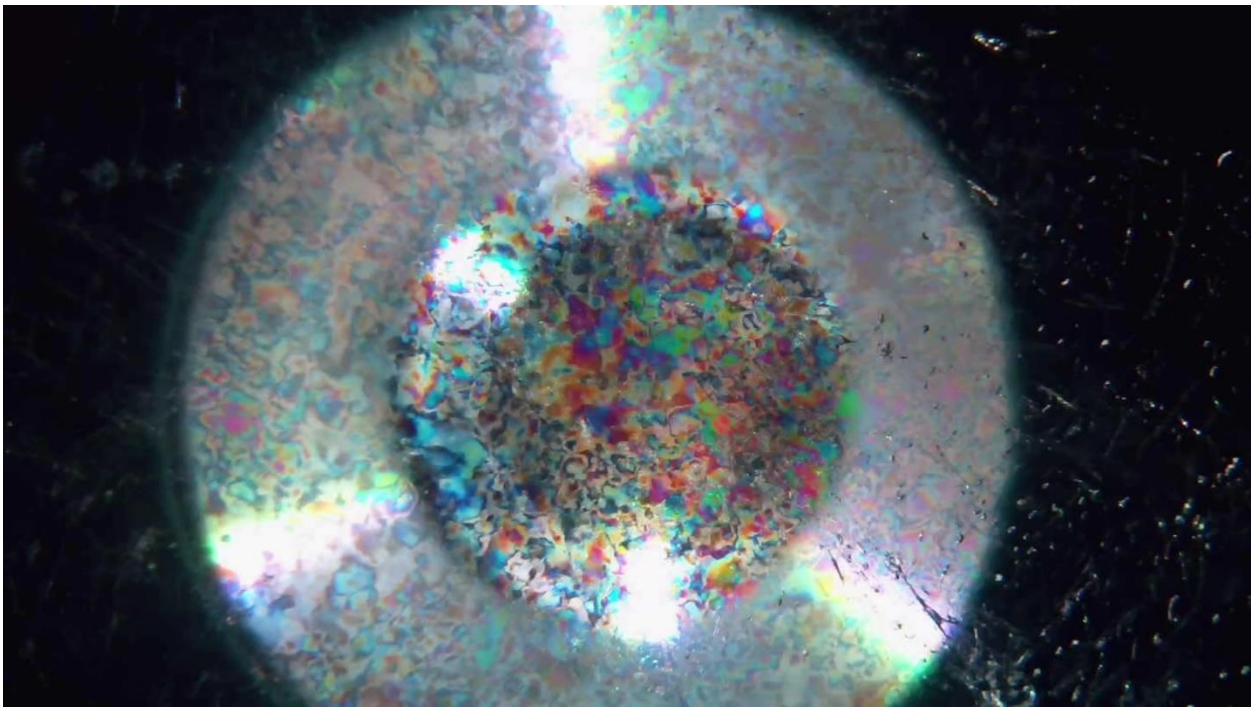

Figure E8 – 6 hours, 0 minutes, 3 seconds

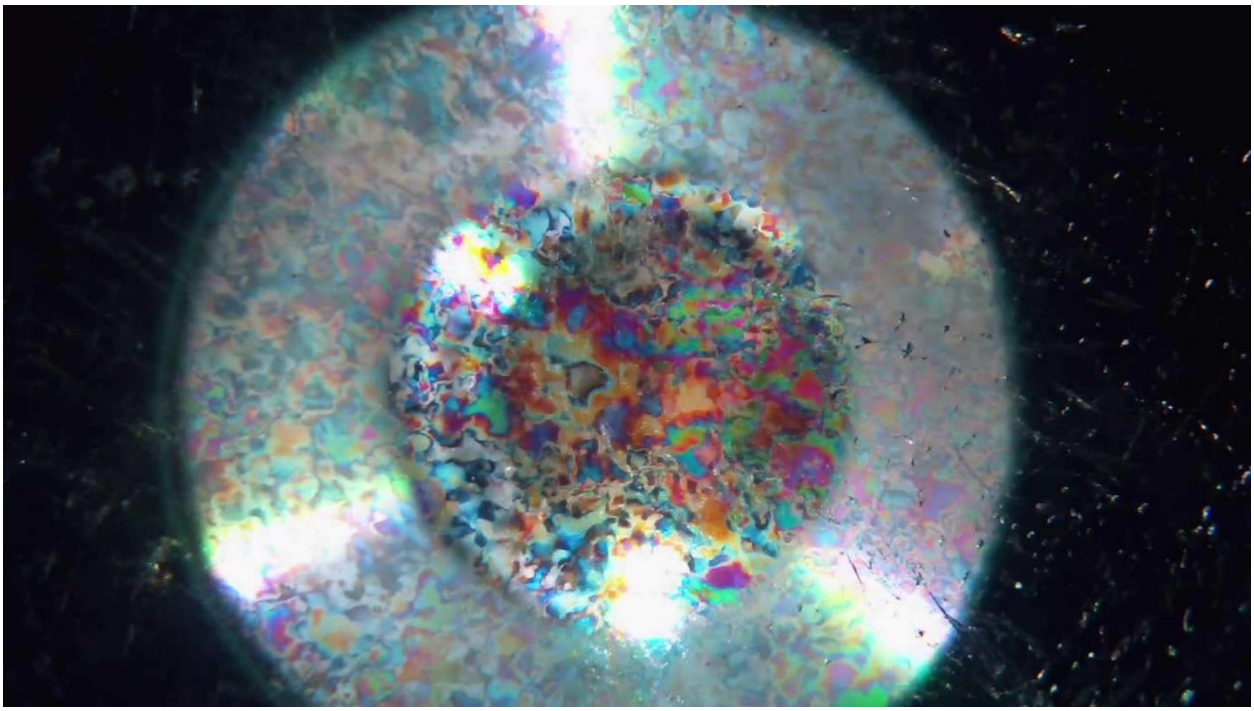

Figure E9 – 8 hours, 0 minutes, 0 seconds

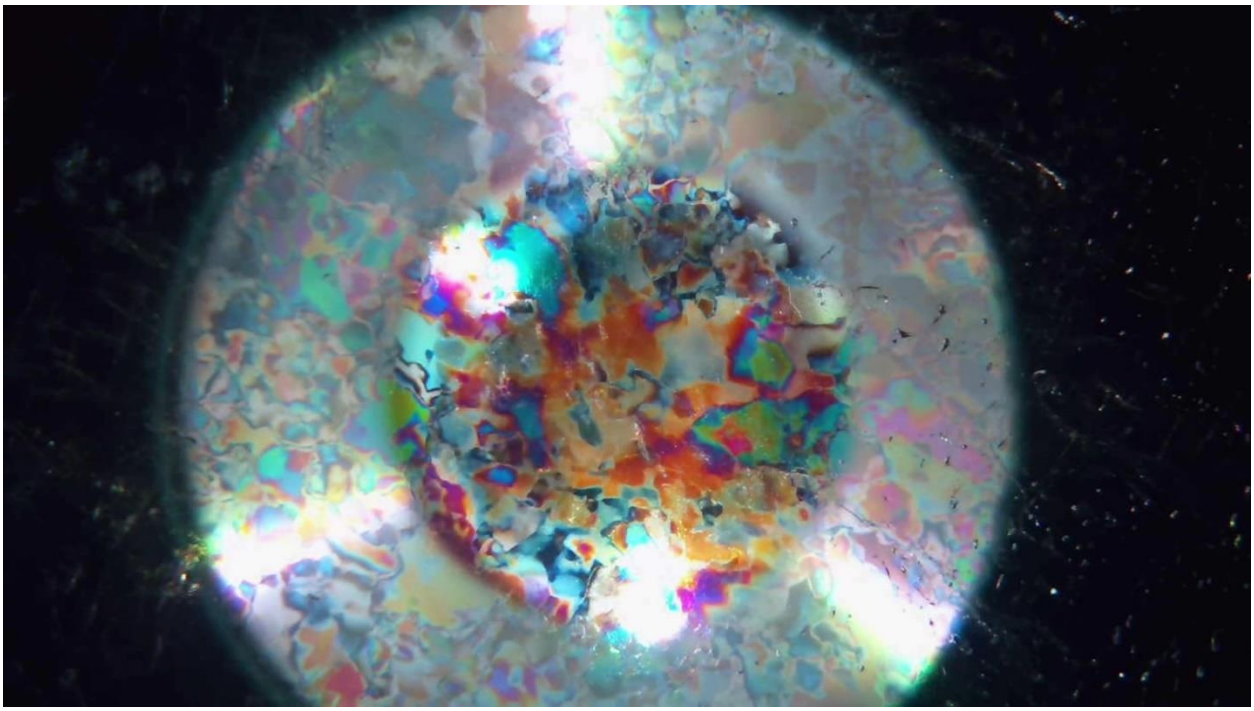

Figure E9 – 15 hours, 0 minutes, 1 second

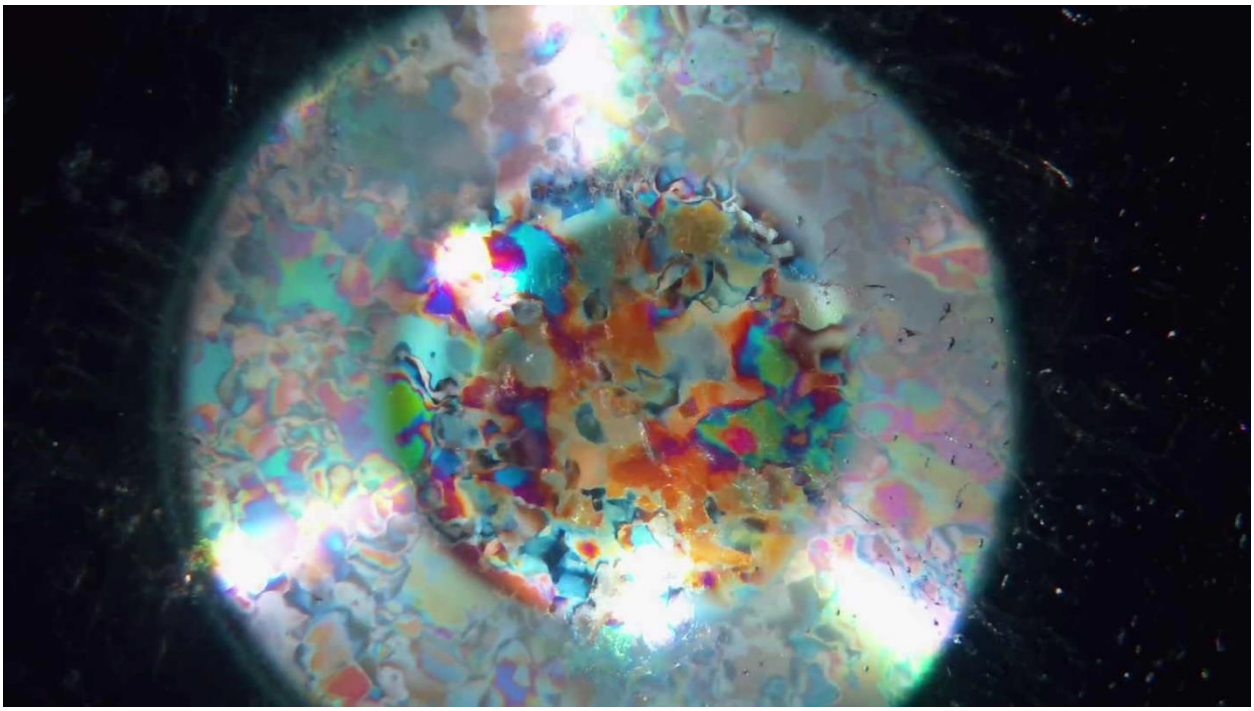

Figure E10 – 17 hours, 0 minutes, 0 seconds

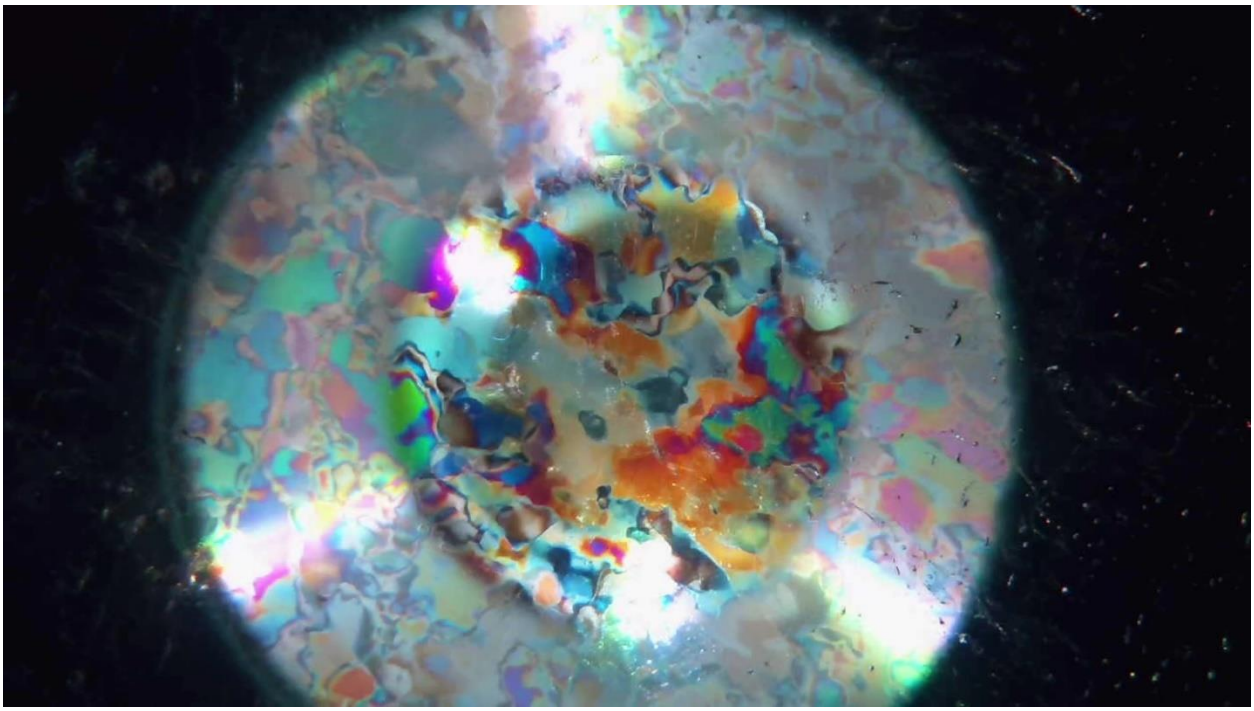

Figure E11 – 20 hours, 0 minutes, 0 seconds

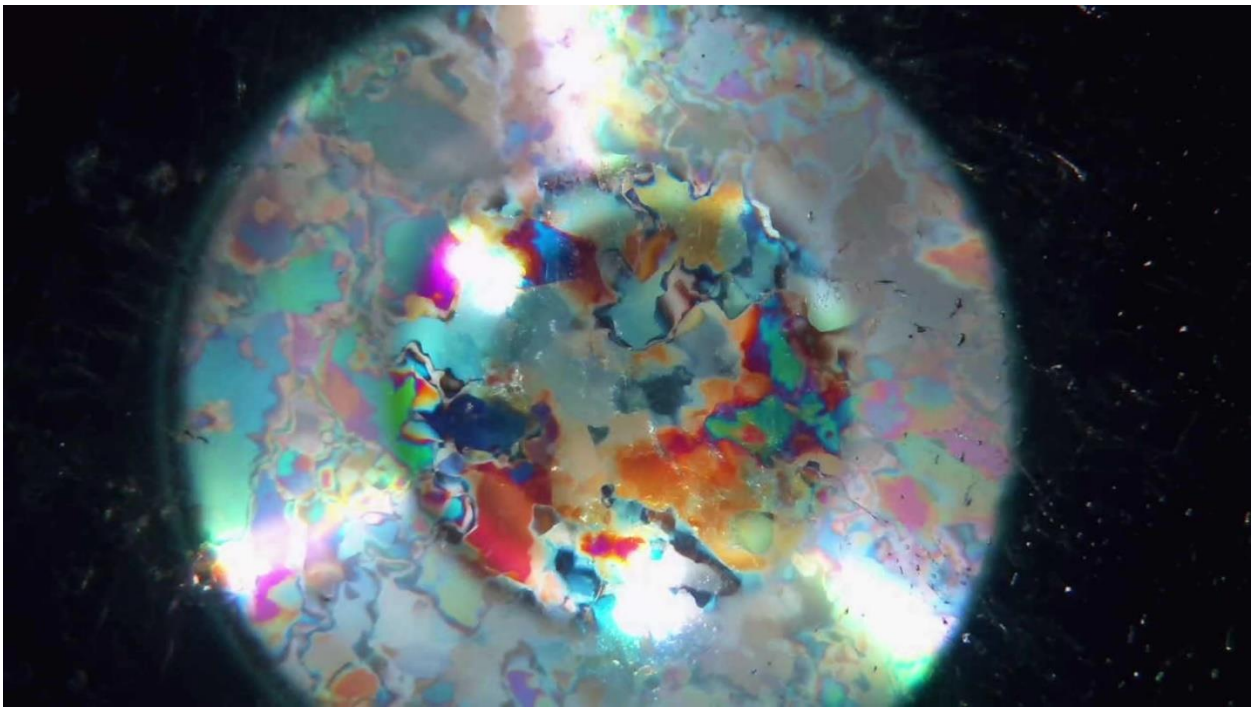

Figure E12 – 22 hours, 0 minutes, 0 seconds

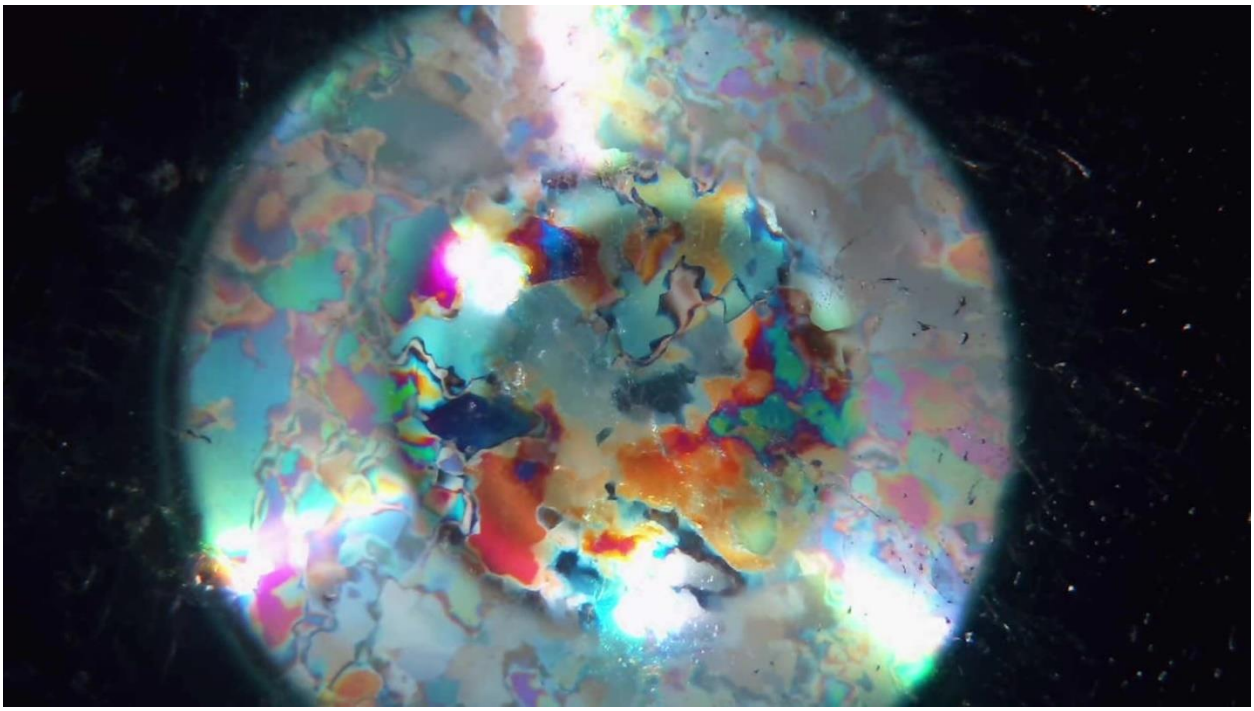

Figure E13 – 23 hours, 55 minutes, 32 seconds

APPENDIX F – Applying Constant Pressure at Melting Point Screenshots

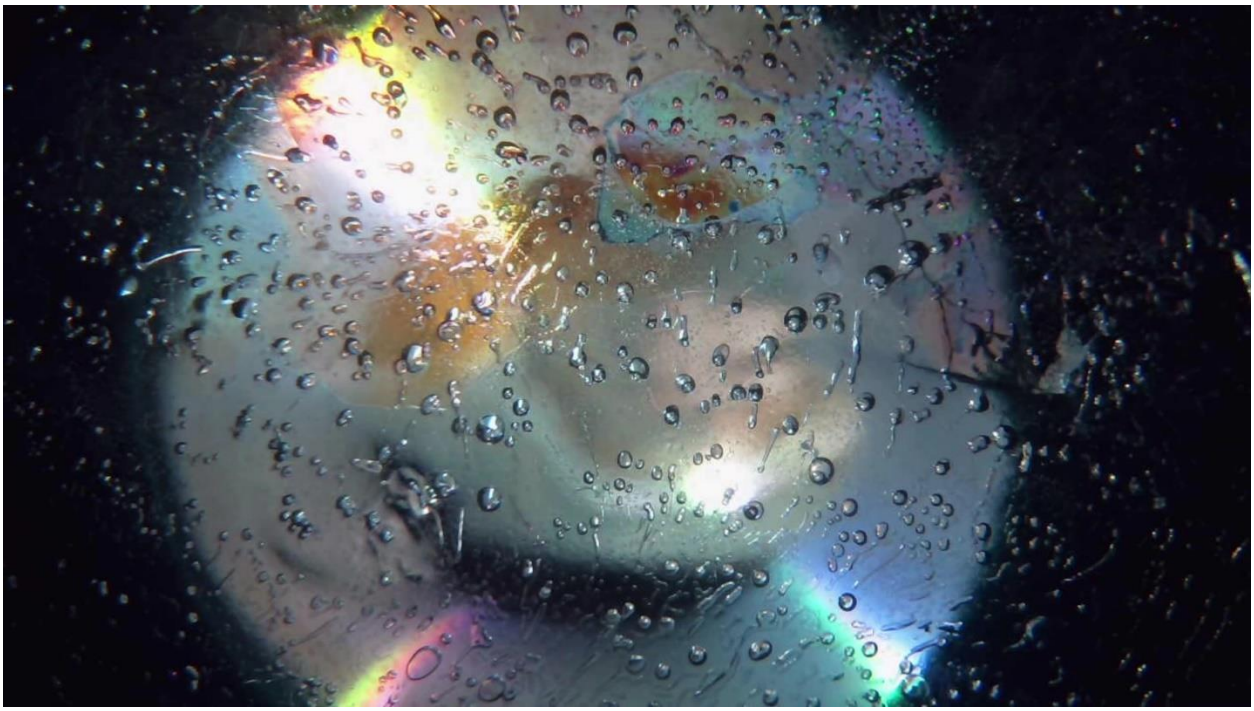

Figure F1 – 0 hours, 0 minutes, 0 seconds

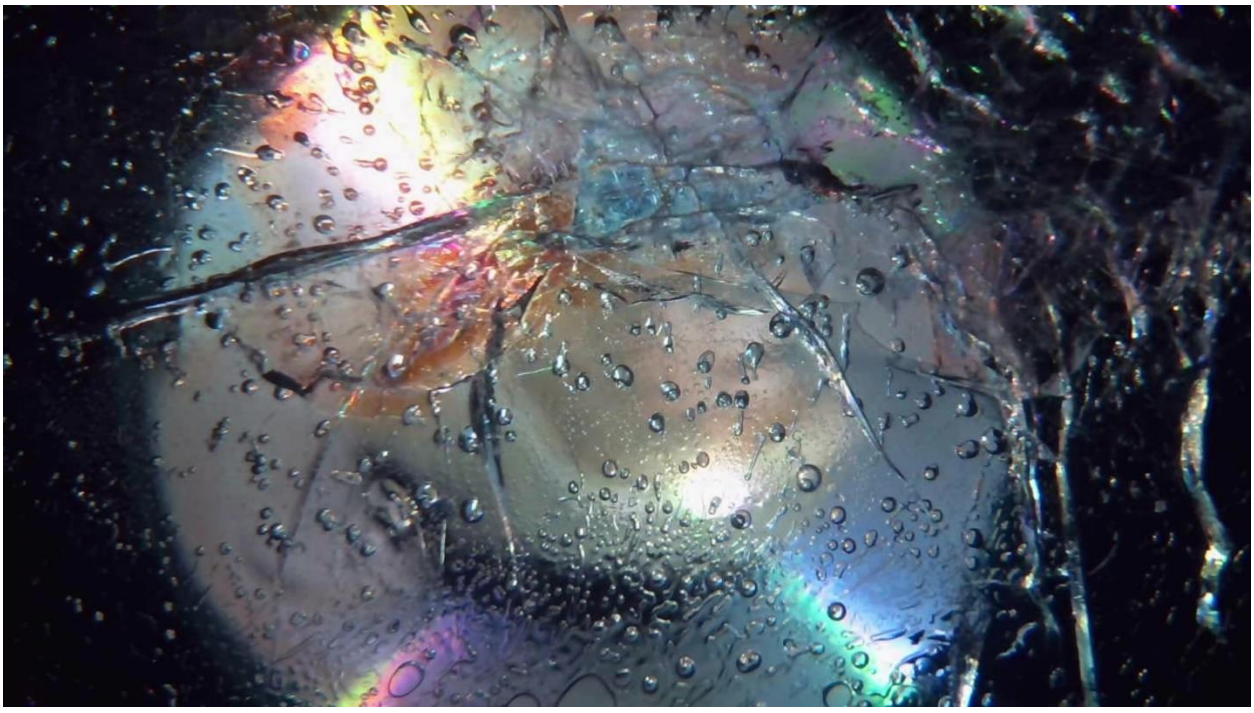

Figure F2 – 0 hours, 1 minutes, 16 seconds

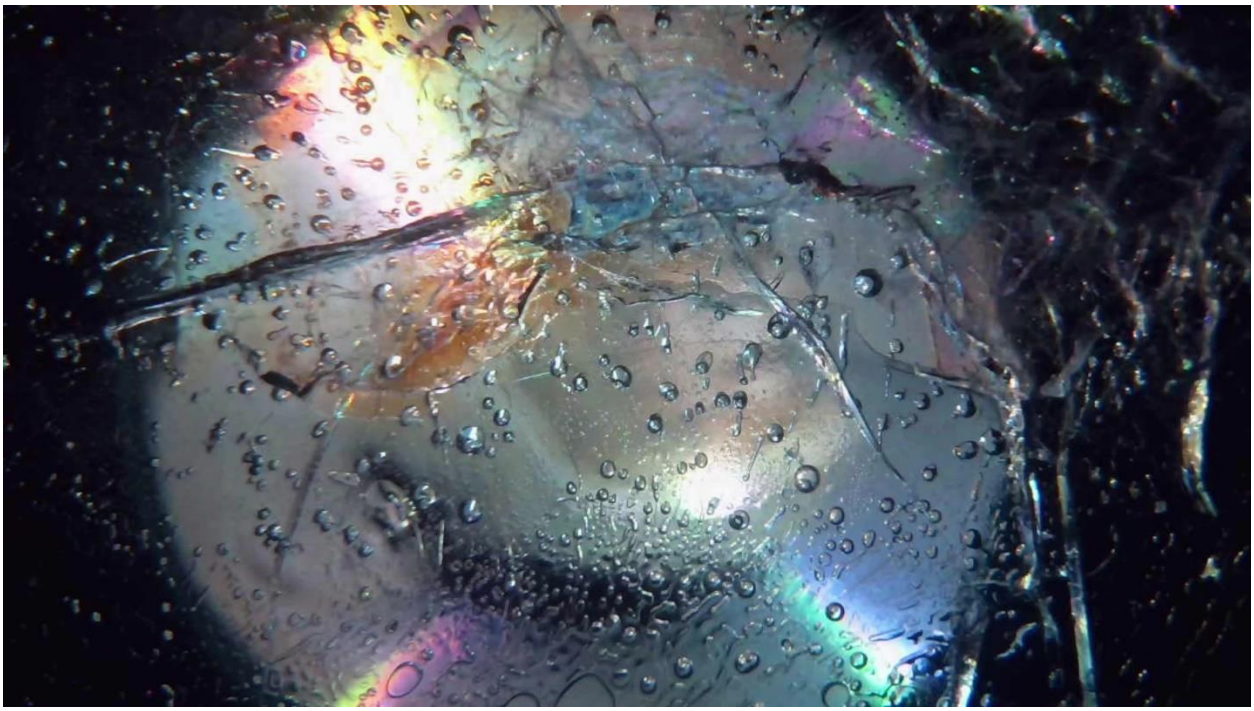

Figure F3 – 0 hours, 1 minutes, 30 seconds

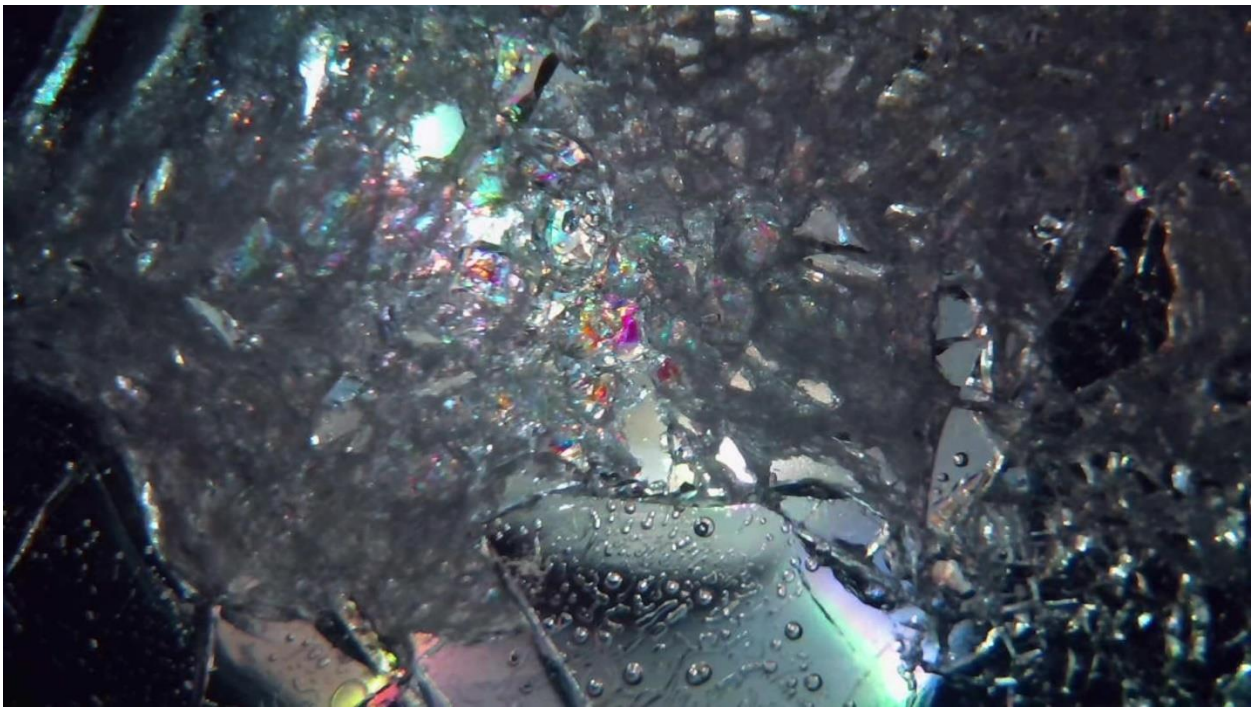

Figure F4 – 0 hours, 2 minutes, 5 seconds

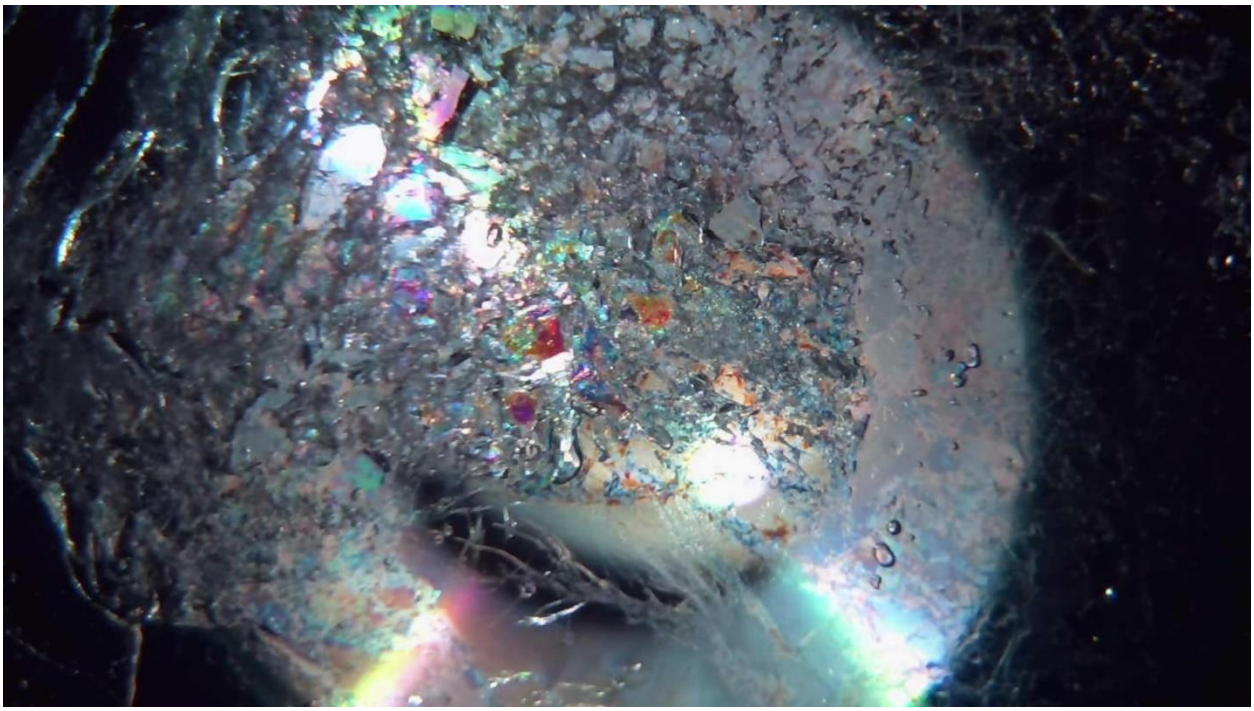

Figure F5 – 0 hours, 3 minutes, 10 seconds

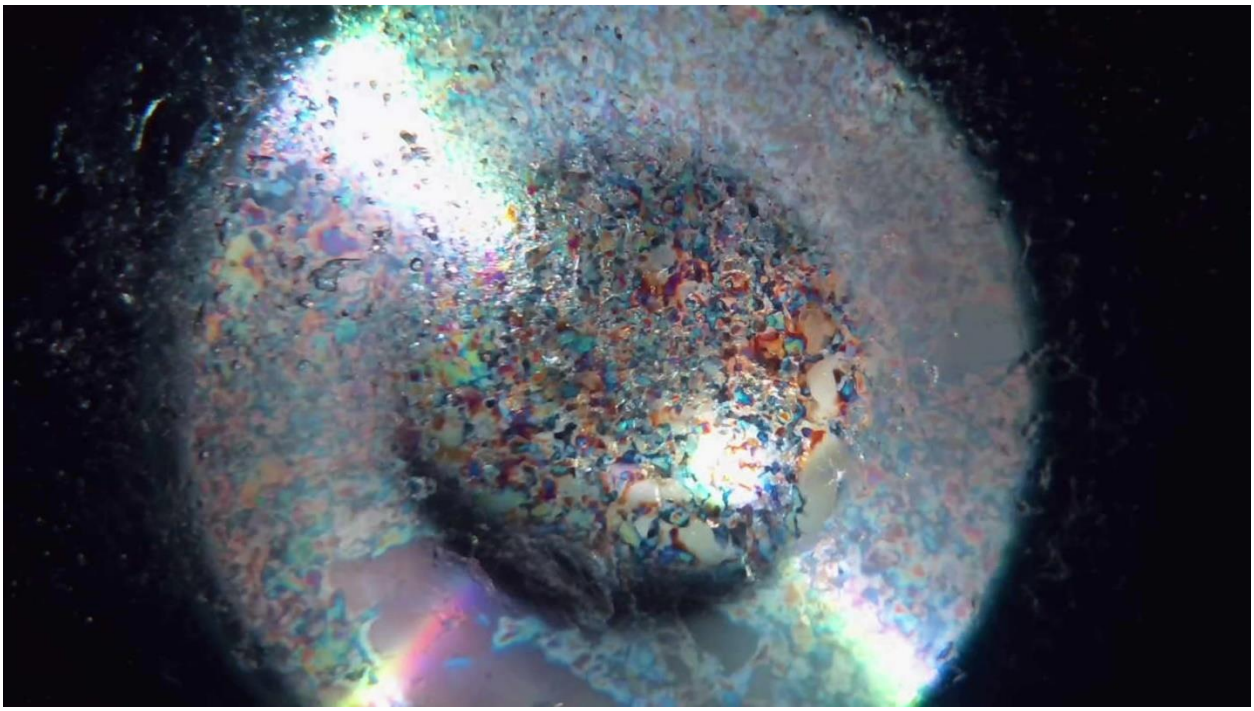

Figure F6 – 0 hours, 10 minutes, 0 seconds

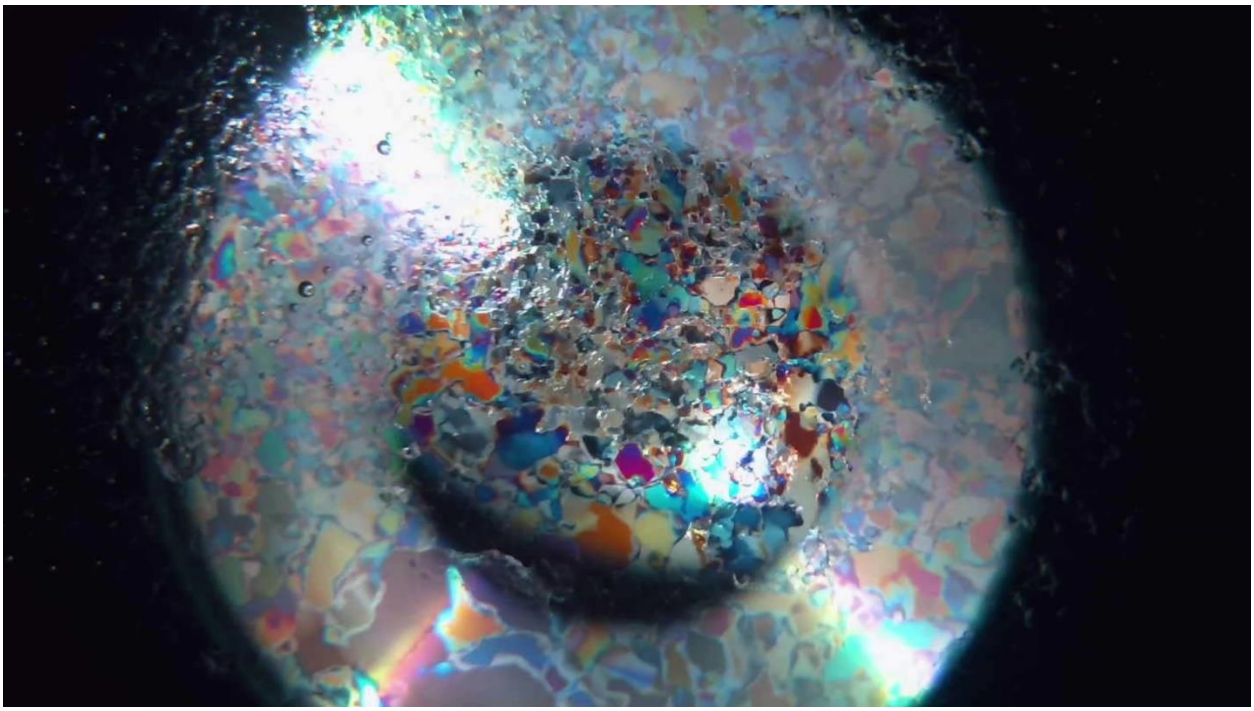

Figure F7 – 0 hours, 30 minutes, 0 seconds

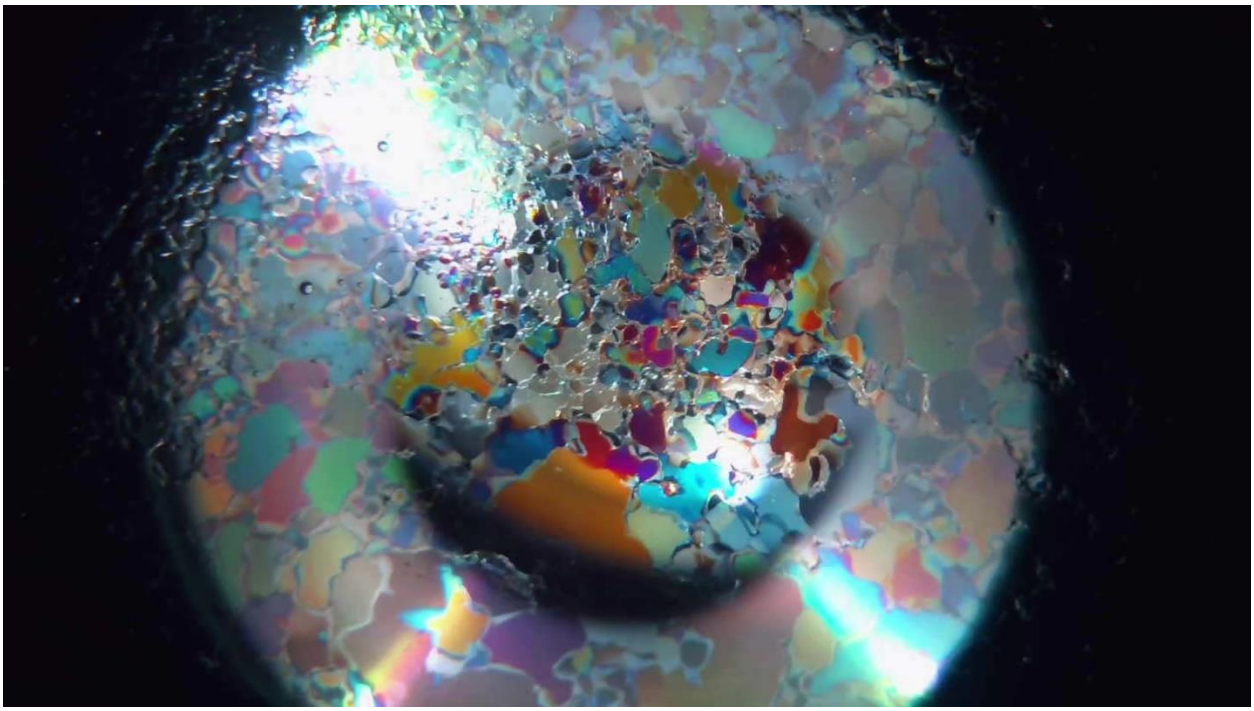

Figure F8 – 1 hour, 0 minutes, 0 seconds

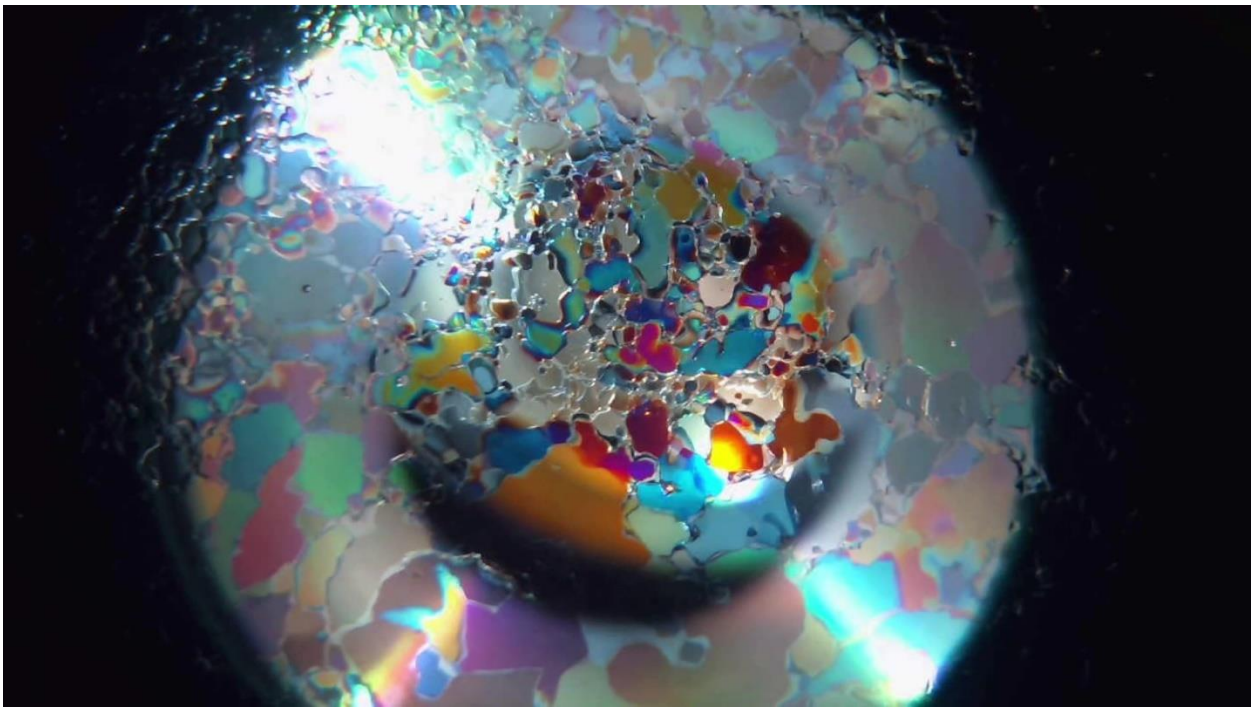

Figure F9 – 1 hour, 30 minutes, 0 seconds

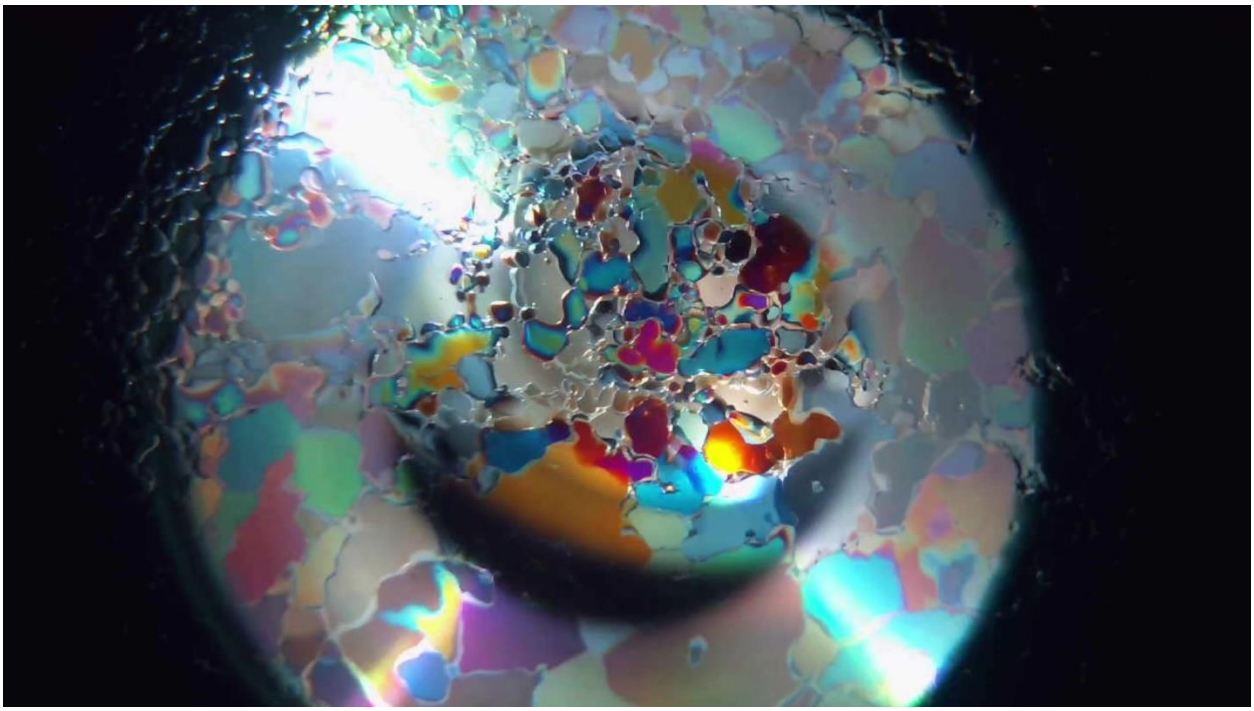

Figure F10 – 2 hours, 0 minutes, 0 seconds

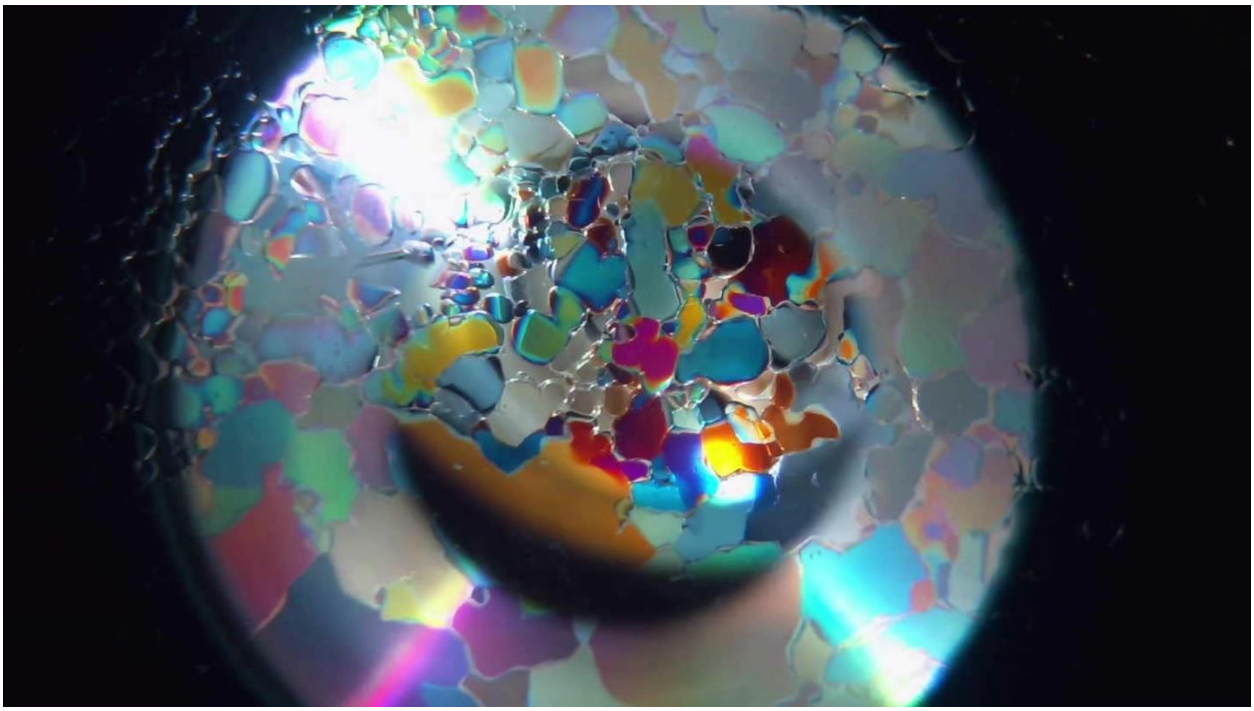

Figure F11 – 5 hours, 0 minutes, 0 seconds

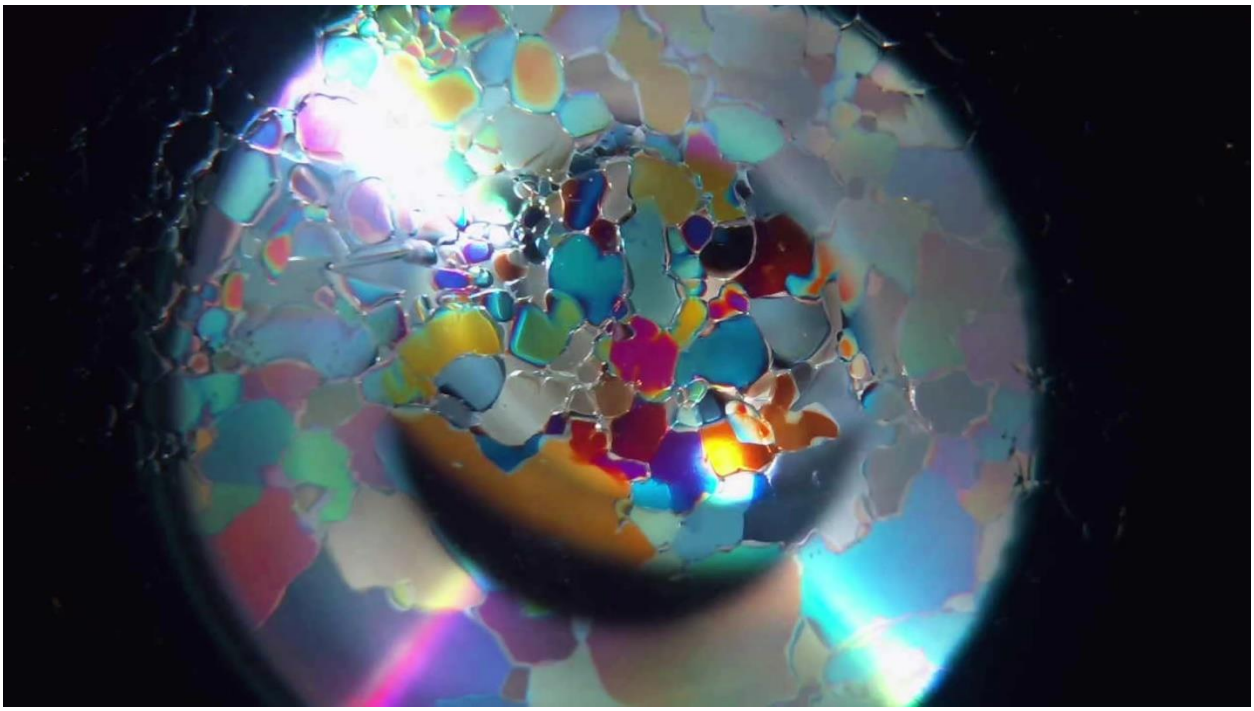

Figure F12 – 7 hours, 0 minutes, 0 seconds

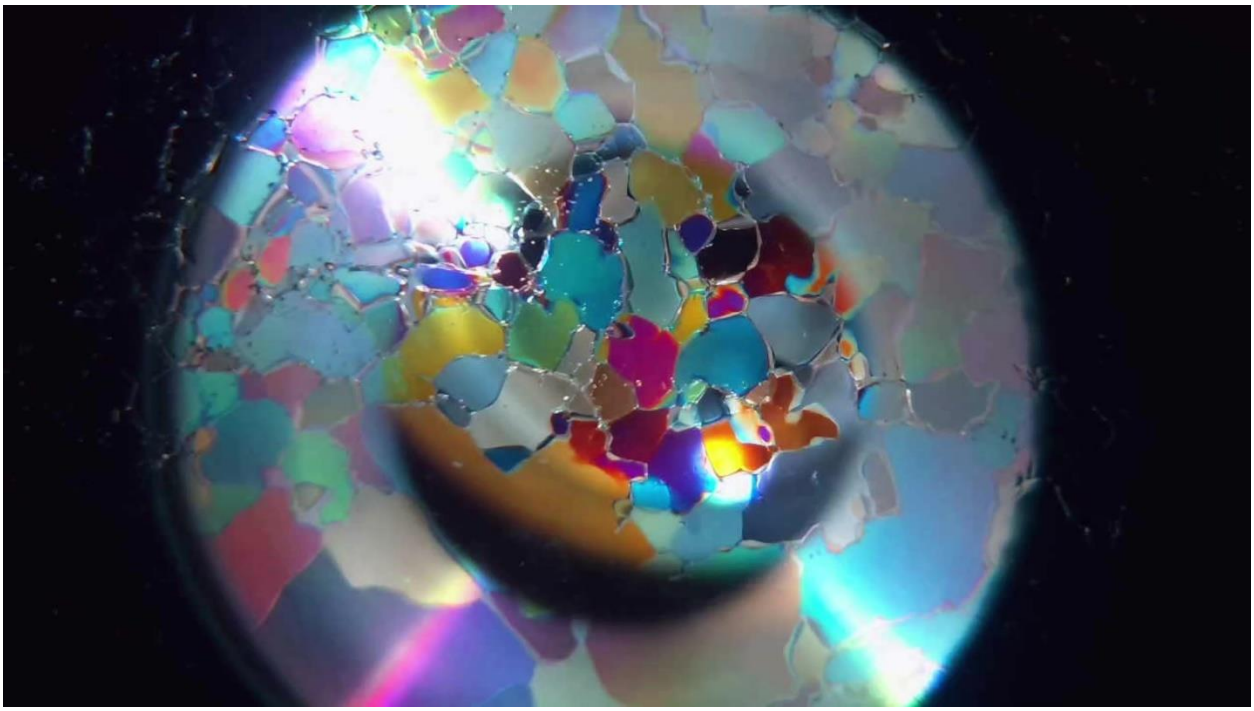

Figure F13 – 9 hours, 0 minutes, 0 seconds

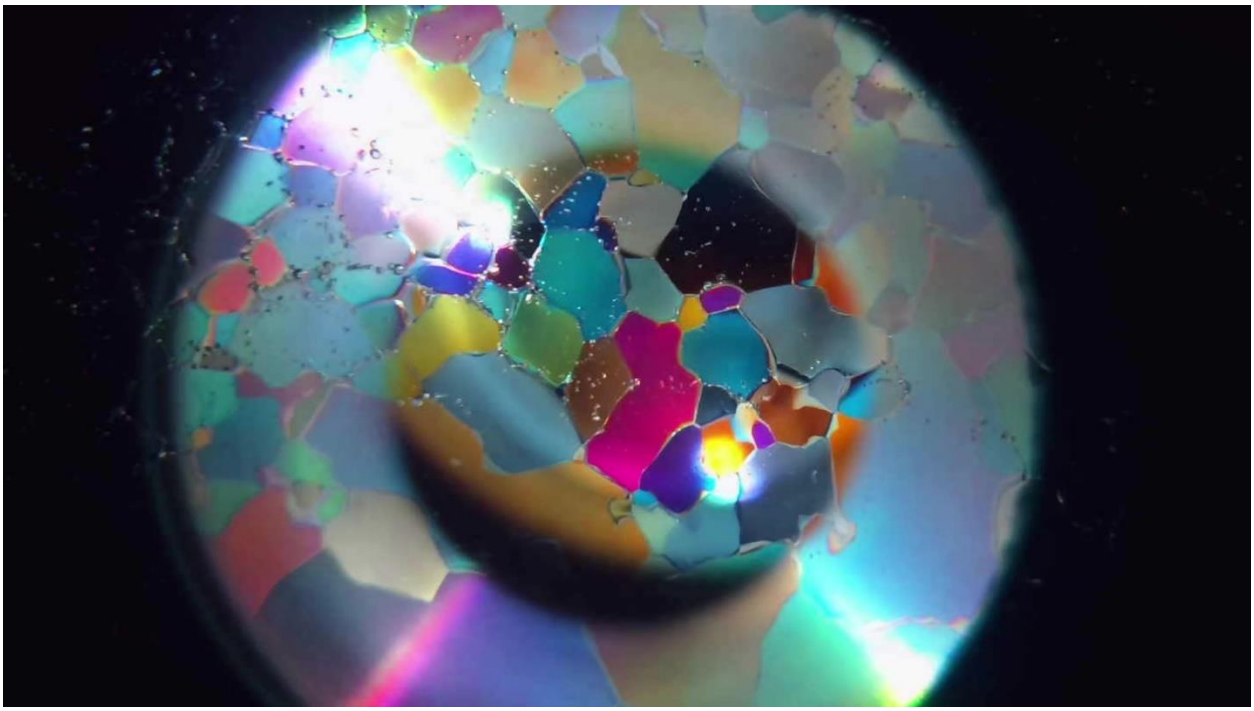

Figure F14 – 22 hours, 0 minutes, 0 seconds

APPENDIX G – Cold Test at Constant Pressure Screenshots

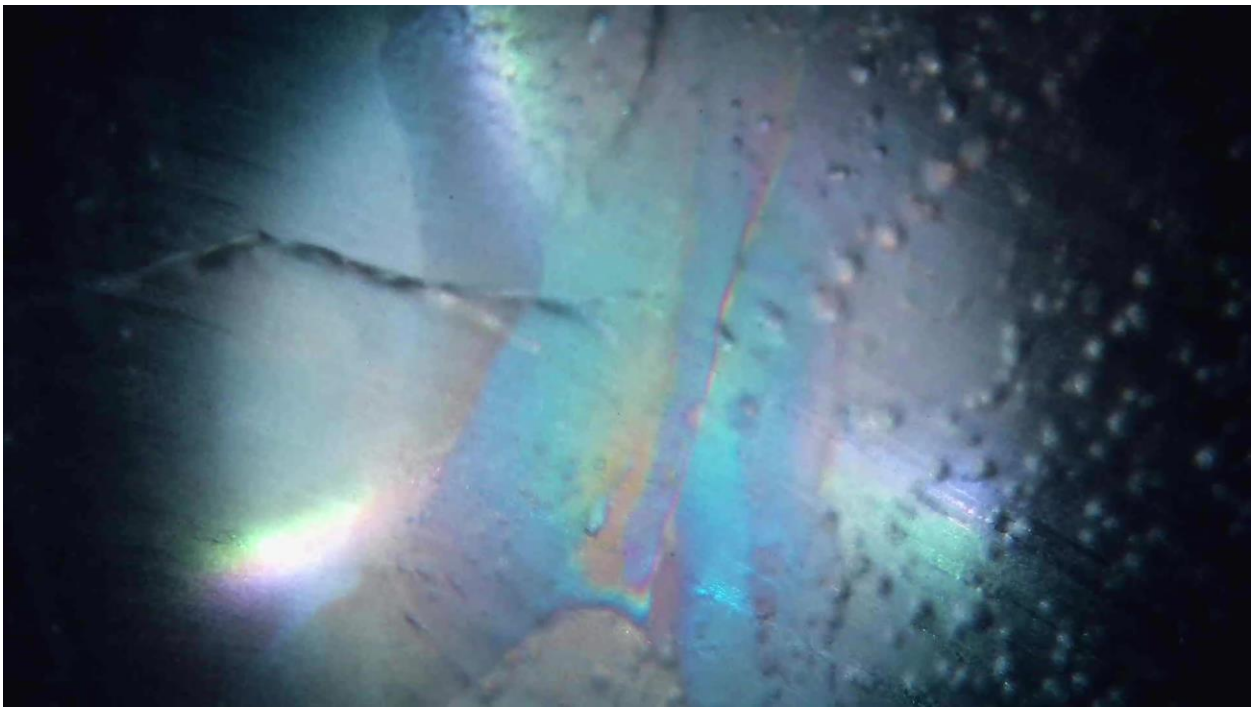

Figure G1 – 0 hours, 0 minutes, 0 seconds

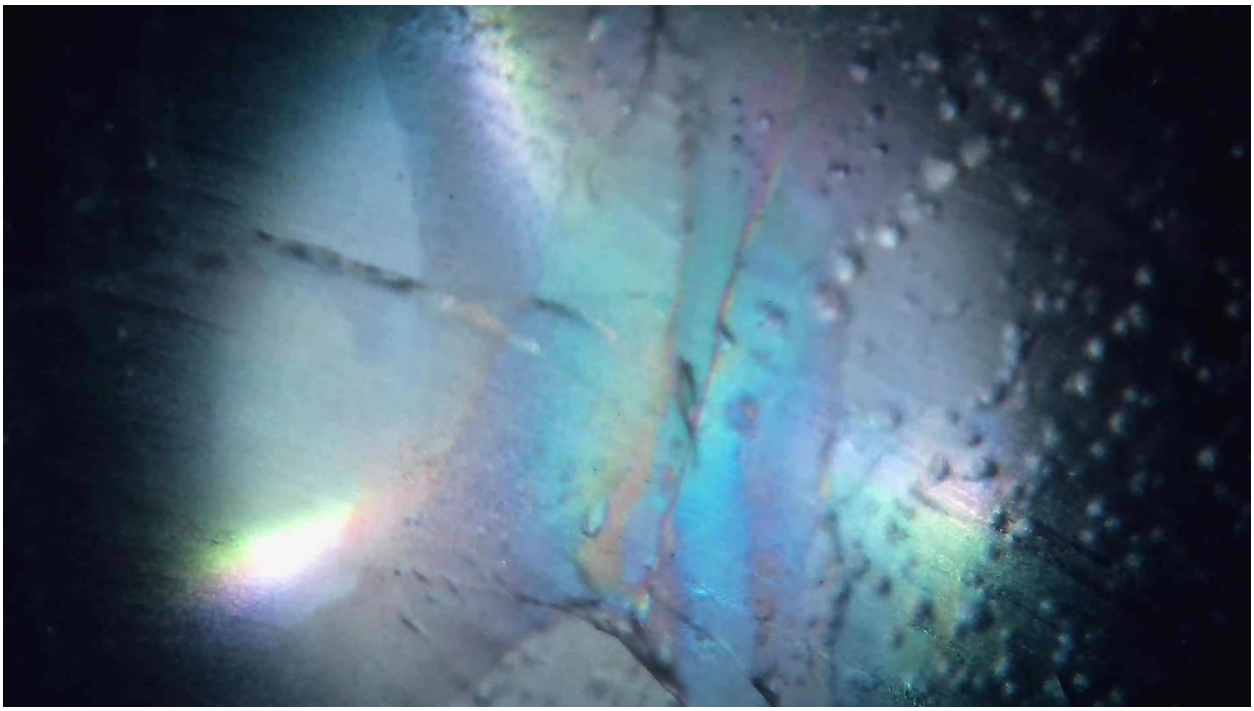

Figure G2 – 0 hours, 1 minute, 22 seconds

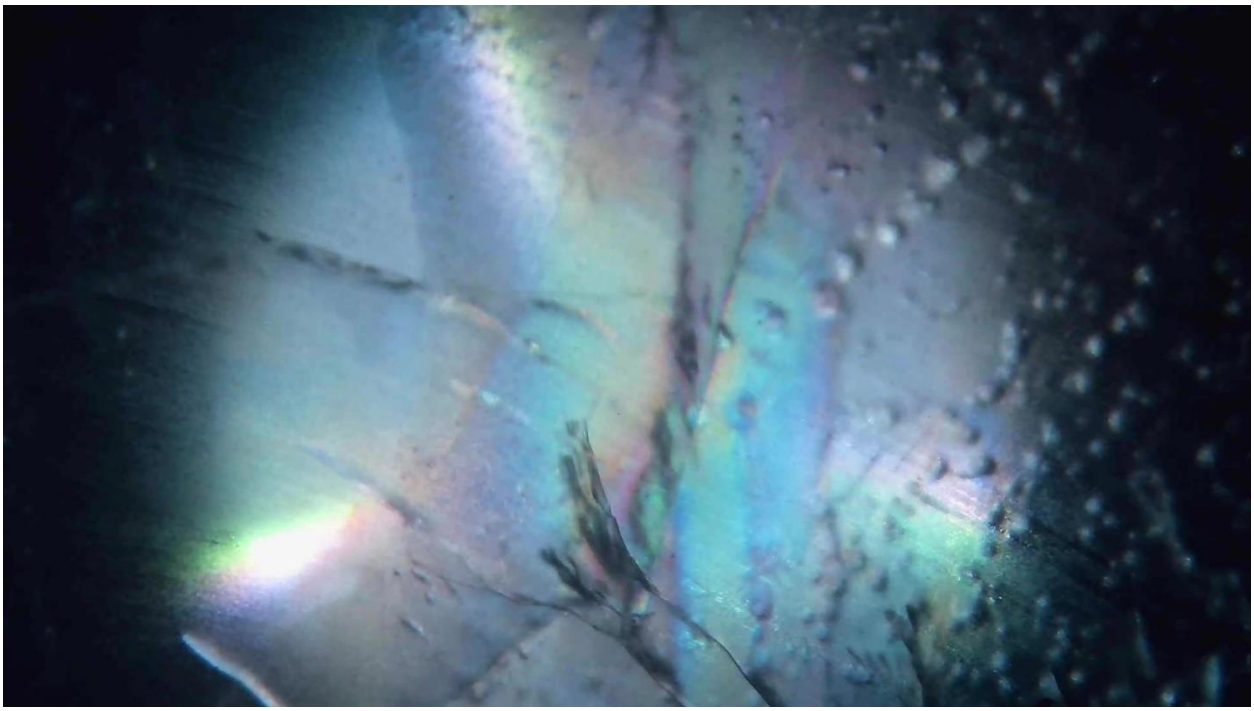

Figure G3 – 0 hours, 1 minute, 45 seconds

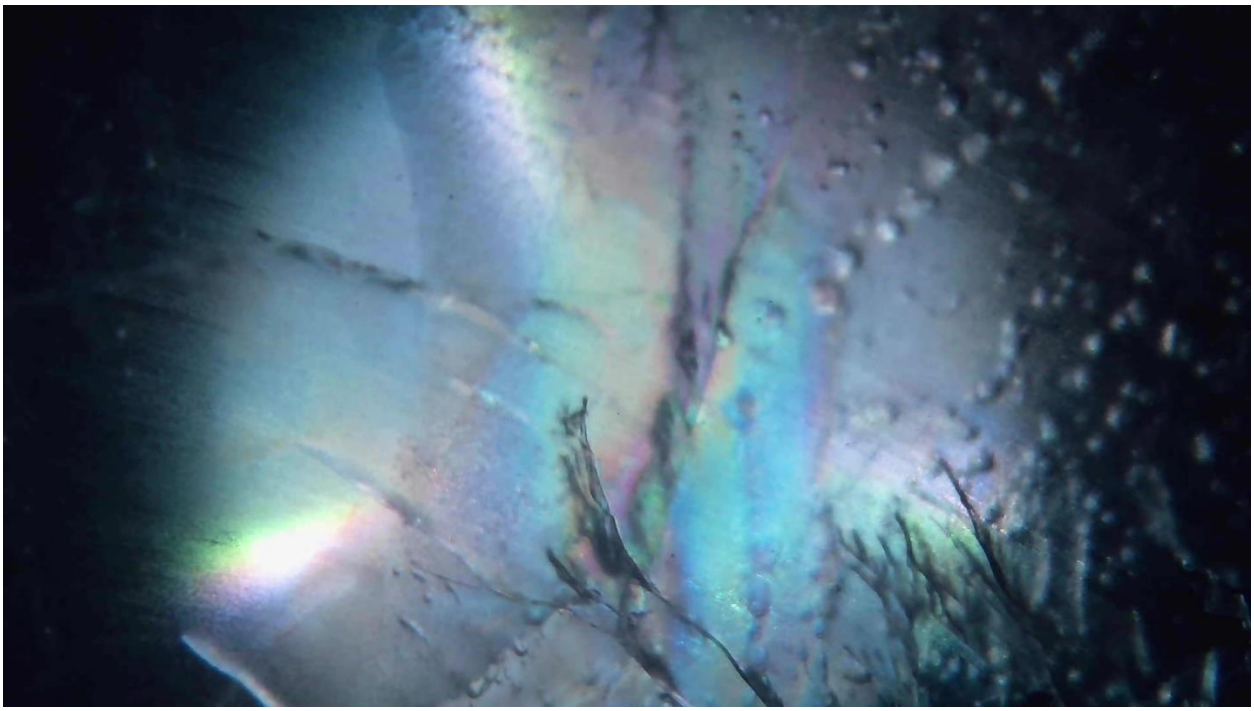

Figure G4 – 0 hours, 2 minutes, 5 seconds

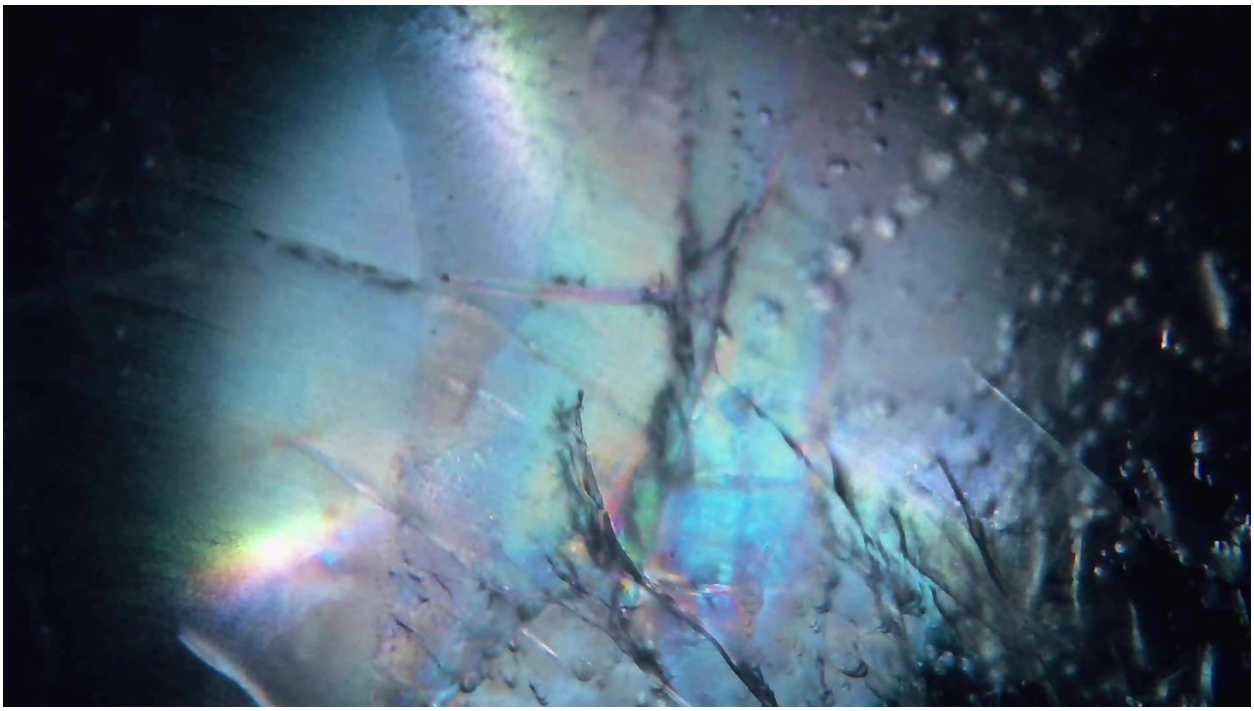

Figure G5 – 0 hours, 3 minutes, 28 seconds

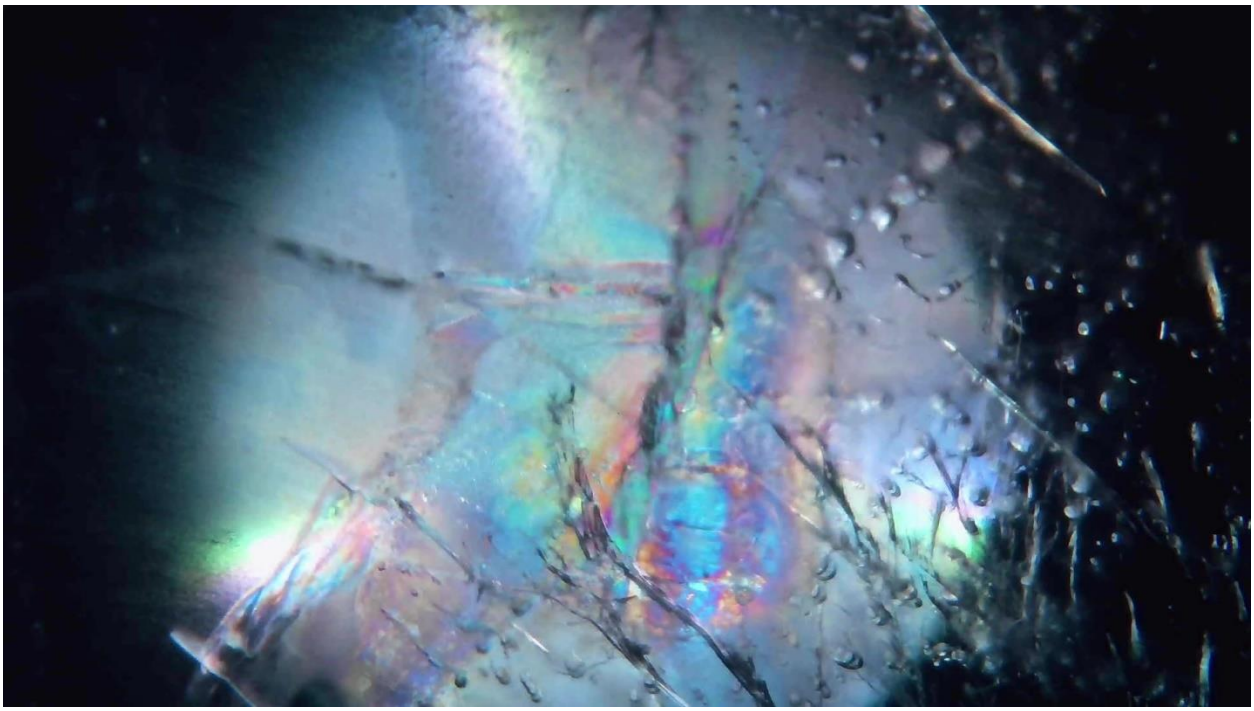

Figure G6 – 0 hours, 15 minutes, 0 seconds

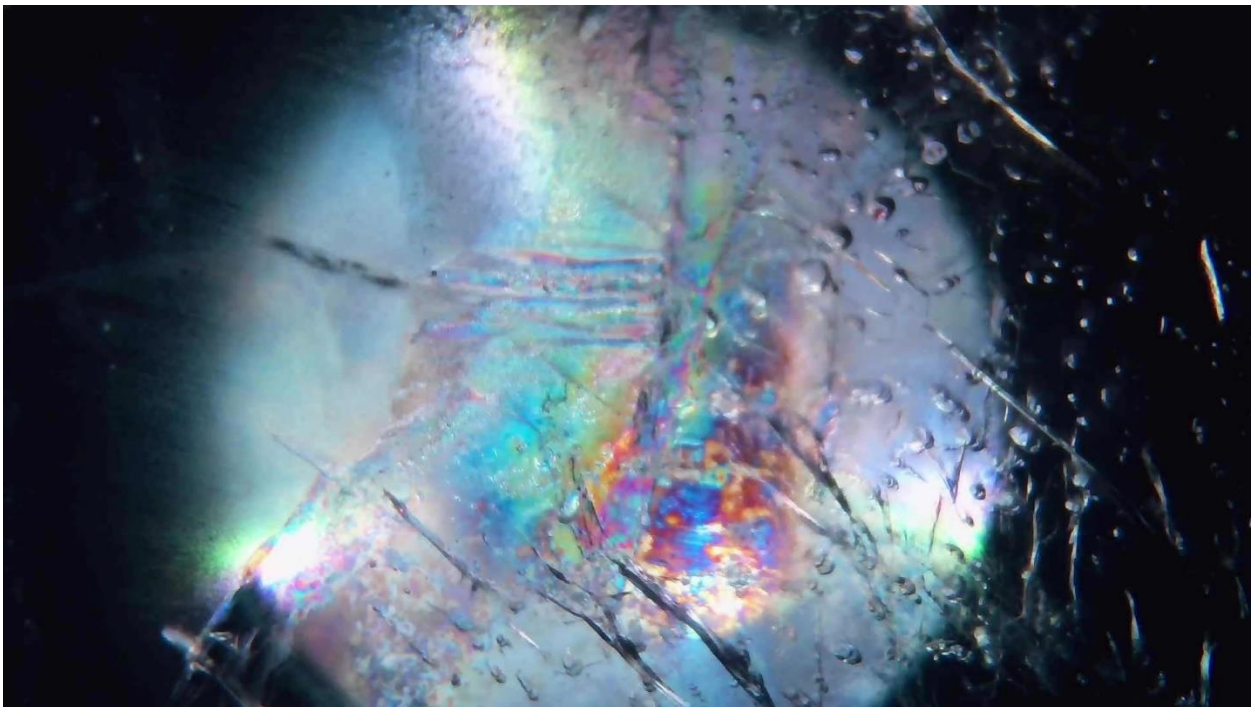

Figure G7 – 1 hour, 0 minutes, 0 seconds

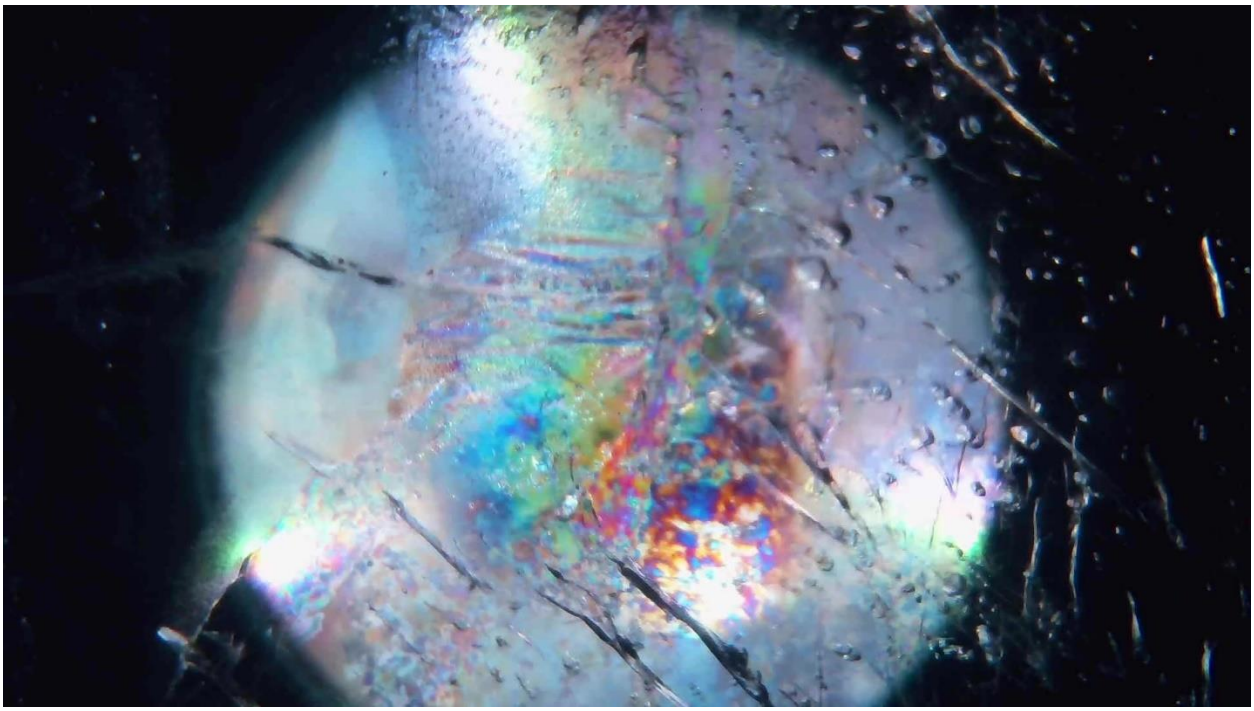

Figure G8 – 2 hours, 20 minutes, 0 seconds

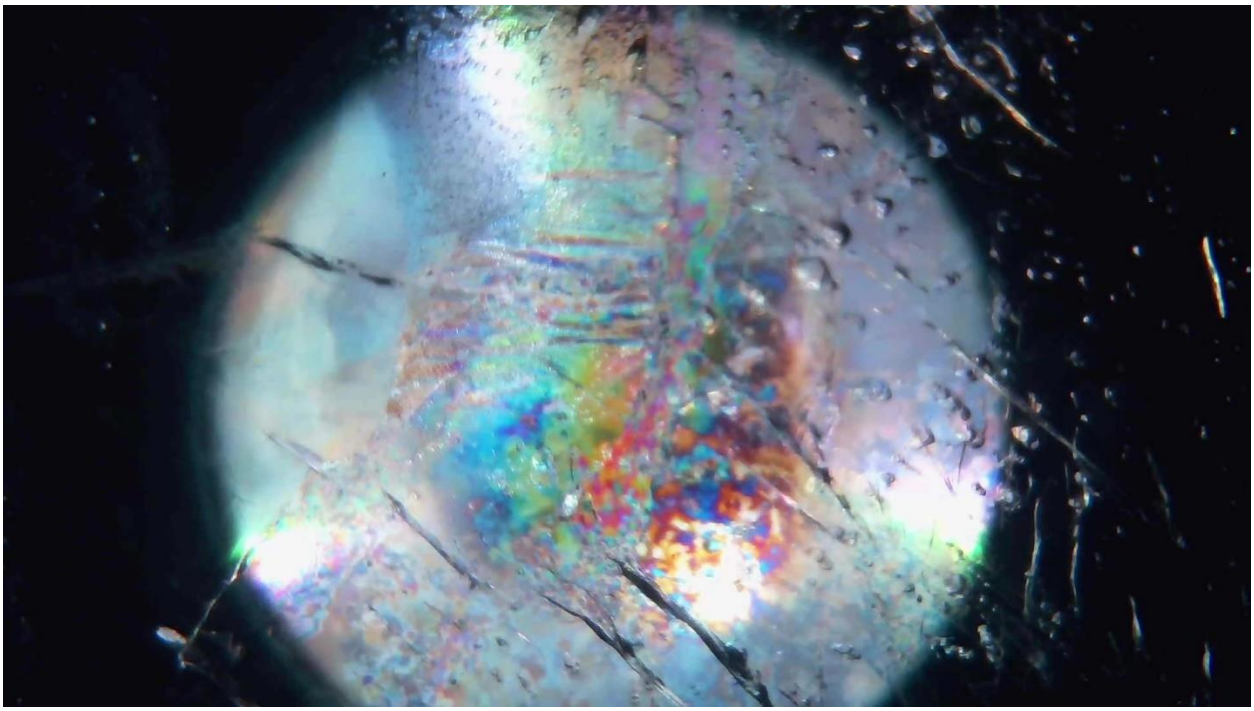

Figure G9 – 5 hours, 0 minutes, 0 seconds

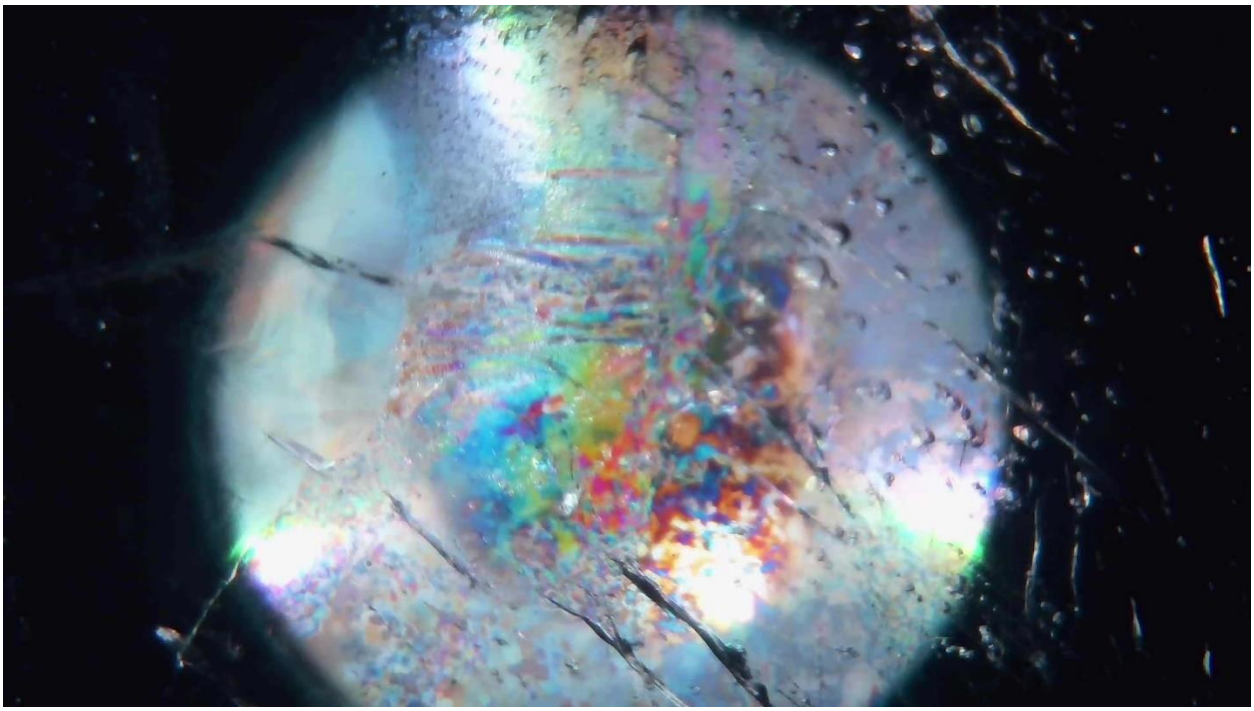

Figure G10 – 10 hours, 0 minutes, 0 seconds

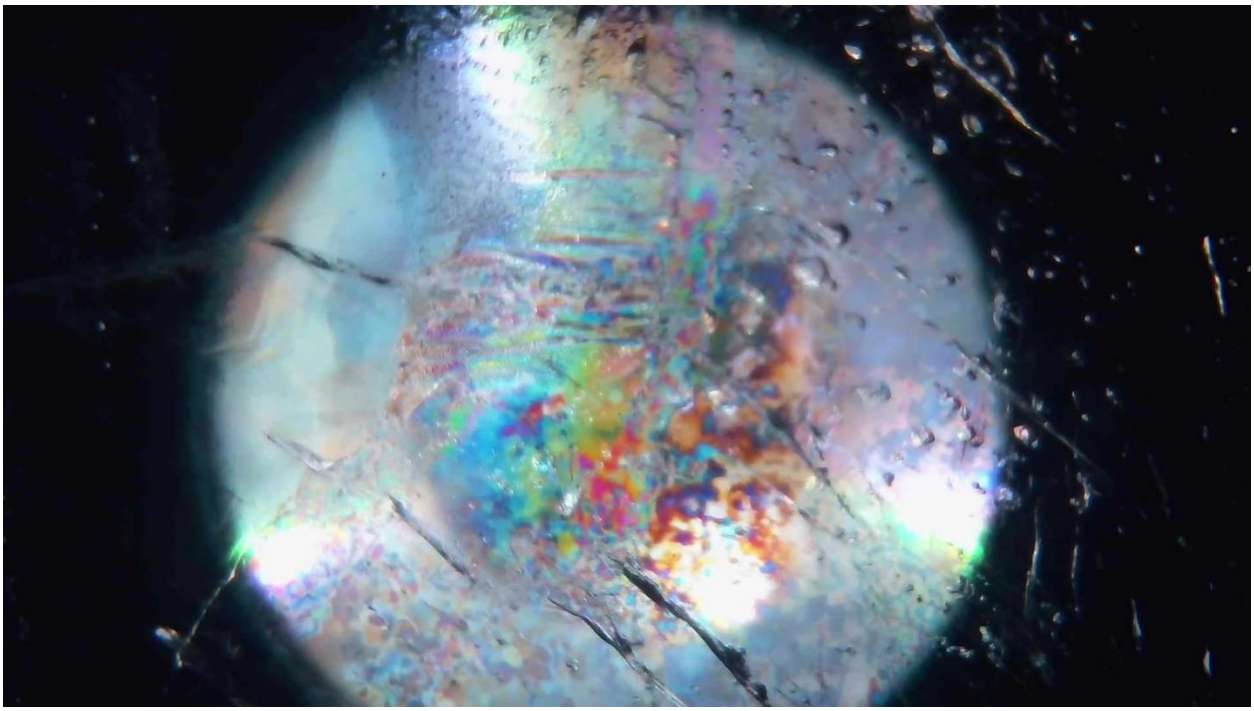

Figure G11 – 15 hours, 0 minutes, 0 seconds

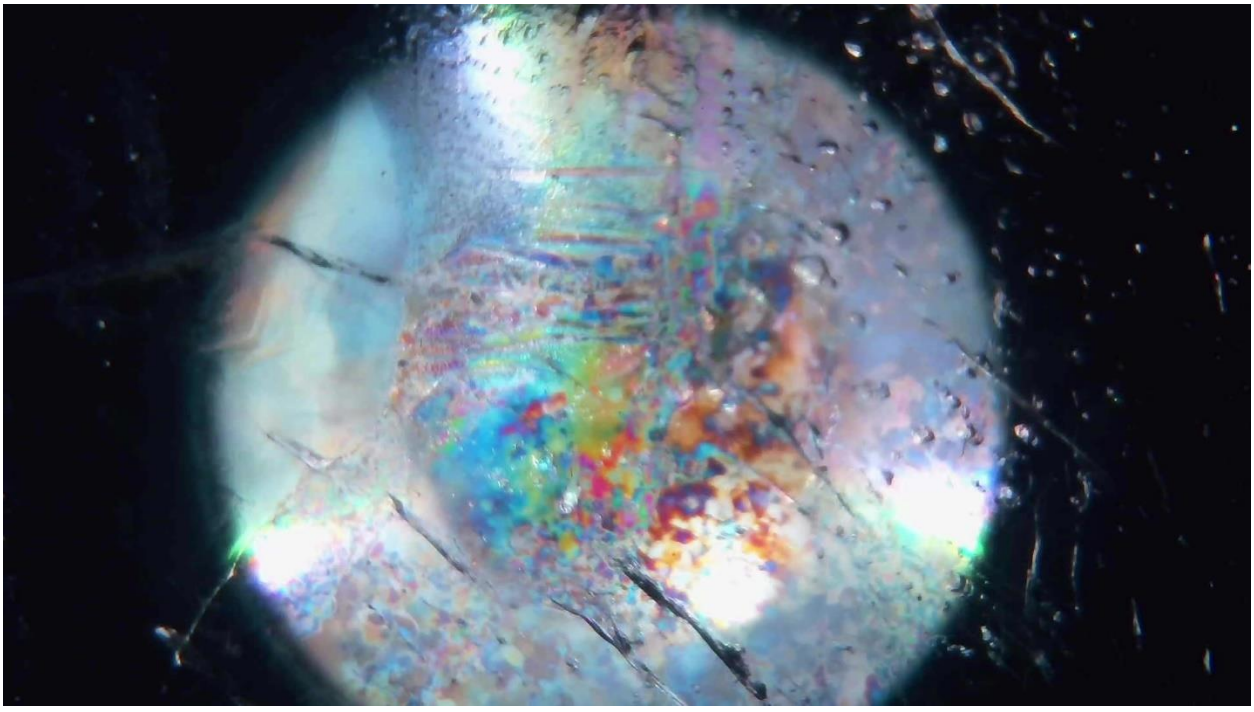

Figure G12 – 20 hours, 0 minutes, 0 seconds

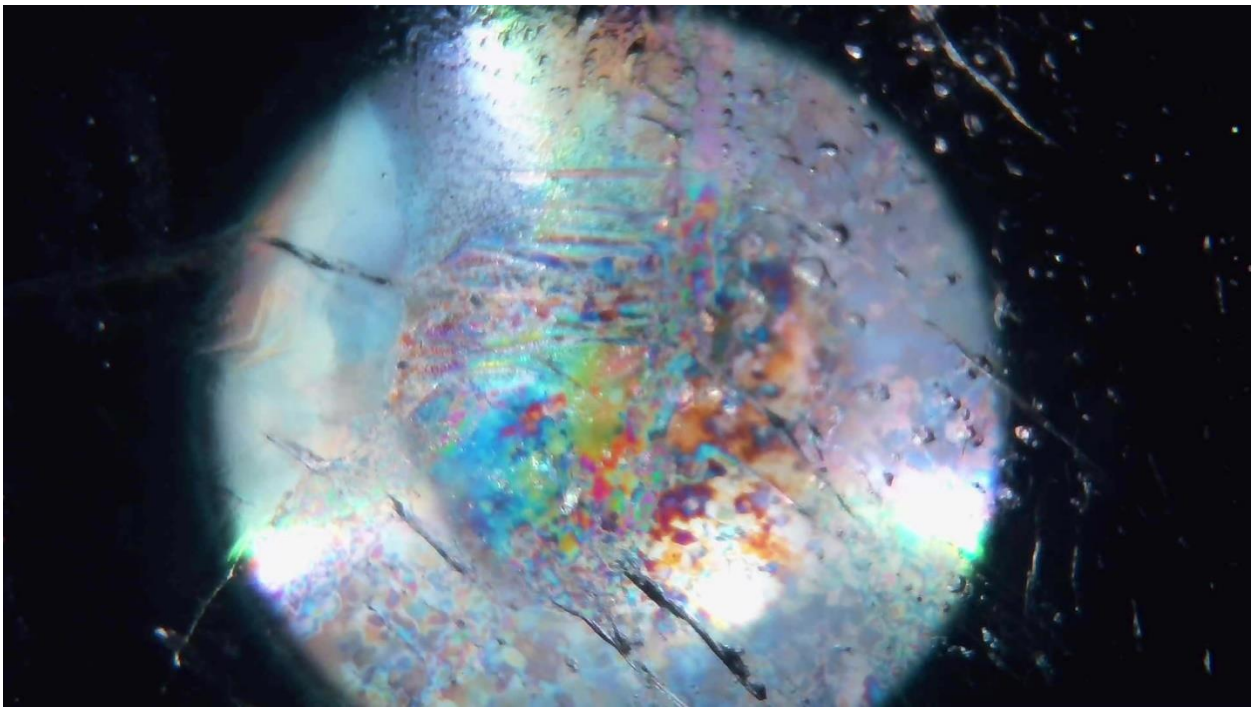

Figure G13 – 23 hours, 58 minutes, 10 seconds